MULTIVARIABLE CONTROL:
DESIGN, ROBUSTNESS, AND NONLINEAR INFERENTIAL CONTROL FOR SEMI-BATCH POLYMERIZATION REACTORS

By
© DERRICK J. KOZUB, M.ENG.

A Thesis
Submitted to the School Of Graduate Studies
in Partial Fulfilment of the Requirements
for the degree
Doctor Of Philosophy

McMaster University
November,1989

MULTIVARIABLE CONTROL

DOCTOR OF PHILOSOPHY (1989) McMASTER UNIVERSITY
(Chemical Engineering) Hamilton, Ontario

TITLE: Multivariable Control: Design, Robustness, And Nonlinear Inferential Control For Semi-Batch Polymerization Reactors

Author: Derrick John Kozub B.Eng. (McGill University)
M.Eng. (McMaster University)

SUPERVISOR: Professor John F. MacGregor

NUMBER OF PAGES: xiv, 309

ABSTRACT

This thesis presents new results in the research area of multiple input/multiple output (MIMO) controller design for chemical processes. The topics considered in this work are: robustness properties of linear MIMO controller designs; the design of approximate inverses for linear MIMO controllers; disturbance prediction in model predictive controller designs; and the development of a nonlinear inferential feedback control strategy for semi-batch copolymerization processes.

A review of robustness analysis procedures based on the use of norm bounded mismatch regions in the frequency domain is presented. These theories are considered for use in the assessment of the relative robustness trends of different MIMO Internal Model Controller designs. Based on these theories, three approaches to analyzing robustness properties are considered: the use of a condition number and singular value analysis on the approximate model inverse; singular value analysis assuming unstructured norm bounded uncertainty; and new procedure based on disk uncertainties in each element of the transfer function matrix that requires the use of structured singular value theory. The problems of conservatism with each approach as a result of unrealistic uncertainty characterizations is discussed, and new results are provided. The approaches are compared and evaluated with different MIMO Internal model controller designs. Compared to previously proposed procedures for relative robustness assessment, new proposed procedure based on disk uncertainties in each element of the transfer is shown to reduce conservatism in analyzing controller design robustness trends.

A general method for obtaining least squares optimal inverses for multivariable Internal Model Controllers (IMCs) is presented. An analytical solution is arrived at using a well known method for optimally factorizing discrete transfer function matrices. The procedure automatically handles unbalanced, noninvertible, and nonsquare systems, and provides controllers with excellent performance and robustness properties. These IMC designs are compared with some of the more traditional IMC designs where tunable diagonal filters are combined with fixed but usually suboptimal inverses. Robustness properties are investigated in simulated mismatch case studies, and with the robustness assessment procedures described above.

A general procedure is proposed for improving disturbance regulation in MIMO Dynamic Matrix Controllers (DMC). The method makes use of autoregressive, integrated moving average disturbance models to provide disturbance predictions, and requires only a simple modification to the DMC algorithm. The method proposed is far more computationally efficient and simple to apply relative to other procedures proposed. Examples are presented were the proposed modification leads to a substantial improvement in DMC disturbance regulation.

A strategy is proposed for estimating and controlling properties of styrene/butadiene rubber (SBR) latex produced in a semi-batch reactor. The nonlinear control strategy features a nonlinear state estimator, a nonlinear open-loop feedforward compensator, and a linear feedback controller to correct for errors in the feedforward control actions. In arriving at a nonlinear state estimator, three approaches, extended Kalman filtering, extended Kalman filtering with global reiteration, and a nonlinear optimization approach were considered. The second approach was found to be most effective and was therefore adopted. The importance of introducing sufficient meaningful nonstationary states is discussed in order to have biased-free state estimates when nonideal conditions exist. Using the knowledge of modelled chemical reaction mechanisms, open-loop feedforward actions are proposed based on establishing conditions for maintaining fixed instantaneous copolymer properties. These open-loop/feedforward policies establish quasi-steady state conditions on the instantaneous copolymer properties to be controlled. This allows for the application of simple feedback control strategies to correct for errors remaining after the open-loop/feedforward actions. The approaches considered for feedback controller design were conventional paired PI, a decoupling and linearizing multivariable transformation approach, and model-based optimal controller design. The second approach was found to be the most convenient for use in the nonlinear inferential feedback control scheme. The performance of the overall nonlinear inferential feedback design strategy proposed in this work is demonstrated to be robust to model mismatch, disturbances, and state initialization errors. In all cases investigated, copolymer property control is greatly improved over a fixed operating policy determined off-line. The proposed strategy is simple and effective alternative to computationally intensive on-line optimization procedures, and has the potential for greatly improving product reproducibility and quality control in polymer manufacturing industries.

ACKNOWLEDGEMENTS

I would like to thank my supervisor, Dr. John F. MacGregor, for his guidance and encouragement which made this project a truly enjoyable and stimulating experience.

I would also like to thank:

Dr. Thomas J. Harris for his assistance in the research related to Internal Model Controller design

Mr. Paul Gossen for being a great friend during some of the most miserable moments of my time spent working on this thesis.

TABLE OF CONTENTS

LIST OF FIGURES

LIST OF TABLES

THESIS INTRODUCTION

1 THESIS INTRODUCTION

The late seventies and early eighties represent an era in chemical process control research where a surge of interest has emerged in approaches to designing multiple input/multiple output (MIMO) feedback controllers. This has been due to both the significant increase in the availability of real-time computer systems, and the economic benefits gained through the application of feedback control to chemical process plants. Although much research has already been carried out in this area, there still remain important problems that need to be addressed. In this thesis, new results are presented in three basic areas of MIMO controller design research. These areas are: design and robustness of approximate inverses for linear MIMO controller design; disturbance prediction in future horizon, model predictive controller design; and nonlinear inferential feedback control for semi-batch polymerization reactors.

1.1 LINEAR MULTIVARIABLE CONTROLLER DESIGN: ROBUSTNESS AND APPROXIMATE INVERSES

A plethora of different optimal and suboptimal model-based MIMO controller design strategies can be found in the literature. However, only relatively few theories have been proven to be practical for use in chemical process plants. These strategies are usually based on input/output transfer function or impulse response type of linear models. These models are convenient for practical use since little effort is often required for an empirical identification relative to the effort usually required to develop detailed mechanistic dynamic models. Furthermore, for a vast range of continuously operating chemical plants, such as found in the petrochemical industries, these model types provide adequate dynamic response prediction when operating close to some optimal nominal condition.

The eighties also represent an era were there has been an increased awareness of the implication of model uncertainty with respect to the performance of time invariant linear MIMO designs. It is often not sufficient for a controller design to perform well at some identified nominal model operating condition. The linear MIMO input/output models traditionally used are low order and/or linearized approximations of the dynamic process behavior of a plant at some nominal operating condition. Changed operating conditions, large disturbances, or large set point changes to new a region of operation during implementation can introduce

significant errors in the dynamic response prediction provided by the linear MIMO model used to design the controller. It is well-known that the consequences of this could include seriously degraded performance and controller instability. Therefore, from a practical point of view, an effective MIMO controller design is one which best compromises nominal performance with robustness to model mismatch.

The problem of analyzing the robustness properties of MIMO controller designs is a very difficult one. The problem is somewhat open ended since any robustness analysis will require a description of the range of possible perturbations from the nominal process model. In most circumstances this information will be unknown, and therefore will have to approximated. Ideally, one would like to select a characterization for MIMO model mismatch that is physically meaningful and at the same time allows a mathematically tractable robustness analysis to be performed in order to avoid exhaustive model mismatch simulation studies. Unfortunately, no theory has yet been proposed where both of these objectives can be met in a straightforward manner.

In chapters two and three a review of different techniques that have been recently popularized for analyzing the robustness properties of MIMO controller designs is presented. The strategies to be investigated are based on independent, norm bounded mismatch regions in the frequency domain, and require the use of singular value (Doyle and Stein, 1981) and structured singular value theories (Doyle, 1982). The mismatch characterization used in these approaches is chosen mainly for mathematical convenience. Unfortunately, this class of uncertainty characterization lacks a clear physical interpretation relative to meaningful types of MIMO model parameter mismatch, and therefore can introduce conservatism into the analysis. Nevertheless, these theories may still be useful for predicting relative robustness trends between different MIMO controller designs. The objective will be to review and evaluate different approaches for predicting relative robustness trends of MIMO controller designs based on these theories. These procedures are used to evaluate the relative robustness properties of different Internal Model Controller designs in the work that follows. New results demonstrating the importance of the model mismatch characterization used in these theories to predict relative robustness trends of MIMO Internal Model Controllers shall be provided. In addition, a new and straightforward procedure for assessing the relative robustness trends of MIMO controllers is proposed. The new measure of relative robustness is based on a meaningful, single parameter disk uncertainty region in the frequency domain. The method leads to less conservatism in predicting relative robustness trends compared to other methods that have been previously proposed. The use of structured singular value theory (Doyle, 1982) is required.

One approach to MIMO controller design, based on linear input/output transfer function models, that has been advocated by a large number of researchers and practitioners has been the Internal Model Control (IMC) concept (Zames, 1979, 1981; Garcia and Morari, 1982, 1985a, 1985b). This concept has been demonstrated to simplify both the design and analysis of the feedback properties of MIMO controllers, and has been shown to posses favorable robustness properties. One stage in the IMC design procedure requires the specification of a stable and causal approximate model inverse. The purpose of the approximate model inverse is to compute realizable and stable input manipulations to cancel observed errors in the outputs from their set points in some optimal or suboptimal manner. A number of authors (Desoer and Chen, 1981; Holt and Morari, 1985a, b; Garcia and Morari, 1985a, b; Morari et al., 1987; Zafiriou and Morari, 1987) have considered the design of IMC inverses. The results of their work demonstrate that the design of these approximate inverses with desirable performance and robustness properties is far from trivial. Because of this, optimal design procedures were proposed only for special limiting cases. In chapter 4, a general and simple method for obtaining analytical expressions for integrated squared error, or linear quadratic optimal (LQ) IMC inverses for any form of linear multivariable input/ouput process model is proposed. The nominal performance and robustness properties of the LQ inverses will be demonstrated and compared to inverses obtained from the more traditional procedures in simulation case studies and with the robustness assessment procedures described above. The proposed design procedure will be shown to provide IMC controllers with excellent performance and robustness properties.

1.2 DISTURBANCE PREDICTION IN DYNAMIC MATRIX CONTROLLERS

Another MIMO controller design procedure that has been found to be very useful for chemical process control application is Dynamic Matrix Control (DMC) (Cutler and Ramaker, 1979). DMC is a finite future horizon, LQ approach to MIMO controller design that makes use of discrete convolution process models. The application of DMC requires that a prediction of the future disturbance trend be made at every control interval to compute feedback control actions. Since the objective in chemical process control is often regulatory, the performance of DMC can depend heavily on the assumptions made concerning the disturbances that enter the process. In the original formulation proposed by Cutler and Ramaker (1979), the assumption was made that the disturbance computed at the current control interval will remain constant over future predicted responses. A number of authors (Garcia and Prett, 1986; Li et al., 1989; Clarke et al., 1987) have reported that such an assumption can sometimes be very poor and seriously limit the performance of DMC. To address this problem.

Li et al. (1989) and Clarke et al. (1987) proposed major modifications to the future model prediction design strategy so that improved disturbance prediction can be carried out. Unfortunately, much of the simplicity and transparency of DMC becomes sacrificed when these modifications are used. In chapter 5, a new and general procedure based on autoregressive integrated moving average disturbance models is proposed for obtaining improved disturbance prediction in DMC. The proposed procedure for disturbance prediction is computationally efficient, and requires only a simple modification to the DMC algorithm. Examples where the proposed modification leads to substantial improved DMC regulation are demonstrated.

1.3 NONLINEAR INFERENTIAL FEEDBACK CONTROL FOR POLYMERIZATION REACTORS

The MIMO control design strategies described above are well suited for vast range of continuously operating chemical processes. However, there exist important types of chemical process control problems where these strategies will be inadequate for obtaining high performance control. Included in this important class of control problems is the control of semi-batch emulsion copolymerization reactions. These type of processes still pose an important challenge for the application of feedback control. Difficulties include significant nonlinearities, absence of steady state, inadequate dynamic models, lack of direct measurements of the properties needed to be controlled, and initial disturbance and/or model mismatch error which must be compensated for quickly during the finite period of batch/semi-batch operation. Relative to continuously operating chemical processes, the design of feedback control strategies for these systems have been studied to a far lesser extent. Much of the research in this area has been focused on the design of off-line, optimal open-loop operating policies. The usefulness of these policies in practice is very limited since no provisions are made to compensate for process variability, model uncertainty, and disturbances. In the polymer manufacturing industry, this problem is important since product reproducibility and copolymer property control are essential (Taylor, 1988).

In chapters 6 through 10, an inferential feedback control strategy is proposed for quality control of copolymer produced in semi-batch emulsion reactors. The production of industrially relevant styrene/butadiene rubber (SBR) copolymer is considered. For the first time, theories related to dynamic polymer modelling, nonlinear state estimation, optimal open-loop policies based on instantaneous copolymer property control, and feedback control are tied together to arrive at simple, yet effective production and

feedback control strategies for producing copolymer latexes meeting a wide range of property specifications. The approach proposed will provide a useful alternative to computationally intensive on-line nonlinear optimization approaches, which in many circumstances, will not be well-suited for industrial application.

The different stages of the development of the nonlinear inferential controller design strategy is divided into 5 chapters. Chapter 6 provides a more complete introduction to the semi-batch control problem addressed in this work. Chapter 7 presents the dynamic SBR reaction model used in this simulation study. Chapter 8 is concerned with the design and evaluation of useful nonlinear state estimators to infer copolymer properties using limited indirect measurement taken from the semi-batch process during operation. The development of practical open-loop operating policies for meeting a wide range of copolymer property specifications is discussed in chapter 9. Finally the design of feedback controllers for the semi-batch problem is covered in Chapter 10. Chapter 10 also ties together all the research from chapters 6 through 10, where the effectiveness of the proposed nonlinear inferential feedback control scheme under both ideal and nonideal simulated process operating conditions is demonstrated. In chapters 7 through 10, new research contributions are also made in the areas of polymer modelling, nonlinear state estimation, optimal open-loop operating policies for copolymer property control, and feedback controller design.

ROBUSTNESS OF LINEAR MIMO CONTROLLERS

2 ROBUSTNESS OF LINEAR MIMO CONTROLLERS

2.1 INTRODUCTION

Transfer function models used to design multiple input/multiple output (MIMO) controllers for chemical processes are almost always linear and/or low order approximations to the true process dynamics at some nominal operating region. Changes in plant operating conditions, large disturbances, or large set point changes can often introduce significant error in the dynamic response predictions provided by these models. Therefore, the usefulness of a time invariant, linear MIMO controller design for an application cannot be determined through nominal performance alone. In general, one would like to choose a design that provides the best compromise between nominal performance and stability to model mismatch. As pointed out by Doyle (1987) and Morari and Doyle (1986), a controller design which most effectively compromises between these properties will also exhibit superior performance at mismatch conditions.

This chapter provides a review of some frequency domain techniques that have been recently advocated by a large number of researchers for analyzing the robustness properties of MIMO controllers. Some of these approaches have been proposed as a useful alternative to extensive prior simulation with mismatch models since a necessary and sufficient condition for stability can be determined for a range of plant mismatch. Unfortunately, the range of plant mismatch is restricted to a special type of uncertainty characterization in the frequency domain which is chosen solely for mathematical convenience, and may be totally unrealistic relative to the true range of possible plants. Nevertheless, these theories may still be useful for predicting relative robustness trends for a class of closely related MIMO controller designs. The objective in this chapter will be to demonstrate straightforward uses of these theories for predicting relative robustness trends between different MIMO designs in some general sense. The important limitations of each method shall exposed in order for reader to appreciate the new results that follow. The procedures proposed will be compared in chapter 4, where the relative robustness of different Internal Model Controller designs will be examined in case studies. The work that follows in the next three chapters will provide new results demonstrating the importance of the assumed uncertainty characterization in assessing the relative robustness of different MIMO designs.

The sections that follow in this chapter will provide theoretical background on three different approaches to analyzing MIMO controller robustness. The first method is an adaptation of a well-known procedure used in numerical analysis whereby controller robustness is assessed through a singular value and condition number analysis on the approximate model inverse used in the design. The second approach makes use of a necessary and sufficient condition for MIMO controller stability based on a multiplicative, unstructured norm bounded uncertainty characterization (Doyle and Stein, 1981). The final method makes use of a frequency independent, norm bounded block diagonal mismatch characterization for robustness analysis, and requires the use of Structured Singular Value Theory (μ) (Doyle, 1982). Using this theory, a new index of relative robust stability assuming equal percentage disk uncertainties in each element of the transfer function matrix is proposed. This new index will be shown to provide a much more meaningful and less conservative assessment of relative robustness than the index used in the second approach.

2.2 PRELIMINARY DEFINITIONS

The theory in this chapter concerns the properties of MIMO linear feedback controller designs shown in Figure 2.1.

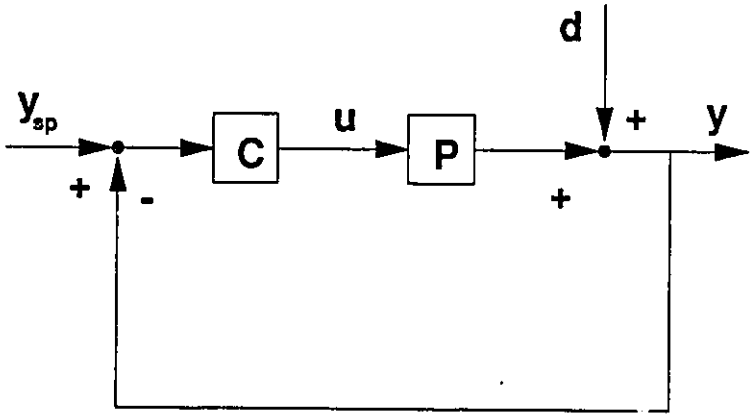

Figure 2.1: Standard MIMO Feedback Control Loop

In this figure, y is the output vector to be controlled, u is the vector of controlled inputs, y_{sp} is the set point vector, d is the disturbance vector, P is the true matrix process transfer function, and C is a fixed linear MIMO controller. The response of y to external inputs y_{sp} and d is given by

$$y = Ty_{sp} + Sd \tag{2.1}$$

where S, the sensitivity matrix operator, is defined by

$$S = (I+PC)^{-1} \tag{2.2}$$

and T, the complementary sensitivity matrix operator, is defined by

$$T = PC(I+PC)^{-1} \tag{2.3}$$

A controller design displaying good disturbance rejection will have an S approximately equal to zero in some norm sense across the entire frequency range or at frequencies where d is significant. Good set point tracking results when T is approximately equal to I across the entire frequency range or at the frequencies where set point changes are being made. Given a nominal process plant transfer function P_n, the nominal sensitivity operator (S_n) and the nominal complementary sensitivity operator (T_n) can similarly be defined as

$$S_n = (I+P_nC)^{-1} \tag{2.4}$$

$$T_n = P_nC(I+P_nC)^{-1} \tag{2.5}$$

In order to evaluate MIMO controller performance and the size of a matrix operator response to a bounded input at a specified frequency $s = i\omega$, an appropriate matrix norm is required. Unlike single input/ single output (SISO) systems, directionality exists with both the inputs and outputs in MIMO processes, and therefore upper and lower matrix norm bounds need to be defined. The most popular choice for an upper bound norm of a complex matrix A is given by the spectral norm

$$\sigma_M[A] = \max_{||x||=1} ||Ax|| = \sqrt{\lambda_{max}[A^*A]} \tag{2.6}$$

where $\sigma_M[A]$ denotes the maximum singular value of matrix A. $\lambda_{max}[A^*A]$ is the largest of the eigenvalues of A^*A that are all real and greater than or equal to 0. $||x||$ is the euclidean norm of x given by

$$||x|| = \sqrt{x^*x} \tag{2.7}$$

with A^* and x^* referring to conjugate complex transposition of A and x respectively. Similarly, a lower bound norm of matrix A is defined according to the minimum singular value $\sigma_m[A]$, given by

$$\sigma_m[A] = \min_{||x||=1} ||Ax|| = \sqrt{\lambda_{min}[A^*A]} \tag{2.8}$$

The physical interpretation of the spectral norm is discussed at great length by Postlethwaite et al. (1981). The deterministic interpretation of the maximum singular value is the maximum ratio of the sum of the energy

densities of the outputs to the sum of the energy densities of the inputs at frequency $s = i\omega$. In stochastic systems, the maximum singular value can be interpreted as the ratio of the sum of the power spectral densities of the outputs to the sum of the power spectral densities of the inputs at frequency $s = i\omega$.

2.3 SINGULAR VALUE ANALYSIS: CONDITIONING OF THE MODEL INVERSE

Singular Value Decomposition (SVD) is a technique commonly applied in numerical analysis for predicting the sensitivity of the solution of a set of linear equations in the form

$$Ax = b \tag{2.9}$$

to perturbations in A and b. This technique can be useful for inferring the frequency dependant closed-loop properties of a MIMO feedback controller design. Figure 2.2 shows a MIMO feedback loop with the true process response represented as

$$y = P_n u + \xi + d \tag{2.10}$$

where ξ is a vector representing stable model mismatch between P and P_n.

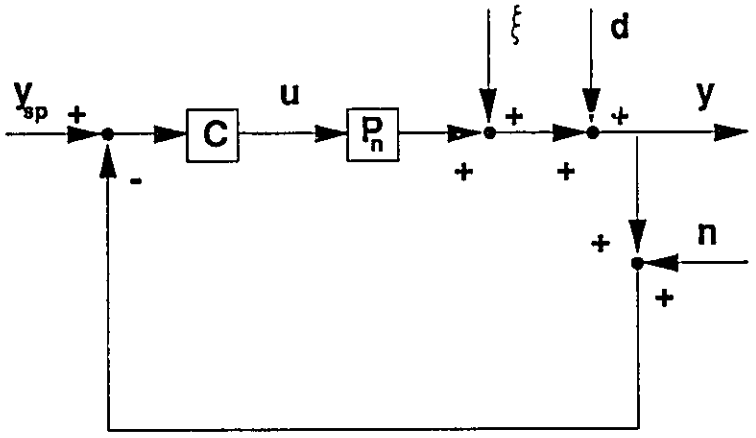

Figure 2.2: Feedback Loop With Model Mismatch And Sensor Noise

For any controller design C, the control manipulation u with respect to d, y_{sp}, mismatch ξ, and additive sensor noise n can be shown to be given by

$$Q^{-1}u = y_{sp} - d - \xi - n \tag{2.11}$$

Relative to (2.9), $A = Q^{-1}$ and $b = y_{sp} - d - \xi - n$. Q^{-1} is the approximation to the process model having a stable and causal inverse in the model reference transformation of Zames (1981) or Internal Model Controller (Garcia and Morari, 1985) (refer to chapter 4 for further details). Q is related to C and P_n through

$$Q = C(I + P_n C)^{-1} \tag{2.12}$$

The ultimate performance and robustness properties of C will depend on the frequency response characteristics of u with respect to y_{sp}, d, ξ, and n. Equation (2.11) shows that the frequency response of u will depend on Q^{-1}, and may be inferred from a frequency dependant SVD analysis on Q^{-1}. Practical considerations usually demand the following:

1) Set point changes and disturbances are typically low frequency inputs to the feedback control loop. Therefore, high performance demands exact model inversion in the low frequency range, which implies that the singular gains of Q^{-1} should be similar to P_n.
2) Large loop gains in the high frequency range can lead to excessive input manipulations, and generally poor performance when high frequency inputs such as n or ξ enter the feedback loop. High frequency loop gains are indicated by a small minimum singular gain of Q^{-1} in the high frequency range, and should be prevented when specifying C.
3) The sensitivity of the control actions as a function of frequency with respect to small changes in y_{sp}, d, ξ, and n will depend on the condition number of Q^{-1}, defined as the ratio of the maximum singular gain to the minimum singular gain of Q^{-1}. The sensitivity of u to model mismatch perturbations ξ is of particular importance since this provides an indication of the robustness of the controller design. The control actions will be very sensitive to these perturbations when the condition number of Q^{-1} is large. Usually process model predictions become more uncertain with increasing frequency, and therefore an effective design would be one with a relatively low condition number in the high frequency range.

The SVD analysis proposed above is a useful and simple technique for a preliminary analysis of the robustness and performance properties of a controller design. One limitation with the approach is the scale dependency of SVD, making the results of this procedure difficult to rely on from an absolute point of view. However, the results from this method may still be useful from the point of view of a relative analysis of different controllers designed for P_n. The usefulness of the results from this technique shall be demonstrated in chapter 4 for comparing different IMC designs.

2.4 ROBUST STABILITY

The multivariable generalization of the Nyquist stability criterion (Rosenbrock, 1974) requires that

$$det\{I+P(s)C(s)\} = 0 \tag{2.13}$$

have no zeros in the right half plane, or similarly,

$$det\{I+P(s)C(s)\} \neq 0 \tag{2.14}$$

for all real s. In an actual process environment, these conditions for stability must hold for a range of plants defined by

$$P(s) \in Region \quad \pi(s) \tag{2.15}$$

The sections to follow will describe a mathematically convenient representation for region $\pi(s)$ that will allow the Nyquist MIMO condition for stability, as stated above, to be nonconservatively applied to $\pi(s)$.

2.5 ROBUST STABILITY: UNSTRUCTURED UNCERTAINTY

An approach that has been recently popular for analyzing the robust stability of feedback controller designs to a range of plants is through the use of an SVD analysis on independent norm bounded perturbations in the frequency domain. Consider the situation where all the uncertainty is lumped into a single, multiplicative output perturbation block M_m, and the range of permissible plants is described by

$$P = (I+M_m)P_n \tag{2.16}$$

where M_m is a stable transfer function matrix belonging to the set $\sigma_M(M_m(i\omega)) < m_m(\omega)$. This type of uncertainty characterization may be used to represent modelling errors in P_n and output sensor error. Using the results of Doyle and Stein (1981), it can be shown that the necessary and sufficient condition for robust stability to the range of perturbations described above is

$$m_m(\omega) \leq \frac{1}{\sigma_M(T_n(i\omega))} \tag{2.17}$$

where T_n, the complementary sensitivity function of the nominal closed-loop system, is given by (2.5).

If a set of possible process transfer functions

$$P \in (P_1, P_2, \ldots, P_i, \ldots, P_p) \tag{2.18}$$

are available through some exhaustive identification study, the bound on $m_m(\omega)$ could be approximated through

$$m_m(\omega) = \max_i \sigma_M[(P_i(i\omega) - P_n(i\omega))P_n(i\omega)^{-1}] \tag{2.19}$$

and the stability condition (2.17) may be used to arrive at tuning parameters in a fixed controller. However, taking such an approach can lead to extreme conservatism in the selection of tuning parameters. Violation of (2.17) from the bound obtained by (2.19) does not imply that the MIMO controller will go unstable. It simply implies that in the set of matrices satisfying $m_m(\omega) < \sigma_M(M_m(i\omega))$ there exists a complex perturbation M_{m_j} that will make the feedback loop go unstable. If M_{m_j} does not correspond to some possible plant mismatch P_i, condition (2.17) is essentially meaningless. Investigations (e.g. McDonald (1987), Palazoglu (1987), McDonald and Palazoglu (1987), Mcdonald et al. (1988)) have shown that the regions of uncertainty mapped out by these complex norm bounded uncertainty descriptions at each frequency were highly conservative relative to the true range of plants encountered in their examples. The same result was also obtained by Bergh (1987) on a catalytic reactor example. An additional, and important source of conservatism that arises from norm bounded perturbation region analyses is the assumption of independence between the range of possible perturbations at different frequencies.

When model mismatch information is not available, a very simple approach for comparing the relative robust stability tolerances of different MIMO controller designs is to compute the frequency dependent upper bound on the allowable mismatch $m_m(\omega)$ from (2.17) for each design. However, when using this measure of relative robust stability tolerance, it is again very important to recognize the severe limitations imposed by the uncertainty region characterization. If condition (2.17) is to be used to address relative robustness, the best one can do is hope that, for a class of closely related controller designs, the relative robust stability trends will at least be captured. However, as will be illustrated in the work presented in chapter 4, such hope does not appear to be justified.

Stability conditions similar to (2.17) can be derived for other common forms of unstructured norm bounded complex perturbations in the frequency domain that enter at one point in the feedback loop. For example, the necessary and sufficient stability condition to additive mismatch of the form

$$P = P_n + M_a \tag{2.20}$$

with $m_a < \sigma_M(M_a)$ is given by

$$m_a \leq \frac{1}{\sigma_M(Q)} \tag{2.21}$$

The necessary and sufficient conditions for stability when only multiplicative input mismatch of the form

$$P = P_n(I + M_{m,i}) \tag{2.22}$$

with $m_{m,i} < \sigma_M(M_{m,i})$ is given by

$$m_{i,n} \leq \frac{1}{\sigma_M(CP_n(I + CP_n)^{-1})} \tag{2.23}$$

This type of uncertainty description may be useful when all the uncertainty exists in the actually implemented value for u. A more detailed discussion on the stability conditions of different types of unstructured norm bounded complex perturbations occurring at one point in the feedback loop can be found in Doyle et al. (1982).

2.6 ROBUST STABILITY: STRUCTURED NORM BOUNDED UNCERTAINTY

The robustness analysis of section 2.5 requires that mismatch between P and P_n be characterized through one block with an upper bound placed on its norm. Mismatch in a real process environment is a result of meaningful perturbations occurring at different locations in the process. When these important meaningful sources of perturbations become lumped into one perturbation block with some arbitrary upper bound placed on its size for mathematical convenience, much useful information about the structure of mismatch in the process becomes lost in the robustness analysis. This makes the robust stability requirement in section 2.5 conservative relative to the real problem on hand.

A currently popular approach to analyzing the robustness properties of MIMO feedback controller designs is through the use of Structured Singular Values (SSV) (Doyle, 1982; Doyle et al., 1982). The SSV approach allows for a nonconservative analysis of the robustness properties of controller designs to multiple independent complex norm bounded perturbations. SSV can be used to reduce conservatism relative to the previous method by allowing for more defined, and more meaningful, structured perturbations in the robustness analysis.

The work that follows will begin with an example to acquaint the reader with the recently developed theory behind norm bounded block diagonal perturbations and the use of SSV to nonconservatively analyze stability to this class of perturbations. The strength and weakness of this method for analyzing relative robustness properties of MIMO controllers shall be exposed in order for the reader to appreciate the work that follows. The aim in this work will be to use this theory to develop a more meaningful one parameter uncertainty characterization relative to the nominal model than the form used in section 2.5 simply for mathematical convenience to compare the relative robustness of different MIMO controller designs. Intuitively, an

uncertainty characterization having a more clear meaning relative to the nominal model should provide a less conservative assessment of relative robustness than a physically meaningless characterization chosen simply for mathematical convenience.

SSV or μ analysis will be introduced with a simple example where two independent, norm bounded perturbation blocks are present. Consider the situation where the permissible range of processes is characterized by

$$P(s) = (I + L_o(s)\Delta_o(s)R_o(s))P_n(s)(I + L_i(s)\Delta_i(s)R_i(s)) \tag{2.24}$$

where L_o, R_o, L_i, R_i, Δ_o, and Δ_i are stable transfer function matrices, $\sigma_M(\Delta_o) < 1$, and $\sigma_M(\Delta_i) < 1$. The block diagram for (2.24) is shown in Figure 2.3.

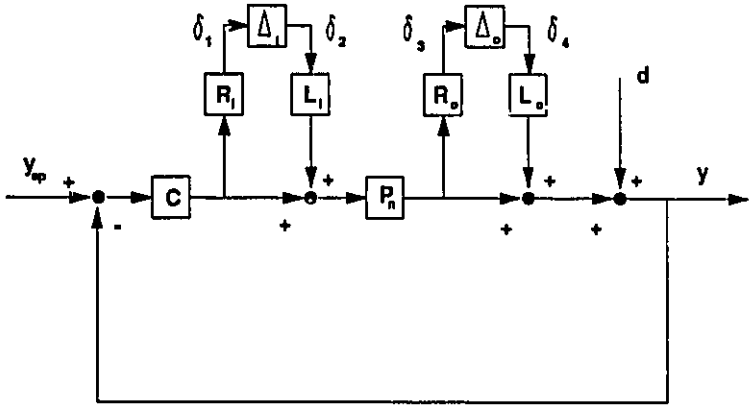

Figure 2.3: Feedback Loop With Unstructured Additive And Multiplicative Uncertainty

In (2.24) and in Figure 2.3, the presence of both unstructured multiplicative input and output mismatch has been assumed. The multiplicative input uncertainty and output uncertainty are given by $L_i(s)\Delta_i(s)R_i(s)$ and $L_o(s)\Delta_o(s)R_o(s)$ respectively. $L_i(s)$, $R_i(s)$, $L_o(s)$, and $R_o(s)$ are fixed weighting transfer function matrices for the uncertainty. These weights are suitably chosen to allow Δ_i and Δ_o at each frequency to independently take on any complex matrix value satisfying $\sigma_M(\Delta_i) < 1$ and $\sigma_M(\Delta_o) < 1$. The range of complex matrices Δ_o and Δ_i norm bounded by one defines the ranges of permissible plant perturbation through (2.24). The mismatch region characterization was chosen to make the robustness analysis mathematically tractable. Unfortunately, the mismatch region has no clear physical interpretation relative to parameter and order mismatch between matrix transfer functions.

The robustness analysis of section 2.5 is not well suited to analyze the robust stability of process (2.24) with a fixed C since two perturbation blocks, Δ_o and Δ_i, are present. To get around this problem, one might propose to transform the two perturbation uncertainty block into one equivalent uncertainty block. For instance, suppose the two block uncertainty structure is transformed into a one block multiplicative output uncertainty description as given below

$$P = (I + M_m)P_n \tag{2.25}$$

Equating (2.25) to (2.24) to solve for M_m leads to

$$M_m = [(I + L_o\Delta_o R_o)P_n(I + L_i\Delta_i R_i) - P_n]P_n^{-1} \tag{2.26}$$

To apply the necessary and sufficient condition for stability on (2.25) based on (2.17), a bound on the maximum singular value of M_m must be assigned to characterize the range of matrix perturbations that M_m can take on. This may be approximated through

$$\sigma_M(M_m) < \sup_{\Delta_i,\Delta_o} \sigma_M[((I + L_o\Delta_o R_o)P_n(I + L_i\Delta_i R_i) - P_n)P_n^{-1}] = m_m \tag{2.27}$$

with $\sigma_M(\Delta_o) < 1$ and $\sigma_M(\Delta_i) < 1$. However in doing so, conservatism is introduced since a single bound on $\sigma_M(M_m)$ will permit a larger range for M_m than (2.26) will allow when mapped out with the permissible Δ_o and Δ_i. In other words, the region

$$M_m \in [(I + L_o\Delta_o R_o)P_n(I + L_i\Delta_i R_i) - P_n]P_n^{-1} \mid \sigma_M(\Delta_o), \sigma_M(\Delta_i) < 1 \tag{2.28}$$

is a subset of

$$M_m \in \mathfrak{I}^{m\times m} \mid \sigma_M(M_m) < m_m \tag{2.29}$$

Therefore, through the transformation, one introduces more perturbations than actually exist, making the stability condition (2.17) only sufficient for the assumed true range of uncertainty described by (2.24). This is a limitation of the norm bounded, perturbation block approach, requiring that the theory be extended to multiple perturbation blocks with norm bounds in order for necessary and sufficient conditions to be derived.

The first step in the stability analysis of the feedback loop is the isolation of the norm bounded perturbations from the fixed elements in the feedback loop. This is done through the transformation of the feedback loop into an interconnection block diagonal structure (Doyle, 1982; Doyle et al., 1982). Returning to example (2.24), this is achieved by severing the feedback loop in Figure (2.3) at perturbation block Δ_i and Δ_o. Defining y, δ_1, δ_3, as loop outputs and y_{sp}, d, δ_2, and δ_4 as loop inputs, the following relationships may be derived:

$$y = T_n y_{sp} + S_n P_n L_i \delta_2 + S_n L_o \delta_4 + S_n d \tag{2.30}$$

$$\delta_1 = R_i C S_n y_{sp} - R_i C S_n P_n L_i \delta_2 - R_i C S_n L_o \delta_4 - R_i C S_n d \tag{2.31}$$

$$\delta_3 = R_o P_n C S_n y_{sp} + R_o P_n (I - C S_n P_n) L_i \delta_2 - R_o T_n L_o \delta_4 - R_o T_n d \tag{2.32}$$

Defining

$$\delta_o = \begin{bmatrix} \delta_1 \\ \delta_3 \end{bmatrix} \tag{2.33}$$

$$\delta_i = \begin{bmatrix} \delta_2 \\ \delta_4 \end{bmatrix} \tag{2.34}$$

and transforming (2.30) to (2.32) into matrix form leads to

$$\begin{bmatrix} y \\ \delta_o \end{bmatrix} = \begin{bmatrix} M_{1,1} & M_{1,2} & M_{1,3} \\ M_{2,1} & M_{2,2} & M_{2,3} \end{bmatrix} \begin{bmatrix} y_{sp} \\ d \\ \delta_i \end{bmatrix} \tag{2.35}$$

with

$$M_{1,1} = T_n \tag{2.36}$$

$$M_{1,2} = S_n \tag{2.37}$$

$$M_{1,3} = \begin{bmatrix} S_n P_n L_i & S_n L_o \end{bmatrix} \tag{2.38}$$

$$M_{2,1} = \begin{bmatrix} R_i C S_n \\ R_o P_n C S_n \end{bmatrix} \tag{2.39}$$

$$M_{2,2} = \begin{bmatrix} -R_i C S_n \\ -R_o T_n \end{bmatrix} \tag{2.40}$$

$$M_{2,3} = \begin{bmatrix} -R_i C S_n P_n L_i & -R_i C S_n L_o \\ R_o P_n (I - C S_n P_n) L_i & -R_o T_n L_o \end{bmatrix} \tag{2.41}$$

Using the relationship

$$\delta_i = \Delta \delta_o \tag{2.42}$$

with

$$\Delta = \begin{bmatrix} \Delta_i & 0 \\ 0 & \Delta_o \end{bmatrix} \tag{2.43}$$

(2.35) can be represented in the feedback diagram shown in Figure 2.4.

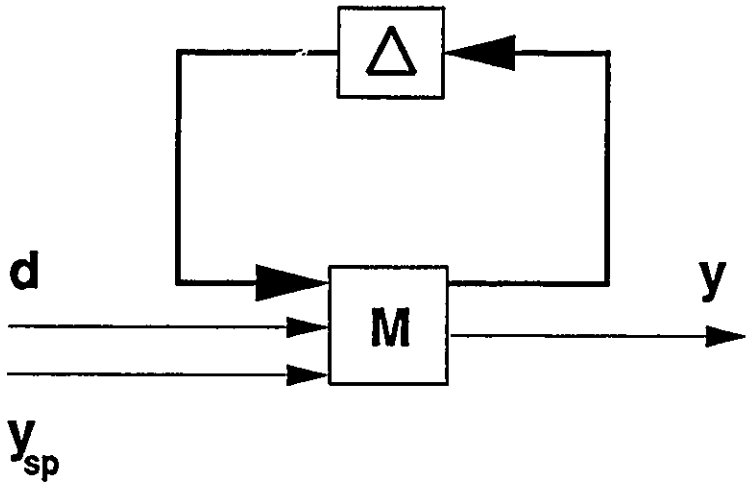

Figure 2.4: Interconnection Stucture For Multiple Perturbation Robustness Analysis

Figure 2.4 represents a general interconnection block diagonal perturbation feedback structure. The perturbation matrix is given by Δ and is block diagonal with respect to independent norm bounded matrix blocks Δ_j with $\sigma_M(\Delta_j) < 1$. The interconnection matrix M, as indicated in (2.35), is a fixed function of C, P_n, and perturbation weighting matrices $L_j(s)$ and $R_j(s)$. This transformation can be similarly performed on any feedback loop having any number of perturbation blocks and of different dimensions. Using equations (2.35), (2.42), and (2.43), the closed-loop response of y can be shown to be given as

$$y = M_{1,1}y_{sp} + M_{1,2}d + M_{1,3}\Delta(I - M_{2,3}\Delta)^{-1}M_{2,1}y_{sp} + M_{1,3}\Delta(I - M_{2,3}\Delta)^{-1}M_{2,2}d \tag{2.44}$$

Since M, Δ, y_{sp}, and d are all assumed to be stable, stability of y will only depend on the stability of $(I - M_{2,3}\Delta)^{-1}$. Stability of $(I - M_{2,3}\Delta)^{-1}$ is equivalent to the requirement that the loop shown in Figure 2.5 also be stable.

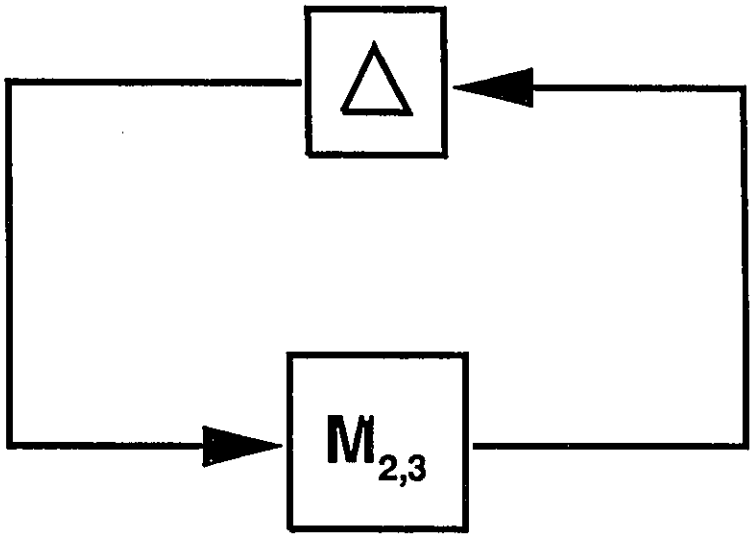

Figure 2.5: Interconnection Block Diagram For Robust Stability Analysis

At this point, the robustness analysis requires a necessary and sufficient condition for the stability of the feedback loop shown in Figure 2.5 with Δ block diagonal and each element norm bounded by 1. Unfortunately, arriving at such a condition is no simple matter. The only situation where a very simple solution for a nonconservative condition for robust stability can be derived is the case where Δ is full, containing only one perturbation block. In this case, the necessary and sufficient condition for robust stability with stable Δ and $M_{2,3}$ has been proven by Doyle (1987) to be

$$\sigma_M[M_{2,3}(i\omega)] \leq 1 \quad \forall \quad \omega \geq 0 \tag{2.45}$$

This stability condition can be used to derive the results shown in section 2.5 for the cases of a single unstructured norm bounded perturbation block, where the appropriate $M_{2,3}$ is chosen for the different locations of the perturbation block in the feedback loop. However, when Δ is not full, but rather block diagonal as a result of multiple perturbation blocks, condition (2.45) is only sufficient for robust stability. Therefore, the robustness analysis requires the introduction of a different norm, other than the maximum singular value, that leads to necessary and sufficient conditions for a nonconservative robustness analysis with norm bounded block diagonal perturbations. Doyle (1982) has derived the properties of this norm and called it the Structured Singular Value (SSV) or μ. The mathematical definition of μ as a function of a complex matrix A is given by

$$\mu(A) = \left\{ \begin{array}{c} 0 \quad \textit{if} \quad \textit{no} \quad \Delta \in \Delta^{\bullet} \quad \textit{solves} \quad \det\{I - A\Delta\} = 0 \\ \textit{or} \\ \dfrac{1}{\min\limits_{\Delta \in \Delta^{\bullet}} \sigma_M(\Delta) \quad \textit{satisfying} \quad \det\{I - A\Delta\} = 0} \end{array} \right\} \tag{2.46}$$

where Δ^* refers to the set of all block diagonal matrices of appropriate dimension in the problem with no limit on the upper norm of Δ_j (i.e. $\sigma_M(\Delta_j) < \infty$). The optimization problem posed in (2.46) to define μ is not convenient to apply to compute μ. Doyle (1982) has shown, using derived properties of μ, that a much more useful approach to estimating μ is through

$$\max_{U \in U^*} \rho(UA) \leq \mu(A) \leq \inf_{D \in D^*} \sigma_M(DAD^{-1}) \tag{2.47}$$

where U^* refers to the set of block diagonal unity matrices U with block structure of appropriate dimensions for Δ, D^* refers to the set of real block diagonal matrices D of the form

$$D = Diag\{d_1 I_1, d_2 I_2, \ldots, d_m I_m\} \tag{2.48}$$

where d_j are real positive scalars and I_j are unit matrices matching the dimensions of perturbation blocks Δ_j, and m refers to the number of perturbation blocks. The left hand side of the inequality (2.47) is always an equality but may involve multiple local maxima in the optimization problem. The right hand side of the inequality provides a tight upper bound for μ and can be shown to be convex with respect to D. Use of the right hand inequality is the recommended approach since the optimization problem is far more simple to solve. It has been reported (Doyle et al., 1982) that this approach leads to good results and does not introduce significant error for many cases tried.

Using the norm defined above, it can be shown (Doyle et al., 1982) that the necessary and sufficient conditions for robust stability to norm bounded perturbations with each block norm bounded by 1 is given by

$$\mu(M_{2,3}(i\omega)) \leq 1 \quad \forall \quad \omega \geq 0 \tag{2.49}$$

Condition (2.49) is referred to as the small μ theorem. This theorem is applicable to feedback control problems without any restriction on the number of diagonal perturbation blocks Δ_j and the dimension of each perturbation block. The only condition that needs to be satisfied is that both Δ and $M_{2,3}$ be stable, which frequently will be the case. The extension of this theory to the case of unstable perturbations is addressed by Foo and Postlethwaite (1988).

From a theoretical point of view, μ analysis offers a very elegant approach to the analysis of robust stability of MIMO feedback controllers. It is one of the very few theories capable of addressing stability of MIMO feedback loops to multiple perturbations in a nonconservative manner. Unfortunately, from a practical point of view, the theory can only be applied conservatively to real process control problems. The problem with the theory is the region of permissible complex matrix perturbations for Δ_j with an upper bound on its

norm arose from mathematical convenience rather than from engineering physical significance. As was previously stated in section 2.5, a range of matrix perturbations characterized with an upper bound on its norm is yet to manifest itself as a realistic characterization of the range of mismatch that really can occur in a real process control problem. To make this point more clear, consider the very simple example of a first order SISO process with transfer function

$$P(s) = \frac{k}{s+p} \tag{2.50}$$

Suppose error in both k and p are known to exist. Let us represent the true k and p relative to a nominal k_n and p_n as

$$k = (1+r_k\Delta_k)k_n \qquad \Delta_k \in \Re \qquad |\Delta_k| < 1 \tag{2.51}$$

$$p = (1+r_p\Delta_p)p_n \qquad \Delta_p \in \Re \qquad |\Delta_p| < 1 \tag{2.52}$$

where $r_k(\omega)$ and $r_p(\omega)$ are real frequency dependant weights. The true process response is given by

$$P(s) = (1+r_k\Delta_k)P_n\frac{1}{1+\frac{r_pP_n}{p_n+s}\Delta_p} \tag{2.53}$$

where

$$P_n = \frac{k_n}{p_n+s} \tag{2.54}$$

The block diagram for this process is given in Figure 2.6.

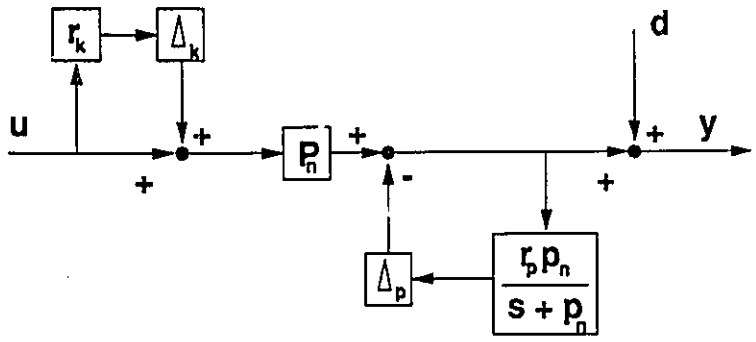

Figure 2.6: Gain And Lag Mismatch Representation In A SISO Process

Condition (2.49) will only lead to a sufficient condition for stability for the robustness stability analysis in this problem due to the fact that Δ_k and Δ_p can be complex in the μ analysis. This introduces more possible perturbations than really exists, and therefore conservatism in the analysis.

As mentioned in the introduction to this chapter, the aim of this work is to provide some meaningful measure of relative robust stability of different MIMO controllers, that will reduce some of the conservatism of the results shown in section 2.5. The problem with SSV analysis is that some meaningful structure for model mismatch perturbation must be proposed along with suitable perturbation weights $R_j(s)$ and $L_j(s)$ that are truly indicative of the magnitude of uncertainty as a function of frequency. In a typical process environment, much effort is usually required to arrive at a single nominal multivariable transfer function model. Such a model will often be obtained empirically, and provide little insight to proposing a suitable characterization for model mismatch. Even if one would propose a simple characterization for the mismatch in each element, such as ranges in gains, time constants, and delays in a first order structure, the number of perturbation blocks and the uncertainty information needed to be specified would become excessive for practical use. The amount of identification studies needed to gain sufficient information about the nature of the process mismatch would practically never be achievable. If such information were available, one would argue that this information would be better served in designing a superior nonlinear or adaptive feedback controller, rather than in the use of accessing the robustness of a fixed feedback controller. Nevertheless, the problem to be addressed in this work, is can a more meaningful single parameter MIMO uncertainty characterization in terms of P_* be proposed relative to section 2.5 to compare the robust stability of different MIMO controllers in some qualitative sense using μ theory. Intuitively, an uncertainty characterization with a more clearly defined physical interpretation relative to the nominal model should give a clearer and less conservative prediction of relative robustness than a characterization lacking any physical significance.

Kouvaritakis and Latchman (1985) proposed that an additive element-by-element disk uncertainty region at each frequency, centered on the nominal model Nyquist plot of each transfer function element be used to characterize MIMO mismatch regions. This corresponds to reducing the MIMO unstructured uncertainty problem to individual SISO unstructured uncertainty regions. This uncertainty characterization is shown in Figure 2.7 for element $P_{i,j}$.

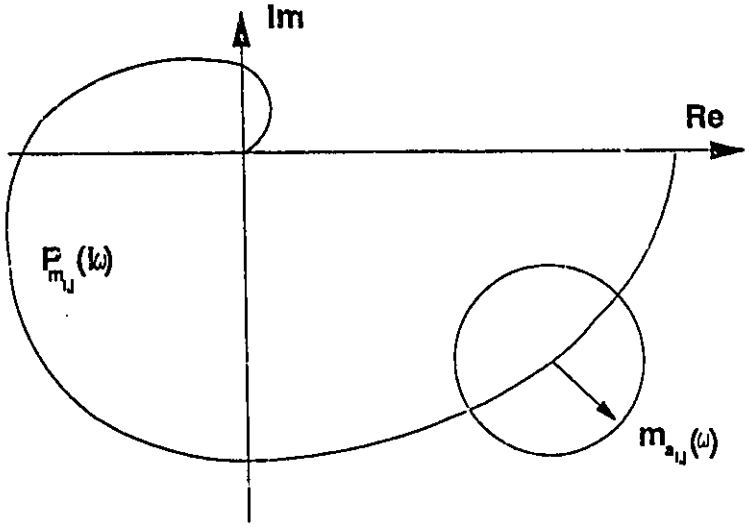

Figure 2.7: Disk Uncertainty Region For Transfer Function Element

The range of possible process responses is given by

$$P = P_n + M_a \tag{2.55}$$

with the frequency response of $M_{a_{i,j}}$ restricted to a disk given by

$$\left|M_{a_{i,j}}(i\omega)\right| = \left|P_{i,j}(i\omega) - P_{n_{i,j}}(i\omega)\right| < m_{a_{i,j}}(\omega) \tag{2.56}$$

The range of process plants contained within (2.56) will still be very conservative relative to possible types of mismatch that really can occur. Two important sources of conservatism are the restriction to a circular disk shape region at each frequency, and the assumption that mismatch points in a disk region at one frequency ω are totally uncorrelated with those in disk regions at other frequencies. Nevertheless, it is assumed that the introduction of more structure into the uncertainty description relative to the type used in section 2.5 will at least provide some reduction in the degree of conservatism, and therefore provide a better indication of the relative robustness trends of closely related controller designs.

The element-by-element uncertainty approach requires one to specify $m_{a_{i,j}}(\omega)$ bounds for each i and j element of M_a as a function of ω. With this information almost always absent, some reasonable assumption must be made. To address the relative robust stability tolerances of different controller designs, the assumption will be made that the size of the uncertainty disk in each element will be proportional to the norm of its corresponding nominal response at each frequency, that is

$$M_{a_{i,j}}(i\omega) = \kappa(\omega)\left|P_{n_{i,j}}(i\omega)\right|\Delta_{i,j}(\omega) \tag{2.57}$$

where $\kappa(\omega)$ (Kappa), is a positive real number at each frequency representing a multiplicative uncertainty factor for the nominal process response, and $\Delta_{i,j}$ is a norm bounded complex number satisfying $|\Delta_{i,j}(i\omega)| < 1$. The maximum $\kappa(\omega)$, or the amount by which the % disk uncertainty in all elements of P_n can be increased at each frequency before the closed-loop system goes unstable may be used as a general index of robustness. No claim is made that this uncertainty characterization will predict the true relative stability robustness of different controller designs. However, we believe that this Kappa uncertainty characterization will be much more reasonable than the very conservative condition of (2.17) for addressing this issue.

The computation of the maximum $\kappa(\omega)$ at each frequency that may be tolerated before the closed-loop system goes unstable will require a μ analysis for robust stability. The feedback loop with the additive element-by-element disk uncertainty has been derived by Skogestad and Morari (1987), and is shown in Figure 2.8, where

$$\Delta = Diag\{\Delta_{1,1}, \Delta_{2,1}, \ldots, \Delta_{n,1}, \Delta_{1,2}, \Delta_{2,2}, \ldots, \Delta_{n,2}, \ldots, \Delta_{n,n}\} \tag{2.58}$$

$$\Delta_{i,j} \in \mathfrak{I}^{1x1} \quad | \quad |\Delta_{i,j}| < 1 \tag{2.59}$$

$$L^{nxn^2} = [I_1^{nxn} | I_2^{nxn}| \quad \ldots\ldots \quad |I_n^{nxn}] \tag{2.60}$$

$$R^{n^2xn} = \begin{bmatrix} \underline{a}_1 & \underline{0} & \underline{0} & . & . & . & \underline{0} \\ \underline{0} & \underline{a}_2 & \underline{0} & . & . & . & \underline{0} \\ . & . & . & . & . & . & . \\ . & . & . & . & . & . & . \\ . & . & . & . & . & . & . \\ \underline{0} & \underline{0} & \underline{0} & . & . & . & \underline{a}_n \end{bmatrix} \tag{2.61}$$

$$\underline{a}_i = \begin{bmatrix} |P_{n_{1,i}}| \\ |P_{n_{2,i}}| \\ . \\ . \\ . \\ |P_{n_{n,i}}| \end{bmatrix}_{nx1} \tag{2.62}$$

$$\underline{0} = \begin{bmatrix} 0 \\ 0 \\ 0 \\ . \\ . \\ . \\ 0 \end{bmatrix}_{nx1} \tag{2.63}$$

R and L serve to transform the element-by-element disk uncertainty representation into a block diagonal structure and also to weight the perturbations as a function of frequency.

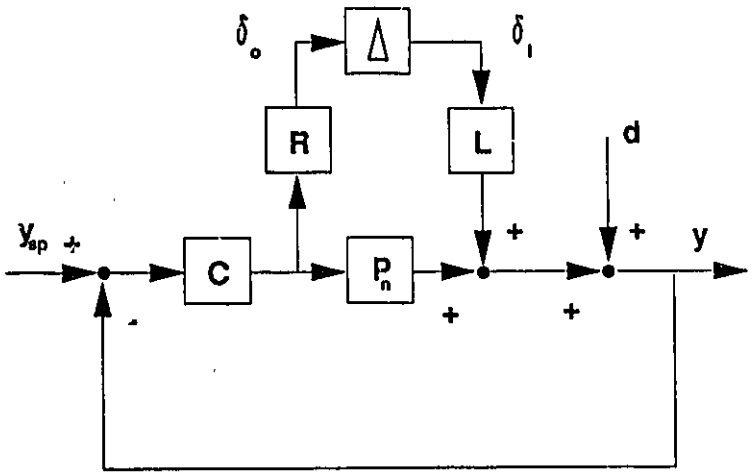

Figure 2.8: Additive Mismatch Uncertainty

In arriving at (2.62) $M_{a_{i,j}}(i\omega) = |P_{m_{i,j}}(i\omega)|\,\Delta_{i,j}$ has been assumed, and $\kappa(\omega)$ will be determined. The feedback loop in Figure 2.8 can be transformed into the block diagonal interconnection structure of Figure 2.4, where

$$\begin{bmatrix} y \\ \delta_{oi} \end{bmatrix} = M \begin{bmatrix} y_{sp} \\ d \\ \delta_i \end{bmatrix} \tag{2.64}$$

$$M = \begin{bmatrix} T_n & S_n & S_nL \\ RCS_n & -RCS_n & -RCS_nL \end{bmatrix} \tag{2.65}$$

Using the small μ theorem, the necessary and sufficient condition for robust stability to the type of uncertainty description above is given by

$$\kappa(\omega) \leq \frac{1}{\mu(M_{2,3}(i\omega))} \tag{2.66}$$

where

$$M_{2,3} = -RCS_aL \tag{2.67}$$

In the work that follows, the computation of $\mu(M_{2,3}(i\omega))$ is estimated from the upper bound of (2.47). The optimization was carried out using an unconstrained conjugate direction optimization routine.

In the work to follow, $\kappa(\omega)$ will be used to evaluate the relative robustness properties of different MIMO controller designs. It will be demonstrated that this new index, although still conservative relative to the real unknown mismatch problem, will provide better prediction of the relative robustness trends of different MIMO designs in some qualitative general sense relative to the stability condition presented in section 2.5.

2.7 SUMMARY

This chapter provided theoretical background on three different frequency domain approaches to analyzing robustness properties of MIMO controller designs. The objective of this chapter was to demonstrate the use of these methods for assessing relative robustness trends of different MIMO controller designs. The use of these procedures shall be demonstrated and compared in chapter 4, were the relative robustness trends of different Internal Model Controller designs will be examined.

The first relative robustness assessment strategy was based on a singular value and condition number analysis of the approximate model inverse used in the controller design. It was shown that controller designs having an approximate model inverse with a low condition number and high minimum singular gain at all frequencies will display good robustness properties. By comparing the minimum singular value and condition number of different MIMO designs, a general assessment of relative robustness can be carried out. The limitation with this procedure is the scale dependency of the analysis, making it very difficult to rely on for an absolute relative robustness assessment.

The second method of relative robustness assessment makes use of a singular value analysis on independent norm bounded perturbations in the frequency domain. If one assumes a single, unstructured multiplicative output perturbation block for the characterization of model mismatch, the results of Doyle and Stein (1981) can be used to a provide a necessary and sufficient condition for robust stability. The condition to be satisfied may be used as an index for assessing the relative robustness of different MIMO designs. The problem with this approach is that the uncertainty characterization lacks any physical interpretation relative to meaningful types of process model mismatch. The unrealistic nature of the uncertainty characterization may lead to conservatism when predicting relative robustness trends.

The final approach to robustness analysis described was based on an independent, norm bounded block diagonal perturbation mismatch characterization in the frequency domain, and requires the use of structured singular value theory (Doyle, 1982). By using this theory, a more meaningful and less conservative single parameter uncertainty characterization than the one used in the second method was proposed. The uncertainty characterization was based on equal percentage disk uncertainties in each element at every frequency relative to the nominal transfer function matrix. The amount by which the percent disk uncertainty radii in all elements of the model transfer function can be increased at each frequency and still maintain stability of the closed-loop system was proposed as a measure of robustness. This new measure of relative robustness ($\kappa(\omega)$) can be obtained through a structured singular value analysis. By plotting $\kappa(\omega)$ versus ω, the relative robustness of various controller designs can be compared. The uncertainty characterization used in this approach may still be very conservative relative to possible mismatch that really can occur in a control problem. However, the introduction of a more meaningful structure in the uncertainty description relative to one used in the second approach should provide some reduction in the degree of conservatism, and therefore provide a better indication of relative robustness trends of closely related controller designs.

2.8 NOTATION

A	complex square matrix
b	complex vector
C	multivariable feedback control block matrix transfer function
D	diagonal similarity scaling matrix
D^*	set of possible D matrices
d	disturbance input to feedback loop
e	output error from set point
i	square root of -1
I	unit matrix
k	first order gain in SISO process
k_n	nominal first order gain in SISO process
L	left perturbation weighting matrix for SSV analysis with equal percentage disk uncertainty in each MIMO transfer function element

L_i	left perturbation weighting matrix for unstructured input uncertainty
L_o	left perturbation weighting matrix for unstructured output uncertainty
m	number of perturbation blocks
m_a	upper bound index for stability with unstructured additive mismatch
m_m	maximum singular value of M_m
$m_{m,i}$	upper bound index for stability with unstructured multiplicative input mismatch
$m_{a_{i,j}}$	radius of disk uncertainty for element (i,j)
M	interconnection matrix for μ analysis
M_a	additive uncertainty matrix transfer function
M_m	multiplicative output perturbation transfer function matrix
n	additive output sensor noise
p	first order pole location in SISO process
p_n	nominal first order pole location in SISO process
P	true process matrix transfer function
P_i	mismatch matrix process transfer function model
P_n	nominal process matrix transfer function
Q	approximate model inverse in controller design
r_k	transfer function weighting for SISO gain error in μ analysis
r_p	transfer function weighting for first order SISO pole error in μ analysis
R	right perturbation weighting matrix for SSV analysis with equal percentage disk uncertainty in each MIMO transfer function element
R_i	right perturbation weighting transfer function matrix for unstructured multiplicative input uncertainty
R_o	right perturbation weighting transfer function matrix for unstructured multiplicative output uncertainty
s	Laplace transform operator
S	sensitivity matrix operator
T	complementary sensitivity matrix operator
T_n	nominal complementary sensitivity matrix operator

u manipulated process input vector

U unitary matrix

U^* set of unitary block diagonal matrices

x complex input vector

y process output vector

y_{sp} output set point vector

Greek Letters

δ_i input or output vectors from a block diagonal perturbation block

Δ stable block diagonal perturbation matrix

Δ_i unstructured multiplicative input perturbation block norm bounded by 1

Δ_o unstructured multiplicative output perturbation block norm bounded by 1

κ nominal model equal percentage element-by-element disk uncertainty tolerance

λ_{min} minimum real eigenvalue

λ_{max} maximum real eigenvalue

μ structured singular value

ξ additive output model mismatch

σ_m minimum singular value

σ_M maximum singular value

ω radian frequency

Mathematical Symbols

$\Im$ complex numbers

$\Re$ real numbers

H^2 VERSUS H^∞ CONTROLLER DESIGN: A REVIEW AND SOME COMMENTS

3 H^2 VERSUS H^∞ CONTROLLER DESIGN: A REVIEW AND SOME COMMENTS

A well-known approach to MIMO controller design is through the minimization of the Linear Quadratic (LQ) performance objective

$$\underset{C}{\text{Min}} \quad ||J||_2^2 \;=\; \underset{C}{\text{Min}} \quad \int_0^\infty (e^T Q_1 e \;+\; u^T Q_2 u)dt \tag{3.1}$$

where $e = y_{sp} - y$, and Q_1 and Q_2 are positive-semidefinite weighting matrices. Other forms of (3.1) are also possible, such as a penalty on the velocity of the input movements instead of about some mean value. The correct form of the input penalty weights to obtain no offset control depends on the process, and the nature of the disturbance or set point change transfer function. Using Parseval's theorem, equation (3.1) for an optimal regulation can be expressed in the frequency domain as

$$\underset{C}{\text{Min}} \quad ||J||_2^2 \;=\; \underset{C}{\text{Min}} \quad \frac{1}{2\pi}\int_{-\infty}^{\infty} Trace\left[(S_n D_n d)^* Q_1 (S_n D_n d) \;+\; (P_n^{-1} T_n D_n d)^* Q_2 (P_n^{-1} T_n D_n d)\right] \; d\omega \tag{3.2}$$

where P_n is the nominal plant model, D_n is the nominal disturbance transfer function, S_n is the sensitivity matrix operator, T_n is the complementary matrix operator, and * refers to conjugate complex matrix transposition. The solution for a specified P_n and D_n is well-known and simple to arrive at. The result can be found in Johnson and Grimble (1987), Youla et al. (1976) for the continuous time case, Kozub (1986), Kozub et al. (1987), Harris and MacGregor (1987), and Wilson (1970) for the discrete time control problem.

The minimization problem posed in (3.2) demonstrates that the LQ-optimal C is the design that leads to the best compromise of weighted errors and disturbances across the entire frequency domain in a 2-norm sense for the specified P_n and D_n. The problem with this method is that the solution is limited to only one specified P_n and D_n, and does not extend to a range of plants and disturbances that might exist in a real process environment. If a range of plants exists, a brute force formal or informal optimization needs to be carried out to find P_n, D_n, and the set of tuning weights Q_1 and Q_2 that provides the best performance for all possible plants. Because of this, some researchers (Morari and Doyle, 1986; Zames, 1981; Kwakernaak, 1985) have argued that the LQ approach to MIMO controller design is not practically suited for real process control

problems. Nevertheless, the harsh criticism directed toward LQ design is surprising given that so much success has been reported in a wide range of industrial applications with LQ approaches such as Dynamic Matrix Control (DMC) (Cutler and Ramaker, 1979).

One of the most remarkable properties of μ analysis that was presented in the previous chapter is that this theory can be extended to allow both a specified performance and a stability requirement for a range of plants to be addressed simultaneously (Doyle et al. 1982; Doyle 1987). Consider the block diagram interconnection structure shown in Figure 3.1.

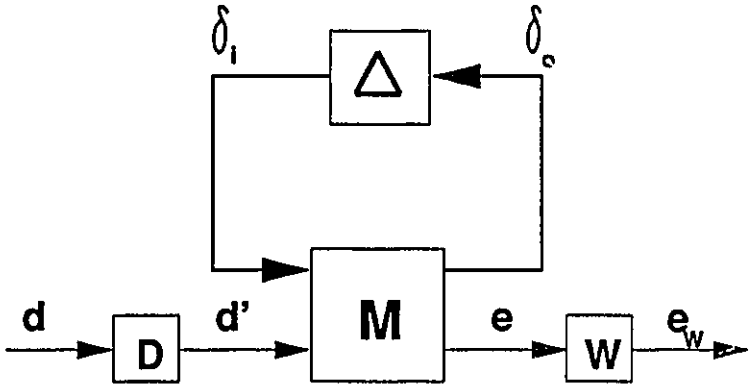

Figure 3.1: Interconnection Sturcture For Robust Stability Analysis

D is the disturbance transfer function or disturbance weight and W is a specified performance weighting transfer function for the output errors. For simplicity, let us assume that the MIMO controller design will be designed specifically for disturbance rejection. The theory that follows extends easily to handle set point change characteristics as well. For the block diagram in Figure 3.1

$$\begin{bmatrix} y \\ \delta_o \end{bmatrix} = M \begin{bmatrix} d' \\ \delta_i \end{bmatrix} \tag{3.3}$$

where

$$M = \begin{bmatrix} M_{1,1} & M_{1,2} \\ M_{2,1} & M_{2,2} \end{bmatrix} \tag{3.4}$$

The response of the weighted errors e_w to d is given by

$$y = [WSD]d \tag{3.5}$$

where

$$S = M_{1,1} + M_{1,2}\Delta(I + M_{2,2}\Delta)^{-1}M_{2,1} \tag{3.6}$$

As an alternative to the LQ performance objective (3.2), suppose that the performance requirement is specified as

$$\underset{\|d\|_2=1}{\text{Max}} \; \|WSDd\|_2 \;=\; \sigma_M(WSD) \;\leq\; 1 \qquad \forall \;\; \omega \geq 0 \tag{3.7}$$

Condition (3.7) represents an ∞-norm performance or robust performance specification to be met by controller design C for all the permissible plants described through the block diagonal norm bounded perturbation structure in Figure 3.1. The performance index requires the specification of a frequency dependant disturbance D and an output performance weight W. D is obtained from some knowledge of the frequency response of disturbances entering the loop or from identified disturbance transfer functions. W is the specified performance weight on e or y from input d. Typically, W will be small in magnitude in the high frequency range were high performance is not demanded and to prevent excessive high frequency input manipulations. At low frequencies, were disturbances usually predominate, W is specified to be large to lead to a design possessing good disturbance rejection. At zero frequency W typically would be set to infinity to ensure integral action in the controller design. Once D and W are specified, tuning parameters p in some standard controller design, such as for example proportional gains, reset times, and derivative terms in PID controllers, are determined so that condition (3.7) is met, if possible. If tuning parameters in a controller design cannot be found so that (3.7) is satisfied some adjustment is made to W to relax the performance specification. Alternatively, an ∞-norm optimal controller design can be carried out (Doyle,1987).

The robust performance specification (3.7) for ranges of plants described through block diagonal norm bounded perturbations can be incorporated in the μ analysis framework. It can be shown (Doyle et al., 1982; Doyle, 1987) that condition (3.7) will be satisfied if and only if

$$det\{I + WSD\Delta_p\} \;\neq\; 0 \qquad \forall \qquad Re(s) > 0 \tag{3.8}$$

where Δ_p, a pseudo perturbation performance block, is a stable transfer function matrix satisfying $\sigma_M(\Delta_p(s)) < 1$. Condition (3.8) implies that the performance index (3.7) can be expressed as an additional robust stability requirement on $(I + WSD\Delta_p)^{-1}$. The added stability requirement can be represented by the addition of an extra feedback loop, as shown in Figure 3.2.

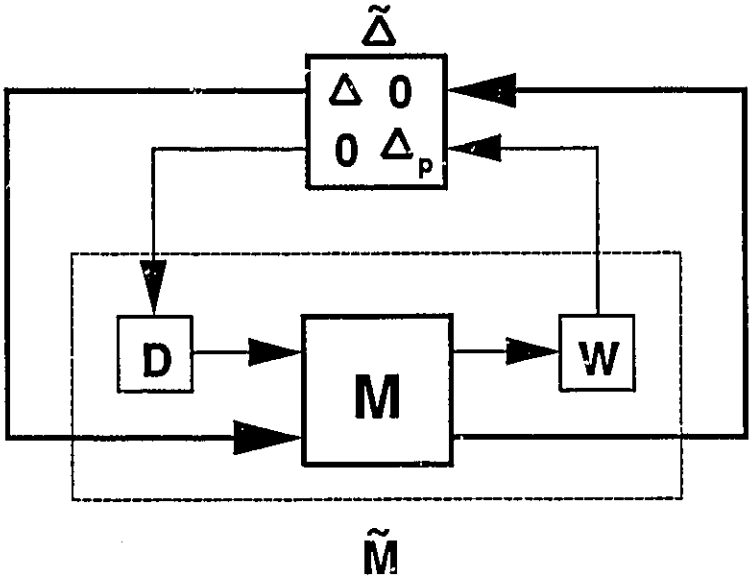

Figure 3.2: Transformation Of Performance Specification Into Stability Analysis

In Figure 3.2, Δ_p can be combined with Δ as an extra diagonal block in $\tilde{\Delta}$. The fixed performance weights, D and W, can be combined in M to form $\tilde{M}$. The transformation leads to Figure 3.3.

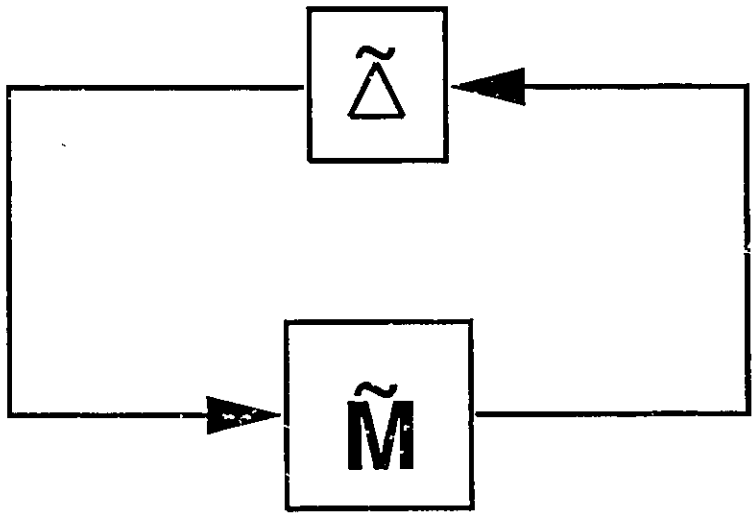

Figure 3.3: Robust Performance Interconnection Block Structure

With this transformation, the robust performance specification (3.7) together with robust stability will be satisfied if and only if

$$\mu(\tilde{M}(i\omega)) \leq 1 \qquad \forall \qquad \omega \geq 0 \tag{3.9}$$

Therefore, from (3.9), tuning parameters in some standard controller design should be selected so that $||\mu(\tilde{M}(i\omega))||_\infty$ is minimized and (3.9) is satisfied. Alternatively, a μ-optimal controller design procedure can be carried out (Doyle, 1987).

At first glance, it would appear that this strategy offers a significant improvement over the LQ approach because a range of plants can be considered in a formal manner in the performance specification to arrive at tuning parameters in some controller design. It would also appear that this method would offer a nice formal procedure to arrive at tuning weights in the LQ controller design earlier described. However, there are serious weaknesses when taking this formal approach to designing controllers. These weaknesses are listed below:

1) The frequency domain objective function (3.7) has no physically meaningful time domain interpretation as does LQ, and is not uniquely related to any particular time domain response.

2) The design requires the specification of a frequency dependant performance weighting matrix $W(s)$. The selection of an appropriate $W(s)$ for a particular control problem is by no means intuitive, mainly because (3.7) lacks a precise time domain interpretation, and virtually no useful guidelines have been proposed. The consequence of a poor guess for $W(s)$ simply to make a physically meaningless index $\mu < 1$ could lead to an overly conservative controller design.

3) In order for the μ methodology to provide a significant improvement over the standard LQ procedure it is necessary that the true range of plants be accurately known and nonconservatively represented through independent norm bounded complex perturbations. A physically meaningful example where this requirement is satisfied is yet to be demonstrated. This issue is of extreme importance due to the ∞-norm performance specification, which is focused on the worst case across the frequency domain. If the worst case results from a perturbation that does not exist in the real process because of a conservative mismatch characterization, the controller design will also be conservative, requiring more detuning than necessary.

4) In a real process environment uncertainty information will never be accurate and likely very difficult to obtain. Therefore, extreme effort made to satisfy (3.7) with questionable mismatch information is questionable.

5) Performance index (3.7) assumes that vector d can take on any complex value such that $||d|| \leq 1$. From the point of view of performance, this is a very conservative range of inputs since in the performance analysis one is usually concerned with complex inputs of the form $u \quad e^{i}$. Therefore, a much larger range of input d are considered than are physically meaningful, introducing conservatism in the design.

6) The H^{∞} design criterion finds the optimal feedback controller for the worst case disturbance at some frequency entering into the process. The worst case may corresponds to an unimportant or infrequent disturbance that may or may not be worthy of consideration. Because this design does not compromise between disturbances at all frequencies, performance of the controller to disturbances that may be more important at other frequencies could be severely degraded as a result of the worst case point.

The problems stated above essentially render the μ robust performance approach inadequate for addressing real world control problems in a straightforward and nonconservative manner. The main obstacle with this approach is that the origins of this theory can be found in the domain of applied mathematics rather than from a practically posed engineering problem. For the sake of mathematical convenience, the approach enforces specific types of uncertainty and performance specifications which are meaningless and not natural for an application engineer to work with in a real world control problem. A more logical procedure for meeting robust performance requirements in some sense would be to work with a meaningful time domain performance criterion, such as ISE or IAE, for a range of plants with a more natural and nonconservative mismatch region characterization for chemical process control problems. It is not known if any useful theory can be developed to meet this goal, but it can at least be stated, that a far greater effort needs to be made in finding more meaningful uncertainty characterizations for nonconservatively analyzing MIMO controller design robustness.

The chapter that follows will examine robustness properties of LQ controller designs in an Internal Model Control (IMC) framework. It will be demonstrated that the LQ procedure can be used to arrive at robust controller designs even though the procedure, at this point in time, lacks any formalism in addressing the robustness issue in a nonconservative manner.

3.1 NOTATION

C	controller transfer function matrix
d	disturbance vector
d'	additive effect of disturbance response on output vector
D_n	disturbance transfer function matrix
e	output error vector
e_w	weighted output error vector
H^2	2 norm
H^∞	infinity norm
J	quadratic performance index
M	interconnection matrix for structured singular value analysis
$\tilde{M}$	interconnection matrix for robust performance analysis
P	true process linear transfer function
Q_1	output error weighting matrix
Q_2	input weighting matrix
S	sensitivity matrix operator
S_n	nominal sensitivity matrix operator
t	time
T_n	complementary sensitivity matrix operator
u	manipulated input vector
W	output error weighting in H^∞ design procedure
y	output vector
y_{sp}	output set point vector

Greek Letters

δ_i	input vector from block diagonal perturbation block
δ_o	output vector from block diagonal perturbation block
Δ	stable block diagonal perturbation transfer function matrix
$\tilde{\Delta}$	block diagonal perturbation block for robust performance analysis
Δ_p	pseudo performance perturbation block
σ_M	maximum singular value
ω	radian frequency

OPTIMAL IMC INVERSES: DESIGN AND ROBUSTNESS CONSIDERATIONS

4 OPTIMAL IMC INVERSES: DESIGN AND ROBUSTNESS CONSIDERATIONS

4.1 INTRODUCTION

The Internal Model Controller (IMC) structure in Figure 4.1 has been advocated recently as a very useful structure for both the analysis and design of multivariable controllers.

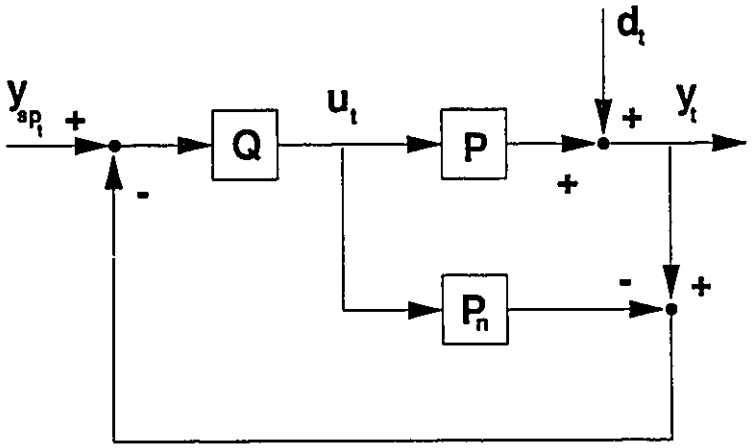

Figure 4.1: Internal Model Controller Block Diagram

In this structure the conventional feedback controller is decomposed into a model prediction block (P_n), and a controller or approximate model inverse block (Q). For a perfect model ($P_n = P$) the closed-loop system is equivalent to the open-loop system given by

$$y = P_n Q(y_{sp} - d) + d \tag{4.1}$$

The benefits of this decomposition into meaningful blocks are that stability and the prevention of steady state offset are both guaranteed for a stable nominal plant (P_n) by simply choosing a stable inverse block (Q) with a gain equal to the inverse gain of P_n. Furthermore, the design of multivariable controllers by directly choosing such a Q is generally much more direct and intuitively more appealing than the design of a feedback controller in the conventional form.

The main theory behind the multivariable IMC structure was laid out by Zames (1979, 1981) who referred to this structure as the model reference transformation. However, because of his use of the symbol Q for the controller block, this form became generally known in the control literature as Q-parameterization. Brosilow (1979) and Garcia and Morari (1982, 1985a, b) were largely responsible for bringing this structure to the attention of the chemical process control community, and the latter authors coined the term "Internal Model Control" to describe it. Since all model-based controllers can be expressed in the IMC structure, it is to be expected that IMC design procedures are closely related to other commonly used designs such as Linear-Quadratic (LQ) control using transfer functions (Harris and MacGregor, 1987), Dynamic Matrix Control (DMC) (Cutler and Ramaker, 1979), Model Algorithmic Control (Richalet et al. 1978; Rouhani and Mehra, 1982) and Inferential Control (Brosilow, 1979).

The design of multivariable IMC controllers requires a procedure for choosing the control block Q. As can be seen from the closed-loop control equation (4.1), perfect control could theoretically be accomplished by choosing Q to be inverse of the process plant model (P_s^{-1}). However, such a controller may not be realizable in practice since it may contain predictive terms, will not be stable if the plant contains RHP zeros, and will lack robustness if the model is not a perfect representation of the plant (P). Therefore, the choice of the controller Q can be viewed as the choice of an approximate model inverse which is stable and causal, and which will provide a good compromise between performance and robustness under most conditions of plant operation. A number of authors (Desoer and Chen, 1981; Holt and Morari, 1985a, b; Garcia and Morari, 1985a, b; Morari et al., 1987; Zafiriou and Morari, 1987) have considered the design of these multivariable controllers. The results of their work demonstrate, in the general case, that the design of an approximate model inverse (Q) with desirable performance and robustness properties is not trivial.

The first objective of this section is to present a general and simple method for obtaining analytical expressions for integrated square error (ISE) or LQ optimal IMC inverses for any form of linear multivariable process model. The process may be of arbitrary complexity including unbalanced time delay structures, noninvertible transfer functions, and nonsquare systems. The method will not only allow one to design stable, causal inverses leading to optimal output performance, but will also allow one to trade off performance, the cost of input manipulations, and robustness in a straightforward manner. The approach requires one to specify a transfer function or impulse response model relating measured or inferred outputs to the process inputs. The solution is directly arrived at using well known, computationally efficient and simple methods for optimally factorizing polynomial matrices into invertible and noninvertible elements.

The second objective of this work is to demonstrate some fundamental differences in the properties of IMC designs obtained by different approaches to selecting the controller Q. To investigate the robustness of the controllers to modelling errors, the designs are analyzed using several methods: (i) examining the conditioning of the invertible model approximation (Q^{-1}) using singular values and condition numbers; (ii) performing a singular value analysis on the closed-loop system assuming unstructured norm bounded uncertainty (Doyle and Stein, 1981); (iii) performing a structured singular value analysis (Doyle, 1982; Skogestad and Morari, 1987) on the closed-loop system assuming equal percentage disk uncertainties in each element of the transfer function matrix; and (iv) performing simulation studies on two processes (a catalytic reactor and a distillation column) for which some actual model uncertainties have been identified experimentally.

4.2 INTERNAL MODEL CONTROLLER DESIGN

The block diagram of the IMC or Q-parameterization structure is given in Figure 4.1, where P represents the true process, P_n the nominal model of the process, and Q the controller. Consider the following discrete right matrix fraction representation of the multivariable process (Harris and MacGregor, 1987)

$$P_n(z^{-1}) = L(z^{-1})[R(z^{-1})]^{-1} \tag{4.2}$$

where $L(z^{-1})$ is a matrix polynomial and $R(z^{-1})$ is a diagonal matrix polynomial in the backward shift operator z^{-1}. We shall restrict ourselves to open-loop stable processes.

There are infinitely many ways of designing the IMC controller Q for the model in (4.2). The only restrictions are that Q be stable and causal (i.e. contain no predictive elements). An optimization approach can be used whereby some index of nominal performance, or some measure of robustness to a class of uncertainties can be optimized. Alternatively, various pole placement or decoupling approaches can be used. Desoer and Chen (1981), employing the latter approach, presented an algorithm for designing Q which yields a decoupled closed-loop system in which all the poles can be chosen by the designer as well as the zeros (except of course the noninvertible zeros which must appear in the closed-loop response). They presented some examples and discussed the limitations imposed by plant dynamics, uncertainties, and noise.

Garcia and Morari (1985a, b), extending their univariate approach (1982), considered a convenient two-stage design whereby they factored Q into two components

$$Q = \tilde{P}_s^{-1}F \tag{4.3}$$

where $\tilde{P}_s^{-1}$ is an approximate model inverse and F is a unit gain tunable filter. The approximate model inverse was taken as

$$\tilde{P}_s^{-1} = P_s^{-1}V \tag{4.4}$$

where P_s^{-1} is the exact model inverse, and V is a polynomial matrix selected to eliminate predictive elements that result from model inversion and replace unstable or ringing zeros in the process model. A very simple method for designing a diagonal V was presented which leads to a decoupled closed-loop response. This decoupled closed-loop IMC design provides an optimal integrated mean square error (ISE) inverse for step disturbances and set point changes if the process model is balanced with respect to time delays and contains no noninvertible zeros. A multivariable process is said to be balanced with respect to time delays if it is possible to manipulate the columns and rows of the process model transfer function such that the minimum delay in each row appears on the diagonal. A process with the same number of inputs and outputs is said to be invertible if the determinant $|L|$ has no finite zeros outside the unit circle in the z-plane. If either of these conditions is not met, the decoupled IMC design procedure will be suboptimal with respect to the ISE criterion. Holt and Morari (1985a, b) have pointed out that in these latter situations ISE optimality requires some interaction in the closed-loop response. Unfortunately, they also showed that the specification of an optimal V is not straightforward. They presented solutions to the inverse only in the limiting case where the weighting in the ISE criterion is placed on all but one output. Zafiriou and Morari (1987) outline a geometric control theory approach for obtaining V for a specified nominal output response and provide a solution for permissible V's leading to a stable and causal Q's for a class of square multivariable processes. To evaluate the performance of inverses these authors also used an ISE output criterion. In this paper we present a general solution to the problem of the optimal inverse design which includes some of the above solutions as special limiting cases.

The proposed choice for the filter block was a diagonal (decoupled) first order exponential filter

$$F = Diag\left\{\frac{1-f_{i,i}}{1-f_{i,i}z^{-1}}\right\} \tag{4.5}$$

where each filter parameter lies in the range $0 \leq f_{i,i} < 1$. When P and P_n are not equal, closed-loop stability cannot be guaranteed for the design with the nominal model. The filter factors are then determined to provide the necessary degree of robustness to model mismatch, and can be conveniently tuned on-line. Increasing the filter factors directly reduces the bandwidth of the complementary sensitivity function $P_n Q$ and improves the robustness of the controller design (Morari and Doyle, 1986). When the filter block (4.5) is combined with a realizable and decoupled approximation of the approximate inverse (4.4), this IMC design can be shown to be the multiple input/multiple output (MIMO) extension of Dahlin's algorithm (1968). The filter factors can be used in a Dahlin sense to adjust the first order time constants of the nominal closed-loop output responses. In this sense the design is also equivalent to that of Desoer and Chen (1981), although conceptually the closed-loop poles $f_{i,i}$ are arrived at from robustness considerations.

4.3 LQ OPTIMAL INVERSE DESIGN

The design of optimal IMC inverses for multivariable systems requires a general design procedure. A trial and error approach of guessing different forms for V until a satisfactory result is realized becomes unmanageable with complicated systems, especially if the process is not invertible nor balanced with respect to time delays. In addition, even if one can find an optimal $\tilde{P}_n^{-1}$ by simple reasoning, it may lead to unacceptable input performance and poor robustness properties.

Garcia and Morari (1985b) suggested that one approach to this problem is to transform it into a future finite horizon, model predictive, linear quadratic (LQ) optimization problem. Such algorithms, for example DMC (Cutler and Ramaker, 1979), have been used extensively in industry. This method yields a very practical and easily implemented solution to the finite horizon LQ problem. However, it does not provide an analytical expression for Q that can be used for analysis of the feedback properties of the controller. The objective of this section is to present a simple and general design procedure for directly obtaining analytical LQ optimal IMC designs for Q. DMC will yield the identical solution to this procedure if both the input and output horizons used in DMC are made large.

The following quadratic performance index will be used for the design of general IMC inverses

$$J = \lim_{N \to \infty} \frac{1}{N} E\left\{ \sum_{i=1}^{N} e_i^T Q_1 e_i + \nabla u_i^T Q_2 \nabla u_i \right\} \tag{4.6}$$

where Q_1 and Q_2 are positive semi-definite weighting matrices, $e_t = y_{sp_t} - y_t$, $\nabla = 1 - z^{-1}$, and E is the expectation operator. In (4.6) we incorporate a penalty on the sum of squares of the velocity of input manipulations to provide a compromise between output performance and the severity of the input manipulations.

The solution which minimizes the quadratic index (4.6) for the classical case of step disturbances and set point changes with the process model (4.2) can be obtained directly from the spectral factorization solution of the Wiener-Hopf equation (Harris and MacGregor, 1987), and is given by

$$Q = \bar{P}_n^{-1} = R\Gamma^{-1} \tag{4.7}$$

Γ is an (nxn) polynomial matrix obtained as the unique invertible and causal solution to the spectral factorization equation

$$\Gamma^* Q_1 \Gamma = L^* Q_1 L + R^* \nabla^* Q_2 \nabla R \tag{4.8}$$

where Γ^* denotes the complex conjugate transpose of $\Gamma(z^{-1})$ (i.e. $\Gamma^T(z)$). Efficient algorithms for computing matrix spectral factors, Γ, can be found in Wilson (1972), Kucera (1979), Jezek and Kucera (1985), Davis and Dickinson (1983), and Harris and Davis (1989). These algorithms have been used to find inverses for systems as large as 12x12. The spectral factorization solution can also be obtained by solving an associated Riccati equation (Tuel, 1968; Georgiou, 1988). A solution for a stable approximate inverse will exist only if the right hand side of the spectral factorization equation (4.8) is nonsingular. Equivalent conditions for the existence of an inverse are given by Wilson (1972), Kucera (1979), and are summarized in Harris and MacGregor (1987).

The design of the spectral factorization inverse (4.7) requires the specification of an output weighting matrix Q_1. Q_1 is usually chosen to be diagonal with the magnitude of each diagonal element reflecting the relative importance of a unit change in each output. The input weighting matrix, Q_2, if taken to be diagonal, can be used to tune the approximate model inverse by adjusting n input weights. Through each input penalty weight, a trade-off between output performance and problems associated with input ringing or harsh input movements can be achieved. This trade-off can be evaluated by simulation or by computing the expected variances or ISE's of the inputs and outputs until an acceptable solution is found. For disturbances entering the feedback loop these variance matrices can be easily computed (Astrom and Wittenmark, 1984; Kwakernaak and Sivan, 1972) from

$$\Sigma_e = \frac{1}{2\pi i}\oint_{|z=1|}(\{I - P_m Q\}\Psi_v)\Sigma_v(\{I - P_m Q\}\Psi_v)^* \frac{dz}{z} \tag{4.9}$$

$$\Sigma_{\nabla u} = \frac{1}{2\pi i}\oint_{|z=1|}(Q\nabla\Psi_v)\Sigma_v(Q\nabla\Psi_v)^* \frac{dz}{z} \tag{4.10}$$

where

$$d_t = \Psi_v(z^{-1})v_t \tag{4.11}$$

In the equations above, Ψ_v represents the disturbance transfer function and v_t is a white noise vector with variance matrix Σ_v. Σ_e and $\Sigma_{\nabla u}$ are the nominal closed-loop output error and manipulated input velocity variance matrices respectively. Alternatively, (4.9) and (4.10) could be used to compute the ISE's for a deterministic disturbance v_t by setting $\Sigma_v = v_t v_t^T$.

4.4 PROPERTIES OF SPECTRAL FACTOR INVERSES

4.4.1 Stability

The spectral factor inverse obtained from (4.7) will always be stable since by design Γ is chosen as the unique solution to (4.8) having all its roots inside the unit circle. Therefore, stability of the closed-loop system will always be guaranteed for the nominal model (Zames, 1981).

4.4.2 Steady State Offset

The spectral factor inverse (4.7) satisfies the condition $Q(z=1) = P_n(z=1)^{-1}$. This property ensures that the closed-loop system will show no steady state offset to asymptotically constant disturbances or set point changes (Desoer and Chen, 1981; Garcia and Morari, 1985a).

4.4.3 Performance

By minimizing the performance index (4.6), it can be shown that for a given weighted ISE of input variations

$$\lim_{N\to\infty} \frac{1}{N} E\left\{\sum_{i=1}^{N} \nabla u_i^T Q_2 \nabla u_i\right\}$$

no inverse will give better performance for the nominal model in terms of the weighted ISE of the output

$$\lim_{N \to \infty} \frac{1}{N} E\left\{ \sum_{i=1}^{N} e_i^T Q_1 e_i \right\}$$

than the spectral inverse (4.7). With no penalty on the input variations (i.e. $Q_2 = 0$), the spectral factor inverse (4.7) gives the inverse having the smallest weighted output ISE among all stable inverses for the nominal model.

4.4.4 Spectral Interpretations

From equation (4.8) the spectrum $\Gamma^* Q_1 \Gamma$ is formed from the weighted process zero matrix spectrum $L^* Q_1 L$ and the spectrum $R^* \nabla^* Q_2 \nabla R$ which is affected by input penalty weight Q_2. This relationship suggests that the method may be interpreted as a pole placement design, where Γ represents an invertible approximation to L, and Q_2 is a tuning matrix used to shift the zeros of Γ.

An alternative form of the spectral factorization equation is obtained by premultiplying the terms in equation (4.8) by R^{-1^*} and post multiplying by R^{-1} to give

$$\tilde{P}_n^* \tilde{P}_n = P_n^* P_n + \nabla^* Q_2 \nabla \qquad (4.12)$$

where Q_1 has been taken, with no loss in generality, as the identity matrix I, and where $\tilde{P}_n = \Gamma R^{-1}$. The approximate model inverse is given by $Q = \tilde{P}_n^{-1}$. From (4.12) it can be seen that the spectrum of the approximate model, $\tilde{P}_n^* \tilde{P}_n$, is obtained by adding to the spectrum of the nominal model, $P_n^* P_n$, the diagonal spectral matrix $\nabla^* Q_2 \nabla$. In the limit where $Q_2 = 0$, the approximate model $\tilde{P}_n$ will be equal to the nominal model P_n, but with all unstable zeros reflected inside the unit circle. When Q_2 is nonzero the approximate model inverse $\tilde{P}_n$ will be a weighted function of two terms on the right hand side of (4.12). At low frequencies ($z = 1$), the first term dominates while at high frequencies the second term becomes important and forces $\tilde{P}_n^* \tilde{P}_n$ to become diagonally dominant in this region. The consequences of this are discussed later in the section on robustness.

4.4.5 Singular Values And Condition Number

The effect of the input weighting matrix Q_2 on the gains of the approximate model $\tilde{P}_n$ can be examined by considering the following singular value analysis. Taking the square root of the eigenvalues (λ_j) of both sides of (4.12) evaluated at $z = e^{i\omega T}$ leads to

$$\sigma_j(\tilde{P}_n(i\omega)) = \sqrt{\lambda_j(P_n^* P_n + \nabla^* Q_2 \nabla)} \tag{4.13}$$

where $\sigma_j(\tilde{P}_n(i\omega))$, $j = 1, \ldots, n$ are the singular gains of $\tilde{P}_n$. Denoting the maximum and minimum singular gains as $\sigma_M(\tilde{P}_n)$ and $\sigma_m(\tilde{P}_n)$ respectively, we can define the condition number as

$$\gamma = \frac{\sigma_M(\tilde{P}_n)}{\sigma_m(\tilde{P}_n)} \tag{4.14}$$

A well-conditioned model has a small condition number at all frequencies. In general, such a model will yield an inverse with good robustness properties. Furthermore, an approximate inverse that leads to small variances of the input manipulations will result from an approximate model having a large minimum singular gain at all frequencies. The spectrum of $\nabla^* Q_2 \nabla$ is diagonal and its elements increase with frequency. It is straightforward to show that a nonzero Q_2 affects the condition number of $\tilde{P}_n$, and can be chosen so that the condition number is reduced at all frequencies $\omega > 0$. An off-line singular value analysis can be performed to check whether any inverse design is well-conditioned and has high minimum singular gains across the entire frequency domain. Note that poor steady state conditioning of the process, is an inherent property of the system and cannot be affected through the spectral factorization inverse design, nor with any other controller design when integral action is required.

4.4.6 Sensitivity Norm Interpretations

The cost function (4.6) can be expressed in the frequency domain form (Kwakernaak and Sivan, 1972; Astrom and Wittenmark, 1984) as

$$\text{Min} \quad \frac{1}{2\pi i} \oint_{|z=1|} Trace\{Q_1 \Phi_e + Q_2 \Phi_{\nabla u}\} \frac{dz}{z} \tag{4.15}$$

where Φ_e and $\Phi_{\nabla u}$ are the spectra of e_t and ∇u_t. The nominal sensitivity matrix S_n, defined by

$$S_n = I - P_n Q \tag{4.16}$$

and the nominal complementary sensitivity matrix

$$T_a = P_a Q \tag{4.17}$$

can be used to express (4.15) as

$$\text{Min}\left\{\|Q_1^{1/2} S_a W_1\|^2 + \|W_2 T_a\|^2\right\} \tag{4.18}$$

where

$$W_1 = \frac{1}{\nabla} \tag{4.19}$$

is the transfer function of the assumed step disturbances or set point changes, and

$$W_2 = Q_2^{1/2} P_a^{-1} \tag{4.20}$$

The cost function (4.18) is similar in form to the criterion used in designing controllers which compromise between performance and robustness (Kwakernaak, 1985; Morari and Doyle, 1986). The difference is that a H^2-norm minimization criterion is used in this case as opposed to a H^∞-norm minimization, and in general, will lead to a controller design with very different performance and robustness properties. In the weighted H^2-norm minimizations criterion (4.18) the weight W_1 on the sensitivity function is large over the low frequency range where the disturbance spectrum is large. When P_a is a typical low pass process, the weight W_2 on the complementary sensitivity function is large at high frequencies where model mismatch is usually the greatest. In general, these weightings are consistent with the trends advocated in the H^∞-norm approaches based on robustness considerations (Kwakernaak, 1985; Doyle and Stein, 1981; Morari and Doyle, 1986).

4.4.7 Nonsquare Systems

In many situations one has a different number of inputs (m) than outputs (n). In particular, with more inputs one has a considerable degree of additional flexibility in designing control systems. Nonsquare spectral inverses are easily obtained (Harris and MacGregor, 1987) by simply using the alternative spectral factorization in (4.8) given by

$$\Gamma_1^* \Gamma_1 = \Gamma^* Q_1 \Gamma \tag{4.21}$$

where Γ_1 is a (mxm) spectral factor. The approximate (mxn) pseudo model inverse to be used in the design is then

$$Q = R \Gamma_1^{-1} K \tag{4.22}$$

where $K = \Gamma_1^*(z=1)^{-1}L^*(z=1)Q_1$ is the scaling factor ensuring no steady state offset to asymptotically constant disturbances or set point changes if $m \geq n$.

4.5 SIMULATION STUDIES: NOMINAL PERFORMANCE

In this section we introduce two example systems with very different dynamics; a pilot plant catalytic reactor, and a pilot plant distillation column, for which models have been identified over a range of operating conditions. In this section we consider the design of various IMC controllers and investigate their nominal performances by computing their expected closed-loop variances using equations (4.9) and (4.10), and by performing simulations. In a later section we investigate how these designs based on a nominal model perform in other operating regions where different models are used.

4.5.1 Example 1: A Packed Bed Catalytic Reactor

The pilot plant packed bed reactor carrying out butane hydrogenolysis reactions over a nickel on silica gel catalyst has been described by Kozub et al. (1987). The outputs to be controlled are propane production rate (y_{1_t}) and % butane conversion (y_{2_t}). These outputs are controlled using hydrogen flow rate (u_{1_t}) and reactor hotspot temperature rise (u_{2_t}). An identification study by Kozub et. al. (1987) led to the model

$$y_t = \begin{bmatrix} \dfrac{1.8z^{-3} - 6.6z^{-4} + 5.2z^{-5}}{1 - z^{-1} + 0.34z^{-2}} & \dfrac{0.54z^{-4}}{1 - 1.3z^{-1} + 0.52z^{-2}} \\ -0.75z^{-3} - 3.4z^{-4} - z^{-5} & \dfrac{0.16z^{-5} + 0.11z^{-6}}{1 - 0.61z^{-1}} \end{bmatrix} u_t \qquad (4.23)$$

where

y_{1_t} = propane production (mmoles/s)

y_{2_t} = % butane conversion

u_{1_t} = hydrogen flow rate ($x10^{-1}$ cc/s)

u_{2_t} = hot spot temperature rise (C)

This process model can be shown to display an initial wrong way propane response with respect to changes in hydrogen flow rate. The model contains one noninvertible zero at -5.5, and a stable ringing zero located at -0.58. One period of time delay imbalance is also present. A right matrix fraction description of this transfer function is given in Kozub (1986).

The following three different IMC controller designs are compared:

Design 1: An LQ optimal inverse obtained by spectral factorization (equations (4.7) and (4.8)) and tuned by adjusting the quadratic performance weights Q_2 to provide an acceptable compromise between the output and input variances (Σ_e and $\Sigma_{\nabla u}$ in equations (4.9) and (4.10)). The output weighting Q_1 is set to I reflecting equal importance on the two outputs.

Design 2: An ISE optimal inverse ($\tilde{P}_n^{-1}$) again obtained by spectral factorization but now with $Q_2 = 0$, and then combined with a diagonal first order filter (F) (equation (4.5)). The controller $Q = \tilde{P}_n^{-1}F$ is tuned by adjusting the diagonal filter parameters.

Design 3: The minimum settling time, decoupled closed-loop inverse design of Garcia and Morari (1985a, b) and Desoer and Chen (1981) given in equations (4.3) and (4.4). In this design the unstable pole resulting from the noninvertible process model zero is reflected inside the unit circle, and the ringing pole arising from the negative real axis zero is shifted to the origin. As with the second design, a diagonal first order filter (4.5) is used to tune the controller.

These designs, together with their calculated nominal closed-loop output and input change ISE's for random step disturbances or set point changes, are summarized in Table 4.1.

TABLE 4.1: NOMINAL PERFORMANCE OF IMC DESIGNS WITH PACKED BED REACTOR MODEL				
Inverse Design: (Q)	Variances			
	e_1	e_2	∇u_1	∇u_2
Design 1: $Q_1 = I$, $Q_2 = Diag(200, 3)$ $f_{1,1} = 0$, $f_{2,2} = 0$	5.0	5.0	0.0071	0.18
Design 2: $Q_1 = I$, $Q_2 = 0$ $f_{1,1} = 0.73$, $f_{2,2} = 0.73$	5.0	5.0	0.0090	1.03
Design 3: Decoupled $f_{1,1} = 0.3$, $f_{2,2} = 0.3$	5.0	5.0	0.0234	2.36

Note that in order to make comparisons all controllers were designed to give the same nominal performance for the outputs. Although all these designs lead to the same output performance, it is evident that the first design using the diagonal elements of Q_2 as tunable parameters leads to significantly lower ISE's for the control actions. The design leading to the highest cost in terms of control actions was the decoupled design. From a practical standpoint, one would generally prefer a design with the smallest control actions for the same degree of performance. Intuitively, this design might also be expected to be more robust to model uncertainty, since it will put less strain on the internal model's ability to predict the output.

The nominal performance of the three IMC designs to an identical sequence of step set point changes is shown in Figures 4.2, 4.3, and 4.4 respectively.

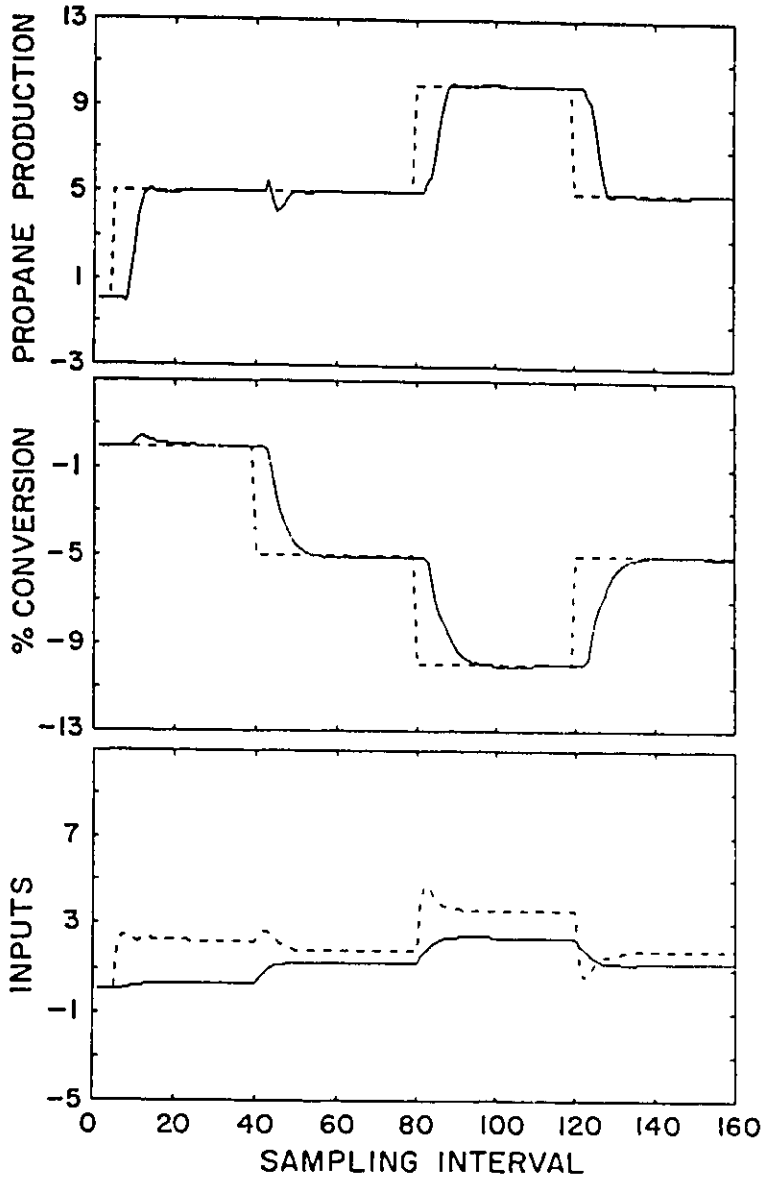

FIGURE 4.2: Nominal Simulated Packed Bed Reactor Control: Design 1
$Q_1 = I$, $Q_2 = Diag(200, 3)$, $f_{i,i} = 0$
Top, (-) propane production; (--) set point
Middle, (-) % butane conversion; (--) set point
Bottom, (-) hydrogen flow rate; (--) hot spot rise

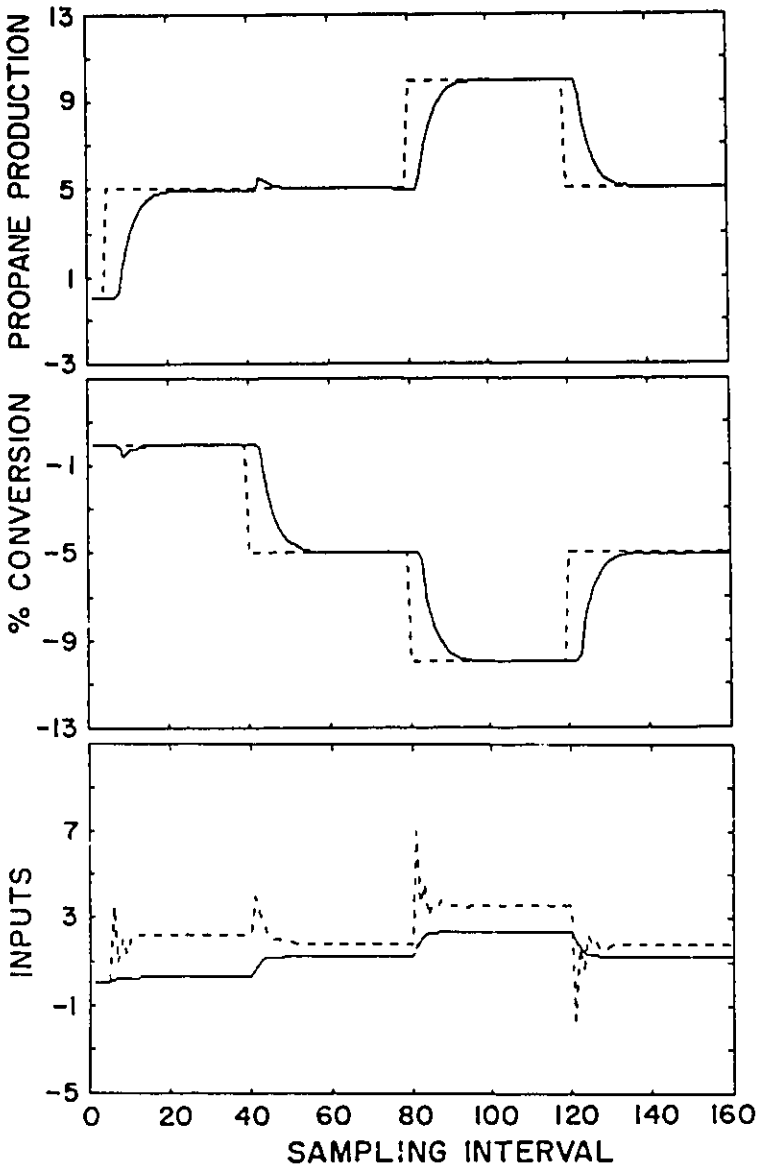

FIGURE 4.3: Nominal Simulated Packed Bed Reactor Control: Design 2
$Q_1 = I, \quad Q_2 = 0, \quad f_{i,j} = 0.73$
curve identification as in Figure 4.2

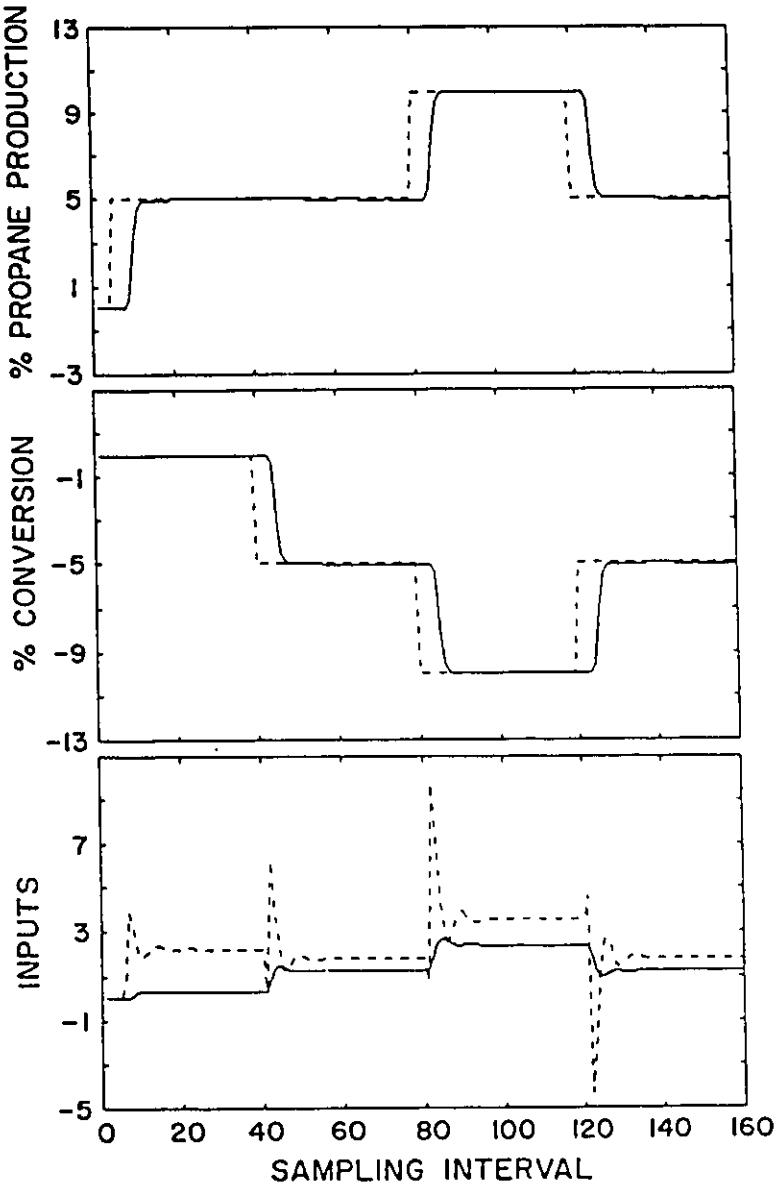

FIGURE 4.4: Nominal Simulated Packed Bed Reactor Control: Design 3
Decoupled, $f_{i,j} = 0.3$
curve identification as in Figure 4.2

The first set point change is a 5 unit increase in the level of propane production (y_{1_t}). The second set point change is a 5 % decrease in butane conversion (y_{2_t}). The third set point change is a simultaneous increase and decrease of 5 units in y_{1_t} and y_{2_t} set points respectively, while the fourth set point change is exactly the reverse of the third. Differences in both the closed-loop output and input responses can be observed in these figures, even though all three controllers were designed for exactly the same output error variances. Unlike the decoupled design, the nominal output response displayed by the first two designs shows some interaction. The input manipulation of design 1 can be seen to be much smoother relative to designs 2 and 3.

This example clearly illustrates that the nominal closed-loop behavior of an IMC design is affected differently by tuning with quadratic weighting matrix Q_2 as opposed to tuning with a diagonal filter. In this particular example, tuning the approximate inverse with Q_2 leads to a better compromise between nominal output performance and the cost of input manipulation than a design where a fixed ISE inverse or decoupling inverse is used with a first order tunable filter.

4.5.2 Example 2: A Binary Distillation Column

The second case study is concerned with the simulated control of overhead composition of water (y_{1_t}) and bottom composition of methanol (y_{2_t}) in a binary methanol/water pilot plant distillation column. The manipulated inputs for control are reflux flow rate (u_{1_t}) and steam flow rate (u_{2_t}) to the reboiler. A detailed description of this pilot plant process is given by Hugo (1989). An identification study made by Hugo (1989) at one region of operation led to a linear continuous transfer function model

$$y(s) = \begin{bmatrix} -\dfrac{4.0}{44.5s+1} & \dfrac{4.0}{60.4s+1} \\ \dfrac{7.4}{60.4s+1} & -\dfrac{12.6}{41.5s+1} \end{bmatrix} u(s) \qquad (4.24)$$

where

y_{1_t} = % mole fraction water in overhead

y_{2_t} = % mole fraction methanol in bottom

u_{1_t} = reflux flow rate (ml/min)

u_{2_t} = steam flow rate (ml/min)

In the control designs to follow, the model was discretized for a control interval of 10 min., corresponding to the sampling frequency of the process gas chromatographs in the actual pilot plant system. When discretized for this sampling interval, it can be shown that the process model is balanced with respect to time delays and contains no unstable zeros.

The following two different IMC designs are compared:

Design 1: The LQ optimal inverse was obtained by spectral factorization and tuned by adjusting both quadratic performance weights Q_1 and Q_2 to meet nominal output performance specifications.

Design 2: The minimum settling time, decoupled closed-loop inverse design procedure together with a tunable diagonal first order filter was used to specify Q. Since the process model is both invertible and balanced with respect to deadtime (no deadtime present), this decoupled design, when taking $f_{i,i} = 0$, is identical to the spectral factorization design (4.8) with $Q_2 = 0$, and any nonzero diagonal choice for Q_1.

The two designs together with their calculated nominal closed-loop output and input change variances or ISE's for random step disturbances or set point changes are summarized in Table 4.2.

TABLE 4.2: NOMINAL PERFORMANCE OF IMC DESIGNS WITH DISTILLATION COLUMN MODEL

Inverse Design (Q)	Variances			
	e_1	e_2	∇u_1	∇u_2
Design 1: $Q_1 = Diag(3.75, 1)$ $Q_2 = Diag(75, 75)$ $f_{1,1} = 0, \quad f_{2,2} = 0$	2.8	2.8	0.059	0.019
Design 2: Decoupled $f_{1,1} = 0.8, \quad f_{2,2} = 0.8$	2.8	2.8	0.136	0.034

Both controllers were designed so that the nominal error variance of each output was the same. As was previously observed in case study 1, the first design using quadratic performance weights to design Q through (4.8) leads to lower ISE's for the control actions for the same nominal output performance specification.

The nominal performance of the two IMC designs to an identical sequence of step set point changes is shown in Figures 4.5 and 4.6.

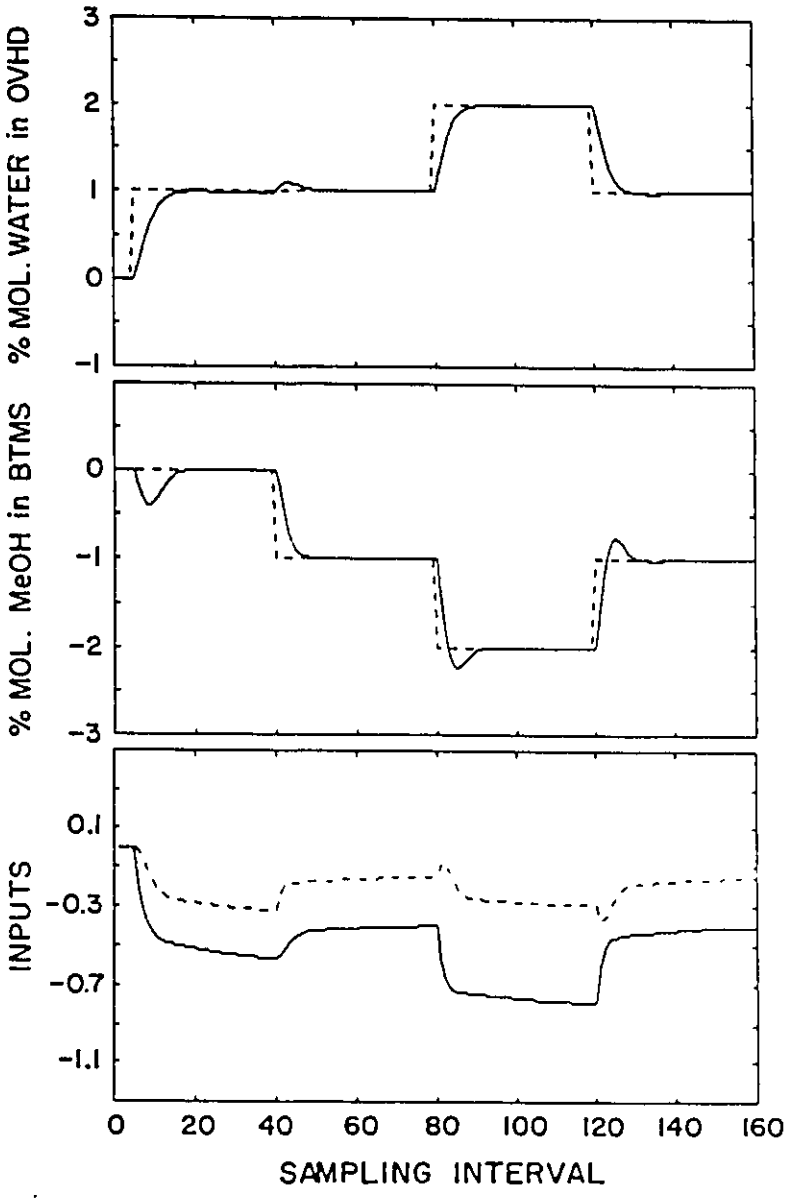

FIGURE 4.5: Nominal Simulated Distillation Column Control: Design 1
$Q_1 = Diag(3.75, 1)$, $Q_2 = Diag(75, 75)$, $f_{i,j} = 0$
Top. (-) % water in overhead; (--) set point
Middle, (-) % methanol in bottom; (--) set point
Bottom, (-) reflux flow; (--) steam flow

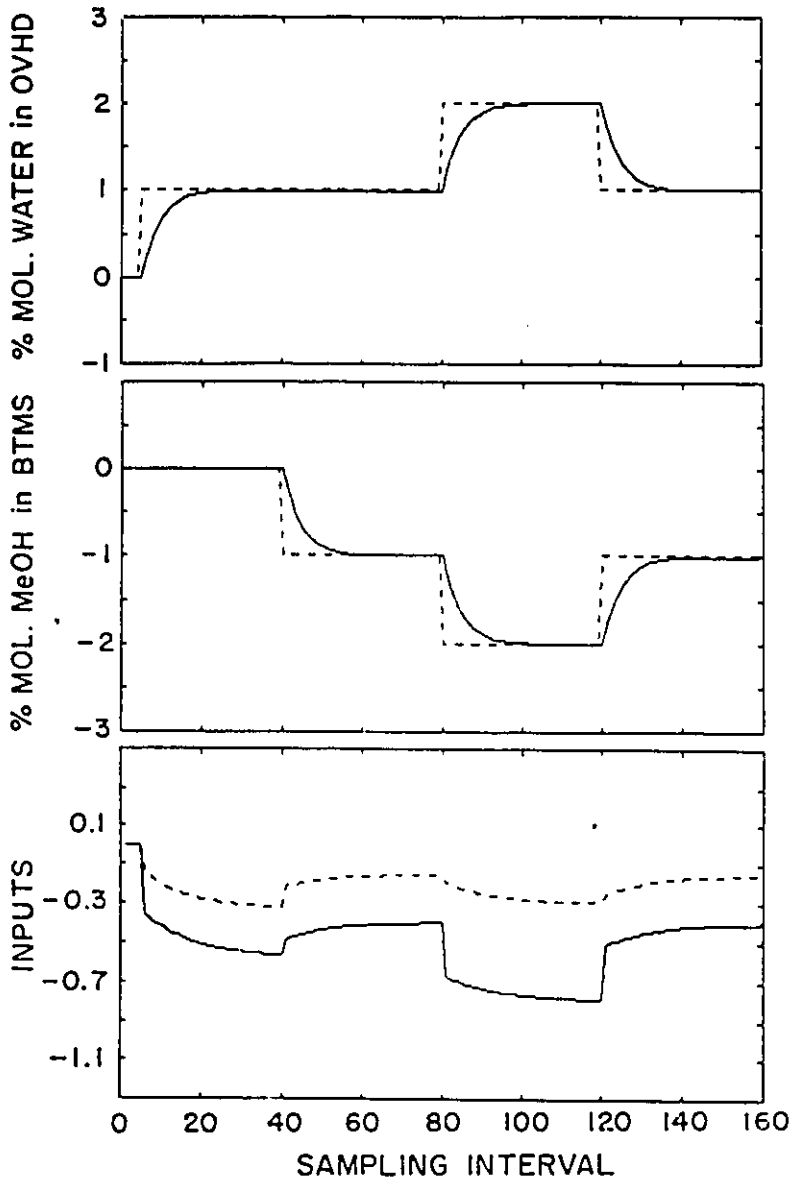

FIGURE 4.6: Nominal Simulated Distilation Column Control: Design 2
Decoupled, $f_{i,i} = 0.8$
curve identification as in Figure 4.5

The first set point change in these simulations is a unit increase in the water composition in the overhead (y_1). The second set point change is a unit decrease in methanol composition in the bottom (y_2). The third change is a simultaneous unit increase and decrease for y_1 and y_2 set points respectively, while the fourth set point change is exactly the reverse of the third. Figures 4.5 and 4.6 show that the response of each design is very different. The first design leads to some interaction in the closed-loop output response, whereas the response of the second design is completely decoupled as expected. Only slight differences can be seen in the closed-loop input responses.

4.6 ROBUSTNESS ANALYSIS

In the following sections we investigate the robustness properties of different IMC designs in four different ways: (i) examining the conditioning of the invertible model approximation (Q^{-1}) using singular values and condition numbers; (ii) performing a singular value analysis on the closed-loop system assuming unstructured norm bounded uncertainty (Doyle and Stein, 1981); (iii) performing a structured singular value analysis (Doyle, 1982; Skogestad and Morari, 1987) on the closed-loop system assuming a one parameter equal percentage disk uncertainty characterization in the frequency domain in each element of the transfer function matrix; (iv) performing simulation studies on the catalytic reactor and distillation pilot plant examples using some experimentally identified model mismatch.

4.6.1 SVD Analysis On Approximate Model Inverses

In this section, the analysis technique outlined in section 2.3 is used to compare the SVD properties of the different IMC designs.

(i) Example 1: SVD Analysis On Packed Bed Reactor Case Study

SVD analyses on the approximate models to be inverted (Q^{-1}) for the three IMC designs in Table 4.1 corresponding to the catalytic reactor example are shown in Figure 4.7.

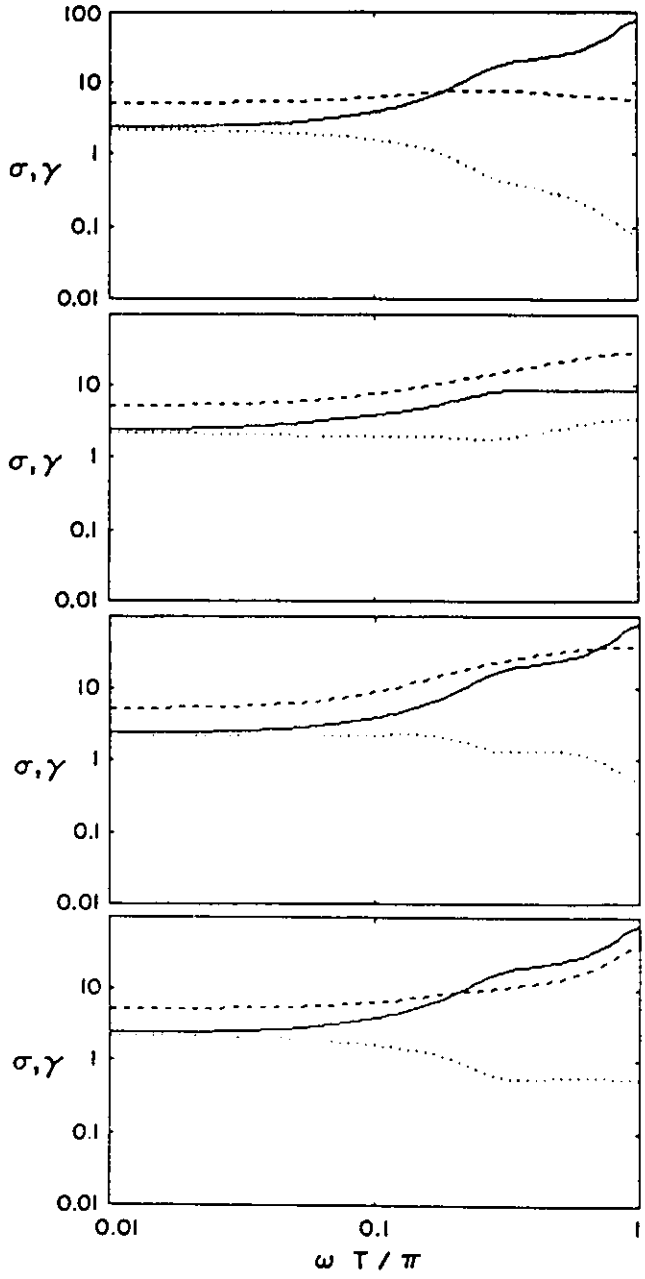

FIGURE 4.7: SVD of Q^{-1}: Packed Bed Reactor Example
Top: nominal model
Second: $Q_1 = I$, $Q_2 = Diag(200, 3)$, $f_{i,i} = 0$
Third: $Q_1 = I$, $Q_2 = 0$, $f_{i,i} = 0.73$
Bottom: Decoupled, $f_{i,i} = 0.3$
(-) γ, (--) σ_M, (..) σ_m

A SVD analysis on the nominal model P_n is also included in this figure as a base against which to contrast the various designs. The SVD of P_n reveals that the nominal model is poorly conditioned at high frequencies and has a small minimum singular gain at frequencies higher than $0.1\pi/T$. This suggests that using an invertible ISE approximate inverse for Q would lead to a design with poor robustness properties based on the arguments in section 2.3. Figure 4.7 also reveals that the SVD properties of P_n and Q^{-1} for the three IMC designs are similar in the frequency range below $0.1\pi/T$, and therefore good performance can be expected from all three designs in that frequency range. However, very significant differences can be seen in the frequency range above $0.1\pi/T$.

The second plot in Figure 4.7 shows the SVD of Q^{-1} for the first (LQ optimal) design that was tuned by adjusting the quadratic performance weight Q_2 in (4.8). The effect that the input penalty matrix Q_2 has on the effective model inverse relative to P_n is to significantly increase the minimum singular gain of Q^{-1} at high frequency. The use of a non-zero Q_2 can also be observed to substantially reduce the condition number of Q^{-1} at high frequency relative to that of the nominal model P_n. This is an expected property of spectral inverse designs as shown earlier in equation (4.13).

The SVD of Q^{-1} for the second design, arrived at with $Q_1 = I$, $Q_2 = 0$, and $f_{i,i} = 0.73$ is shown in the third plot of Figure 4.7. The effect of the filter in this design is to increase both the high frequency minimum and maximum singular gains by the same factor relative to P_n. This results in a reduction in the high frequency loop gains but has no effect on the condition number of Q^{-1} (This is true for all IMC designs using common diagonal filters).

The SVD analysis of the decoupled IMC inverse design, shown in the fourth plot of Figure 4.7 shows a trend similar to the second design, in that the gains of Q^{-1} are increased, but the conditioning is unaffected by the diagonal filters.

(ii) Example 2: SVD Analysis On Distillation Column Case Study

Figure 4.8 shows the SVD analyses of the approximate models to be inverted (Q^{-1}) together with the nominal model P_n for the IMC designs in Table 4.2 corresponding to the pilot plant distillation column example.

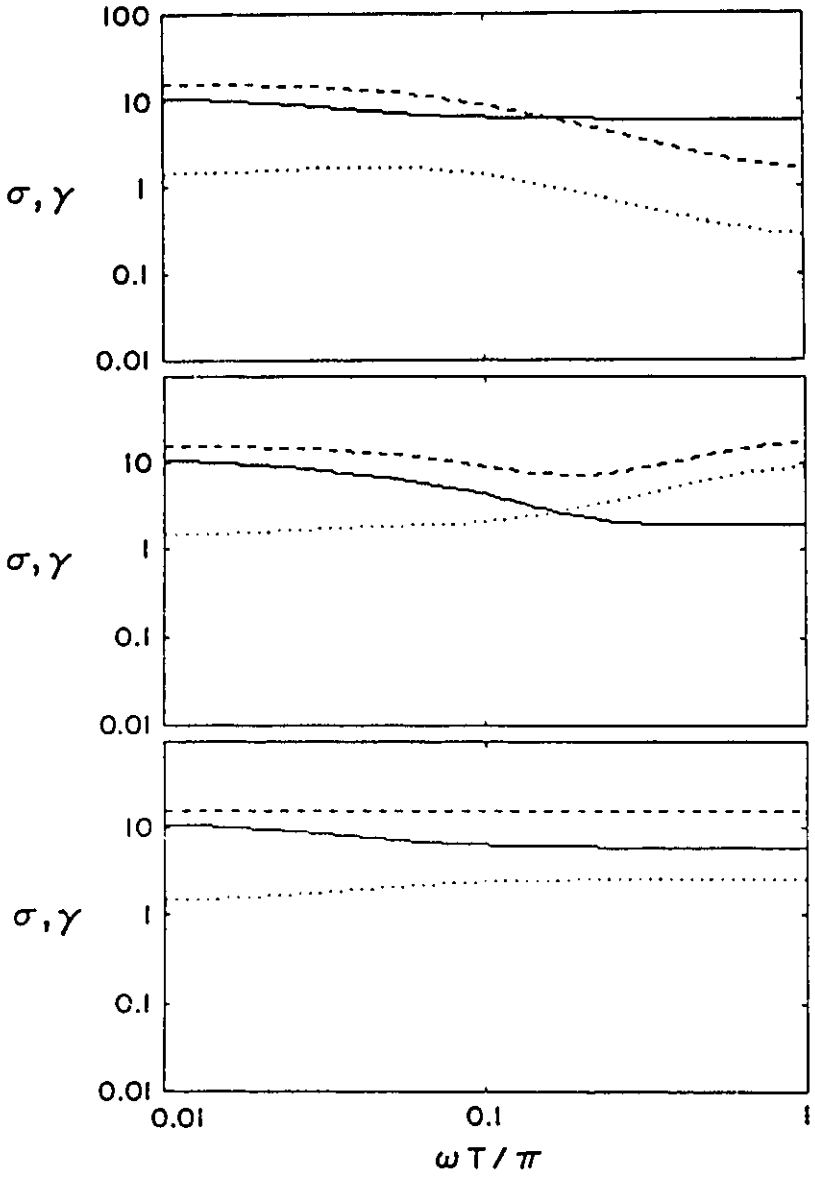

FIGURE 4.8: SVD of Q^{-1}: Distillation Column Example
Top: nominal model
Middle: $Q_1 = Diag(3.75, 1)$, $Q_2 = Diag(75, 75)$, $f_{i,i} = 0$
Bottom: Decoupled, $f_{i,i} = 0.8$
(-) γ, (--) σ_M, (..) σ_m

As in the first case study, the minimum singular value of P_n decreases with increasing frequency, indicating that unacceptably high controller gains at the high frequency range may result if the exact model inverse were used in Q. However, unlike the first case study, the condition number of Q^{-1} decreases slightly with increasing frequency, suggesting that the approximate model inversion design will be less sensitive to high frequency model perturbations. In general, the behavior of this process appears much better over the whole frequency range than the previous reactor example.

The second plot in Figure 4.8 shows the SVD of Q^{-1} corresponding to the first (LQ optimal) design arrived at by adjusting Q_1 and Q_2 in (4.8). This design gives both a significant increase in the minimum singular gain, and an improved condition number of the approximate model Q^{-1} at high frequency compared to P_n. No differences relative to P_n can be seen at low frequencies.

The third plot in Figure 4.8 shows the SVD of Q^{-1} for the decoupled output response IMC design. The effect that the filter has on the effective approximate inverse is, once again, to increase the minimum and maximum singular gains by proportionally the same amount in the high frequency range. The conditioning of the effective model inverse relative to P_n is unchanged. At low frequency no differences between the SVD of P_n and Q^{-1} can be observed.

The results of this example are consistent with the trends observed in the first example. For the same nominal output performance specification, the inverse arrived at through LQ penalty weights Q_1 and Q_2 leads to greatly improved high frequency conditioning and better high frequency gains relative to an IMC inverse design arrived at with a fixed inverse and a tunable diagonal filter. These results clearly demonstrate some advantages in the employing spectral factor inverses (4.8) in IMC designs, and also demonstrate the limitations of IMC designs where fixed inverses are combined with tunable diagonal filters. Admittedly, however, these latter designs are very appealing to use in practice because of their ability to tune them on-line using diagonal filter elements.

4.6.2 Singular Value Analysis: Unstructured Uncertainties

In this section, the index for relative robustness based on multiplicative unstructured norm bounded uncertainty m_m in section 2.5 is used to compare the relative robustness of the different IMC designs.

The upper bound on $m_m(\omega)$ for each of the designs in Table 4.1 is shown in Figure 4.9.

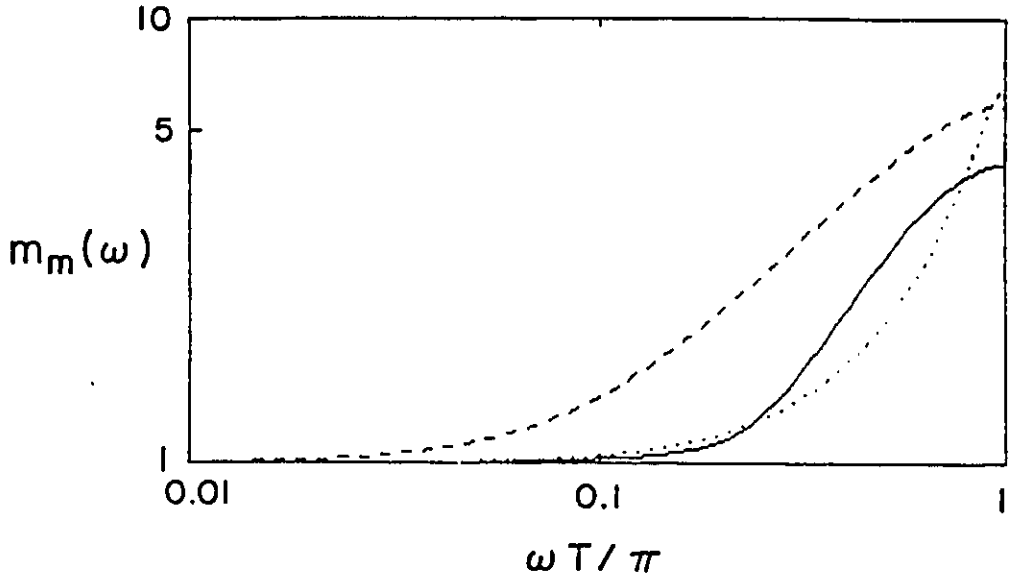

FIGURE 4.9: Unstructured Multiplicative Mismatch Tolerance $m_m(\omega)$: Packed Bed Reactor Example
(-) $Q_1 = I$, $Q_2 = Diag(200, 3)$, $f_{i,i} = 0$
(--) $Q_1 = I$, $Q_2 = 0$, $f_{i,i} = 0.73$
(..) **Decoupled,** $f_{i,i} = 0.3$

The results indicate that the second design, arrived at with a fixed ISE inverse and a tunable diagonal filter, is more robust with respect to stability, except at very high frequency where the decoupled inverse IMC design appears to be slightly better. Robust stability of the first (LQ optimal) design, arrived at by adjusting Q_2 in (4.8), to this unstructured multiplicative uncertainty is predicted to be inferior to the second IMC design. The decoupled IMC design is predicted to be slightly more robust than the first design in some frequency regions but worse in others.

The relative robustness trends of the two IMC designs for the distillation column example in Table 4.2 to independent norm bounded unstructured multiplicative output uncertainty is shown in Figure 4.10.

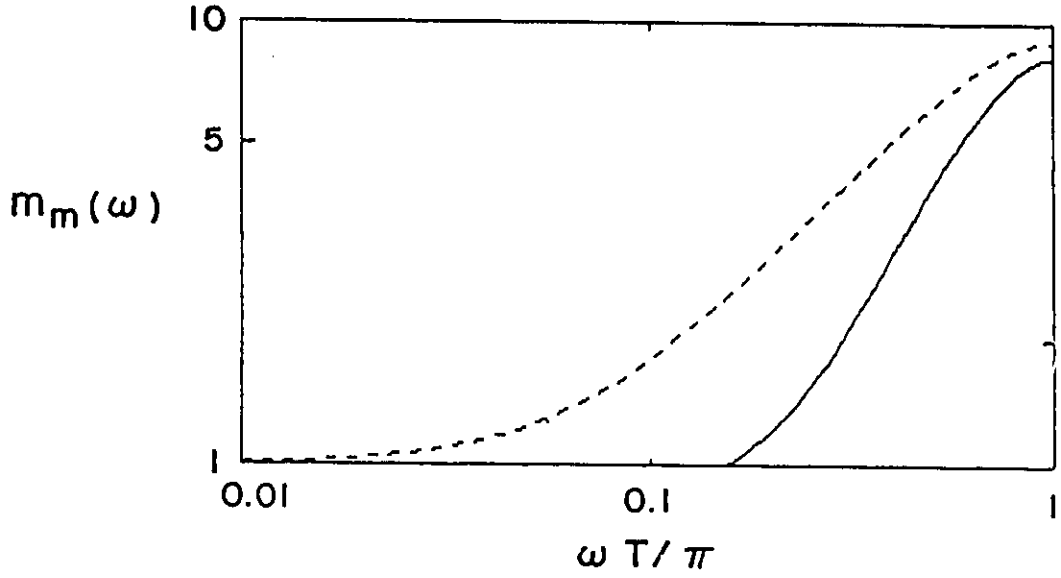

FIGURE 4.10: Unstructured Multiplicative Mismatch Tolerance $m_m(\omega)$: Distillation Column Example
(-) $Q_1 = Diag(3.75, 1)$, $Q_2 = Diag(75, 75)$, $f_{i,i} = 0$
(--) **Decoupled,** $f_{i,i} = 0.8$

At all frequencies, the decoupled IMC design appears to be significantly more tolerant to unstructured multiplicative output uncertainty.

The results of the robust stability analyses from the two examples display a consistent trend. In general, for the same nominal output performance specification, the design where Q was arrived at by adjusting the quadratic performance index weights Q_1 and Q_2 in (4.8) appear significantly less robust to independent unstructured norm bounded uncertainty than the Q designs using the ISE output optimal inverses combined with a tunable diagonal filter. Again, it is important to stress that these trends only pertain to the mismatch characterization described above, and may not provide a reliable indication of the relative robustness of the controllers to the true range of plant mismatch. This will be illustrated in the sections to follow.

4.6.3 Equal Percentage Element-By-Element Uncertainty Analysis

In this section the relative robust stability of the IMC designs are compared using the Kappa (κ) index introduced in section 2.6. This Kappa index represents the amount by which equal percentage disk

uncertainty in all elements of the transfer function can be increased at each frequency before the feedback loop goes unstable. Structured singular value analysis is used to arrive at $\kappa(\omega)$ for the IMC designs considered in this section.

Figure 4.11 shows the maximum κ for closed-loop stability as a function of ω for the packed bed reactor IMC designs in Table 4.1.

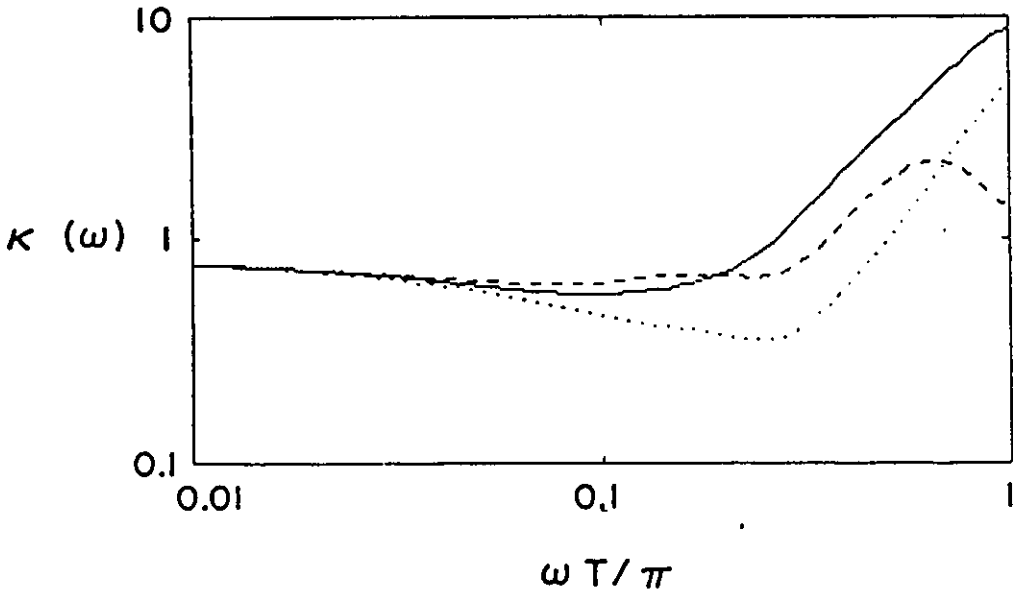

FIGURE 4.11: Element-by-Element Equal % Disk Uncertainty Tolerance $\kappa(\omega)$: Packed Bed Reactor Example
(-) $Q_1 = I$, $Q_2 = Diag(200, 3)$, $f_{i,i} = 0$
(--) $Q_1 = I$, $Q_2 = 0$, $f_{i,i} = 0.73$
(..) **Decoupled,** $f_{i,i} = 0.3$

The relative robust stability limits of the three controller designs for this equal percentage element-by-element disk uncertainty are significantly different from the trends previously shown for the unstructured multiplicative case in Figure 4.9. In the high frequency range, the first IMC design arrived at by tuning Q_2 in spectral factorization equation (4.8) now appears to be the most robust design. Only in the mid frequency range, does this design appear to be slightly less robust than the second design where Q was arrived at with an ISE optimal inverse combined with a diagonal filter. The decoupled design is the least robust of all three IMC designs, except at very high frequencies where it appears to be more robust than the second design. If one makes the assumption that model uncertainty will in general be greater at higher frequencies, then based on these results, one would expect the first design to be the most robust to model perturbations.

Figure 4.12 shows the maximum tolerable $\kappa(\omega)$ for both of the distillation column IMC designs in Table 4.2.

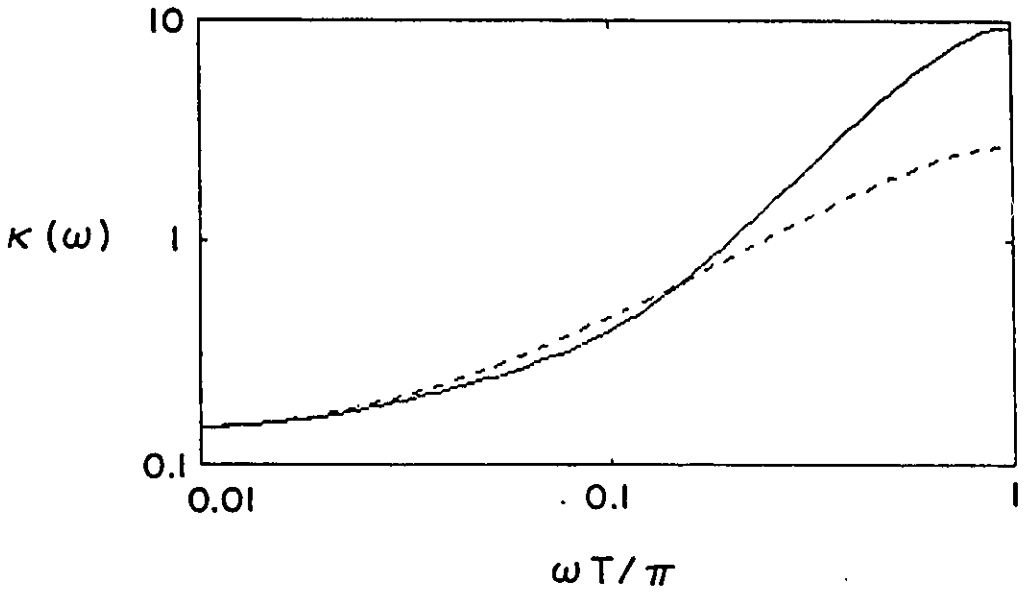

FIGURE 4.12: Element-by-Element Equal % Disk Uncertainty Tolerance $\kappa(\omega)$: Distillation Column Example
(-) $Q_1 = Diag(3.75, 1)$, $Q_2 = Diag(75, 75)$, $f_{i,i} = 0$
(--) Decoupled, $f_{i,i} = 0.8$

Relative to the results from the unstructured uncertainty analysis in Figure 4.10, the robustness trends once again appear to be very different. For the equal percentage element-by-element, disk uncertainty characterization, the LQ inverse design arrived at by adjusting Q_1 and Q_2 in (4.8) appears to be significantly more robust in the high frequency range, and only slightly less robust in the mid frequency range relative to the design with a fixed decoupled ISE inverse combined with a tunable diagonal filter.

The trends observed in both examples appear to be consistent, in that IMC designs arrived at through tuning Q_1 and Q_2 in (4.8) were predicted to be much more robust in the high frequency range and slightly less robust in the mid frequency range to the equal percentage element-by-element disk uncertainty relative to IMC designs with fixed inverses combined with tunable diagonal filters. Furthermore, the robustness trends based on the Kappa analysis using SSV's for this element-by-element uncertainty appear to be almost opposite to those trends using SV's on the much more conservative unstructured multiplicative uncertainty characterization.

The results clearly indicate the importance of the uncertainty characterization in evaluating the robustness trends of different controller designs, and that serious credibility should not be given to any analysis unless the mismatch region characterization can be proven from fundamental modelling considerations to actually represent the forms of mismatch that might be encountered.

4.6.4 Simulation Studies: Robustness

In light of the above results, it may be argued that a more worthwhile approach to addressing relative robustness of different designs is simply to evaluate their performance on identified mismatch models if available, and avoid the problems of conservative disk uncertainty characterizations that existed in the methods above. Of course this approach could lead to very erroneous results if the mismatch cases tested are not indicative of the whole range of plants that will be encountered. In the following two sections, the IMC designs for both the packed bed reactor and distillation column examples will be simulated with different (mismatch) models identified experimentally in some different regions of operation.

(i) Example 1: Simulated Packed Bed Reactor Model Mismatch

An identification study by Onderwater (1985) on the same pilot plant reactor system led to three different transfer function models describing the process dynamics in three very different regions of operation. These three models were used in a simulated study to evaluate the performance of the three different controller designs in Table 4.1 under conditions of model mismatch. The identified mismatch model that led to the worst performance with all three designs was

$$y_t = \begin{bmatrix} \dfrac{-0.8z^{-3} - 0.9z^{-4} + 2.4z^{-5}}{1 - z^{-1} + 0.41z^{-2}} & \dfrac{0.41z^{-4}}{1 - 0.79z^{-1} + 0.23z^{-2}} \\ \dfrac{-4.0z^{-3} + 2.5z^{-4}}{1 - 1.2z^{-1} + 0.59z^{-2}} & \dfrac{0.34z^{-4}}{1 - 0.72z^{-1}} \end{bmatrix} u_t \qquad (4.25)$$

Figures 4.13, 4.14, and 4.15 show the performance of the three IMC designs to the same sequence of step set point changes made in Figures 4.2 to 4.4 but with P set to (4.25) in the simulation.

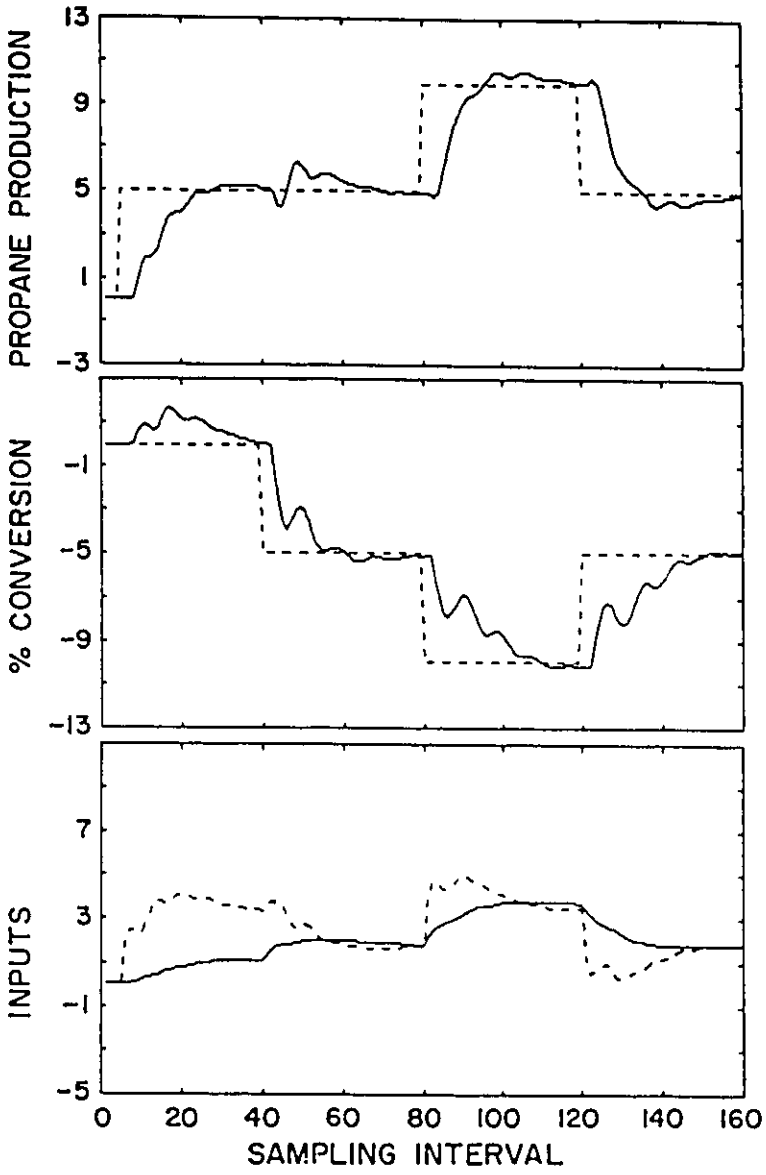

FIGURE 4.13: Simulated Packed Bed Reactor Control With Model Mismatch: Design 1
$Q_1 = I$, $Q_2 = Diag(200, 3)$, $f_{i,j} = 0$
curve identification as in Figure 4.2

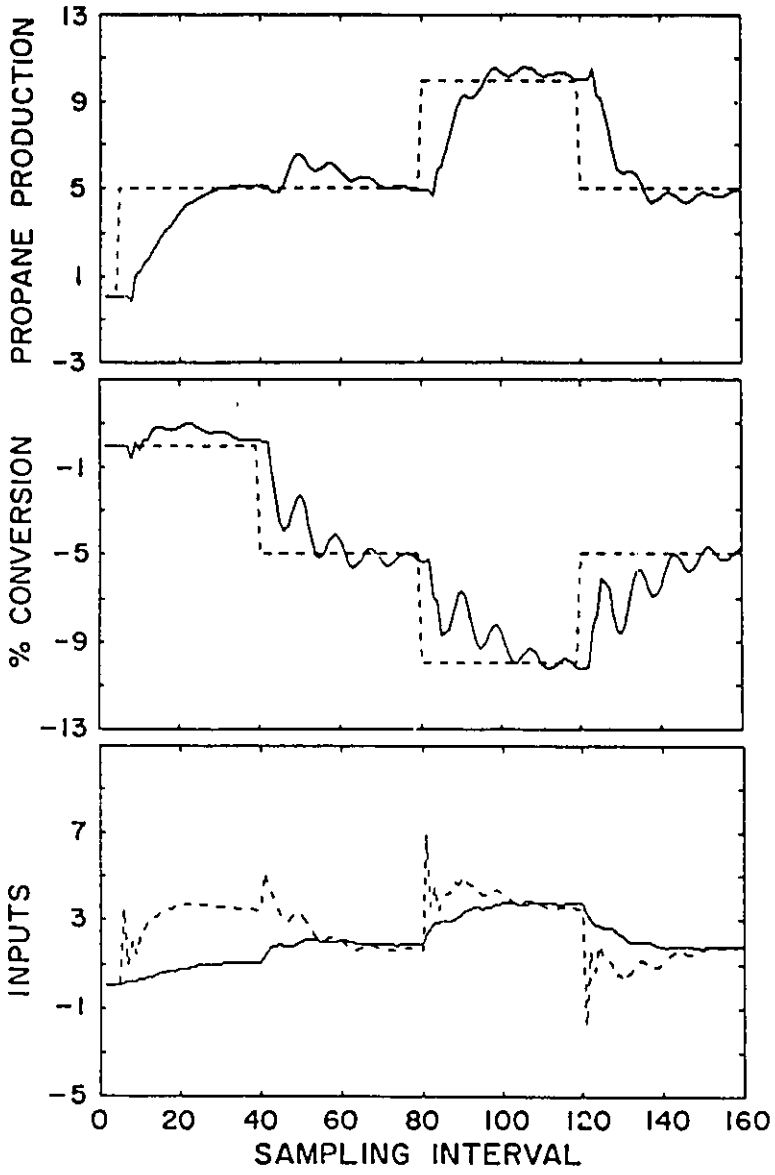

FIGURE 4.14: Simulated Packed Bed Reactor Control With Model Mismatch: Design 2
$Q_1 = 1, \quad Q_2 = 0, \quad f_{i,i} = 0.73$
curve identification as in Figure 4.2

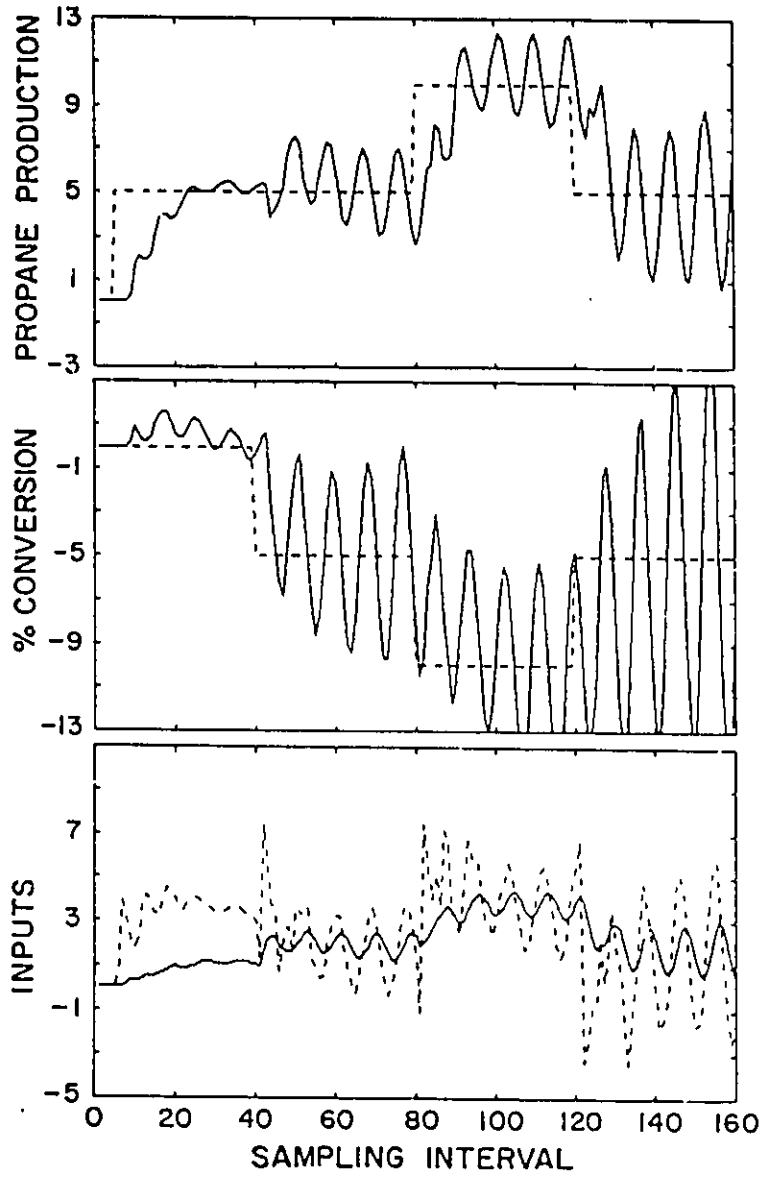

FIGURE 4.15: Simulated Packed Bed Reactor Control With Model Mismatch: Design 3 Decoupled, $f_{i,j} = 0.3$
curve identification as in Figure 4.2

The performance of each IMC design can be observed to be significantly different. The design that was least sensitive and performed the best under these conditions of model mismatch was the LQ inverse design (#1), shown in Figure 4.13. The most sensitive design to the model mismatch was the decoupled design, shown in Figure 4.15, which went unstable after the first set point change. Exactly the same trends were observed when model mismatch simulations were performed using the other two models identified by Onderwater (1985).

(ii) Example 2: Simulated Distillation Column Model Mismatch

An identification made by Hugo (1989) at a slightly different region led to the following approximate linear model

$$y(s) = \begin{bmatrix} -\dfrac{3.7}{49.4s+1} & \dfrac{4.2}{31.5s+1} \\ \dfrac{6.6}{83.2s+1} & -\dfrac{20.0}{49.4s+1} \end{bmatrix} u(s) \qquad (4.26)$$

The same sequence of set point changes that were made in Figures 4.5 and 4.6 were repeated for both IMC designs but with P replaced by (4.26). The results are shown in Figures 4.16 and 4.17.

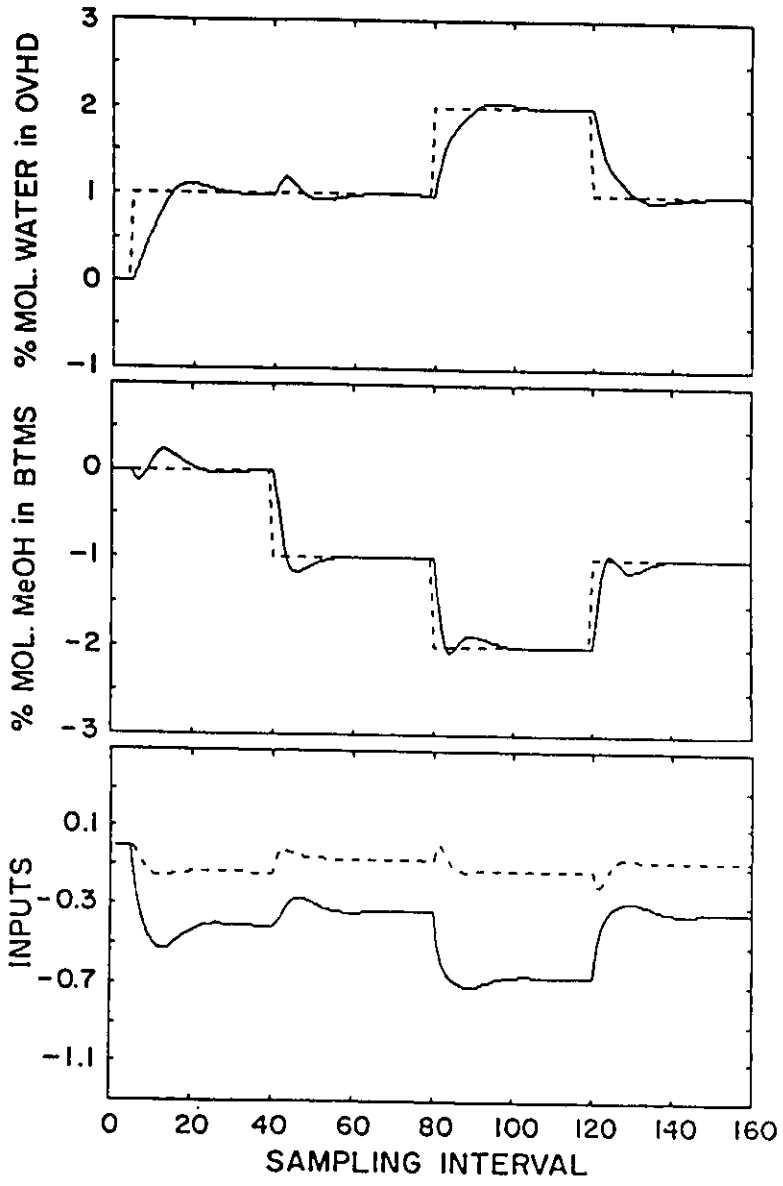

FIGURE 4.16: Simulated Distillation Column Control With Model Mismatch: Design 1
$Q_1 = Diag(3.75, 1)$, $Q_2 = Diag(75, 75)$, $f_{i,l} = 0$
curve identification as in Figure 4.5

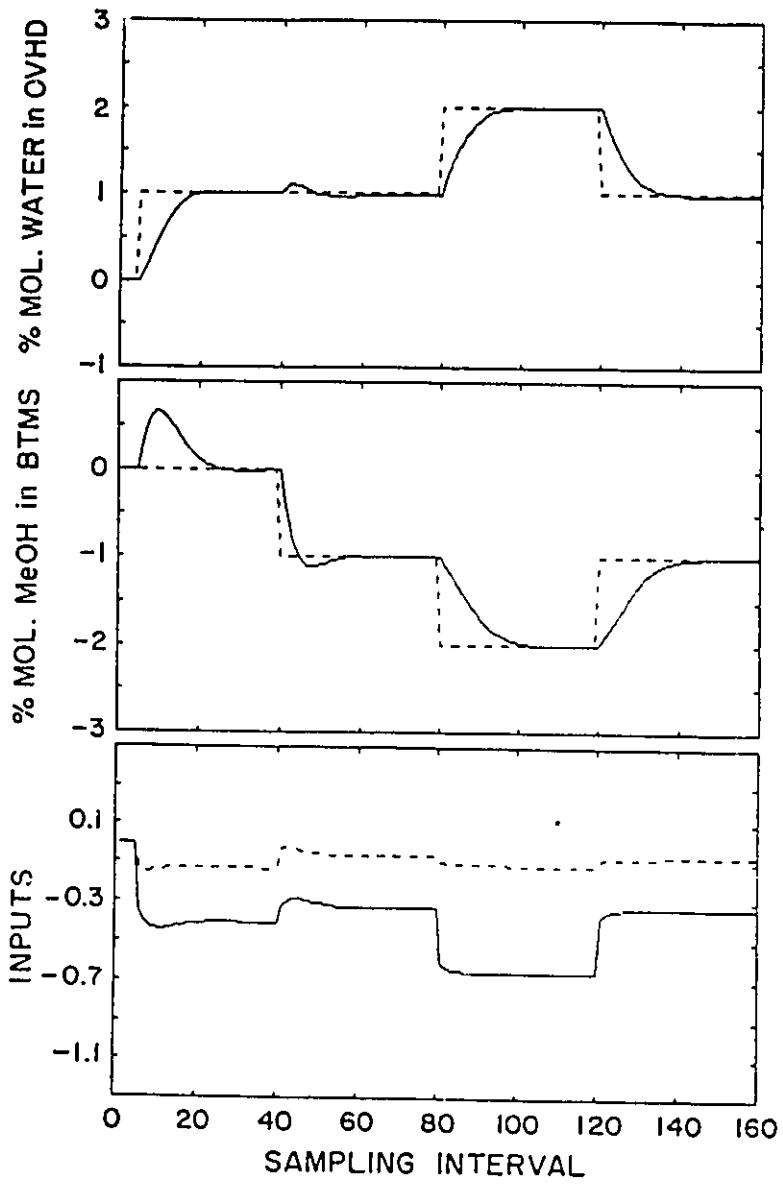

FIGURE 4.17: Simulated Distillation Column Control With Model Mismatch: Design 2 Decoupled, $f_{i,i} = 0.8$
curve identification as in Figure 4.5

Relative to the nominal output responses shown in Figures 4.5 and 4.6, both controlled responses of y_1, are not seriously affected by this particular type of mismatch. However, some significant differences in the responses of y_2, can be seen in these figures. The first IMC design arrived at by adjusting Q_1 and Q_2 in (4.8) led to a much better response in y_2, than the decoupled IMC design.

In both examples considered above, the simulation results appear to be consistent with the robustness trends predicted by the Kappa analysis using structured singular values, and yet again not consistent with those trends predicted by the unstructured singular value analysis.

4.7 SUMMARY AND CONCLUSIONS

The design of Internal Model Controllers (IMC) consists of finding stable and causal approximate model inverse block Q. A matrix spectral factorization approach has been proposed in this chapter as a very straightforward and computationally efficient method for obtaining inverses which yield excellent controller performance and robustness properties. The procedure allows one to arrive at LQ or ISE optimal inverses for any choice of output and input penalty weighting matrices. It automatically handles multivariable process transfer function matrices of arbitrary order, with unbalanced deadtime, with noninvertible zeros, and nonsquare systems. The resulting inverses are shown to provide many desirable properties in IMC controllers including guaranteed nominal stability, no steady state offset, optimal nominal performance, desirable singular values and condition numbers, and excellent robustness properties.

This spectral factorization design approach was compared against two other commonly used IMC design methods: (i) the ISE optimal inverse (most easily obtained via spectral factorization) combined with a tunable, diagonal first order filter, and (ii) the minimum settling time decoupled inverse combined with a tunable, first order diagonal filter.

Two simulation case studies were considered: (i) a multivariable packed bed catalytic reactor, and (ii) a binary distillation column. The results of the simulation studies on nominal performance demonstrated that the different IMC design approaches can lead to very different time domain output and input responses, even when designed to meet the same nominal output ISE performance specifications. As expected, the LQ inverses designed by spectral factorization provide the best nominal performance.

Analyzing the robustness properties of the multivariable controllers is much more difficult. In this work four approaches to robustness analysis were employed to evaluate and compare these IMC designs. Firstly, by examining the condition numbers and singular values of the approximate models being inverted

(Q^{-1}), it was shown that a fundamental problem with designs using diagonal filters is that the condition numbers of the approximate models are not improved by tuning the filter constants. Detuning via diagonal filters simply decreases all the controller gains equally at higher frequencies. On the other hand, the spectral factor inverses tuned by adjusting weights Q_2 in the quadratic objective function are shown to not only decrease the controller gains at high frequencies, but to greatly improve the condition numbers as well.

A second, commonly used approach to robustness assessment, based on a singular value analysis of the nominal closed-loop system and relying upon very conservative unstructured uncertainty characterizations (Doyle and Stein, 1981), was shown to be at odds with all the other robustness assessment methods investigated here. It did not even appear capable of ranking the designs in the correct relative order. This was attributed to the unrealistic unstructured uncertainty characterization used by this method.

The third approach to analyzing the relative robustness of the different MIMO designs made use of a more meaningful and less conservative single parameter uncertainty characterization based on equal percentage disk uncertainties in each element at every frequency relative to the nominal transfer function matrix. The amount by which the percent disk radii in all elements of the model transfer function can be increased at each frequency and still maintain stability of the closed-loop system was used as a measure of robustness. This new measure of relative robustness ($\kappa(\omega)$), introduced in chapter 2, was computed using a structured singular value analysis (Doyle, 1982). By plotting $\kappa(\omega)$ versus ω, the relative robustness of the various controller designs was compared in the frequency range of interest. Performing this analysis on the two examples of this paper showed the spectral factorization designs to be the most robust of the designs considered, particularly in the higher frequency regions.

Finally the relative robustness of the different nominal IMC designs was addressed by performing simulation studies on the two example processes using some mismatch models actually identified from data collected from these processes under different operating conditions. In both cases the simulation studies confirmed the relative robustness rankings indicated by the Kappa index and the singular value analysis on Q^{-1}.

In summary, assessing the relative robustness of various controller designs is very dependant upon the model uncertainty used. Different characterizations can lead to totally contradictory results. It appears that a much more thorough understanding of the nature of the uncertainties is necessary if one is to put much faith in the conclusion of any robustness analysis.

4.8 NOTATION

d_t	output disturbance vector at t
e_t	output error from set point
E	expectation
$f_{i,i}$	first order exponential filter factor for output i
F	IMC filter block transfer function
H^2	quadratic or 2-norm
H^∞	infinity norm
i	square root of -1
J	quadratic cost function
K	scaling matrix for nonsquare approximate inverses
L	left polynomial matrix in process transfer function model
m	number of inputs
m_m	minimum singular value of M_m
M_m	multiplicative output perturbation transfer function matrix
n	number of inputs
N	horizon in quadratic cost function
P	true process matrix transfer function
P_n	nominal process matrix transfer function
$\tilde{P}_n$	approximation to P_n with causal and stable inverse
Q	approximate model inverse in IMC design
Q_1	output error penalty weighting matrix in quadratic cost function
Q_2	input weighting matrix in quadratic cost function
s	Laplace transform operator
S_n	nominal sensitivity matrix operator
t	discrete time sampling period
T	sampling interval

T_n nominal complementary sensitivity matrix operator

u_t input vector at sampling period t

v_t input vector to disturbance transfer function Ψ at period t

V rational matrix operator used to make exact model inverse causal and stable in IMC design

y_t output vector at sampling period t

W_1 matrix transfer function weight on S_n

W_2 matrix transfer function weight on T_n

y_{sp_t} output set point at period t

z^{-1} backward shift operator

Greek Letters

γ condition number

Γ matrix spectral factor polynomial

Γ_1 matrix spectral factor for nonsquare processes

∇ backwards difference operator $(1 - z^{-1})$

κ nominal model equal percentage element-by-element disk uncertainty tolerance

λ_j j'th eigenvalue

σ_j j'th singular value

σ_m minimum singular value

σ_M maximum singular value

Σ_e output error variance matrix

$\Sigma_{\nabla u}$ input move variance matrix

Ψ disturbance matrix transfer function

ω radian frequency

INCORPORATION OF ARIMA DISTURBANCE MODELS IN DYNAMIC MATRIX CONTROLLERS

5 INCORPORATION OF ARIMA DISTURBANCE MODELS IN DMC

5.1 INTRODUCTION

Dynamic Matrix Control (DMC) or Quadratic Dynamic Matrix Control (QDMC) is a finite horizon, linear quadratic (LQ) approach to multiple input/multiple output (MIMO) controller design. DMC appears to have been first introduced by Cutler and Ramaker (1979), and later extended to QDMC by Garcia (1984) to handle constraints on the feasible range of the inputs and outputs. In recent years, this approach has become very popular and has been successfully applied to a wide range of chemical process applications. Its industrial success can be attributed to conceptual simplicity (i.e. no Ricatti, spectral factorization, and/or Diophantine equations involved), favorable robustness properties, and its ability to easily handle operating constraints. DMC/QDMC is a model predictive controller design, and therefore is closely related to other future finite horizon, model predictive controller designs such as Model Predictive Heuristic Control (IDCOM) (Richalet et al., 1978; Froisy and Richalet, 1986), Internal Model Control (IMC) (Garcia and Morari, 1982, 1985b), Model Algorithmic Control (MAC) (Rouhani and Mehra, 1982), Generalized Predictive Control (GPC) (Clarke et al., 1987a, b), and Multivariable Optimal Constrained Control (MOCCA) (Stripada et al., 1985). Therefore the results in this thesis will also apply to the entire class of designs stated above.

The objective in chemical process control problems is often regulatory in nature. Hence the effectiveness of DMC depends heavily on the assumptions made concerning the disturbances that enter the process. The usual assumption made in DMC is that the disturbance computed at the current sampling interval will remain constant over the future predicted responses. This is equivalent to assuming that disturbances enter as decoupled deterministic steps or, in a stochastic sense, behave as independent random walks. This assumption can often lead to poor disturbance regulation in a real process environment. This is especially true when operating under very noisy process conditions or when a noticeable lag (high autocorrelation) can be observed in the disturbances entering the loop. Garcia and Prett (1986) have found that the standard assumption only works well when the measurement noise level is low and the disturbance dynamics are fast and infrequent. Clearly, this is the trend that one would expect from the assumed random walk disturbance characterization.

The importance of disturbance prediction in finite future horizon, model predictive controller designs has been recognized by other researchers. Navratil et al. (1988) and Li et al. (1989) considered the incorporation of a feedback disturbance prediction in the DMC strategy. To achieve this goal, they proposed that the DMC strategy be transformed into a discrete time, state space form so that disturbance filtering and prediction could be realized through the incorporation of a Kalman filter. This modified DMC approach, which they coined Multivariable Optimal, Constrained Control Algorithm (MOCCA), was demonstrated to significantly improve disturbance rejection in the presence of noisy measurements relative to the standard DMC approach in a distillation column and level control example. The unfortunate consequence of their approach is that all the transparency and simplification of DMC becomes lost in a meaningless, and often less well understood, state space framework simply for the sake of improved disturbance forecasting. In addition, more complexity is introduced into the DMC design since an effective disturbance model must be incorporated into the state space process representation together with noise covariance matrices that are needed to tune the Kalman filter. The authors have failed to provide general guidelines for addressing this important latter issue.

Clarke et al. (1987a, b) have also included a feedback disturbance predictor in a DMC type design which they coined Generalized Predictive Control (GPC). Instead of using convolution models, GPC makes use of CARIMA (Controlled Auto-Regressive, Integrated Moving Average) models in the form

$$A(z^{-1})y_t = B(z^{-1})u_{t-1} + \frac{C(z^{-1})}{1-z^{-1}}a_t \tag{5.1}$$

where $A(z^{-1})$, $B(z^{-1})$, and $C(z^{-1})$ are finite order polynomials in z^{-1}, the backward shift operator, and a_t is a Gaussian white noise random shock. These model forms have been popular in self tuning controller applications (Astrom and Wittenmark, 1984). To make disturbance predictions in GPC, a series of p Diophantine equations, where p is equal to the output prediction horizon, need to be solved to obtain p polynomial operators that operate on the measured outputs to provide predictions of the disturbances over p future periods. A computationally efficient procedure is outlined for obtaining these polynomial operators. The drawback with their approach is that a large number of operator polynomials will need to be stored to generate forecasts, especially when large output horizons are taken. Furthermore, their method is not computationally efficient in generating forecasts since different forecasting polynomials are needed for the future disturbance prediction at different future periods of time. Another criticism of GPC is the use of the CARIMA model form which does explicitly separate the process dynamics from the disturbance dynamics. This is important when one wishes to design a controller for a servo application, or for regulation of a disturbance other than the one

identified. When this situation arises, it is crucial to be able to separate the process dynamic terms from the CARIMA model. Surprisingly enough, the authors failed to do so in an example where a random walk disturbance is assumed and they mistakenly choose $C(z^{-1}) = 1$.

The objective in this work is to propose a straightforward approach to predicting disturbances in the DMC/QDMC algorithm. The method of disturbance prediction shall be based on well-known techniques of forecasting using ARIMA (Autoregressive, Integrated Moving Average) stochastic disturbance models (Tiao and Box, 1981; Wilson, 1970). It will be demonstrated that the use of ARIMA models to predict future disturbances requires only a trivial modification to the standard DMC/QDMC algorithm, and that disturbance forecasts can be generated with computational efficiency.

The sections that follow will begin with a brief review of DMC/QDMC for the benefit of readers not familiar with the concept. A general approach to predicting disturbances in DMC will then be outlined, followed by simulation studies showing the benefits of improved disturbance filtering and forecasting.

5.2 MODEL FORMULATION

The heart of DMC/QDMC is the discrete time, step response convolution model employed in the design. This linear model form is given by

$$y(i,t) = \sum_{j=1}^{r}\sum_{l=1}^{n} a(i,j,l)\nabla u(j,t-l) + a(i,j,n)\sum_{j=1}^{r}\sum_{l=n+1}^{\infty} \nabla u(j,t-l) + d(i,t) \qquad (5.2)$$

where

$y(i,t)$: i'th output at interval t

∇: difference operator $(1-z^{-1})$

$u(j,t-l)$: j'th input at interval $t-l$

$a(i,j,l)$: step response coefficient relating effect of $t-l$ past move of the j'th input to output i.

r: number of inputs

$d(i,t)$: effect of process disturbances on output i at interval t

n: finite order approximation to step response convolution model

This model form can be easily obtained from an open-loop step test identification on a process provided that no disturbances are present, and that the level of noise in the process is low. If process noise and/or disturbances are present, well-known time series and process identification techniques (Box and Jenkins, 1976; Tiao and Box, 1981; Wilson, 1970; Kashyap and Rao, 1976) should be used instead. The model obtained from the latter approach can be readily transformed to the step response convolution form needed in DMC/QDMC, and in addition, offer valuable information on the nature of disturbances entering the process that ultimately will lead to improved disturbance prediction in the DMC algorithm.

5.3 DMC FORMULATION

The objective of the DMC/QDMC approach is to best match the prediction of the output over an output horizon of p intervals into the future to a target set point using m future control moves. Using (5.2) we may predict the $t+k$ future output from a current sampling interval t by

$$y(i,t+k) = \sum_{j=1}^{r}\sum_{l=1}^{k} a(i,j,l)\nabla u(j,t+k-l) + y^{\circ}(i,t+k) + d(i,t+k) \tag{5.3}$$

where

$$y^{\circ}(i,j+k) = \sum_{j=1}^{r}\sum_{l=k+1}^{n} a(i,j,l)\nabla u(j,t+k-l) + a(i,j,n)\sum_{l=n+1}^{\infty}\nabla u(j,t+k-l) \tag{5.4}$$

In (5.3) it can be seen the prediction of output i at future interval $t+k$ consists of three components. The first term represents the effect that unknown future input moves will have on $y(i,t+k)$. The second term represents the effect on $y(i,t+k)$ of input moves already made on the process. In (5.4) it is shown that this term can be computed through the step response convolution model. It is not necessary that this model form be used to compute $y^{\circ}(i,j+k)$. If a transfer function model or a state space representation (Navratil et al., 1988) of the process is used to compute $y^{\circ}(i,t+k)$, it can be shown that the computational efficiency of DMC/QDMC can be substantially improved. The final contribution to $y(i,t+k)$ is the effect of the future unknown disturbance $d(i,t+k)$. This term will also account for model mismatch, and if the process is nonlinear, mismatch due to the linear representation of the process. The standard assumption taken in DMC is

$$d(i,t+k/t) = d(i,t) \tag{5.5}$$

which indicates that the disturbance is assumed fixed at $d(i,t)$ over the future output prediction horizon. In section 5.6 a more general procedure shall be outlined to predict $d(i,t)$.

Having defined the prediction of one output at k future periods, we similarly proceed in predicting the effect of r inputs over m future moves on w outputs over p future periods. These predictions are summarized below:

$$e_{k+1} = A\nabla U_k \tag{5.6}$$

A: Dynamic matrix of MIMO system

$$A = \begin{bmatrix} A(1,1) & A(1,2) & \cdots & A(1,r) \\ A(2,1) & A(2,2) & \cdots & A(2,r) \\ \vdots & \vdots & \cdots & \vdots \\ A(w,1) & A(w,2) & \cdots & A(w,r) \end{bmatrix}_{(wp)\times(rm)} \tag{5.7}$$

$A(i,j)$: Dynamic matrix relating p future responses of output i to m future moves in input j

$$A(i,j) = \begin{bmatrix} a(i,j,1) & 0 & 0 & 0 & \cdots & 0 \\ a(i,j,2) & a(i,j,1) & 0 & 0 & \cdots & 0 \\ a(i,j,3) & a(i,j,2) & a(i,j,1) & 0 & \cdots & 0 \\ \vdots & \vdots & \vdots & \vdots & \cdots & \vdots \\ \vdots & \vdots & \vdots & \vdots & \cdots & \vdots \\ a(i,j,m) & a(i,j,m-1) & a(i,j,m-2) & \cdots & \cdots & 0 \\ \vdots & \vdots & \vdots & \vdots & \cdots & \vdots \\ \vdots & \vdots & \vdots & \vdots & \cdots & \vdots \\ a(i,j,p) & a(i,j,p-1) & a(i,j,p-2) & \cdots & \cdots & a(i,j,p-m+1) \end{bmatrix}_{p\times m} \tag{5.8}$$

$e(k+1)$: Projection of the error between the output and set point over p future periods if no further input moves are made

$$e_{k+1} = \begin{bmatrix} Y_{sp}(1) \\ Y_{sp}(2) \\ \vdots \\ Y_{sp}(w) \end{bmatrix}_{(wp)\times 1} - \begin{bmatrix} Y^*(1) \\ Y^*(2) \\ \vdots \\ Y^*(w) \end{bmatrix}_{(wp)\times 1} - \begin{bmatrix} D(1) \\ D(2) \\ \vdots \\ D(w) \end{bmatrix}_{(wp)\times 1} \tag{5.9}$$

$Y_{sp}(i)$: Set point vector for output i over horizon p

$$Y_{sp}(i) = \begin{bmatrix} y_{sp}(i,t+1) \\ y_{sp}(i,t+2) \\ \cdot \\ \cdot \\ \cdot \\ y_{sp}(i,t+p) \end{bmatrix}_{px1} \tag{5.10}$$

$Y^*(i)$: Vector of the predicted effect of past input moves on output i over p future intervals

$$Y^*(i) = \begin{bmatrix} y^*(i,t+1) \\ y^*(i,t+2) \\ \cdot \\ \cdot \\ \cdot \\ y^*(i,t+p) \end{bmatrix}_{px1} \tag{5.11}$$

$D(i)$: Vector predicting effect of disturbances on output i over p future periods

$$D(i) = \begin{bmatrix} d(i,t+1/t) \\ d(i,t+2/t) \\ \cdot \\ \cdot \\ \cdot \\ d(i,t+p/t) \end{bmatrix}_{px1} \tag{5.12}$$

∇U_k: Vector of all future input moves

$$\nabla U_k = \begin{bmatrix} \nabla U(1) \\ \nabla U(2) \\ \cdot \\ \cdot \\ \cdot \\ \nabla U(r) \end{bmatrix}_{mx1} \tag{5.13}$$

$\nabla U(j)$: Vector of m future input moves for input j

$$\nabla U(j) = \begin{bmatrix} \nabla u(j,t) \\ \nabla u(j,t+1) \\ \cdot \\ \cdot \\ \cdot \\ \nabla u(j,t+m-1) \end{bmatrix}_{mx1} \tag{5.14}$$

At this point all that remains in the DMC/QDMC algorithm is an approach for computing ∇U_k in (5.6) which is optimal in some sense.

5.4 CONTROL MOVE COMPUTATION

In DMC/QDMC the best sequence of control moves ∇U_k is found through the minimization of the linear quadratic (LQ) performance index

$$J = \frac{1}{2}\{ \sum_{i=1}^{m}\sum_{k=1}^{p}(y_{sp}(i,t+k)-y(i,t+k))^2 W(i,k) + \sum_{j=1}^{r}\sum_{k=1}^{m}\nabla u(j,t+k-1)^2 R(j,k) \quad (5.15)$$

Relative to (5.6), equation (5.15) can also be expressed as

$$J = \frac{1}{2}\{ (e_{k+1}-A\nabla U_k)^T W(e_{k+1}-A\nabla U_k) + \nabla U_k^T R \nabla U_k \} \quad (5.16)$$

W is a diagonal weighting matrix for the process outputs. W is typically used to scale the outputs or assign a relative importance between the outputs in a MIMO control problem. R is a diagonal input move penalty weighting matrix. This matrix is used to tune the DMC/QDMC controller so that control actions are acceptable.

It can be shown that the minimization of (5.16) with respect to ∇U_k can also be represented in the standard QP form given below:

$$\underset{\nabla U_k}{\text{Min}} \left\{ \frac{1}{2}\nabla U_k^T (A^T W A + R)\nabla U_k - e_{k+1}^T W A \nabla U_k \right\} \quad (5.17)$$

If no input constraints are present, the solution for ∇U_k in (5.17) is given by

$$\nabla U_k = \bar{A}^{-1} e_{k+1} \quad (5.18)$$

where $\bar{A}^{-1}$, the pseudo dynamic matrix inverse, is given by

$$\bar{A}^{-1} = (A^T W A + R)^{-1} A^T W \quad (5.19)$$

If linear constraints are present, such as for example on the feasible range of the inputs as

$$u(j)_{low} \le u(j,t+k-1) \le u(j)_{high} \qquad j=1,r \quad k=1,m \quad (5.20)$$

the QDMC approach is taken whereby (5.17) is solved on-line using any constrained QP routine.

The optimal control action in DMC/QDMC is recalculated on-line at every control interval t, and only the control action called for at sampling interval t is applied. In this way the controller can adapt immediately to unaccounted for disturbances and mismatch between the true process and the model by reforming the projected error vector e_{k+1} at every sampling interval and recomputing ∇U_k.

5.5 MODELLING OF DISTURBANCES

The objective of this work is to extend the DMC/QDMC concept in a straightforward manner to handle more general types of disturbances. To do so, information on the nature of disturbances entering the process must be provided. A powerful, and well-known technique for identifying disturbance trends from discrete process data is through multivariate time series analysis (Box and Jenkins, 1976; Tiao and Box, 1981; Kashyap and Rao, 1976; Goodwin and Payne, 1977; Wilson, 1970). This technique may be used to identify MIMO process transfer functions and disturbance models in many different canonical forms. The work that follows will make use of ARIMA (Auto Regressive, Integrate Moving Average) disturbance models as suggested by Tiao and Box (1981). The form of these disturbance models is given by

$$d_t = \phi(z^{-1})^{-1}\theta(z^{-1})\nabla^{-q}a_t \tag{5.21}$$

where

$$\theta(z^{-1}) = I + \theta_1 z^{-1} + \ldots\ldots + \theta_e z^{-e} \tag{5.22}$$

$$\phi(z^{-1}) = I + \phi_1 z^{-1} + \ldots\ldots + \phi_v z^{-v} \tag{5.23}$$

$$d_t = \begin{bmatrix} d(1,t) \\ d(2,t) \\ \cdot \\ \cdot \\ \cdot \\ d(w,t) \end{bmatrix} \tag{5.24}$$

and a_t is assumed to be a vector sequence of random shocks, identically independent and normally distributed with zero mean and covariance matrix Σ_{a_t}. It is assumed that $det\{\phi(z^{-1})\}$ and $det\{\theta(z^{-1})\}$ will have no roots in z that lie outside the unit circle. Nonstationarity of d_t is accounted for by the integer $q > 0$. Nonstationarity of d_t is essential if integral action is to be present in the DMC/QDMC design.

A left matrix fraction form is used in (5.21). This form was chosen over a right matrix fraction form since the former offers advantages in computational efficiency. However, a right fraction form can also be applied to the results that follow, and will only require slight modifications. The ARIMA disturbance model form was also chosen over other MIMO disturbance model forms for basically two reasons. First the dynamics of the disturbance transfer function are separated from dynamic terms associated with the process transfer function. This is important when one chooses to design the controller for a disturbance that is different from the type identified. This would likely be the situation when one identifies a stationary disturbance model and

would prefer a nonstationary disturbance model so that integral action will be present in the DMC/QDMC design. The second reason for using the ARIMA structure is the computational efficiency and simplicity that the form offers in generating forecasts relative to other forms where solutions to Diophantine equations are required (Clarke et al., 1987; Kashyap and Rao, 1976).

The disturbance model given by (5.21) has been assumed to be stochastic. This assumption may be relaxed in the results to follow by assuming that a_t is zero mean but has a probability distribution other than Gaussian. The deterministic case would be represented by a_t having a probability distribution which is zero most of the time and infrequently takes on some nonzero value (MacGregor, 1984). Any identified deterministic disturbance model can be transformed into the form given by (5.21). However, when doing so, one must pay strict attention to the assumption made on (5.21), mainly that $\theta(z^{-1})$ is causal (i.e. inverse has no predictive terms) and invertible (i.e. $det\{\theta(z^{-1})\}$ has no roots in z outside the unit circle). If the conditions on $\theta(z^{-1})$ do not hold, this polynomial matrix must be replaced by its invertible and causal least squares error approximation. The modification is obtained through the matrix spectral factorization equation (refer to chapter 4 for details)

$$\theta_D(z^{-1})\theta_D^T(z) = \theta(z^{-1})\theta^T(z) \tag{5.25}$$

where $\theta(z^{-1})$ is the unique invertible and causal replacement to the deterministically derived $\theta_D(z^{-1})$.

5.6 PREDICTION OF FUTURE DISTURBANCES

Given (5.21), the objective will be to outline a simple and computationally efficient procedure for generating $d_{t+k/t}$ for $k = 1$ to p.

Suppose at sampling interval t we wish to make a prediction of the disturbance at future interval $t+k$ ($d_{t+k/t}$). Using (5.21), d_{t+k} is given by

$$d_{t+k} = \phi(z^{-1})^{-1}\theta(z^{-1})\nabla^{-c}a(t+k) \tag{5.26}$$

By performing simple long division on the rational elements of the polynomial matrix fraction, (5.26) can be modified to

$$d_{t+k} = \Psi(z^{-1})a_{t+k} + \phi(z^{-1})^{-1}T(z^{-1})\nabla^{-c}a_t \tag{5.27}$$

where

$$\Psi(z^{-1}) = I + \Psi_1 z^{-1} + \ldots + \Psi_{k-1}z^{-k+1} \tag{5.28}$$

$$T(z^{-1}) = T_0 + T_1 z^{-1} + \ldots\ldots + T_n z^{-n} \tag{5.29}$$

The first term in (5.27) contains future unknown random shocks which cannot be predicted. The second term contains present and past information and represents the minimum mean squared error forecast of the disturbance. Hence the minimum variance prediction of d_{t+kt} is given by

$$d_{t+kt} = \phi(z^{-1})^{-1} T(z^{-1}) \nabla^{-q} a_t \tag{5.30}$$

Equation (5.30) is only suited for generating a single forecast at k future sampling periods. When generating forecasts for the DMC/QDMC projected error vector e_{k+1}, we require $k = 1$ to $k = p$ forecasts of d_{t+kt}. In general, $T(z^{-1})$ changes with different k step ahead forecasts. If (5.30) were used, p separate finite difference equations to forecast the disturbances would be required, as in the method of Clarke at al. (1987). To avoid this, a more efficient method of generating a large number of forecasts based on the forecast update equation of Box and Jenkins (1976) is employed. Let (5.21) be instead represented in convolution form as

$$d_t = (I + \Psi_1 z^{-1} + \Psi_2 z^{-2} + \ldots\ldots) a_t \tag{5.31}$$

We can express the $t+k$ step ahead disturbance forecast at origins t and $t-1$ as

$$d_{t+kt} = \Psi_k a_t + \Psi_{k+1} a_{t-1} + \Psi_{k+2} a_{t-2} + \ldots\ldots \tag{5.32}$$

$$d_{t+kt-1} = \Psi_{k+1} a_{t-1} + \Psi_{k+2} a_{t-2} + \Psi_{k+3} a_{t-3} + \ldots\ldots \tag{5.33}$$

Subtraction of (5.33) from (5.32) leads to

$$d_{t+kt} = d_{t+kt-1} + \Psi_k a_t \tag{5.34}$$

The first term in (5.34) represents the disturbance prediction at the previous interval. The second term is a correction added to the old forecast from the new information made available. Note that a_t is obtained through

$$a_t = d_t - d_{tt-1} \tag{5.35}$$

Equation (5.34) when combined with just one finite difference equation of the form (5.30) to forecast d_{t+p+1t} provides a simple method for generating p forecasts at successive intervals. Note that this method requires the storage of only three matrix polynomials, $T(z^{-1})$, $\Psi(z^{-1})$, and $\Phi(z^{-1})$ to generate all the disturbance forecasts over p future outputs. This approach is clearly far more efficient than that of Clarke at al. (1987) were p matrix polynomials are required.

In summary, the recommended algorithm for generating disturbance forecasts in the DMC/QDMC projected error vector e_{k+1} is outlined below:

1) Compute a_t from (5.35).

2) Compute forecasts $d_{t+1|t}$ through $d_{t+p|t}$ using (5.34).

3) Compute $d_{t+p+1|t}$ using (5.30) for next interval.

4) Update all storage information for next time through.

5.7 COMMON ARIMA MODEL FORMS

In this section three ARIMA disturbance model forms, that are commonly encountered in chemical processes are discussed in terms of their effect on disturbance prediction in DMC/QDMC.

The first type of disturbance model that is often encountered is a random walk. Relative to (5.21), this disturbance type is represented by $q = 1$, $\phi(z^{-1}) = I$, $\theta(z^{-1}) = I$, leading to

$$d_t = \nabla^{-1} a_t \tag{5.36}$$

This model represents a drifting disturbance with a changing mean level. This disturbance trend would be observed in processes where the dynamics of the disturbances are fast relative to the sampling interval and the level of measurement noise is low compared the disturbances that enter. It can be shown that for this case

$$\Psi_k = I \qquad k = 1, p \tag{5.37}$$

$$T_k(z^{-1}) = I \qquad k = 1, p \tag{5.38}$$

and that

$$d_{t+k|t} = d_t \qquad k = 1, p \tag{5.39}$$

Note that the optimal forecast equation (5.39) is identical to the type used in the standard DMC/QDMC algorithm proposed by Cutler and Ramaker (1979).

The second common disturbance model is an integrated moving average model of degree 1. Relative to (5.21), this model form is given by $q = 1$, $\phi(z^{-1}) = I$, $\theta(z^{-1}) = I + \theta_1 z^{-1}$, leading to

$$d_t = (I + \theta_1 z^{-1}) \nabla^{-1} a_t \tag{5.40}$$

This disturbance model form is well suited for representing processes where the dynamics of the disturbances are fast relative to the sampling period and the measurements are highly corrupted by additive noise. The optimal forecasts for this case are generated by

$$\Psi_k = I + \theta_1 \qquad k = 1, p \tag{5.41}$$

$$T_k(z^{-1}) = I + \theta_1 \qquad k = 1, p \tag{5.42}$$

or

$$d_{t+k|t} = (I+\theta_1)(I+\theta_1 z^{-1})^{-1} d_t \qquad k=1,p \tag{5.43}$$

Note that for this case $T(z^{-1})$ is also a constant matrix, independent of p, and that forecasts of $d_{t+k|t}$ are the same regardless of k. Hence the disturbance predictor given by (5.43) is a first order exponential filter of the type used in the Internal Model Control (IMC) algorithm proposed by Garcia and Morari (1985b). This filter form is also commonly used in SPC applications (MacGregor, 1988). The only difference between (5.43) and the filter design used in IMC is that θ_1 in the former approach is permitted to be a full matrix, and thus has the advantage of including multivariable disturbance interactions in the forecasts.

The optimal filter given by (5.41) to (5.43) only requires a very simple modification to the DMC/QDMC algorithm. For a similar disturbance trend as (5.40), Navratil et al. (1988) and Li et al. (1989) instead chose a roundabout approach whereby they reformulated the DMC concept in a state space framework and added on a Kalman filter to provide improved disturbance prediction. Clearly, the results from this section show that the use of the ARIMA disturbance model form leads to far less effort and greater transparency compared to the state space method.

The final disturbance form to be discussed will be the first order integrated autoregressive form with $q=1$, $\theta(z^{-1})=I$, $\phi(z^{-1})=(I+\phi_1 z^{-1})$, and d_t given by

$$d_t = (I+\phi_1 z^{-1})^{-1}\nabla^{-1} a_t \tag{5.44}$$

This model is well suited to representing the effect of random step disturbances with first order dynamics lags that are commonly encountered in chemical processes. The poles of the lags are indicated by the ϕ_1 matrix. For this disturbance form, Ψ_k and $T_k(z^{-1})$ will be different for each k. The consequence of the forecasts for this disturbance model would be to provide some phase lead to the DMC/QDMC design in order to track in more rapidly to the exponential change in the output. This will be demonstrated in the examples that follow.

5.8 SIMULATION CASE STUDIES

The examples that follow were selected to show the benefits of the proposed forecaster in the DMC/QDMC strategy. All simulations that follow will be performed using a nominal SISO process transfer function given by

$$P_n = \frac{0.2z^{-2}}{1-0.8z^{-1}} \tag{5.45}$$

No constraints on the manipulated input were considered, and therefore, DMC was applied. The output and input horizons in all of the DMC designs that follow were selected to be 10 and 9 respectively.

5.8.1 Stochastic First Order Integrated Moving Average Disturbance

In this case study the disturbance model was assumed to follow a stochastic, nonstationary first order moving average trend given by

$$d_t = \frac{1-0.9z^{-1}}{\nabla} a_t \tag{5.46}$$

with $var\{a_t\} = 1$. A very noisy and drifting trend is exhibited by this disturbance model.

Table 5.1 summarizes the simulated performance of two different DMC designs in regulating disturbance (5.46).

TABLE 5.1: DMC PERFORMANCE WITH STOCHASTIC NONSTATIONARY MOVING AVERAGE DISTURBANCE

Design	$Var\{e_t\}$	$Var\{\nabla u_t\}$
1: $R = 0.5I, W = I$ Optimal Disturbance Prediction	1.07	0.03
2: $R = 2I, W = I$ Standard Disturbance Assumption	1.07	0.4

The table displays the calculated variances of the output error and the input moves in regulating the disturbance over 200 points. The first design was arrived at by selecting a penalty weight of 1 on the output error, a penalty weight of 0.5 on the input moves, and made use of the optimal disturbance forecaster modification of section (5.6) in the design. The second design was arrived at using $R = 2I$ and $W = I$, and made the standard DMC assumption that $d_{t+k|t} = d_t$. The results in Table 5.1 clearly show that the design 1 was significantly superior to design 2. For the same output error variance, design 1 required far less input action than design 2, even though less penalty weighting was placed on the input moves of the former. A design with far less input action

for the same level of performance would always be the preferred choice by plant personnel, and intuitively, would be expected to be more robust since less demand will be placed on the model in predicting future outputs.

5.8.2 Stochastic Nonstationary First Order Autoregressive Disturbance

In this case study, the disturbance is stochastic and follows an integrated, first order autoregressive trend. The disturbance model is given by

$$d_t = \frac{1}{\nabla(1-0.9z^{-1})}a_t \tag{5.47}$$

where $var\{a_t\} = 0.01$. Unlike the previous disturbance model, this process follows a less noisy, smoother drifting trend.

Table 5.2 shows the simulated performance of two different DMC designs from 200 data points.

TABLE 5.2: DMC PERFORMANCE WITH STOCHASTIC NONSTATIONARY AUTOREGRESSIVE DISTURBANCE

Design	$Var\{e_t\}$	$Var\{\nabla u_t\}$
1: $R = 0.5I, W = I$ Optimal Disturbance Prediction	0.1	0.22
2: $R = 0, W = I$ Standard Disturbance Assumption	0.13	0.25

The first DMC design used an input penalty weighting of $R = 0.5I$ and an output penalty weighting of $W = I$. Disturbance model (5.47) was used to forecast the disturbance. The second design placed no penalty weight on the input moves and makes the standard DMC disturbance prediction. The results in Table 5.2 show that design 1 was superior to design 2 in both the computed output error and input move variances. Note that design 2, the most tightly tuned standard DMC design ($R = 0$), could not match the performance of a penalized DMC design (design 1) with optimal disturbance prediction.

5.8.3 Deterministic Integrated First Order Autoregressive Disturbance

In this section the performance of the two DMC designs presented in Table 5.2 are again considered but with a_t in (5.47) assumed to be deterministic instead of Gaussian as in section 5.8.2. Throughout simulations that follow, a_t is fixed at 0 except at sampling period 10 where it takes on a value of 0.1. Hence the process at sampling interval 10 becomes subjected to a step disturbance with a first order exponential lag that asymptotically will increase the process output by 1 unit if no feedback control is applied.

Figures 5.1 and 5.2 show the performance of designs 1 and 2 respectively in Table 5.2 to the deterministic disturbance. The output performance of design 1 in Figure 5.1 with optimal disturbance prediction can be clearly seen to out perform the most tightly tuned standard DMC design in Figure 5.2 in regulating the disturbance. Furthermore, it can be shown that variance of input moves taken by design 1 is lower than that of design 2 even though design 1 displayed superior output performance.

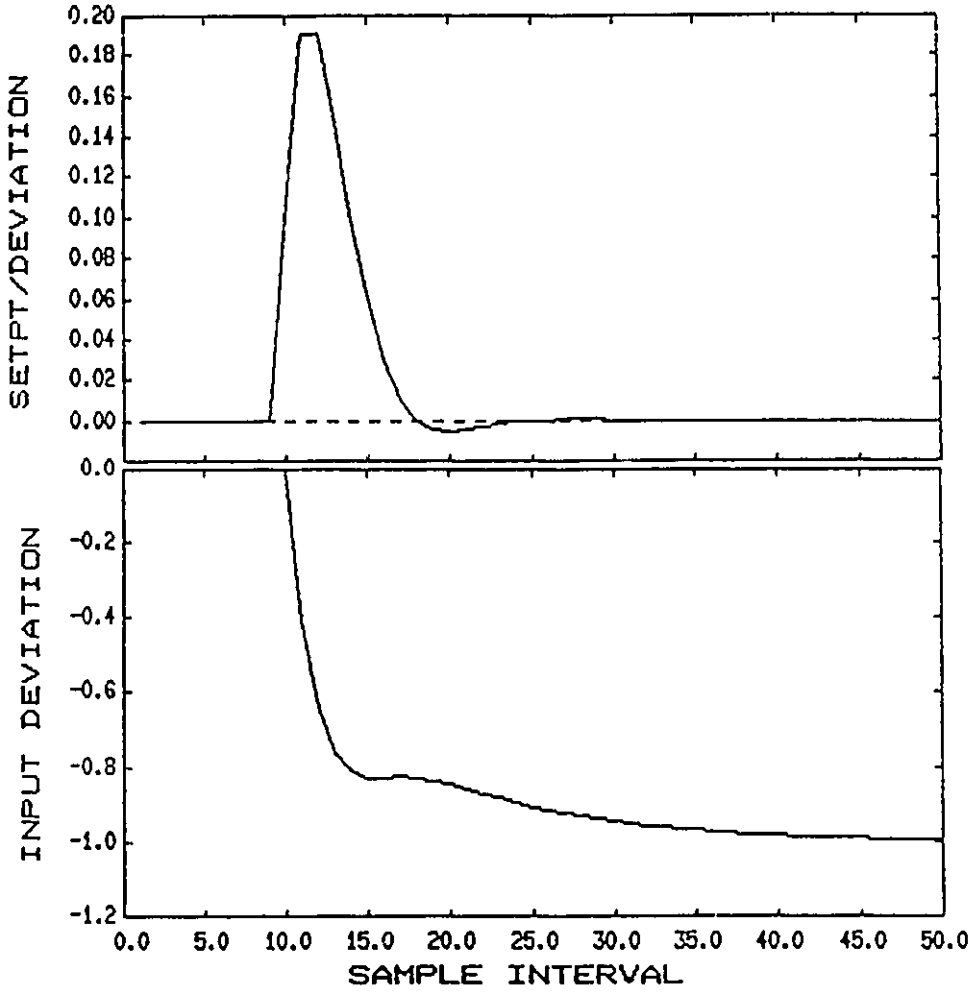

FIGURE 5.1: DMC Performance With Optimal Disturbance Prediction
Top: (-) output; (--) set point
Bottom: input response

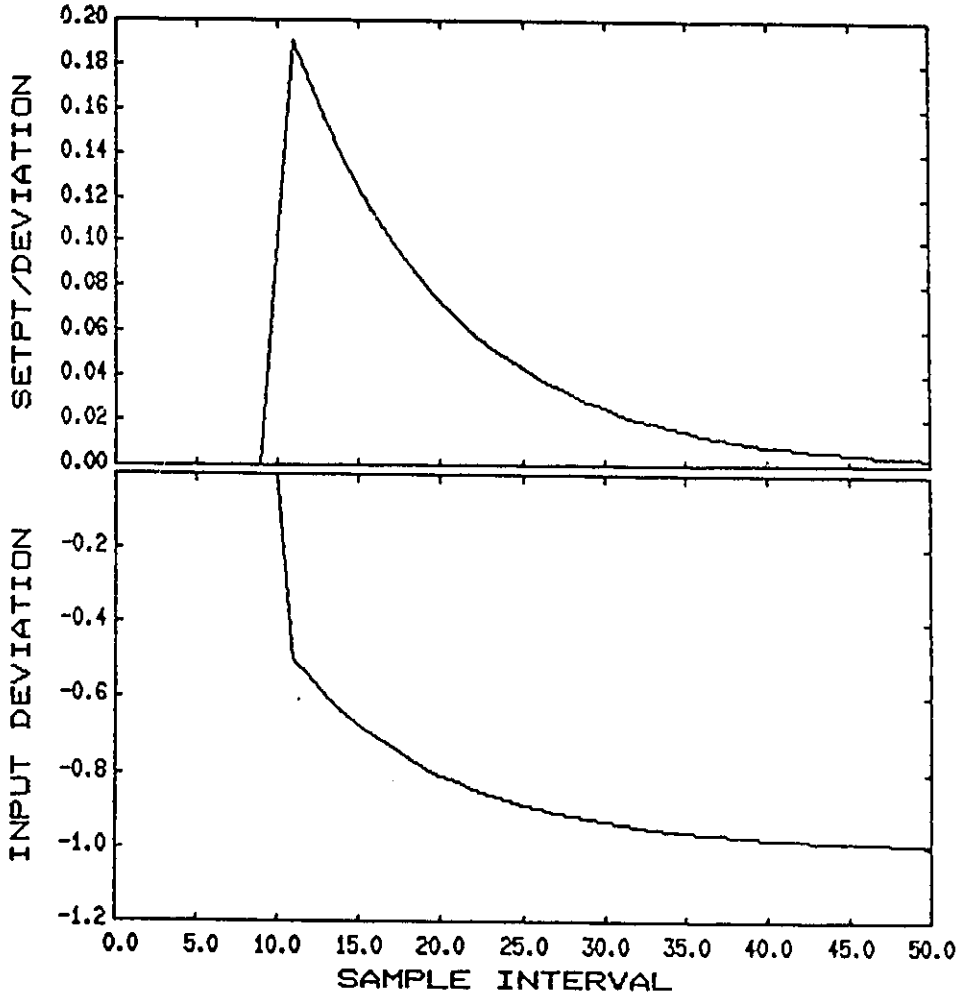

FIGURE 5.2: DMC Performance With Standard Disturbance Assumption
Top: (-) output; (--) set point
Bottom: input response

5.9 CONCLUSION

In this work a straightforward addition to the standard DMC/QDMC algorithm has been proposed to provide a general procedure to optimally forecast disturbances for future unknown output horizons. The formal approach, in principle, should lead to improved regulatory control when the standard DMC assumption of $d_{t+kH} = d_t$ is suboptimal. The method makes use of well-known ARIMA disturbance models that can be identified empirically from process data or from derived deterministic disturbance transfer functions. The mathematics involved in generating the forecast equations is trivial, requiring nothing more than the division of finite order polynomials. On-line computation of disturbance forecasts is computationally efficient, and only requires the evaluation of one matrix finite difference polynomial operator together with one recursive update equation p times. Only three matrix polynomial operators need to be stored.

The benefits of the proposed modification to the DMC/QDMC algorithm were demonstrated in three case studies. Both stochastic and deterministic disturbances were considered. In all cases considered, the modified DMC/QDMC design out performed a DMC design with the standard disturbance assumption in terms of both output error and cost of input manipulations.

5.10 NOTATION

$a(i,j,l)$	step response coefficient of input j on output i at lag l
a_t	Gaussian white noise random shock vector
A	dynamic matrix of MIMO process
$\bar{A}^{-1}$	pseudo dynamic matrix inverse
$A(i,j)$	dynamic matrix of output i with input j
$A(z^{-1})$	finite order polynomial in z^{-1} in CARIMA model form (eq. 5.1)
$B(z^{-1})$	finite order polynomial in z^{-1} in CARIMA model form (eq. 5.1)
$C(z^{-1})$	finite order polynomial in z^{-1} in CARIMA model form (eq. 5.1)
$d(i,t)$	effect of process disturbances on output i at interval t
d_t	vector representing additive effect of disturbances on the outputs at interval t
$D(i)$	vector holding disturbance effect prediction on output i over p future periods

$e(k+1)$	vector containing the projected error in all outputs over p future periods if no control actions are taken
J	quadratic cost function
k	future control interval
m	number of future input moves to be made in DMC
n	finite order approximation to step response convolution model
p	future output horizon in DMC
r	number of inputs
R	matrix holding all input move weightings over future horizon p
$R(i,k)$	t'th input move weighting at future period k
t	control interval
$T(z^{-1})$	left matrix polynomial in minimum variance ARIMA disturbance forecaster
$u(j,t-l)$	j'th input at interval t-l
$\nabla U(j)$	vector of m future input moves for input j
∇U_k	vector holding all future inputs moves at t
w	number of outputs
W	matrix containing the weighting for all output errors over p future periods
$W(i,k)$	output i error weighting at future period k
$y(i,t)$	response of output i at sampling period t
y^*	effect on output i of input moves already made on future predictions
$Y^*(i)$	vector of the predicted effect of past input moves on output i over p future intervals
$Y_{sp}(i)$	set point vector for output i over horizon p
z^{-1}	backwards shift operator

Greek Letters

∇	difference operator $(1-z^{-1})$
$\theta(z^{-1})$	right matrix polynomial in z^{-1} in MIMO ARIMA disturbance model
$\phi(z^{-1})$	left matrix polynomial in z^{-1} in MIMO ARIMA disturbance model
$\Psi(z^{-1})$	infinite order matrix polynomial representating convolution form of ARIMA disturbance model

STATE ESTIMATION AND CONTROL FOR SEMI-BATCH COPOLYMERIZATION REACTORS

6. STATE ESTIMATION AND CONTROL FOR SEMI-BATCH COPOLYMERIZATION REACTORS: INTRODUCTION

Semi-batch processes still pose an important challenge for the application of feedback control. This is especially true when faced with semi-batch, emulsion polymerization reactors. Difficulties include significant nonlinearities, absence of a steady state, inadequate dynamic models, lack of direct measurements of the properties needed to be controlled, and initial disturbance and/or model mismatch error which must be compensated for quickly during the finite period of batch/semi-batch operation. These operating characteristics essentially render useless much of the vast range of conventional and advanced linear model-based feedback control strategies, such as described in chapters 4 and 5, developed mainly for petrochemical continuous time type of processes. Furthermore, open-loop optimal control policies developed specifically for batch/semi-batch reactors contain no provisions to compensate for process variability and uncertainty.

Limited work has been reported concerning the development of inferential feedback control strategies for polymerization reaction processes. Often the focus is only on one particular aspect of the batch/semi-batch control problem. The purpose of the remainder of this thesis will be to propose a nonlinear, inferential feedback control strategy to improve quality control and product reproducibility of hot Styrene/Butadiene rubber (SBR) latex produced from an initially seeded semi-batch reactor. SBR is an industrially important synthetic rubber with widespread applications. The grade of SBR to be considered would find practical application in the production of adhesives, tire cord, carpet backing, coatings for textiles, paper, wood, and leather, liquid floor polishes, and as a fabric binder. Although this work pertains to the manufacture of SBR latex, it is expected that much of the ideas to follow can be applied to other semi-batch problems.

The block diagram of the control structure proposed in this work is shown in Figure 6.1.

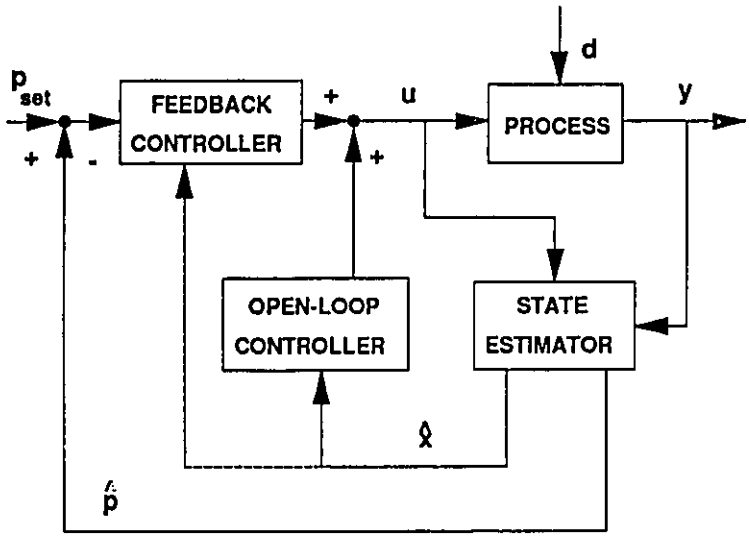

Figure 6.1: Nonlinear Inferential Feedforward/Feedback Control Strategy

It is consists of a nonlinear state estimator to infer copolymer properties (p) to be controlled from the available measurements (y), a feedforward control action block derived from some optimal instantaneous open-loop copolymer property control policy, and a linear or nonlinear feedback controller to compensate for errors still existing after the feedforward/open-loop actions are applied. The correct implementation of existing theories related to nonlinear state estimation, optimal open-loop polymer property control, and feedback control to the problem posed above are examined and evaluated. For the first time these theories are tied together to propose simple, but yet effective, production strategies for meeting a wide range of copolymer property specifications with limited variability from target specifications. The proposed control scheme will offer a simple alternative to computationally intensive on-line nonlinear optimization approaches, which in many circumstances, would not be considered practical.

The presentation of the semi-batch control scheme will be divided into 4 chapters. In chapter 7, the dynamic nonlinear SBR reaction model used in this simulation study is presented. Chapter 8 provides a discussion and some new results on the correct design and evaluation of nonlinear state estimators for copolymer property inference from limited, indirect measurements obtained from a semi-batch process. The development of useful open-loop operating policies for meeting a wide range of copolymer property specifications is covered in chapter 9. Chapter 10 deals with the design of linear and nonlinear feedback control strategies to compensate for errors in the open-loop optimal control actions when nonideal operating conditions are encountered. This final chapter also ties together all the work on the semi-batch copolymer control problem and demonstrates the effectiveness of the proposed scheme in Figure 6.1.

DYNAMIC MODEL FOR THE EMULSION COPOLYMERIZATION OF STYRENE/BUTADIENE

DYNAMIC MODEL FOR THE EMULSION COPOLYMERIZATION OF STYRENE/BUTADIENE

7. INTRODUCTION TO MODEL DEVELOPMENT

This chapter will provide a brief summary of the emulsion copolymerization styrene/butadiene rubber (SBR) model developed in this work for the purpose of a nonlinear feedback control study. It is expected that the reader is familiar with copolymer emulsion reaction modelling. Background material on emulsion copolymer reaction modelling can be found in Hamielec and Hoffman (1986), Ugelstad and Hansen (1976), and Rawlings and Ray(1988). A detailed study on the reaction modelling of SBR can be found in Broadhead(1984) and Broadhead et al. (1985). The model to be presented is a subset of the more general model proposed by Broadhead(1984) and Broadhead et al. (1985) with some modifications, and will pertain to the production of hot SBR latex using a thermal water soluble initiator in a semi-batch mode of operation. The original SBR model proposed by Broadhead(1984) was completely redone. Corrections have been made and more mechanistic detail has been added relative to the original work. Kinetic parameters and other paremeters used in the model can be found in Broadhead(1984).

7.2. INITIATION

This work will be concerned with the production of hot SBR latex using only one water soluble thermal initiator. The thermal initiator has been assumed to be potassium persulphate. All radical initiation is assumed to take place in the water phase. The molar balance on the moles of initiator is given by

$$\frac{dI_w}{dt} = F_{I_w} - k_d[I_w]_w V_w \tag{7.1}$$

7.3. PROPAGATION

The equations governing the reaction of each monomer to produce copolymer are given by

$$\frac{dM_s}{dt} = F_{M_s} - \Phi_s[M_s]_p \frac{\bar{n}N_p V_w}{N_A} \tag{7.2}$$

$$\frac{dM_b}{dt} = F_{M_b} - \Phi_b[M_b]_p \frac{\bar{n}N_p V_w}{N_A} \tag{7.3}$$

$$\frac{dP_s}{dt} = \Phi_s[M_s]_p \frac{\bar{n}N_p V_w}{N_A} \tag{7.4}$$

$$\frac{dP_b}{dt} = \Phi_b[M_b]_p \frac{\bar{n}N_p V_w}{N_A} \tag{7.5}$$

where Φ_s and Φ_b are pseudo rate constants defined as

$$\Phi_s = k_{pss}k_{pbb} \frac{r_s[M_s]_p + [M_b]_p}{k_{pbb}r_s[M_s]_p + k_{pss}r_b[M_b]_p} \tag{7.6}$$

$$\Phi_b = k_{pss}k_{pbb} \frac{r_b[M_b]_p + [M_s]_p}{k_{pbb}r_s[M_s]_p + k_{pss}r_b[M_b]_p} \tag{7.7}$$

In the equations above, it has been assumed that both long chain assumption I and II are applicable (Brash and Hamielec, 1986). Property calculations based on a monodispersed particle size distribution have also been assumed. For conditions when nucleation time is very fast relative to particle growth time or when the reactor is initially seeded, this simplifying assumption is not expected to introduce significant error.

The total conversion and conversion of each monomer are commonly specified properties for monitoring reaction progress, and can be easily computed from the differential states defined above. These conversions are defined below:

Styrene Conversion

$$X_s = \frac{P_s}{P_s + M_s} \tag{7.8}$$

Butadiene Conversion

$$X_b = \frac{P_b}{P_b + M_b} \tag{7.9}$$

Total Conversion

$$X = \frac{P_s + P_b}{P_s + P_b + M_s + M_b} \tag{7.10}$$

An important property of the copolymer produced is its composition. The cumulative copolymer compositions are computed from the monomer and reacted monomer material balances by

$$\overline{F}_a = \frac{P_a}{P_a + P_b} \tag{7.11}$$

$$\overline{F}_b = \frac{P_b}{P_a + P_b} \tag{7.12}$$

The instantaneous copolymer compositions are given by

$$F_a = \frac{\Phi_a[M_a]_p}{\Phi_a[M_a]_p + \Phi_b[M_b]_p} \tag{7.13}$$

$$F_b = 1 - F_a \tag{7.14}$$

7.4. CHAIN TRANSFER AGENT

A single chain transfer agent (CTA) or modifier is assumed to be present in the organic phases to provide control over molecular weight properties. The differential equation corresponding to the depletion of CTA is given by

$$\frac{dCTA}{dt} = F_{CTA} - k_{fCTA}[CTA]_p \frac{\overline{n}N_p V_w}{N_A} \tag{7.15}$$

where

$$k_{fCTA} = k_{fsCTA}\phi_a + k_{fbCTA}\phi_b \tag{7.16}$$

$$\phi_a = \frac{k_{pba}f_{ap}}{k_{pba}f_{ap} + k_{pab}f_{bp}} \tag{7.17}$$

$$\phi_b = 1 - \phi_a \tag{7.18}$$

In this work, the properties of the modifier pertain to n-dodecyl mercaptan.

7.5. WATER AND SOAP

Water and soap (emulsifier) are inert as far as the copolymerization reaction kinetics are concerned but yet play an important role in the emulsion reaction progress. The presence of soap in the water phase leads to the formation of micelles which, when stung by a water phase radical leads to the formation of a polymer

particle. The parameter values used for the emulsifier in this study correspond to those of sodium lauryl sulphate. The differential equations corresponding to the water volume and moles of soap for the semi-batch mode of operation are given by

$$\frac{dV_w}{dt} = F_{V_w} \tag{7.19}$$

$$\frac{dE}{dt} = F_E \tag{7.20}$$

7.6. REACTIVE IMPURITIES

Huo et al. (1988) have demonstrated the significant, but different, effects of both water soluble and organic phase soluble reactive impurities on the progress of emulsion polymerization. The presence of a reactive impurity in both the water and organic phases has been added to the model to account for meaningful disturbances for the purpose of this control study. The material balance equations for the organic and water phase impurities are given by

$$\frac{dIm_p}{dt} = F_{Im_p} - k_{Im_p}[Im_p]_p \frac{\bar{n}N_pV_w}{N_A} \tag{7.21}$$

$$\frac{dIm_w}{dt} = F_{Im_w} - k_{Im_w}[Im_w]_w [R]_w V_w \tag{7.22}$$

The parameters for the organic phase reactive impurity in this work correspond to 4-ter-butyl catechol (TBC) which is an inhibitor added to stabilize the monomer during storage. Due to lack of data, parameters for the water phase impurity were guessed at, and assumed to represent dissolved oxygen which inhibits the reaction by consuming water phase radicals.

7.7. PARTICLE AND AVERAGE NUMBER OF RADICALS COMPUTATION

Significant modifications have been made in the particle generation and average number of radicals per particle ($\bar{n}$) calculations relative to Broadhead(1984). Huo et al. (1988) have demonstrated the significance of impurities in both the water and organic phases on N_p and $\bar{n}$. The effect of impurities on these terms have been added to the model. The computation of n has been also modified to account for the effect of micellar

nucleation on $\bar{n}$ which was neglected by Broadhead(1984) and Huo et al.(1988). The collision theory model for particle generation assuming no significant radical desorption, presence of a single water phase reactive impurity, negligible water phase radical termination, and no significant homogeneous nucleation is given by

$$\frac{d(N_p V_w)}{dt} = \frac{N_A R_{in} A_{mf}}{A_{mf} + \varepsilon A_p + k^*_{Im_w}[Im_w]_w} \tag{7.23}$$

where

$$\varepsilon = \frac{C_p}{C_m} \tag{7.24}$$

$$k^*_{Im_w} = \frac{k_{Im_w}}{C_m} \tag{7.25}$$

$$R_{in} = 2fk_d[I_n]_w \tag{7.26}$$

$$A_{mf} = TSA - A_p \tag{7.27}$$

$$A_p = (6(\pi N_p V_w)^{1/2} V_p)^{2/3} \tag{7.28}$$

$$TSA = a_{sa}(E - [E]_{cmc} V_w) \tag{7.29}$$

The model takes two approaches to computing $\bar{n}$. The first approach makes the instantaneous termination assumption where it is assumed that there only two types of particles: particles with a single radical (N_{p_1}) and particles without a single radical (N_{p_0}). The differential equation for $N_{p_1} V_w$ is given by

$$\frac{d(N_{p_1} V_w)}{dt} = \rho_m V_w + \rho_p V_w \frac{N_p - 2N_{p_1}}{N_p} - N_{p_1} V_w k_{Im_p}[Im_p]_p \tag{7.30}$$

where

$$\rho_m = N_A C_m A_m [R]_w \tag{7.31}$$

$$\rho_p = N_A C_p A_p [R]_w \tag{7.32}$$

$$[R]_w = \frac{2fk_d[I]_w}{C_m A_{mf} + C_p A_p + k_{Im_w}[Im_w]_w} \tag{7.33}$$

With N_p and N_{p_1} determined from (7.23) and (7.30) respectively, $\bar{n}$ is computed as

$$\bar{n} = \frac{N_{p_1}}{N_p} \tag{7.34}$$

It has been observed through simulation studies that the stationary state hypothesis on (7.30) can lead to some significant error in computing $\bar{n}$. For this reason (7.30) has been added to model as an additional differential equation.

Another well-known approach to computing $\bar{n}$ is through the Smith-Ewart equation (Ugelstad and Hansen, 1976) where a balance is made on the number particles of a class containing q radicals, and a stationary state hypothesis is applied assuming no particle nucleation. The general solution for $\bar{n}$ was first derived by O'Toole(1965) and later extended by Hamielec and Hoffman(1986) to account for organic phase reactive impurities. Assuming a monodispersed particle population with property calculations based on the volume average particle size D_p and case II emulsion kinetics, the solution for $\bar{n}$ is given by

$$\bar{n} = \frac{a}{4}\frac{I_m(a)}{I_{m-1}(a)} \tag{7.35}$$

where $I_m(a)$ is a modified Bessel function of order m and parameter a and

$$a = \sqrt{8\alpha} \tag{7.36}$$

$$\alpha = \frac{\rho_p N_A V_p}{N_p^2 V_w k_{tp}} \tag{7.37}$$

$$m = \frac{N_A k_{Im_p} [Im_p]_p V_p}{N_p V_w k_{tp}} \tag{7.38}$$

Batch styrene homopolymerization studies were carried out to compare $\bar{n}$ predictions based on equations (7.34) and (7.35). Figure 7.1 shows conversion, N_p, and $\bar{n}$ with time for styrene produced in a batch mode with particles produced through micellar nucleation. The recipe for the simulated batch run is given below:

M_s:	24.4 *gmol*
P_s:	0.0 *gmol*
In:	0.03 *gmol*
E:	0.53 *gmol*
Im_p:	1.5×10^{-4} *gmol*
Im_w:	0.0 *gmol*
V_w:	4.8 *l*
T:	55° *C*

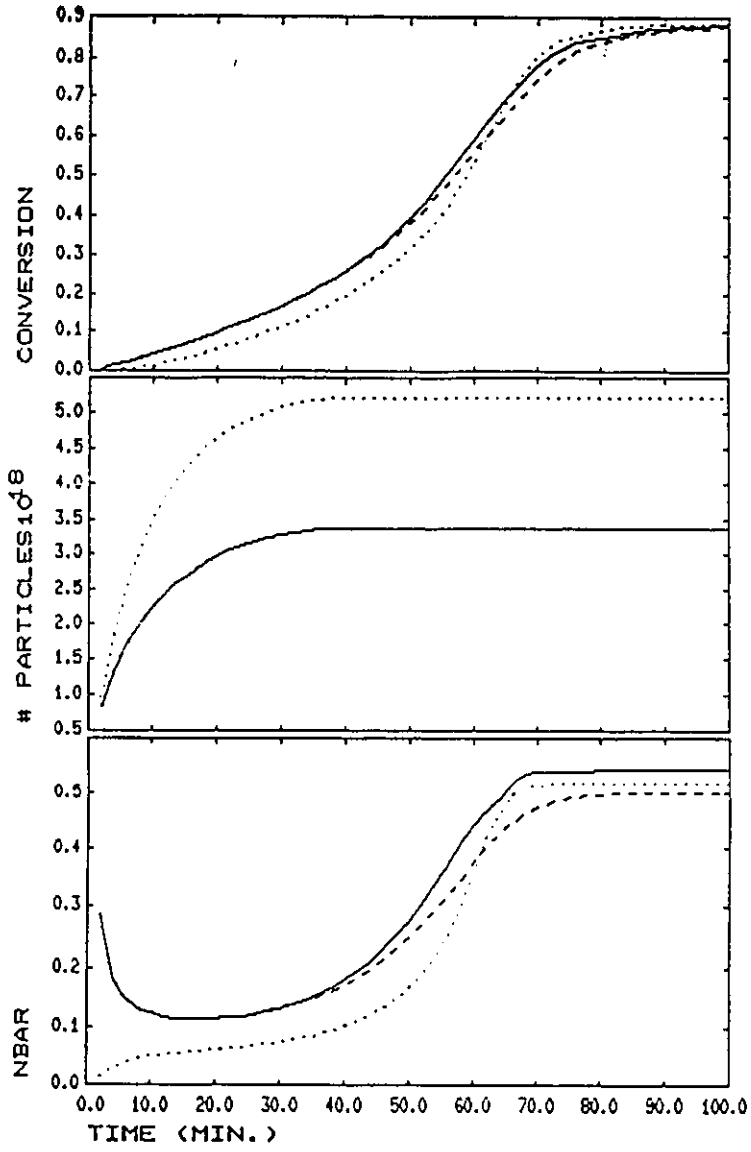

FIGURE 7.1: Effect of $\overline{n}$ Modelling on Batch Styrene Polymerization With Nucleation
Top: conversion; Middle: N_p; Bottom: $\overline{n}$
$\overline{n}$ obtained from: (7.34) (--); (7.35) (..); hybrid (7.34) & (7.35) (-)

In these figures, the response where $\bar{n}$ is computed from (7.34) is indicated by (--), and the response where $\bar{n}$ is computed through (7.35) is indicated by (..). The plots clearly show that the two different models for $\bar{n}$ lead to significant differences in X_s, N_p, and $\bar{n}$. The instantaneous termination model (7.34) predicts a larger $\bar{n}$ in the early period of the batch reaction because the effect of particle generation on $\bar{n}$ which leads to increased $\bar{n}$ is accounted for in the model. The initial larger $\bar{n}$ leads to a higher initial conversion, as is shown in Figure 7.1(a). The instantaneous termination model predicts a smaller particle number than the Smith-Ewart model due to the initial higher $\bar{n}$ that leads to larger particles initially because of the higher conversion. The larger particles adsorb more soap, leaving less free micelles for particle nucleation. At higher conversions, when no nucleation is present, the Smith-Ewart model (7.35) led to higher $\bar{n}$ predictions. This results because (7.35) can allow for more than one radical to exist in a particle when diffusion controlled termination occurs at larger particle sizes and conversions. These results suggest that neglecting the effect of micellar nucleation on $\bar{n}$ can lead to significant errors in the prediction of $\bar{n}$ when nucleation is present.

Figures 7.2 shows the results of a simulated batch styrene homopolymerization where the reactor is initially seeded, and no further nucleation takes place. The recipe for this batch run is given below:

M_s:	24.4 *gmol*
P_s:	0.06 *gmol*
In:	0.03 *gmol*
Im_p:	$1.5x10^{-4}$ *gmol*
Im_w:	0.0 *gmol*
N_p	$2x10^{-18}$ l^{-1}
V_w:	4.8 *l*
T:	55° *C*

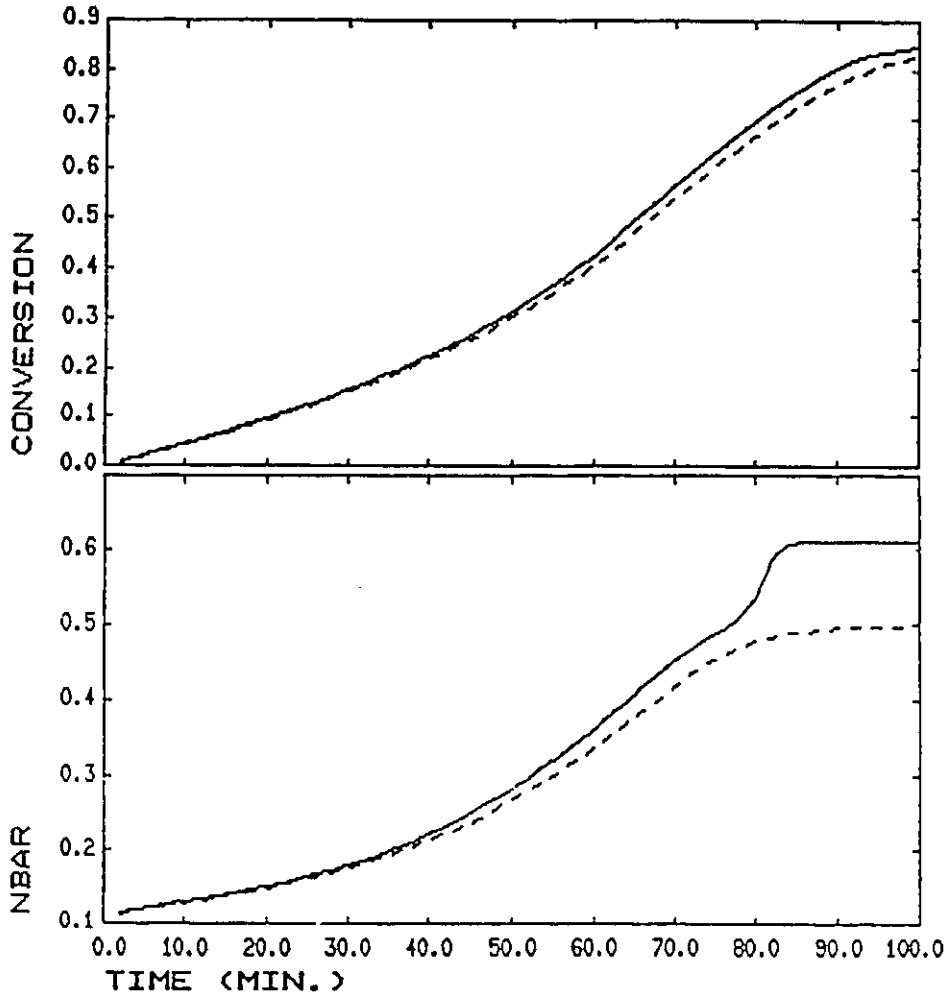

FIGURE 7.2: Effect of $\overline{n}$ Modelling on Seeded Batch Styrene Polymerization
Top: conversion; Bottom: $\overline{n}$
$\overline{n}$ obtained from: (7.34) (--); (7.35) (..); hybrid (7.34) & (7.35) (-)

The results in Figure 7.2 show that both models led to the same $\overline{n}$ and conversion predictions at low conversion. However, at higher conversion and larger particle sizes, the Smith-Ewart model (7.35) leads to higher $\overline{n}$ prediction due to the effects of diffusion controlled termination being accounted for. These results suggest that the stationary state hypothesis used to compute $\overline{n}$ in (7.35) appears to be valid for the seeded case when no nucleation is present.

Based on the results above, it was decided to compute both $\overline{n}$'s in the computer model and choose the larger of the two. Basically this meant that during early stages of reaction when micellar nucleation is present (7.34) is used to compute $\overline{n}$, and during high conversion stages of reaction when diffusion controlled termination becomes significant (7.35) is used. The result of using this policy is indicated by (-) in Figures 7.1 and 7.2. For the first simulation where micellar nucleation occurs, this policy led to significantly different predictions relative to both (7.34) and (7.35), with the exception of the N_p prediction that matched the prediction based on (7.34). For the seeded case shown in Figure 7.2, the policy proposed meant using the Smith-Ewart model (7.35) throughout the simulation.

7.8. MOLECULAR WEIGHT AND BRANCHING FREQUENCY

The differential equations used by Broadhead(1984) for the prediction of zero, first, and second moments, and the tri and tetra branch frequencies, have been modified to include the effect of a reactive particle phase impurity. The assumption in the molecular weight development are that transfer reactions and not termination reactions are important, dead chains greatly outnumber live polymer chains, and that copolymer composition drift is not significant. These assumptions are considered to be reasonable for the operating conditions studied in this work. The differential equations used are

$$\frac{d(V_pQ_0)}{dt}=\left(\frac{C_i[CTA]_p}{[M]_p}+C_m+\frac{C_{lm_p}}{[M]_p}-\frac{C_p^{\bullet\bullet}Q_1}{[M]_p}\right)k_p[M]_p[R]_pV_p \tag{7.39}$$

$$\frac{d(V_pQ_1)}{dt} = k_p[M]_p[R]_pV_p \tag{7.40}$$

$$\frac{d(V_pQ_2)}{dt}=\frac{2\left(1+\frac{C_p^{\bullet\bullet}Q_2}{[M]_p}\right)\left(1+\frac{C_i[CTA]_p}{[M]_p}+C_m+\frac{C_p^{\bullet}Q_2}{[M]_p}+\frac{C_p^{\bullet\bullet}Q_2}{[M]_p}\right)}{\frac{C_i[CTA]_p}{[M]_p}+C_m+\frac{C_p^{\bullet}Q_1}{[M]_p}+\frac{C_{lm_p}[lm_p]_p}{[M]_p}}k_p[M]_p[R]_pV_p \tag{7.41}$$

$$\frac{d(V_pQ_0Bn_3)}{dt} = C_p^{\bullet}Q_1k_p[R]_pV_p \tag{7.42}$$

$$\frac{d(V_p Q_0 Bn_3)}{dt} = C_p^{**} Q_1 k_p [R]_p V_p \tag{7.43}$$

where

$$C_t = \frac{k_{fCTA}}{k_p} \tag{7.44}$$

$$C_m = \frac{k_{fm}}{k_p} \tag{7.45}$$

$$C_p^* = \frac{k_{fp}^*}{k_p} \tag{7.46}$$

$$C_p^{**} = \frac{k_{fp}^{**}}{k_p} \tag{7.47}$$

$$C_{Im_p} = \frac{k_{Im_p}}{k_p} \tag{7.48}$$

$$k_p = \phi_s(k_{pss} f_{sp} + k_{psb} f_{bp}) + \phi_b(k_{pbs} f_{sp} + k_{pbb} f_{bp}) \tag{7.49}$$

$$k_{fm} = \phi_s k_{fs} f_{bp} + \phi_b k_{fb} f_{bp} \tag{7.50}$$

$$k_{fp}^* = (\phi_s k_{fsx} + \phi_b k_{fbx}) \overline{F}_b \tag{7.51}$$

$$k_{fp}^{**} = \phi_s \overline{F}_b (0.17 k_{s12} + 0.83 k_{s14}) + \phi_b \overline{F}_b (0.17 k_{b12} + 0.83 k_{b14}) \tag{7.52}$$

$$[R]_p = \frac{\overline{n} N_p V_w}{V_p N_A} \tag{7.53}$$

Expressions for ϕ_s and ϕ_b are given are given by (7.17) and (7.18).

Assuming composition drift is not appreciable, the cumulative number and weight average molecular weights are computed as

$$\overline{M_{W_N}} = \left(M_{W_s} \overline{F}_s + M_{W_b} \overline{F}_b\right) \frac{Q_1}{Q_0} \tag{7.54}$$

$$\overline{M_{W_W}} = \left(M_{W_s} \overline{F}_s + M_{W_b} \overline{F}_b\right) \frac{Q_2}{Q_1} \tag{7.55}$$

Similarly, instantaneous number and weight molecular weight averages are computed as

$$M_{W_N} = \left(M_{W_s} F_s + M_{W_b} F_b\right) \frac{d(V_p Q_1)}{d(V_p Q_0)} \tag{7.56}$$

$$M_{W_w} = \left(M_{W_s}F_s + M_{W_b}F_b\right)\frac{d(V_pQ_2)}{d(V_pQ_1)} \tag{7.57}$$

7.9. DISTRIBUTION OF SPECIES BETWEEN PHASES

The expressions above require information on the distribution of the species between water, particle, and monomer phases that exist during an emulsion reaction. In the model developed, it has been assumed that the reactor will be operated at high pressure under an inert nitrogen blanket. Therefore the presence of monomer, particularly butadiene, in the overhead gas phase has been assumed to be negligible. Due to the lack of detailed mass transfer and thermodynamic data, the model makes the simplifying assumption of an equilibrium distribution of each species according to constant partition coefficients of the form

$$K_{imw} = \frac{[i]_m}{[i]_w} \tag{7.58}$$

$$K_{iwp} = \frac{[i]_w}{[i]_p} \tag{7.59}$$

$$K_{imp} = \frac{[i]_m}{[i]_p} = K_{imw}K_{iwp} \tag{7.60}$$

where K_{ijk} indicates the partition coefficient of species i between phases j and k. These partition coefficients together with phase volumes can be used to determine the concentration of a species in any of the three phases (refer to Broadhead(1984)). In this work the model of Broadhead(1984) has been extended to allow prediction of the equilibrium swollen particle composition or monomer partitioning between the monomer droplet and polymer particle phases(K_{smp} & K_{bmp}) according the Flory-Huggins theory of polymer solutions (Ugelstad et al., 1985) if requested. Using this theory, the unknown equilibrium volume fraction compositions of styrene and butadiene monomer in the monomer droplet and polymer particle phases, given by v_{sm}, v_{bm}, v_{sp}, and v_{bp} respectively, is determined through the solution of nonlinear equations:

Styrene Monomer Balance

$$0 = \frac{v_{sp}V_pd_s}{M_{W_s}} + \frac{v_{sm}V_md_s}{M_{W_s}} - M_s + \frac{v_{sp}d_sK_{swp}V_w}{M_{W_s}} \tag{7.61}$$

Butadiene Monomer Balance

$$0 = \frac{v_{bp}V_pd_b}{M_{W_b}} + \frac{v_{bm}V_md_b}{M_{W_b}} + M_b + \frac{v_{bp}d_pK_{bwp}V_w}{M_{W_b}} \tag{7.62}$$

Styrene Monomer Partial Molar Free Energy Balance

$$0 = \ln(v_{sp}) + (1 - m_{sb})v_{bp} + v_{pp} + v_{bp}^2 x_{sb} + v_{pp}^2 x_{sp} + v_{bp} v_{pp}(x_{sb} + x_{sp} - x_{bp} m_{sb})$$

$$+ \frac{4 M_{W_s} \tau}{D_p d_s RT} - \ln(v_{sm}) - (1 - m_{sb}) v_{bm} \quad - v_{bm}^2 x_{sb} \qquad (7.63)$$

Butadiene Monomer Partial Molar Free Energy Balance

$$0 = \ln(v_{bp}) + (1 - m_{sb}^{-1})v_{sp} + v_{pp} + v_{sp}^2 x_{sb} m_{sb}^{-1} + v_{pp}^2 x_{bp} + v_{sp} v_{pp}(x_{sb} m_{sb}^{-1} + x_{bp} - x_{sp} m_{sb}^{-1})$$

$$+ \frac{4 M_{W_b} \tau}{D_p d_b RT} - \ln(v_{bm}) - (1 - m_{sb}^{-1}) v_{sm} - v_{sm}^2 x_{sb} m_{sb}^{-1} \qquad (7.64)$$

where

Volume Fraction Polymer In Particle Phase

$$v_{pp} = 1 - v_{sp} - v_{bp} \qquad (7.65)$$

Swollen Particle Volume

$$V_p = \frac{P_s M_{W_s} + P_b M_{W_b}}{d_p v_{pp}} \qquad (7.66)$$

Approximate Partial Molar Volume Ratio

$$m_{sb} = \frac{M_{W_s} d_b}{d_s M_{W_b}} \qquad (7.67)$$

Volume Average Swollen Particle Diameter

$$D_p = \sqrt[3]{\frac{6 V_p}{\pi N_p V_w}} \qquad (7.68)$$

Interaction Parameters

$$x_{sp} = \frac{M_{W_s}(\delta_s - \delta_p)^2}{RTd_s} - \frac{W_{sp}}{R} \qquad (7.69)$$

$$x_{bp} = \frac{M_{W_b}(\delta_b - \delta_p)^2}{RTd_b} - \frac{W_{bp}}{R} \qquad (7.70)$$

$$x_{sb} = \frac{M_{W_s}(\delta_s - \delta_b)^2}{RTd_s} - \frac{W_{sb}}{R} \qquad (7.71)$$

Partition Coefficients

$$K_{smp} = \frac{v_{sm}}{v_{sp}} \tag{7.72}$$

$$K_{bmp} = \frac{v_{bm}}{v_{bp}} \tag{7.73}$$

The system of nonlinear equations is numerically solved. It is important to note that this theory only applies when a monomer droplet phase is present, as is explained in the next section.

The solution of the monomer volume fractions according to Flory-Huggins requires a prediction of the particle surface tension (τ). In this work the surface tension is predicted according to the method proposed by Hansen and Ugelstad (1979), where they suggested that particle interfacial tension be approximated using

$$\tau = \tau_0 - B \ln\left(\frac{[E]_w}{A} + 1\right) \tag{7.74}$$

The concentration of soap in the water phase ($[E]_w$), when below the critical micelle concentration (CMC), is modelled by assuming a modified Langmuir adsorption isotherm for adsorbance of emulsifier on the particles, given by

$$E_{abs} = \frac{\theta[E]_w}{\alpha + [E]_w} \tag{7.75}$$

where

$$\theta = \frac{A_p(\alpha_s + CMC)}{a_{ss}CMC} \tag{7.76}$$

A molar balance on the moles of soap in the reactor leads to

$$E = [E]_w V_w + E_{abs} \tag{7.77}$$

From equations (7.75) and (7.77) $[E]_w$ is computed for use in (7.74). The solution for $[E]_w$ is given by

$$[E]_w = \frac{-(\theta + \alpha_s V_w - E_{abs}) + \sqrt{(\theta + \alpha_s V_w - E_{abs})^2 + 4\alpha_s E_{abs} V_w}}{2V_w} \tag{7.78}$$

Figure 7.3 shows the simulated results of conversion, monomer and particle volumes, and partition coefficients K_{smp} and K_{bmp} respectively for a batch SBR run with operating conditions and the initial charge as specified below:

M_s:	12.2 *gmol*
M_b:	12.2 *gmol*
In:	0.03 *gmol*
E:	0.2 *gmol*
Im_p:	$1.25x10^{-5}$ *gmol*
Im_w:	0.0 *gmol*
V_w:	4.8 *l*
T:	55° *C*

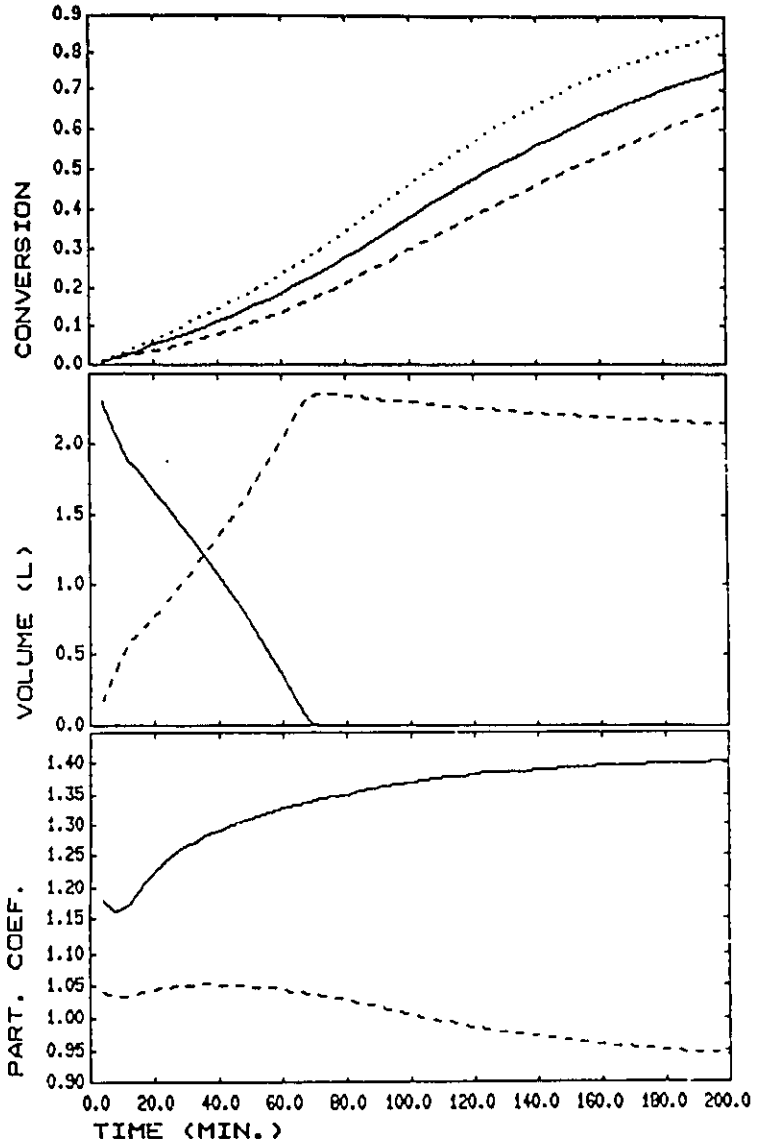

FIGURE 7.3: Simulated Batch SBR Run Using Flory-Huggins Partitioning Prediction
Top: X (-), X_s (--), X_b (..)
Middle: V_m (-), V_p (--)
Bottom: K_{smp} (-), K_{bmp} (--)

Figures 7.3(a) and 7.3(b) show that a monomer droplet phase will be present only at low conversion since the Flory-Huggins model predicts a large degree of particle swelling based on the parameters that were obtained from the literature (Ugelstad and Hansen, 1979; Billmeyer, 1984). The partition coefficients, shown in Figure 7.3(c), can be observed to go through a moderate change during the course of reaction when V_m is present and the particle size is still small. At high conversion very little change can be observed. The lack of experimental data to obtain a suitable semi-empirical fit for prediction together with the relatively small changes in the partition coefficients over the course of the reaction still support the use of constant partition coefficients as a reasonable simplification without introducing serious prediction error.

In the work in subsequent chapters, the assumption of constant partition coefficients will be taken.

7.10. PHASE VOLUMES

In the original model proposed by Broadhead(1984), ideal solution properties are assumed (volumes are additive), and the solubility of the organic and water phases were assumed negligible for computing monomer droplet, particle, and water phase volumes. It is also assumed that density of copolymer produced is approximately constant through the course of reaction. Differential equations for V_o and V_p were used to compute these volumes. This approach was not taken in the model developed in this work because it was considered inconsistent and unnecessary to introduce these two additional differential states when they can be easily computed from previously defined differential states. The total organic phase volume is estimated by

$$V_o = \frac{M_s M_{W_s}}{d_s} + \frac{M_b M_{W_b}}{d_b} + \frac{P_s M_{W_s} + P_b M_{W_b}}{d_p} \tag{7.79}$$

If constant partitioning is used for K_{swp} and K_{bwp}, the swollen particle volume (V_p) and monomer droplet phase volume (V_m) is numerically computed using Newton's method from

$$0 = \frac{P_s M_{W_s} + P_b M_{W_b}}{d_p} + \frac{M_{W_s} M_s V_p}{d_s((V_o - V_p)K_{swp} + V_w K_{swp} + V_p)} - V_p + \frac{M_{W_b} M_b V_p}{d_b((V_o - V_p)K_{bwp} + V_w K_{bwp} + V_p)} \tag{7.80}$$

$$V_m = V_o - V_p \tag{7.81}$$

It has been found that this approach always gives a V_m that is greater than or equal to zero, and hence offers an advantage over the approach taken by Broadhead(1984) where numerical discontinuities are encountered due to the possibility of a negative V_m being calculated when the monomer droplet phase disappears. If Flory-Huggin's theory is used, V_p is computed using (7.66), and V_m is computed from (7.81). If V_m is determined to be less than zero from (7.81) then V_p and V_m are instead given by

$$V_p = V_o \tag{7.82}$$

$$V_m = 0 \tag{7.83}$$

7.11. DIFFUSION CONTROLLED TERMINATION AND PROPAGATION

The Smith-Ewart equation described in section 7.7 requires an estimate of the termination rate constant. Because of the high level of conversion in a polymer particle during a emulsion reaction, radical termination is often diffusion controlled. At very high conversions monomer propagation can also become diffusion controlled. The free volume theory of Harris et al. (1981), applied to emulsion polymerization, is used to model diffusion controlled termination when $V_f < V_{fcat}$ as

$$k_{tp} = k_{tpsat} \exp\left[-A_t\left(\frac{1}{V_f}-\frac{1}{V_{fcat}}\right)\right] \tag{7.84}$$

and diffusion controlled propagation when $V_f < V_{fcrp}$ as

$$k_p = k_{p0} \exp\left[-B_t\left(\frac{1}{V_f}-\frac{1}{V_{fcrp}}\right)\right] \tag{7.85}$$

where

$$V_f = (0.025+a_s(T-T_{gs}))v_{sp} + (0.025+a_b(T-T_{gb}))v_{bp} + (0.025+a_p(T-T_{gp}))v_{pp} \tag{7.86}$$

Unlike the model of Broadhead(1984) where a fixed glass transition temperature of the copolymer T_{gp} is used, T_{gp} is estimated using the semi-empirical model proposed by Bueche (1962)

$$T_{gp} = \frac{T_{gps}+(k_g T_{gpb}-T_{gps})v_{fpb}}{1+(k_g-1)v_{fpb}} \tag{7.87}$$

where k_g is an experimentally determined constant.

7.12. ENERGY BALANCES AND TEMPERATURES

Energy balances on both the CSTR reactor and cooling jacket were made by Broadhead(1984) assuming perfect mixing in both sections. The reactor energy balance leads to the differential equation

$$\frac{d\left(\sum_i M_i Cp_i(T-T_{ref})\right)}{dt} = \sum_i F_{i,in} Cp_i(T_{in}-T_{ref}) - R_{pa}\Delta H_{pa} V_p - R_{pb}\Delta H_{pb} V_p - UA_j(T-T_j) - Q_R \qquad (7.88)$$

The summations in the equation above are taken over styrene, butadiene, water, and the copolymer. An energy balance on the cooling jacket is given by

$$\frac{dT_j}{dt} = \frac{F_{jw} Cp_w (T_{j,in}-T_j) + UA_j(T-T_j) - Q_j}{d_w V_j Cp_w} \qquad (7.89)$$

Temperature control of the reactor is achieved by a continuous time PI controller which adjusts $T_{j,in}$ of the cooling jacket according to

$$T_{j,in} = T_{j,o} + K_p e + \frac{K_p}{R_I} I_{Te} \qquad (7.90)$$

with I_{Te} determined from

$$\frac{dI_{Te}}{dt} = T_{set} - T \qquad (7.91)$$

The implementation of the controller has been modified for correct handling of input saturation when it occurs. When input saturation occurs, $T_{j,in}$ is set to its bound and the integration of (7.91) is stopped only when the reset action alone is the cause of saturation.

7.13. PARTICLE SIZE

Unswollen polymer particle size is often an important property of a copolymer latex and can be determined on-line by turbidity and light scattering techniques (Korti, 1988). The model predicts the average particle size according to a volume average, and is given by

$$D_{P_w} = \sqrt[3]{\frac{6(P_a M_{W_a} + P_b M_{W_b})}{\pi d_p N_p V_w}} \qquad (7.92)$$

This average particle size would be consistent with the measurements indicated above for the case of a particle size distribution which is approximately monodispersed. For batch reaction with a short period of nucleation or with an initially seeded reactor, a monodispersed assumption is expected to be reasonable.

7.14. NUMERICAL SOLUTION

The system of ordinary differential equations described above is solved numerically using a stiff differential equation solver "LSODAR" obtained from ODEPACK.

7.15. NOTATION

a	parameter in modified Bessel function
a_i	difference in thermal expansion coefficients above and below the glass transition point for i
a_{se}	emulsifier surface covering potential
A	constant in (7.74)
A_t	constant used in k_{tp} prediction
A_{mf}	free micellar area
A_p	particle area
B_d	constant in diffusion controlled propagation rate constant prediction (7.85)
B	constant in (7.74)
Bn_3	frequency of copolymer chains with tri branch points
Bn_4	frequency of copolymer chains with tetra branch points
C_i	ratio of i'th rate constant to k_p
C_m	collision theory rate constant for micelle radical capture
C_p	collision theory rate constant for polymer particle radical capture
C_p^*	ratio of $k_{k_p}^*$ to k_p
C_p^{**}	ratio of k_{fp}^{**} to k_p
CMC	critical micelle concentration
Cp_i	heat capacity of i

CTA	moles of chain transfer agent
d_i	density of i
D_p	volume average particle size
e	error from set point in PI temperature controller
E	moles of emulsifier
E_{abs}	moles emulsifier adsorbed on particles
f	initiator efficiency constant
f_{bp}	molar fraction of butadiene monomer in monomer contained within the polymer particle phase
f_{sp}	molar fraction of styrene monomer in monomer contained within the polymer particle phase
F_{M_b}	molar feed rate of butadiene
F_{CTA}	molar feed rate of chain transfer agent
F_E	molar feed rate of emulsifier
F_{I_n}	molar feed rate of initiator
F_{M_s}	molar feed rate of styrene
F_b	instantaneous butadiene copolymer composition
F_s	instantaneous styrene copolymer composition
$\overline{F}_b$	cumulative butadiene copolymer composition
$\overline{F}_s$	cumulative styrene copolymer composition
F_{V_w}	volumetric feed rate of water
ΔH_{pb}	heat of polymerization of butadiene
ΔH_{ps}	heat of polymerization of styrene
$I_m(a)$	modified Bessel function of order m and parameter a
Im_p	moles of organic phase reactive impurity
Im_w	moles of water phase reactive impurity
I_n	moles of initiator
I_{Te}	integrated error in PI temperature controller

k_{b12} rate constant for bound butadiene radicals with 1,2 internal copolymer double bonds

k_{b14} rate constant for bound butadiene radicals with 1,4 internal copolymer double bonds

k_{fb} rate constant for bound butadiene radical transfer to butadiene monomer

k_{fCTA} pseudo copolymer rate constant of chain transfer agent

k_{fbCTA} rate constant of butadiene bound radicals with chain transfer agent

k_{fbx} rate constant for radical transfer of bound butadiene radicals with copolymer

k_{fsCTA} rate constant of styrene bound radicals with chain transfer agent

k_{fsx} rate constant for radical transfer of bound styrene radicals to copolymer

k_{fm} pseudo copolymerization rate constant for radical transfer to monomer

k_{fp}^{*} overall rate constant for radical transfer to copolymer chains

k_{fp}^{**} pseudo copolymerization rate constant for radical reaction with internal copolymer double bonds

k_{fs} rate constant for bound styrene radical transfer to butadiene monomer

k_{Im_p} pseudo copolymerization rate constant of organic phase impurities with particle phase radicals

k_{Im_w} pseudo copolymerization rate constant of water phase impurities with water phase radicals

$k_{Im_w}^{*}$ ratio of k_{Im_w} to C_m

k_d initiator decomposition rate constant

k_g constant used to predict copolymer glass transition temperature in (7.87)

k_p pseudo overall copolymerization propagation rate constant

k_{p0} constant used for diffusion controlled termination prediction in (7.85)

k_{pbb} homopolymerization propagation rate constant of butadiene

k_{pbs} propagation rate constant of bound butadiene chain ends with styrene

k_{psb} propagation constant of bound styrene chain ends with butadiene

k_{pss} homopolymerization propagation rate constant of styrene

k_{s12} rate constant for bound styrene radical reaction with 1,2 internal double bonds

k_{s14} rate constant for bound styrene radical reaction with 1,4 internal double bonds

k_{tp} overall copolymer termination rate constant

k_{tpsat} termination rate constant of fully swollen polymer particles

K_{ijk} partition coefficient of the concentration of species i between phases j and k

K_p proportional constant term in PI controller

m order of modified Bessel function obtained from (7.38)

m_{ij} partial molar volume ratio of i to j

M_b moles of butadiene

M_s moles of styrene

M_{W_i} molecular weight of component i

$\overline{M_{W_i}}$ cumulative i'th average molecular weight

$\bar{n}$ average number of radicals per particle

N_A Avogadro's number

N_p number of polymer particles per volume unit of water

N_{p_1} number of polymer particles containing a single radical

P_b moles of reacted butadiene bound in copolymer

P_s moles of reacted styrene bound in copolymer

Q_i i'th copolymer moment per volume polymer particle phase

Q_R reactor heat loss rate

r_b copolymerization reactivity ratio of bound butadiene radicals

r_s copolymerization reactivity ratio of bound styrene radicals

R gas constant

R_I reset constant in PI controller

$[R]_i$ radical concentration in phase i

R_{in} rate of initiation

R_{pb} rate of polymerization of butadiene

R_{ps} rate of polymerization of styrene

P_s moles of reacted styrene bound in copolymer

t time

T	reactor temperature
T_{gi}	glass transition temperature of i
T_{gpb}	glass transition temperature of polybutadiene
T_{gps}	glass transition temperature of polystyrene
T_{in}	feed temperature
T_j	cooling jacket temperature
$T_{j,in}$	jacket inlet temperature
T_{set}	temperature set point
TSA	total micellar covering area
v_{fpb}	volume fraction of polybutadiene in copolymer
v_{ij}	volume fraction of i in phase j
V_f	free volume
V_{fcrp}	critical free volume for start of diffusion controlled termination
V_{fsat}	free volume of fully swollen polymer particle
V_i	volume of phase i
W_{ij}	entropic contribution to x_{ij}
x_{ij}	interaction parameter per molecular of compound i with compound j
X	overall monomer conversion
X_b	butadiene conversion
X_s	styrene conversion

Subscripts

b	butadiene
cmc	critical micelle concentration
j	jacket
m	monomer droplet phase
N	number average
o	organic phase

p	polymer or polymer particle phase
s	styrene
w	water or water phase
W	weight average

Greek Letters

α	expression obtained from (7.36)
α_a	adsorption parameter for emulsifier in (7.75)
δ_i	solubility parameter of component i
ε	radical capture efficiency
θ	adsorption parameter for emulsifier in (7.76)
ρ_m	radicle entry rate to micelles
ρ_p	radical entry rate to particles
τ	particle surface tension
τ_0	surface tension constant in (7.74)
ϕ_b	fraction of bound butadiene radical ends
ϕ_s	fraction of bound styrene radical ends
Φ_b	pseudo copolymerization rate constant for butadiene
Φ_s	pseudo copolymerization rate constant for styrene

STATE ESTIMATION FOR SEMI-BATCH EMULSION POLYMERIZATION REACTORS

8. STATE ESTIMATION FOR SEMI-BATCH EMULSION POLYMERIZATION REACTORS

8.1. INTRODUCTION

This chapter will be concerned with the first problem commonly encountered when faced with controlling batch/semi-batch processes, namely the estimation of nonlinear internal process model dynamic states from a limited set of related measurements. These state estimators are necessary for tracking and filtering the states of the process and for computing on-line model-based feedback control actions. The problem of state estimation in nonlinear systems has been covered extensively in the literature. A review of different methods is beyond the scope of this work, and can be found in Seinfeld (1970), Ekyhoff (1974), Hsia (1977), Young (1981), and Bekey and Saridis (1982). Three approaches to the state estimation problem are considered in this work, and are illustrated and compared on simulations of the semi-batch emulsion copolymerization of styrene/butadiene rubber (SBR) using the semi-theoretical nonlinear model described in the previous chapter.

The first approach to nonlinear state estimation is extended Kalman filtering (Jazwinski, 1970). A limited number of applications of this theory in the chemical process industry can be found in the literature, and a review of the applications of this method to various chemical processes can be found in Gilles (1986,1987). The theory behind extended Kalman filtering is well known and well understood. On the other hand, the correct formulation of the extended Kalman filter to make it useful for application in a real process environment is understood to a far lesser extent. The common error in judgement when formulating these filters is neglecting the incorporation of the correct nonstationary disturbance and/or parameter states needed to eliminate bias between the true and model predicted response when nonideal prediction mismatch situations arise. When this mistake is made, the designer often attempts to mask the problem by increasing the noise associated with the process states, with the unfavorable result of arriving at a noisy state estimator that hides the bias problem. Examples where this mistake has been made are demonstrated in Hamilton et al. (1973) in a double effect evaporator problem and Wells (1971) in a stirred tank reactor problem. Examples with continuous processes can also be found where unmeasured nonstationary states were correctly included in the extended Kalman

filter formulation. Ahlberg and Cheyne (1976), in an industrial application of extended Kalman filtering to the polymerization of butyl synthetic rubber, discuss the importance of accounting for unmeasured nonstationary reactive impurity disturbances and parameter variations. Jo and Bankoff (1976) demonstrate the application of extended Kalman filtering in an experimental study on the continuous solution polymerization of vinyl acetate. In their work, meaningful nonstationary stochastic inhibitor disturbance and model mismatch parameter states are incorporated in filter to provide bias free state estimates for the experimental conditions considered. Hubbard and DaSilva (1982) and Allison and Taylor (1986) demonstrate the necessary incorporation of unmeasured nonstationary feed disturbance composition states in extended Kalman filter applications to continuous cement blending and pH control problems respectively. The same considerations discussed above would be expected to be necessary in any real industrial application, where imprecise models are usually applied and unmeasurable disturbances exist.

The incorporation of meaningful or fictitious nonstationary disturbance and/or parameter states in an extended Kalman filter is not a sufficient requirement for it to be useful in a real process environment. It must be demonstrated to be robust to any unaccounted disturbance, parameter, and structural types of mismatch, and shown to contain sufficient nonstationary disturbance and parameter states so that model predicted measured outputs will always be consistent with actual measurements in the region of operation. Parrish and Brosilow (1988) have stressed that if the latter requirement is not satisfied, the state estimator may still lead to biased estimates, preventing the possibility of integral action if feedback control is applied. Therefore, from a practical point of view, Kalman filters formulated and evaluated with a perfect model assumption and with all disturbances information known fail to address the problems of state estimation in a real chemical process environment. Even if some nonstationary disturbance and model mismatch states are included, the requirement for consistency may not be satisfied.

Examples of the application of extended Kalman filtering to batch/semi-batch processes can be found in the literature. Schuler and Suzhen (1985) and Schuler and Papadopoulou (1986) successfully applied extended Kalman filtering to estimate properties of polystyrene in a solution batch reactor. In their work a perfect model was assumed, and the effect of unaccounted reactive impurities or model mismatch was not considered. Dimitratos et al. (1989) applied extended Kalman filtering to a seeded semi-batch emulsion vinyl acetate/n-butyl acrylate copolymerization reactor. Sources of nonstationary disturbances or model parameter mismatch were not considered. They assumed that the effect of process disturbances can be modelled as zero mean white noise shocks added to the deterministic model states. Such an assumption is unrealistic in a real process environment since model or disturbance mismatch will usually introduce a nonzero bias between the

deterministic and true model states. MacGregor et al. (1986) applied extended Kalman filtering to infer state properties in a batch polystyrene latex reactor where a reactive impurity was present and initially unknown. A nonstationary state to compensate for the initially unknown impurity level was not included in their filter formulation. Their results showed that the performance of the filter was sensitive to errors in the unknown initial impurity disturbance level. Ramirez (1987) successfully applied a Kalman filter to a batch beer fermentation problem. The Kalman filter was formulated according to a deterministic model without the inclusion of any nonstationary disturbance or parameter states. Their Kalman filter was then combined with a sequential parameter estimator to indirectly account for model mismatch in only a single model parameter. Stephanopoulos and San (1984) propose a strategy for state estimation and filtering in batch, semi-batch, and continuous bioreactors using extended Kalman filtering with a very simplified reactor model. In their formulation, nonstationary growth parameter states are included in the filter to account for all possible observed responses. San and Stephanopoulos (1984) successfully applied this approach to a semi-batch fermentation reactor over a wide range of operating conditions.

Unlike previously reported applications on Kalman filtering, the first objective in this work will be to provide new useful and practical results on the application of this theory to a semi-batch copolymerization problem where the important issues of nonstationary disturbance and parameter variations, errors in the initialization of disturbances and parameter states, and consistency are formally addressed for evaluation in a real process environment.

The second approach to the problem of state estimation arises from a problem of particular importance to batch/semi-batch problems. Due to the finite time of operation of a batch or semi-batch process, rapid convergence of the state estimates to their correct values from state initialization errors is necessary in order for effective feedback control to be applied. A modification to the standard extended Kalman filter is proposed where it is reiterated from the beginning at every sampling interval with new estimates of the initial unknown state estimates in order to improve the convergence properties of the filter. The unknown initial states are obtained by combining a second extended Kalman filter with the standard extended Kalman filter which provides updated estimates of the unknown initial states.

The final approach considered for nonlinear state estimation uses nonlinear optimization methods to minimize some suitably chosen objective function. This approach was suggested by Jang et al. (1986) and compared to extended Kalman filtering in a simple simulation study on a CSTR reactor carrying out a first order exothermic reaction with a noisy measurement. They found the former approach to be far superior in terms of the speed of tracking, robustness in the presence of errors in modelling the system, noise statistics,

and in terms of the ability to handle nonlinearities in the system. Unfortunately, their results are impossible to critically evaluate because no information was provided on the formulation and tuning of the extended Kalman filter used in their work. It is possible that such a poor formulation of the extended Kalman filter may have been the cause of the drastically poorer relative performance. In this work, the on-line optimization approach is once again compared to extended Kalman filtering, but in this case to the SBR semi-batch problem stated above, where the results will be demonstrated to be far different from those obtained by Jang et al. (1986).

The work in this chapter will be presented in three sections. The first section will briefly review each of the state estimation procedures. The second describes the semi-batch nonlinear SBR polymerization process that will be the case study used in this chapter. The third section will present results on the formulation and relative performance of the state estimation approaches for the semi-batch SBR estimation problem where it will be assumed that the sources of nonstationary disturbance and parameter mismatch will be correctly accounted for in the state estimation scheme. Finally, the issue of consistency will be examined, where the problem of unaccounted for model mismatch will be addressed through the incorporation of carefully selected fictitious nonstationary mismatch states.

8.2. MODEL FORMULATION

The approaches that follow will be concerned with batch/semi-batch processes described by a set of nonlinear ordinary differential equation states in the form

$$\frac{dx^d}{dt} = f^d(x,u,t) \tag{8.1}$$

$$y = h(x,u,t) \tag{8.2}$$

$$x_0 = x(t=0) \tag{8.3}$$

where x represents the complete vector of internal states, x^d is the modelled deterministic subset of the differential state vector x described through (8.1), y is the vector of measured outputs that is related to x through (8.2), and u is a time varying vector of known manipulated inputs. The state vector x is assumed to be made up of a deterministic component x^d and a stochastic component x^s. Included in x^s are model parameter

and disturbance states that may vary with time in some stochastic manner and may be unknown initially. These states are needed to eliminate bias in the state estimates when operating under nonideal model mismatch situations. The dynamics of x^s, given by

$$\frac{dx^s}{dt} = f^s(x,u,t) \tag{8.4}$$

are usually unknown. The common assumption of the dynamics of these states in the state estimation procedures is $f^s(x,u,t) = 0$. This assumption will work well provided x^s does not change substantially with time in some correlated manner.

Generally stated, the state estimation problem will be to predict the internal states $x(t)$ from a limited set of sampled measurements $y(t_k)$. It is assumed that some elements of x_0 will be initially unknown, and that some states will be time varying disturbances and/or fixed parameters that must be estimated.

8.3. NONLINEAR STATE ESTIMATION

In the sections to follow, the basic theory behind three different strategies for state estimation in nonlinear processes will be reviewed.

8.3.1. The Extended Kalman Filter

The solution to the finite time optimal filtering and estimation problem for linear processes with independent additive Gaussian white noise on the states and outputs is well known and was first laid down by Kalman (1960). This theory has been extended to nonlinear systems (Jazwinski, 1970) to provide a suboptimal filter with the same structure as that used for linear systems. Only the results are summarized below.

Given the current estimate of the state vector $x(t_k \mid t_k)$, the state vector prediction at t_{k+1} $x(t_{k+1} \mid t_k)$ is obtained by

$$x^d(t_{k+1} \mid t_k) = x^d(t_k \mid t_k) + \int_{t_k}^{t_{k+1}} f^d(x,u,t)dt \tag{8.5}$$

$$x^s(t_{k+1} \mid t_k) = x^s(t_k \mid t_k) \tag{8.6}$$

In (8.6) $f^s(x,u,t)$ has been assumed to be zero according to the discussion in section 8.2. Performing a local linearization and discretization of state models (8.1) and (8.4) at conditions $x(t_{k+1} \mid t_k)$gives

$$x_{k+1} = A_k x_k + w_k \tag{8.7}$$

where

$$x_{k+1}^d = A_k^d x_k^d + A_k^s x_k^s + w_k^d \tag{8.8}$$

$$x_{k+1}^s = x_k^s + w_k^s \tag{8.9}$$

$$x_k = \begin{bmatrix} x_k^d \\ x_k^s \end{bmatrix} \tag{8.10}$$

$$A_k = \begin{bmatrix} A_k^d & A_k^s \\ 0 & I \end{bmatrix} \tag{8.11}$$

A_k is the Jacobian matrix of $f(x,u,t)$ with respect to $x(t_{k+1} \mid t_k)$, and w_k is a zero mean, Gaussian white noise vector with covariance matrix R_w. This latter white noise vector w_k is introduced to account for errors in the right hand side of (8.7) arising from modelling errors, and errors due to linearization. The disturbance or parameter states x^s are shown in equation (8.9) to vary according to a nonstationary random walk where w_k^s represents the amount of change occurring between sampling intervals. R_w is usually specified to be diagonal both for convenience and for lack of information regarding covariances. Its diagonal elements (variances) are chosen to reflect the total possible error in each row of (8.7) over the interval t_k to t_{k+1}, or the amount of change that can be expected between sampling periods for the case of disturbances and parameters.

The measurements are, in general, a nonlinear function of the states and controls, given by

$$y_k = h(x_k, u_k, t_k) + v_k \tag{8.12}$$

where v_k is again assumed to be a zero mean Gaussian white noise vector of measurements errors with covariance matrix R_v. This covariance matrix is usually easily obtained from replicated measurement data.

When a new observation y_{k+1} becomes available at t_{k+1}, the states are estimated iteratively through the filter equation

$$x_{k+1|k+1} = x_{k+1|k} + K_k\{y_{k+1} - h(x_{k+1|k}, u_{k+1}, t_{k+1})\} \tag{8.13}$$

where K_k is the Kalman gain at t_k. Given (8.7) and (8.12) with R_w, R_v, a prior initial state estimate x_0 having a Gaussian distribution with covariance matrix P_0 in the initial estimation error, the Kalman gain K_k is determined so that the variance of the estimation error $e = (x_k - x_{k|k})$, denoted by

$$Tr[P_k] = Tr[E\{(x_k - x_{k|k})(x_k - x_{k|k})^T\}] \tag{8.14}$$

is minimized. For nonlinear systems, an approximate optimal solution for K_k given R_w, R_v, and P_0 is updated with every new observation using the equations given below:

$$P_{k+1|k} = A_k P_{k|k} A_k^T + R_w \tag{8.15}$$

$$K_k = P_{k+1|k} H_k^T (H_k P_{k+1|k} H_k^T + R_v)^{-1} \tag{8.16}$$

$$P_{k+1|k+1} = P_{k+1|k} - K_k H_k P_{k+1|k} \tag{8.17}$$

In the equations above, H_k represents the Jacobian matrix of $h(x,u,t)$ with respect to $x_{k+1|k}$, and $P_{k|k}$ is the covariance matrix of the estimation error in $x_{k|k}$ at t_k.

Equations (8.13) and (8.15) to (8.17) define the extended Kalman filter. This set of update equations provides a very simple approach to infer nonlinear process states given a limited set of measurements corrupted with added white noise. The main difficulty with this approach is that the filter is derived from the statistics of the added Gaussian white noise terms w_k and v_k, and often this information is unknown. If a serious error in judgement is made selecting R_w, R_v, and P_0 the extended Kalman filter could provide poor biased estimates of the nonlinear states. Because of this much insight together with prior simulation is usually required to arrive at an acceptable set of tuning parameters.

8.3.2. Reiterative Extended Kalman Filter

The extended Kalman filter described in section 8.3.1 closely approximates the true solution to the nonlinear estimation problem for Gaussian w_k and v_k about a known nonlinear reference trajectory given by (8.1), (8.2), and (8.4), provided that x_0 is known exactly at the start. When x_0 is initially not known, Jazwinski (1970) suggests that the extended Kalman filter be restarted from the beginning with each new measurement using an updated estimate for $x_{0|t_k}$. This modification, although simple in principle, can lead to a substantial increase in the computational effort in the state estimation procedure, depending on the difficulty of back calculating x_0 given x_{t_k}. When initially unknown states have no dynamics (i.e. $dx_i/dt = f_i(x,u,t) = 0$) the modification is trivial since the extended Kalman filter is simply restarted with x_{i_0} equal to the most recent estimate of $x_i(t_k \mid t_k)$. However, when the initially unknown states have dynamic terms (i.e. $dx_i/dt = f_i(x,u,t) \neq 0$), the computational effort can increase substantially relative to the standard extended Kalman filter, requiring the solution to a system of nonlinear equations with integral expressions to obtain

$x_{0|t_k}$. Instead of a direct solution, a recursive nonlinear parameter estimation procedure can be combined with the standard extended Kalman filter to estimate the initial unknown states using the results from well-known sensitivity analyses. More details on this approach will be provided in the sections to follow.

If feedback control is to be applied to a batch/semi-batch process rapid convergence to initially unknown disturbance and parameter states is required due to the finite operation time. The modification proposed above should lead to improved convergence relative to the standard extended Kalman filter provided disturbance and parameter variations are not significant during the period where the reiteration is to be carried out. The reiteration procedure would only be required during the early stages of nonlinear estimation until convergence to the unknown x_0 is achieved, and therefore, would not expected to lead to excessive computation relative to the standard extended Kalman filter approach.

8.3.3. Nonlinear Optimization Approach

Jang et al. (1986) suggest an approach to nonlinear state estimation through a nonlinear optimization of some specified objective function of the measured and predicted outputs with respect to unknown process states over a finite horizon. The logical choice for an objective function to infer states from would be the minimization of

$$J(x_0) = \sum_{t=1}^{n}\sum_{j=1}^{m}\sum_{b=1}^{m}(y_{j,t}^{M}-y_{j,t})(y_{b,t}^{M}-y_{b,t})(R_v)_{j,b}^{-1} + \sum_{a=1}^{s}\sum_{b=1}^{s}(x_{a,0}^{p}-x_{a,0})(x_{b,0}^{p}-x_{b,0})(P_0)_{a,b}^{-1} \qquad (8.18)$$

which provides maximum likelihood estimates of unknown state vector x_0 assuming measured outputs of the form (8.12) with zero mean Gaussian v_t having a specified covariance R_v. In (8.18) $y_{j,t}^{M}$ and $y_{j,t}$ refer to the j'th measured and model predicted output measurements at sampling interval t. The indices n, m, and s represent the number of sampled periods, measurements, and states respectively. The vectors x_0 and x_0^p represent the estimated and prior estimate of parameter and disturbance states that are unknown at time $t = 0$. The second term in (8.18) is included to allow for prior information on unknown states x_0^p with covariance P_0 to be included in the state estimation problem.

The optimal solution for x_0 in (8.18) may be found using gradient based methods such as Levenberg-Marquardt, quasi-Newton, and conjugate gradient approaches. The gradient of the objective function with respect to x_0 may be estimated using finite difference approximations, or alternatively, can be estimated through sensitivity analysis. Using the chain rule for differentiation, it can be shown that the gradient can be estimated by

$$\frac{\partial J(x_0)}{\partial x_{i,0}} = -2\sum_{t=1}^{n}\sum_{j=1}^{m}\sum_{b=1}^{m}\left(\frac{\partial y_{j,t}}{\partial x_{i,0}}\right)(y^{M}_{b,t}-y_{b,t})(R_v)^{-1}_{j,b} - 2\sum_{b=1}^{s}(x^{p}_{b,0}-x_{b,0})(P_0)^{-1}_{i,b} \tag{8.19}$$

where

$$\frac{\partial y_{j,t}}{\partial x_{i,0}} = \sum_{k=1}^{s}\left(\frac{\partial h(x,u,t)}{\partial x_{k,t}}\right)\left(\frac{\partial x_{k,t}}{\partial x_{i,0}}\right) \tag{8.20}$$

$$\frac{d}{dt}\left(\frac{\partial x_{k,t}}{\partial x_{i,0}}\right) = \sum_{a=1}^{s}\left(\frac{\partial f(x,u,t)}{\partial x_{a,t}}\right)\left(\frac{\partial x_{a,t}}{\partial x_{i,0}}\right) \tag{8.21}$$

Relative to extended Kalman filtering, the nonlinear optimization approach requires a much greater computational effort, especially when a multivariable nonlinear estimation problem is involved. The computational procedures would make this approach impractical for many state estimation problems. It has been argued by Jang et al. (1986) that the benefit of this approach relative to extended Kalman filtering is that it can be applied with no prior knowledge of the process statistics, and that R_v can be arbitrarily set to I for convenience. Such a blind approach to selecting the weighting parameters could seriously degrade the state estimation procedure when the noise level in the measurements are significantly different. In addition, multiple measurements obtained from a similar sensor would be expected to display some correlation, and would not be correctly accounted for in the parameter estimation procedure.

Another problem with the nonlinear optimization approach is the assumption that unknown disturbances or parameter are fixed during the optimization horizon. When time varying disturbances or rapidly changing conditions are present, such an assumption could introduce serious error in the state estimates. This problem can only be dealt with if prior knowledge is available concerning the unknown parameter trends, which rarely would be the case.

8.4. CASE STUDY: STATE ESTIMATION FOR A SEMI-BATCH SBR POLYMERIZATION REACTOR

The nonlinear state estimation approaches described in the previous sections will be used to estimate the minimal internal model states in a semi-batch stirred tank reactor where the free radical emulsion copolymerization of styrene/butadiene rubber (SBR) is occurring. The reactor is assumed to be initially seeded with polystyrene seeds, with no significant nucleation occurring during the reaction. In this study only styrene and butadiene will be fed to the reactor, and the reactor will be assumed to be operated isothermally. This

mode of operation was chosen for simplicity, with the results extending easily to the more general case of changing inlet flows of more components and changing operating conditions that may occur when feedback control is applied.

In essentially all free radical polymerizations, the major source of disturbances arises from reactive impurities. Huo et al. (1988) demonstrated that both water soluble and monomer soluble reactive impurities consume radicals in free radical polymerizations which in turn significantly affects all the material balance states in the reactor. It will be assumed that reactive impurities can be present in both monomer feeds, and that the impurity level in the initial reactor charge is unknown. It is also assumed that there may be significant error in the number of particle seeds (N_p) in the reactor either due to an initial wrong starting estimate, coagulation, or further nucleation at the start of the reaction. In this work errors in the initial estimates of the reactive impurities in the reactor, reactive impurity inlet flow rates, and number of particles will be taken to be the major cause of deviation between the true and model predicted process response.

Simulation of the SBR process requires the integration of deterministic ordinary differential equation (ODE) states listed below:

- M_s : moles of unreacted styrene
- M_b : moles of unreacted butadiene
- P_s : moles of styrene bound in copolymer
- P_b : moles of butadiene bound in copolymer
- I_n : moles of unreacted thermal initiator
- CTA : moles unreacted chain transfer agent
- V_pQ_0 : product 0'th moment and particle volume
- V_pQ_1 : product 1'st moment and particle volume
- V_pQ_2 : product 2'nd moment and particle volume
- $V_pQ_0Bn_3$: product V_pQ_0 and trifunctional branch frequency
- $V_pQ_0Bn_4$: product V_pQ_0 and tetrafunctional branch frequency

These states provide the minimal information needed to compute copolymer properties of interest for feedback control, such as copolymer composition, conversion, branching and crosslinking, number and weight average molecular weight, polydispersity, and average particle size. Details on the model development and the form of the differential equations describing these states can be found in the previous chapter. The model also includes differential states corresponding to a single impurity in both the water and organic phases, and are listed below:

- Im_p : moles of unreacted organic phase impurity

- Im_w : moles of unreacted water phase impurity

These states are included in the model according to the discussion above, and are used to predict the effect of impurity disturbances on the reactor progress. The inlet feed rates of the impurities and the particle concentration, previously described as an important source of model prediction error, are included as parameters in the SBR model.

A subset of the differential equation states described above will be used in the nonlinear state estimation procedures to follow. The subset of states will differ depending on the state estimation routine used.

8.4.1. State Observability

In order for a state estimation strategy to converge to the correct solution, it is necessary for the unknown internal model states to be uniquely related to the limited set of sampled measurements. During operation, periodic sampling from a small bleed taken from the reactor will be made to allow for some on-line measurements. In this study, it will be assumed that the following on-line measurements will be available:

- y_1 : M_s moles of styrene in the reactor inferred from an on-line G.C. analysis on a sample taken from the bleed

- y_2 : M_b moles of butadiene in the reactor inferred from an on-line G.C. analysis on a sample taken from the bleed

- y_3 : D_p average unswollen particle size from dynamic light scattering

- y_4 : CTA moles of unreacted chain transfer agent obtained from on-line chemical analysis on a sample taken from the bleed

The nonlinear relationship between average unswollen particle size D_p and the model states is given by

$$D_p = \sqrt[3]{\frac{6(P_s M_{W_s} + P_b M_{W_b})}{\pi d_p N_r V_w}} \tag{8.22}$$

The assumption will be made that the bleed can be sampled every 10 minutes, with the results of the measurement analyses provided only just before the next sampling interval. Accommodation must be made in the state estimation approaches for the delay resulting from the measurement analyses. It will also be expected that these measurements will be corrupted with significant sensor noise.

Schuler and Suzhen (1985) have shown that polymer reaction models can be divided into two subsystems. The first subsystem contains differential states and variable parameters related to material balance properties. In this case study, these states and parameters would refer to M_r, M_b, P_s, P_b, CTA, I_n, Im_w, Im_p, V_pQ_1, N_p, F_{Im_p}, and F_{Im_w}. The second subsystem is made up of differential states associated with molecular weight and branch frequency properties, and in this work would refer to V_pQ_0, V_pQ_2, $V_pQ_0Bn_3$, and $V_pQ_0Bn_4$. The two subsystems are shown in Figure 8.1.

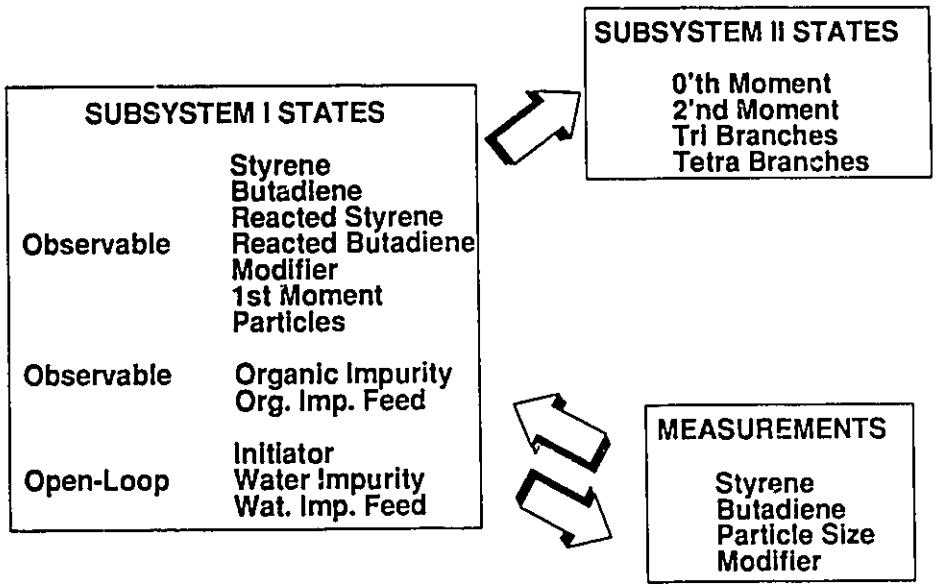

FIGURE 8.1: State Observability In SBR Process

The figure indicates that states in the first subsystem effect states in the second subsystem, but no feedback exists from the states of the second subsystem to the first. The measurements are also shown to provide information only on the material balance states of subsystem I, and are not affected by the states in subsystem II. Because no feedback on measured information is available on the states of the second subsystem, these states are not observable. However, they may be predicted if the important states of the first subsystem are known, and the relationship between these states and their influence are modelled accurately. Unfortunately,

sensors do not exist for polymer latex that would provide needed information of the states of subsystem II to meet observability requirements, forcing one to rely on conditional predictions based on the model in the state estimation procedure.

All states in subsystem I are not observable from measurements y_1 to y_4 alone. It can be shown that sufficient information is available to estimate M_s, M_b, P_s, P_b, CTA, and V_pQ_1 together with parameter N_p from the measurements if only a subset of the remaining states are included in the estimator. The problem is due to states Im_p, Im_w, and I_a together with inlet flow rate parameters F_{Im_p} and F_{Im_w} which do not satisfy observability requirements when all terms are not known. It can be shown that a unique solution for these terms cannot be found from the available measurements when unknown. Given this physical limitation, one subset of these states and parameters above must be either fixed a priori or inferred open-loop through the model, while the remaining set will be estimated through the nonlinear estimation algorithm. This step may introduce significant bias in some of the these state estimates, but still allow the important states that are needed for property calculations for control to be free from bias. In the work that follows, the differential state Im_p and disturbance parameter F_{Im_p} will be estimated. Im_p was selected over Im_w since the latter typically represents the effect of oxygen poisoning. This impurity usually causes an initial period of inhibition followed by the expected reaction progress if no more of this impurity is added during the semi-batch run. Therefore, it will be assumed that the state estimation routine will be started after any period of inhibition, and that the amount of oxygen in the monomer feeds can be reasonably approximated from known solubilities.

The set of states M_s, M_b, P_s, P_b, CTA, Im_p, V_pQ_1 together with parameters N_p and F_{Im_p} can be shown to meet observability requirements. Observability would also be met if CTA was neglected as both a state and measurement in the state estimation problem. The CTA measurement provides information on the radical concentration in the reactor which is already obtained through the M_s and M_b measurements, and therefore will only provide confirmation on the reaction progress if model mismatch is not serious. The CTA is included to improve the prediction of the molecular weight properties. The molecular weight properties in the SBR process are strongly influenced by radical chain transfer to CTA. Therefore, improved knowledge of the amount of CTA should provide improved molecular weight property predictions.

8.5. SIMULATION STUDIES WITHOUT MODEL MISMATCH

The first set of simulation studies will be concerned with estimating the minimum number of deterministic states specified in section 8.4 in order to compute copolymer properties for feedback control. It will be assumed that the model proposed in the previous chapter on modelling is correct. The true recipe of the initial charge and the operating conditions are listed below:

Initial Charge

M_a	: 0.1 *gmol*
M_b	: 0.1 *gmol*
P_a	: 0.04 *gmol*
P_b	: 0.0 *gmol*
I_n	: 0.03 *gmol*
E	: 0.01 *gmol*
Im_w	: 0.0 *gmol*
Im_p	: $1.25x10^{-5}$ *gmol*
N_p	: $2x10^{17}$ l^{-1}
V_w	: 4.8 *l*
CTA	: 0.0275 *gmol*

Operating Conditions

T	: 55° *C* (constant)
F_{M_a}	: 0.00871 *gmol*/min (constant)
F_{M_b}	: 0.00871 *gmol*/min (constant)
F_{Im_p}	: $1.09x10^{-6}$ *gmol*/min (constant)

The state estimation algorithms to follow will be initialized with the same recipe and operating conditions as above with the exception of three initialization errors:

Initialization In State Estimation Algorithms

Im_p	: 0.0 *gmol*
N_p	: $1x10^{17}$ l^{-1}
F_{Im_p}	: 0.0 *gmol*

For convenience in the state estimation routines, the state variables in the work that follows shall be scaled as indicated below:

Variable	Scale Factor

M_s	: 1
M_b	: 1
P_s	: 1
P_b	: 1
Im_p	: $1x10^5$
N_pV_w	: $1x10^{-17}$
F_{Im_p}	: $1x10^6$
CTA	: 100
V_pQ_0	: 1000
V_pQ_1	: 1
V_pQ_2	: 0.001
$V_pQ_0Bn_3$	: $1x10^4$
$V_pQ_0Bn_4$	: $1x10^4$

The effect of the initialization errors in Im_p, N_p, and F_{Im_p} on the model predicted open-loop response on states $M_s, M_b, P_s, P_b, Im_p, CTA, V_pQ_0, V_pQ_1, V_pQ_2, V_pQ_0Bn_3$, and $V_pQ_0Bn_4$ is shown in Figure 8.2. The results clearly indicate that the three errors lead to a substantial deviation in predicting the progress of the reactor states.

The measurements in a real process environment will be expected to be corrupted with noise. In the simulations to follow, the measurements will be corrupted with additive Gaussian white noise with the variances indicated below:

Output			Variance
y_1	:	M_s	0.002 $gmol^2$
y_2	:	M_b	0.002 $gmol^2$
y_3	:	D_p	200 $\overset{o}{A}^2$
y_4	:	CTA	$2x10^{-7}$ $gmol^2$

The variances of y_1 and y_2 were deduced from limited data provided by experimental work performed by Hoffman (1984) and Campbell (1985), where an on-line G.C. was used for monomer conversion estimation. The variance for y_3 was estimated based on data obtained from Korti(1989) where on-line dynamic light scattering measurements were used for polystyrene particle size measurements. Without any on-line sensor currently available for CTA measurement, the variance listed above was simply a reasonable guess of what one might hope to achieve. Due to lack of data, the covariances of the measurements have been assumed to

be zero. In practice, this assumption would be expected to be poor for both y_1 and y_2, since both of these measurements are obtained from the same sensor (G.C.). However, replicate measurements on a few standard mixtures could be used to estimate this.

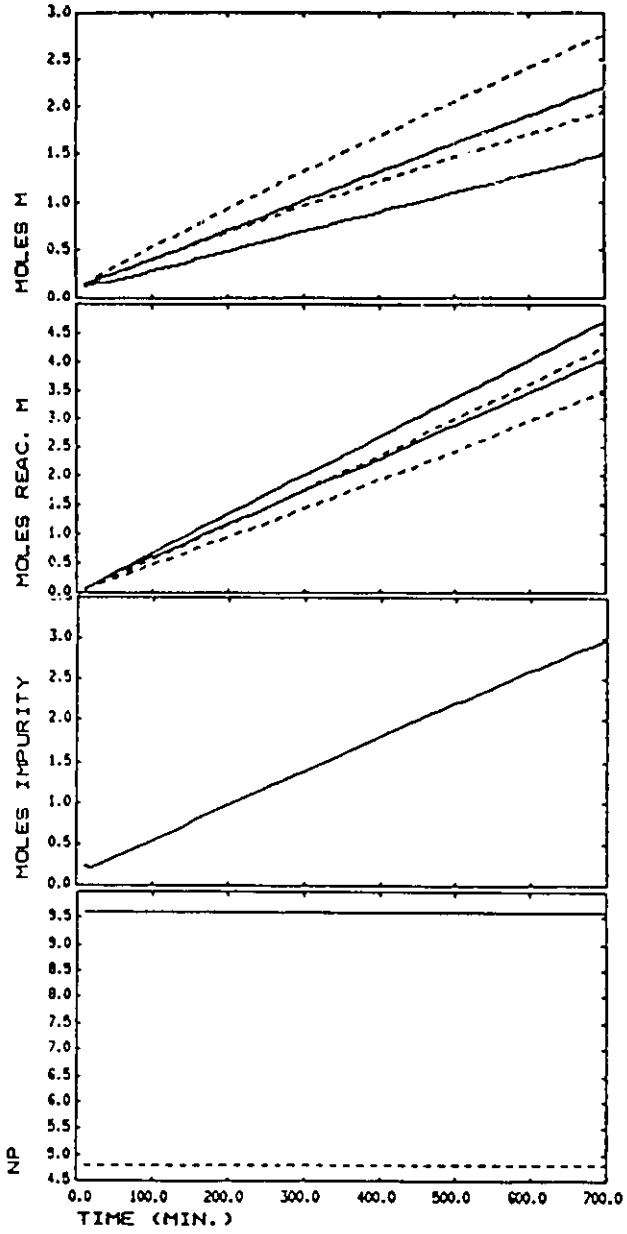
MOLES M
MOLES REAC. M
MOLES IMPURITY
NP
TIME (MIN.)
0.0
100.0
200.0
300.0
400.0
500.0
600.0
700.0

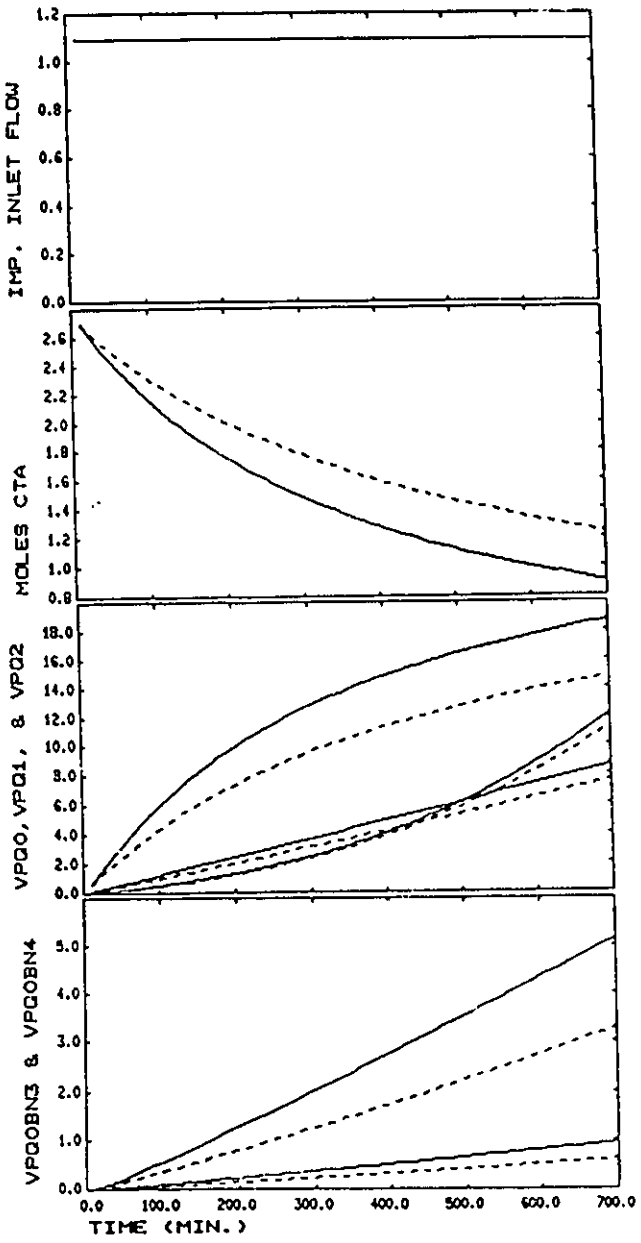

FIGURE 8.2: Effect Of Initialization Errors On Model Predicted Open-loop Response
(-) Actual Response; (--) Predicted
(a) M_r & M_b; (b) P_r & P_b; (c) Im_p; (d) N_p
(e) F_{Im_p}; (f) CTA; (g) V_pQ_0, V_pQ_1, & V_pQ_2; (h) $V_pQ_0Bn_3$ & $V_pQ_0Bn_4$

8.5.1. Extended Kalman Filter Formulation And Simulation

The objective of this section will be first to demonstrate the importance of the correct incorporation of nonstationary disturbance and parameter states to eliminate bias, and second, to tune and evaluate the extended Kalman filter for SBR emulsion state estimation.

As mentioned in the introduction, a common mistake that is made when formulating an extended Kalman filter is neglecting to include a reasonable set of nonstationary stochastic states that could explain the reasons for deviations between the model and the process. Neglecting these nonstationary states will lead to a Kalman filter that has no integrating capabilities that can eliminate these deviations. The sources of nonstationary bias can be due to disturbances or incorrect model parameters. To demonstrate the effect of this error in the estimation procedure, the extended Kalman filter will be formulated and applied using the minimal state vector

$$x^T = (M_s, M_b, P_s, P_b, Im_p, CTA, V_p Q_0, V_p Q_1, V_p Q_2, V_p Q_0 Bn_3, V_p Q_0 Bn_4)$$

needed for property calculations, and measurement vector

$$y^T = (M_s, M_b, D_p, CTA)$$

The extended Kalman filter was tuned with

$$R_w = Diag(0.001, 0.001, 0.001, 0.001, 1, 0.001, 0.001, 0.001, 0.001, 0.001, 0.001)$$

$$R_v = Diag(0.002, 0.002, 200, 0.002)$$

$$P_0 = Diag(0.01, 0.01, 0.01, 0.01, 10, 0.01, 0.01, 0.01, 0.01, 0.01, 0.01)$$

Im_p, F_{Im_p}, and N_p are set incorrectly in the extended Kalman filter as specified in the previous section. Figures 8.3(a) to 8.3(f) show the true (-) states compared to their one step ahead ($x_{k|k-1}$) state predictions. Figures 8.3(g) to 8.3(j) show the true measurements compared to their filtered estimates $y_{k|k}$. It is clearly evident in these figures that the extended Kalman filter leads to an unacceptable bias problem.

The poor performance of this extended Kalman filter can be easily explained. The deterministic states used in the extended Kalman filter posed above assume that each state and output will be in error by only zero mean white noise components w_k and v_k respectively. Therefore, the extended Kalman filter is unable to account for the nonzero mean bias between the true states and the filtered states due to the incorrect specification of Im_p, F_{Im_p}, and N_p. Often when this mistake is made, the designer attempts to mask the problem by introducing

a very large R_w. An example where this had been done is demonstrated in Hamilton et al. (1973). The consequence of taking such action is to remove the significance of the contribution of the deterministic modelled component $A_k x_k$ in the linearized and discretized state space model

$$x_{k+1} = A_k x_k + w_k \tag{8.23}$$

as a result of the large covariance matrix associated with w_k. This essentially reduces the state space model (8.23) to

$$x_{k+1} = w_k \tag{8.24}$$

which simply models all states as random walks with very large variances. The extended Kalman filter becomes a noisy state estimator in order to hide the bias problem, and provides poor present and future prediction of the progress of the process since the modelled deterministic component of the states is lost. In the example shown in Figure 8.3, the bias problem cannot be effectively removed with tuning of R_w and R_v.

The results above clearly indicate that F_{Im_p} and $N_p V_w$ must be included in the extended Kalman filter as a nonstationary disturbance and parameter state respectively. These states are assumed to be fixed deterministically (i.e. $f_i(x,u,t)=0$) and vary as a random walk according to (8.9). With these states added to the extended Kalman filter, the estimation problem becomes estimating

$$x^T = \left(M_s, M_b, P_s, P_b, Im_p, N_p V_w, F_{Im_p}, CTA, V_p Q_0, V_p Q_1, V_p Q_2, V_p Q_0 Bn_3, V_p Q_0 Bn_4\right)$$

using measurements $y^T = (M_s, M_b, D_p, CTA)$.

The next problem to be addressed is the selection of tuning matrices R_w, R_v, and P_0. For deterministic states, the diagonal elements of R_w were initially selected to allow for approximately a maximum 10% error in the model predictions at each sampling period. For nonstationary states $N_p V_w$ and F_{Im_p}, the corresponding diagonal elements of R_w were initially selected to roughly represent the maximum change that would be expected between sampling periods under real process operating conditions. These initial tuning parameters were only used as a first pass, and adjustments were made through repeated simulations until an acceptable compromise between speed of convergence and state smoothing was found. It was found that

R_w =

$$Diag(5x10^{-6}, 5x10^{-6}, 5x10^{-6}, 5x10^{-6}, 5x10^{-6}, 1x10^{-4}, 1x10^{-6}, 5x10^{-6}, 5x10^{-6}, 5x10^{-6}, 5x10^{-6}, 5x10^{-6}, 5x10^{-6})$$

led to acceptable performance. R_v was set to $Diag\,(0.002, 0.002, 200, 0.002)$ in accordance with the discussion in section 8.5. The diagonal elements of P_0 were chosen to reflect the expected variance in the initial error of the state estimates. For Im_p, N_pV_w, and F_{Im_p}, the variances in the initial estimates would be based on the range of the expected initial values from the history of past process operations. The variance of the initial error in the deterministic states that are assumed known at the start are based on the expected accuracy of the measurement procedure used in computing these states at $t = 0$. The use of an arbitrarily large P_0 that is often made in computing off-line Kalman filter gains for linear systems was not found to be acceptable since such a choice led to initial large excursions in the state predictions before converging. An acceptable choice was found to be

$$P_0 = Diag\,(0.0001, 0.0001, 0.0001, 0.0001, 1, 5, 1, 0.0001, 0.0001, 0.0001, 0.0001, 0.0001, 0.0001)$$

Figure 8.4 shows the performance of the correctly formulated extended Kalman filter, where in Figures 8.4(a) to 8.4(h) the true states x_k (-) are compared to $x_{k|k-1}$ (--), and the true measurements y_k (-) are compared to the filtered measurements $y_{k|k}$ (--) in Figures 8.4(i) to 8.4(l). The results show that the extended Kalman filter leads to bias free estimates in all the states and measurements. After about 10 measurements, Im_p, F_{Im_p}, and N_pV_w can be observed to converge to their true values. All filtered state estimates can be observed to be smooth and not severely influenced by the measurement noise.

In section 8.4.1, the states V_pQ_0, V_pQ_2, $V_pQ_0Bn_3$, and $V_pQ_0Bn_4$ were pointed out to be not observable from the measurements. Nevertheless, these states were included in the extended Kalman filter in the work above. Predictions of these states are improved by including them in the filter since the best estimates of the observable states are used in their prediction, and feedback information from errors in the observable states is used to correct the prediction of nonobservable states through the associated Kalman gain. This strategy differed from that used by Schuler and Suzhen (1985) where nonobservable states were left out from the Kalman filter formulation and predicted open-loop with the filtered estimates of the observable states. Intuitively, the approach taken here should be more effective since the error of integration of the nonobservable states from initialization errors in the observable states will be corrected from the feedback information.

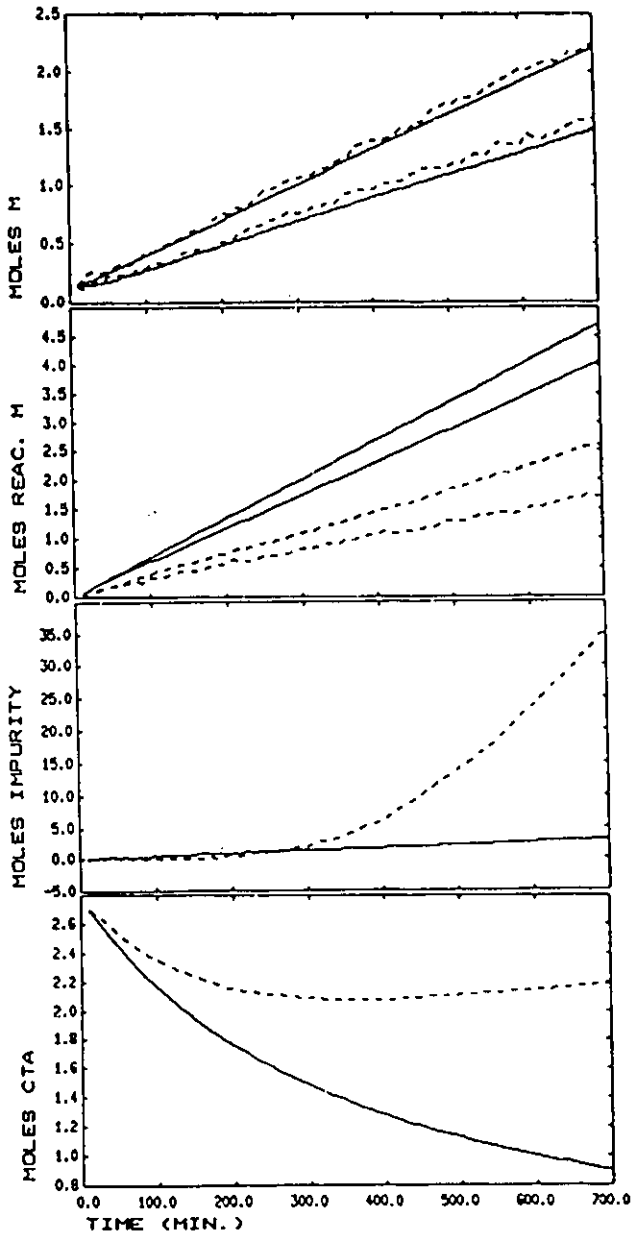
MOLES M
MOLES REAC. M
MOLES IMPURITY
MOLES CTA
TIME (MIN.)
0.0
100.0
200.0
300.0
400.0
500.0
600.0
700.0

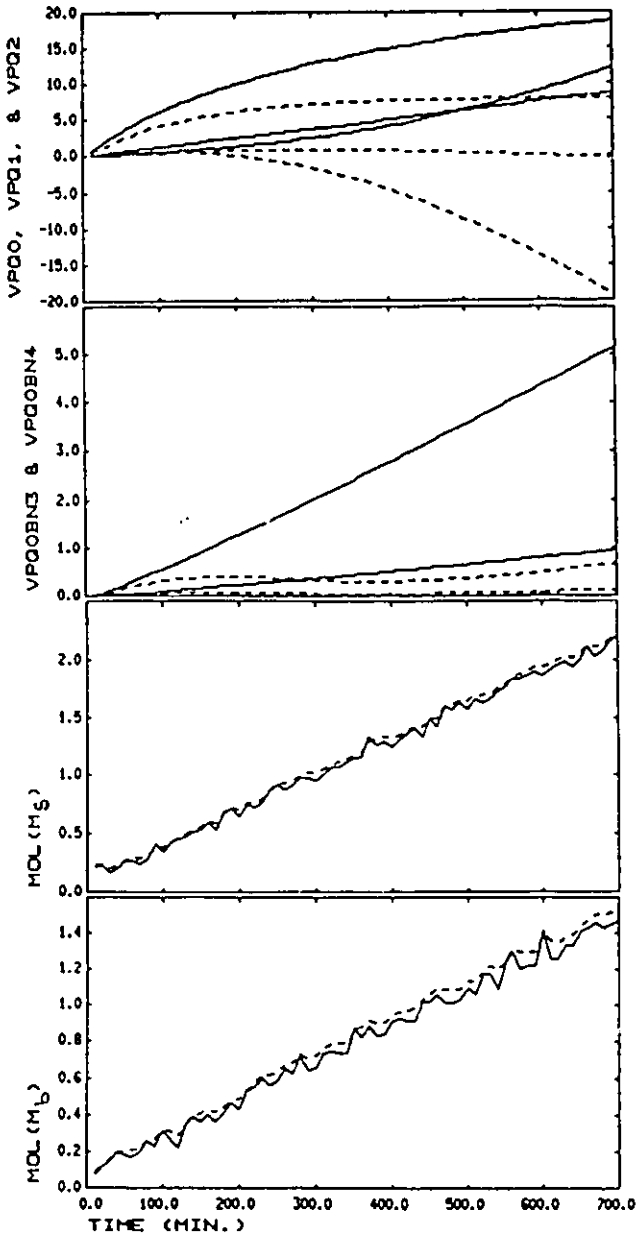
VPQ0, VPQ1, & VPQ2
VPQQBN3 & VPQQBN4
MOL(M_S)
MOL(M_D)
TIME (MIN.)
0.0
100.0
200.0
300.0
400.0
500.0
600.0
700.0

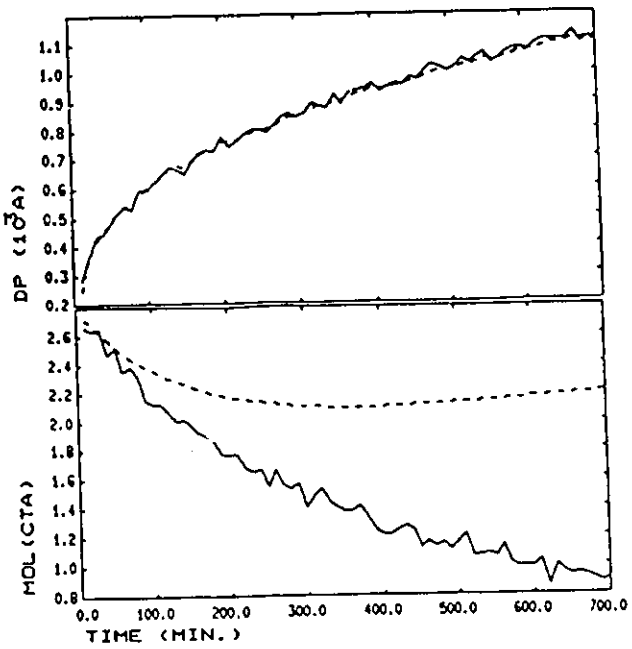

FIGURE 8.3: Extended Kalman Filter Without Nonstationary States
(-) Actual Response; (--) Predicted
(a) M_a & M_b; (b) P_a & P_b; (c) Im_p; (d) CTA;
(e) V_pQ_0, V_pQ_1, & V_pQ_2; (f) $V_pQ_0Bn_3$ & $V_pQ_0Bn_4$
(-) Measured y; (--) y_{kk}
(g) M_a; (h) M_b; (i) D_p; (j) CTA

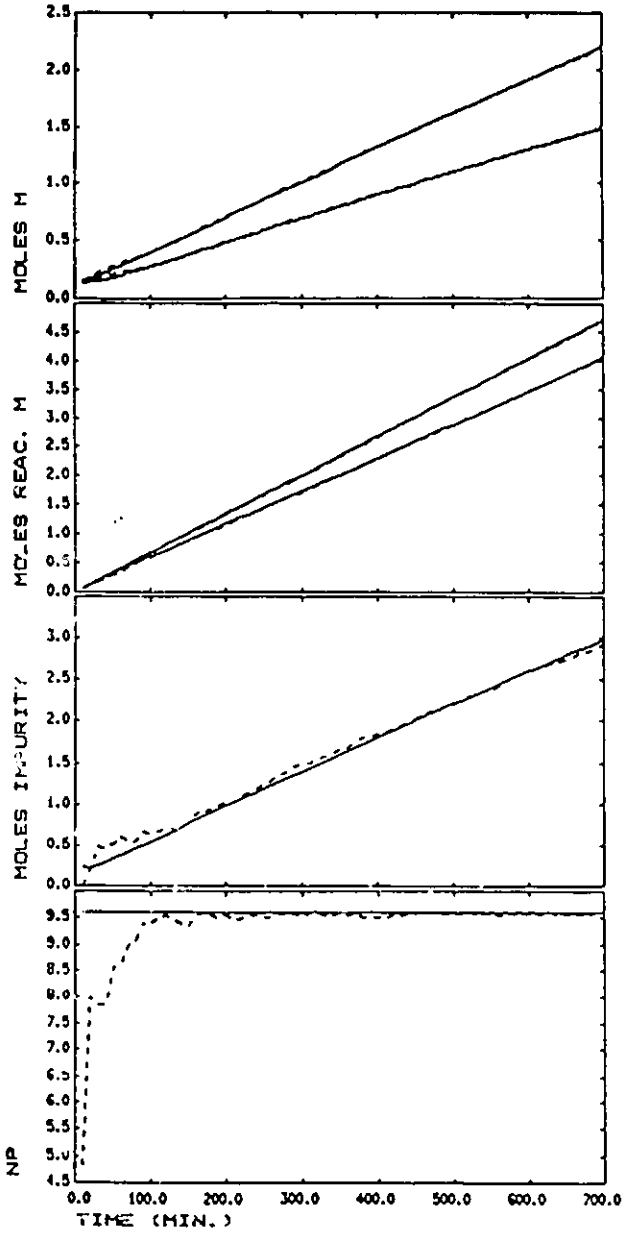
MOLES M
MOLES REAC. M
MOLES IMPURITY
NP
TIME (MIN.)
0.0
100.0
200.0
300.0
400.0
500.0
600.0
700.0

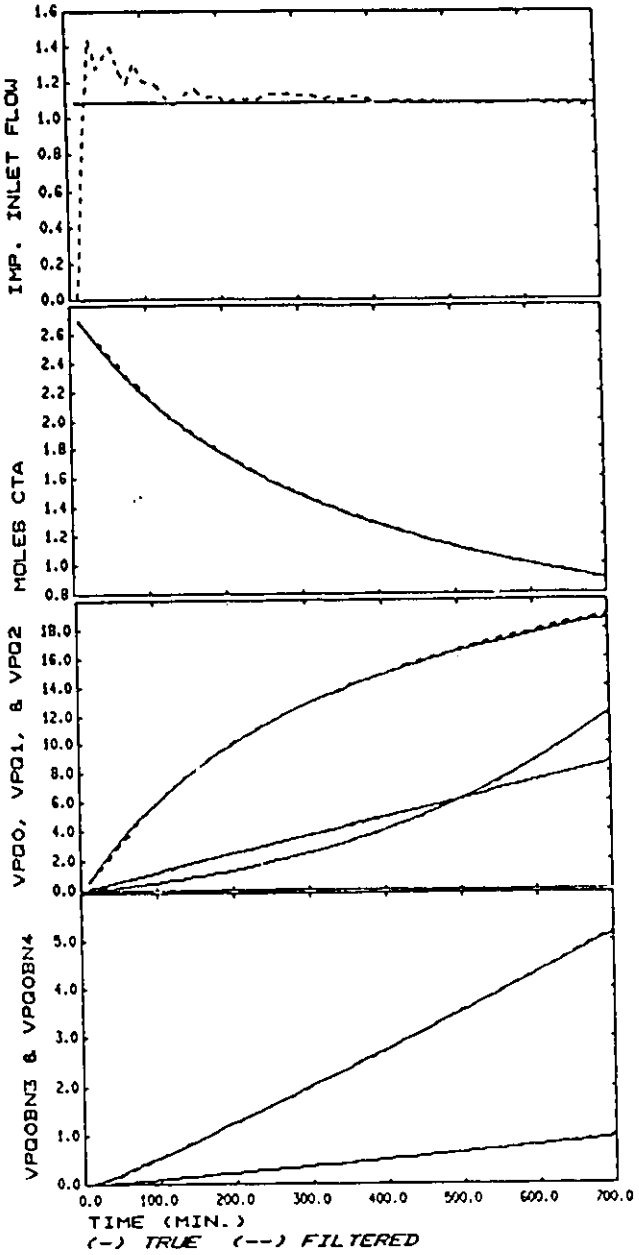
IMP. INLET FLOW
MOLES CTA
VPOO, VPO1, & VPO2
VPOOBN3 & VPOOBN4
TIME (MIN.)
(-) TRUE (--) FILTERED

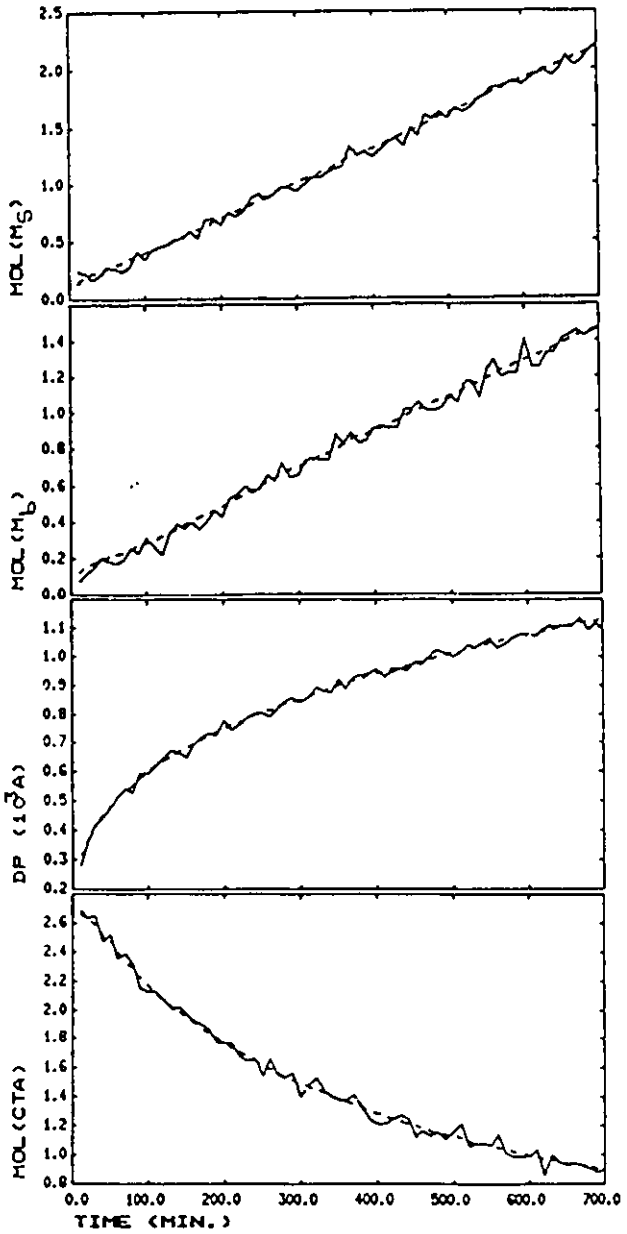

FIGURE 8.4: Extented Kalman Filter: Correct Formulation
(-) Actual Response; (--) Predicted
(a) M_s **&** M_b**; (b)** P_s **&** P_b**; (c)** Im_p**; (d)** N_p
(e) $\bar{F}_{Im_p}$**; (f)** CTA**; (g)** V_pQ_0**,** V_pQ_1**, &** V_pQ_2**; (h)** $V_pQ_0Bn_3$ **&** $V_pQ_0Bn_4$
(-) Measured y**; (--)** $y_{k/k}$
(i) M_s**; (j)** M_b**; (k)** D_p**; (l)** CTA

8.5.2 Reiterative Extended Kalman Filter Formulation And Simulation

The results from the previous section have demonstrated that the problem with the regular extended Kalman filter is that it is slow to recover from poor guesses of the initial state vector x_0. The reason for this is that the extended Kalman filter is a purely recursive estimator that never goes back to reprocess past initial data containing a lot of information on x_0. In section 8.3.2, it was pointed out that the performance of the extended Kalman filter to initialization errors in x_0 may be improved by adding an estimator for x_0 which processes early data to gradually improve the estimate in x_0, and reiterating the regular extended Kalman filter from $t = 0$ with all past data when a new measurement point is available.

Recognizing that the major uncertainties in the state estimation problem are the unknown initial values for the states Im_p, $N_p V_w$, and F_{Im_p}, it would seem logical to try to estimate these from the incoming data. This can be accomplished by defining a second extended Kalman filter with states $x^{2T} = \left(Im_{p_0}, N_p V_{w_0}, F_{Im_{p_0}}\right)$ and $dx_i^2/dt = 0$. The discrete form of the state space model with added stochastics becomes

$$x_{k+1}^2 = x_k^2 + w_k^2 \tag{8.25}$$

Since the state vector x^2 is initially unknown and assumed fixed throughout the entire semi-batch run, the logical choice for R_w would be 0. Ljung and Soderstrom (1987) has shown that the Kalman filter that results from his formulation is essentially a recursive least-squares parameter estimator with no discounting as a result of the specification $R_w = 0$.

Figure 8.5 shows a schematic of the reiterative extended Kalman filter approach.

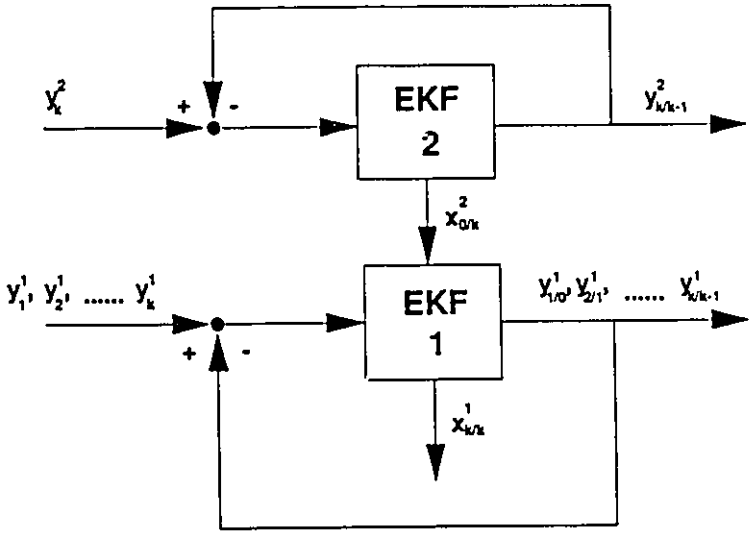

Figure 8.5: Reiterative Extended Kalman Filter

EKF 1 refers to the regular extended Kalman filter described in section 8.4.1, while EKF 2 refers to the second extended Kalman filter that provides estimates of the unknown initial states. At the y_k^2 measurement, EKF 2 provides a recursive estimate of the unknown initial states $x_{0|k}^{2\,T} = (Im_{p_0}, N_p V_{w_0}, F_{Im_{p0}})$ which is sent to EKF 1. EKF 1 is reiterated from $t = 0$ with y_1^1 to y_k^1 using the updated estimate of x_0^1 to get $x_{k|k}^1$.

In order to avoid excessive computations in the reiterative extended Kalman filter approach, only a minimal number of measurements needed to satisfy the observability condition are used in EKF 2. The vector of measurements was selected to be $y^{2T} = (M_s, M_b, D_p)$. The output vector is predicted from the integration of the minimal number of SBR model differential equations required in order to speed up computation time. These correspond to the states M_s, M_b, P_s, P_b, Im_p, and I_n. At every sampling interval the integration is repeated from $t = 0$ with $x_{k|k-1}^2$ to obtain the predicted measurements $y_{k|k-1}^2$. When the measurements are computed, the Jacobian matrix of $y_{k|k-1}^2$ with respect to $x_{k|k-1}^2$ is also estimated using sensitivity equations (8.20) and by adding additional differential equations defined by (8.21).

Figure 8.6 shows the performance of the proposed reiterated extended Kalman filter. Throughout the entire simulation, EKF 1 was restarted from $t = 0$ with estimates of the unknown initial states at $t = 0$ provided at every sampling period by EKF 2. EKF 2 was tuned using $R_w = 0$, $R_v = Diag(0.002, 0.002, 200)$, and $P_0 = Diag(1, 25, 1)$. The extended Kalman filter being reiterated (EKF 1) was exactly the same as in section 8.5.1 with the correct nonstationary states and the same tuning parameter matrices. As before, these plots display the true states x_k (-) against the one step ahead filtered values $x_{k|k-1}$ (--), and the true measurements y_k^M (-) against their filtered values $y_{k|k}$ (--) obtained from the reiterated extended Kalman filter. The plots clearly reveal that the reiterated extended Kalman filter converges significantly faster to the true states compared to the regular extended Kalman filter shown in Figure 8.4. The reiterated extended Kalman filter appears to be very close to the true states in about 5 sampling periods, whereas the regular extended Kalman filter takes about 10 sampling periods. The results also indicate that there appears to be very little benefit in reiterating after about 12 measurement periods, even through the estimates of the initial states, shown in Figure 8.6(i), do not appear to converge until 30 sampled measurements. Figure 8.6(i) shows that Im_{p_0}, $N_p V_{w_0}$, and $F_{Im_{p0}}$ eventually converge to their true values of $1.12x10^{-5}$ $gmol$, $2x10^{17}$ l^{-1}, and $1.09x10^{-6}$ $gmol$ respectively.

The computation time of the reiterative extended Kalman filter was much greater and not practical relative to the standard extended Kalman filter, with most of the computing time being spent on the reiterations

of later sampled measurements. However, when the reiterations are applied only for the first few sampling periods, thereby requiring only short integration times, the increased computational time was found to be insignificant, making the approach useful for practical purposes.

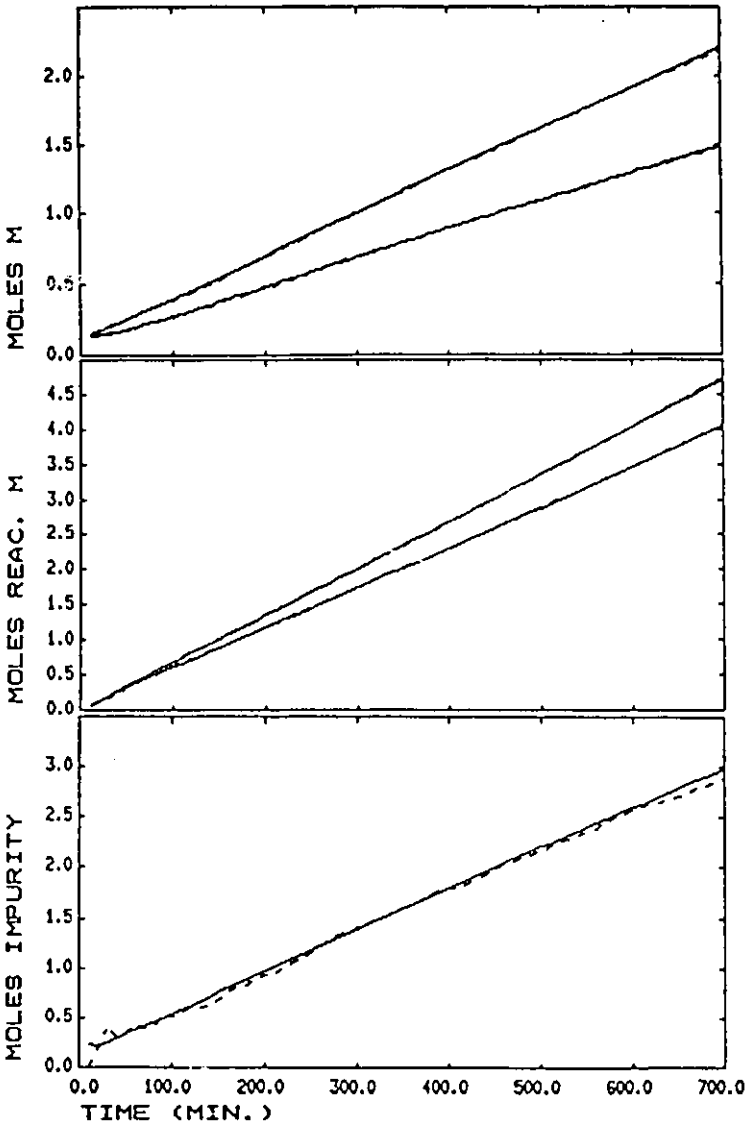
MOLES M
2.0
1.5
1.0
0.5
0.0
MOLES REAC. M
4.5
4.0
3.5
3.0
2.5
2.0
1.5
1.0
0.5
0.0
MOLES IMPURITY
3.0
2.5
2.0
1.5
1.0
0.5
0.0
0.0
100.0
200.0
300.0
400.0
500.0
600.0
700.0
TIME (MIN.)

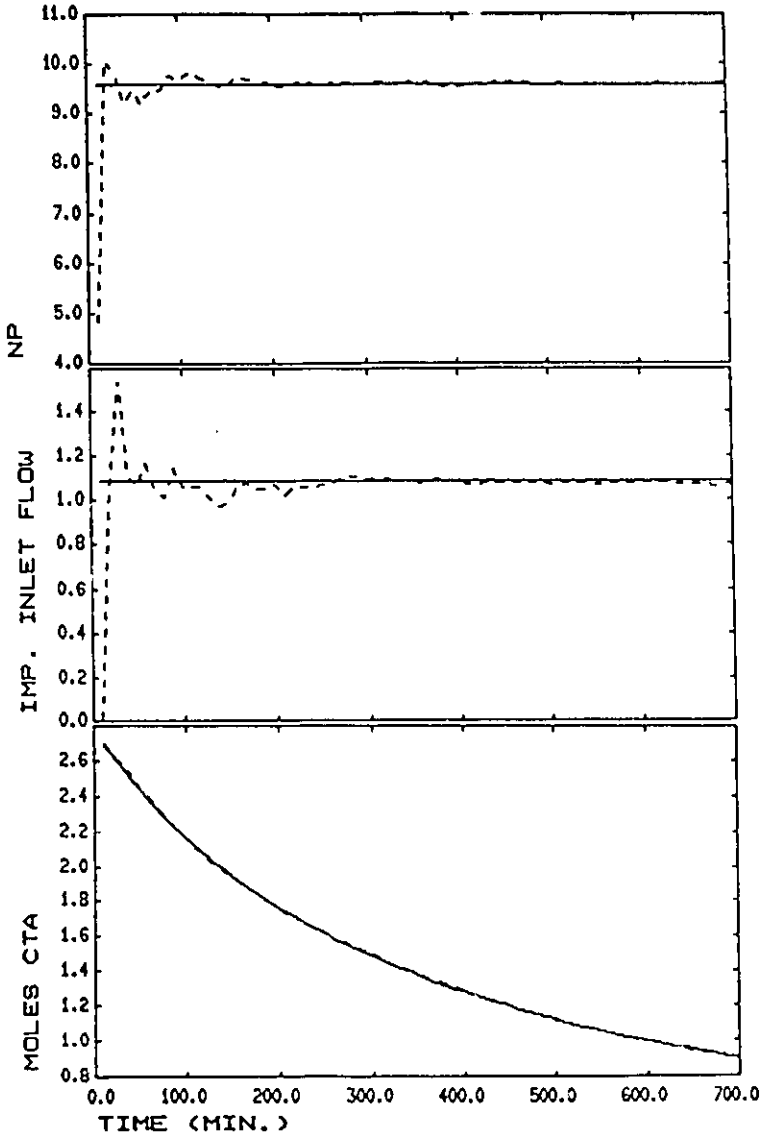
NP
11.0
10.0
9.0
8.0
7.0
6.0
5.0
4.0
IMP. INLET FLOW
1.4
1.2
1.0
0.8
0.6
0.4
0.2
0.0
MOLES CTA
2.6
2.4
2.2
2.0
1.8
1.6
1.4
1.2
1.0
0.8
0.0
100.0
200.0
300.0
400.0
500.0
600.0
700.0
TIME (MIN.)

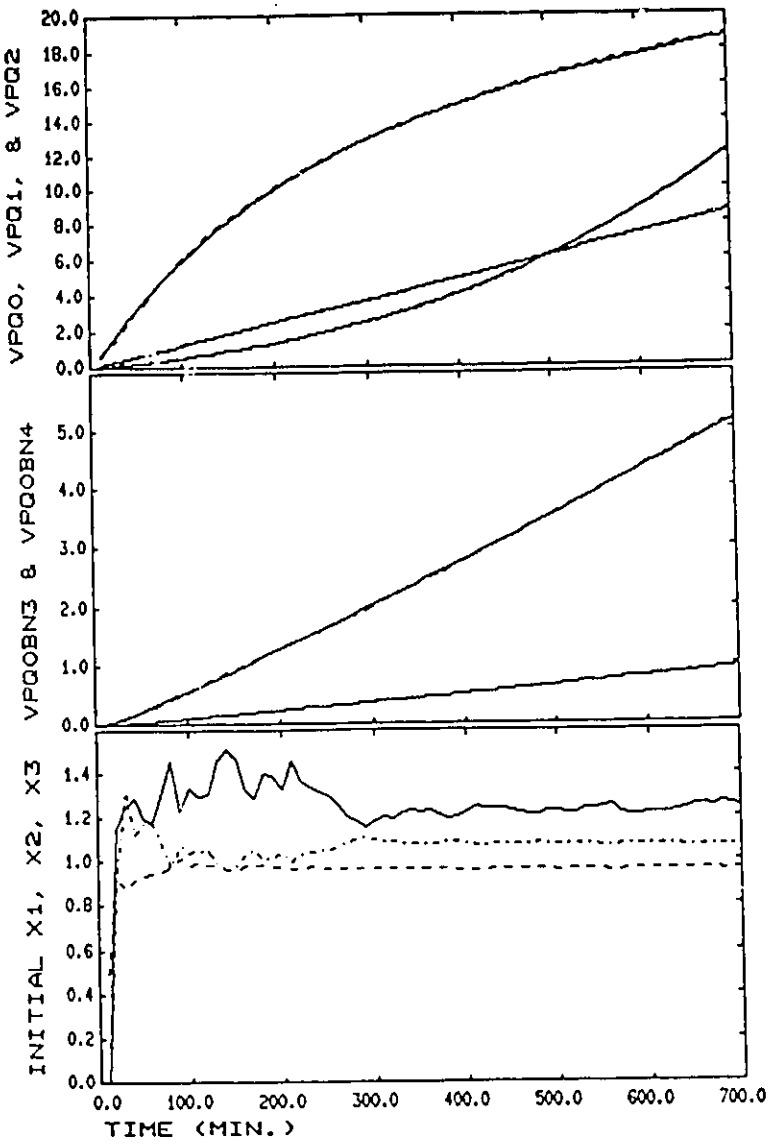

FIGURE 8.6: Reiterative Extented Kalman Filter
(-) Actual Response; (--) Predicted
(a) M_a & M_b; (b) P_a & P_b; (c) Im_p; (d) N_p
(e) F_{Im_p}; (f) CTA; (g) V_pQ_0, V_pQ_1, & V_pQ_2; (h) $V_pQ_0Bn_3$ & $V_pQ_0Bn_4$
(i) Im_{p_0} (-), $N_{p_0}/10$ (--), $F_{Im_{p0}}$ (..)

8.5.3. Nonlinear Optimization Approach Formulation And Simulation

The nonlinear optimization approach of Jang et al. (1987), described in section 8.3.3 was applied to the SBR semi-batch estimation problem. The objective function to be minimized with respect to unknown initial states $x_0^T = \left(Im_{P_0}, N_p V_{w_0}, F_{Im_{P_0}}\right)$ is given by (8.18). In order to reduce computation time, only a minimal number of measurements are used to satisfy observability requirements. The measurements used in the on-line optimization approach are $y^T = (M_s, M_b, D_p)$, and are computed from the model by integrating only the differential equations corresponding to M_s, M_b, P_s, P_b, Im_p, and I_a. The gradient of (8.18) with respect to x_0 was obtained using sensitivity equations (8.19) and (8.20). This approach was found to be faster than using forward differencing to estimate the gradient and was also found to give a better estimate of the gradient at the optimum in several test cases tried. Several quasi-Newton and conjugate gradient algorithms were evaluated for solving the optimization problem posed above. From the results of several test cases, it was decided to use the unconstrained optimization routine "CONMIN" obtained from the "TOMS" library that uses a Beale restarted conjugate gradient algorithm. More computationally efficient methods may exist for solving the optimization problem in this work (Beigler, 1984). However, this issue is not the point of this section. The main issue in this work is the potential performance of this approach to nonlinear state estimation.

The weighting R_v^{-1} on the squared differences between the model predicted measurements and the measured values was taken to be $Diag(1/0.002, 1/0.002, 1/200)$, the inverse of the covariance matrix of the measurements. This corresponds to the maximum likelihood weighting for the assumed statistics of the measurements. The optimization problem was resolved at every sampling interval, and the optimization horizon was taken from $t = 0$ to the most recent sampled measurements.

Figure 8.7 shows the performance of the nonlinear optimization approach with no prior information on the initial estimates assumed (i.e. $P_0^{-1} = 0$). The $x_{k|k-1}$ predictions from the optimization estimator can be observed to converge to their true values. Relative to the standard extended Kalman filter, shown in Figure 8.4, the nonlinear optimization approach led to improved convergence since all the present and past data are used in the latter approach. However, relative to the reiterated extended Kalman filter approach, shown in Figure 8.6, the convergence of the nonlinear optimization approach was slightly inferior.

The optimal estimates for x_0 are shown in Figure 8.7(i). After about 25 samples the initial estimates can be seen to converge to their correct values. The optimization routine ran into difficulty in the initial sampling periods where an excessive number of function evaluations where encountered to meet the convergence specification on the gradient. During this time it was found that the Hessian at the solution was nearly positive

semidefinite. The explanation for this can be found through an identifiability condition analysis on the optimization problem posed at every sampling interval. The covariance matrix of x_0 can be shown to be given by $(X^T R_v^{-1} X)^{-1}$, where X is the matrix of sensitivity coefficients (Beck and Arnold, 1977; Jang et al., 1986) whose elements are obtained from (8.20). Since $|(X^T R_v^{-1} X)^{-1}| = |(X^T X)^{-1}|\,|R_v^{-1}|$, an indication of the size of the covariance of estimates x_0 can be found by examining $|(X^T X)^{-1}|$. If this term is large, it is expected that a nearly singular least squares error problem has been posed due to a lack of sufficient measurement points. A plot of $\log|(X^T X)^{-1}|$ vs. time is shown in Figure 8.7(j). In this figure it can be observed that $|(X^T X)^{-1}|$ is extremely large at the first measurement point and decreases rapidly by several orders of magnitude during the first 5 sampling periods. Hence early erratic behavior of the initial estimates together with the nonpositive definite Hessian at the solution are explained from the results of the identifiability analysis. From a Bayesian point of view, an improvement in the conditioning of the least squares error problem can be made by specifying a nonzero P_0 to the prior estimate of x_0. It was found that taking such action to improve the conditioning of the least squares problem led to an unacceptable, very slowly converging nonlinear estimator.

The CPU time of the simulation on a Vax 750 without floating point acceleration of the nonlinear optimization approach was about 18 hours, which was tremendous and not practical relative to the reiterative extended Kalman filter time of about 5 hours and the standard extended Kalman filter time of about 6 minutes. For practical implementation, the on-line horizon approach must be speeded up by improving upon the computation used above and by solving the optimization problem less frequently. Even if a substantial improvement can be realized, such as through the approach suggested by Beigler (1984), it is doubtful that the performance of the nonlinear optimization approach as a state estimator can be improved over the reiterative extended Kalman filter method.

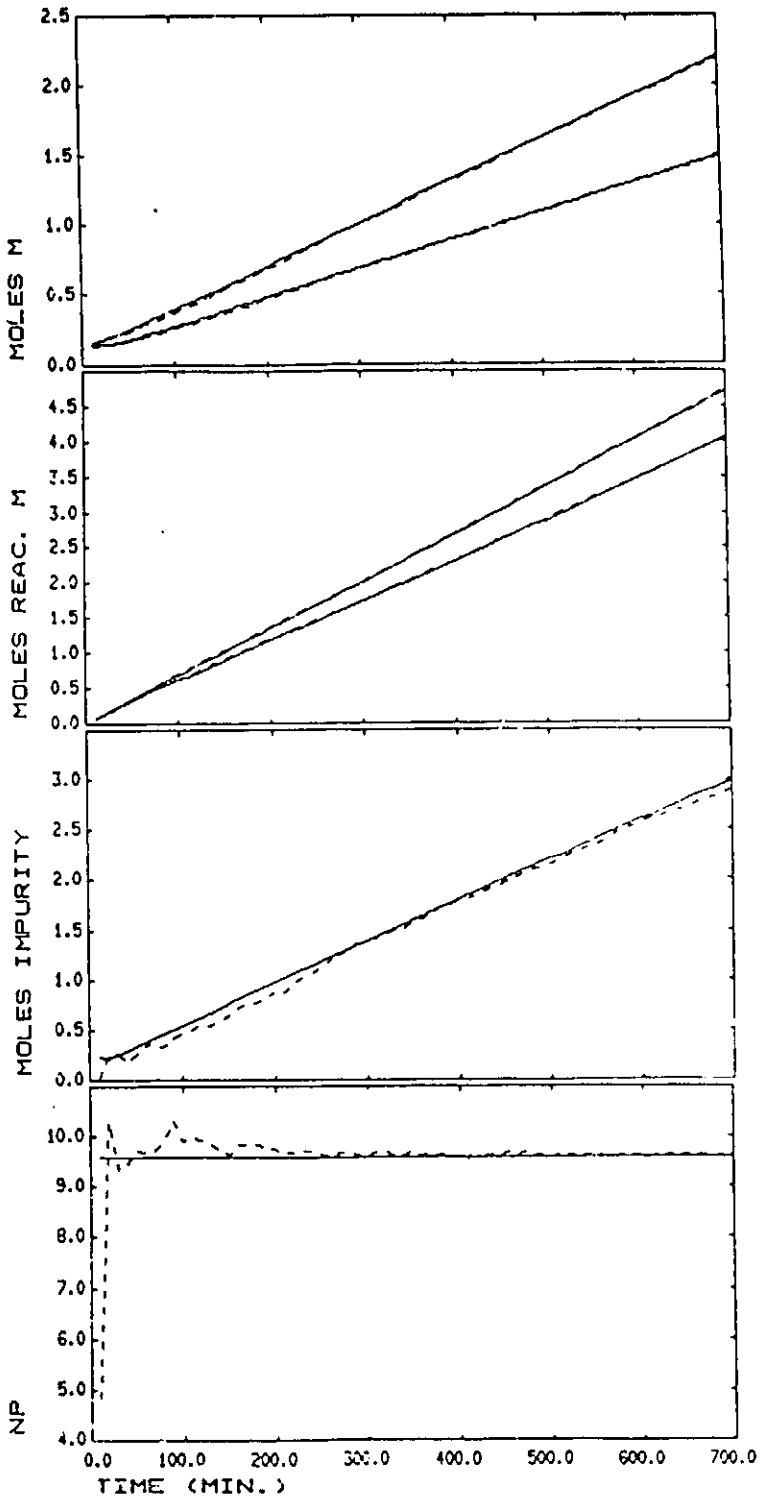
MOLES M
2.5
2.0
1.5
1.0
0.5
0.0
MOLES REAC. M
4.5
4.0
3.5
3.0
2.5
2.0
1.5
1.0
0.5
0.0
MOLES IMPURITY
3.0
2.5
2.0
1.5
1.0
0.5
0.0
NP
10.0
9.0
8.0
7.0
6.0
5.0
4.0
0.0
100.0
200.0
300.0
400.0
500.0
600.0
700.0
TIME (MIN.)

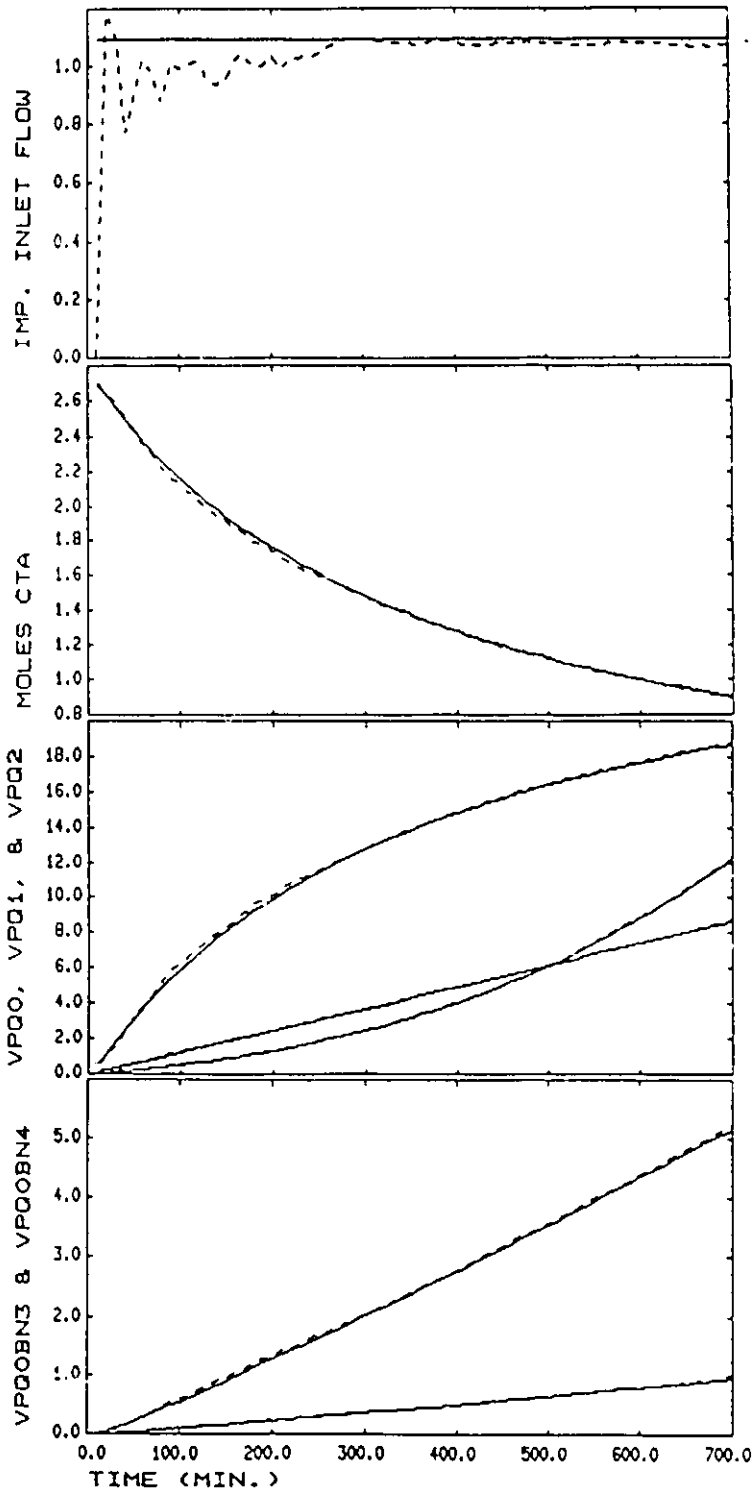
IMP. INLET FLOW
1.0
0.8
0.6
0.4
0.2
0.0
MOLES CTA
2.6
2.4
2.2
2.0
1.8
1.6
1.4
1.2
1.0
0.8
VPQ0, VPQ1, & VPQ2
18.0
16.0
14.0
12.0
10.0
8.0
6.0
4.0
2.0
0.0
VPQOBN3 & VPQOBN4
5.0
4.0
3.0
2.0
1.0
0.0
0.0
100.0
200.0
300.0
400.0
500.0
600.0
700.0
TIME (MIN.)

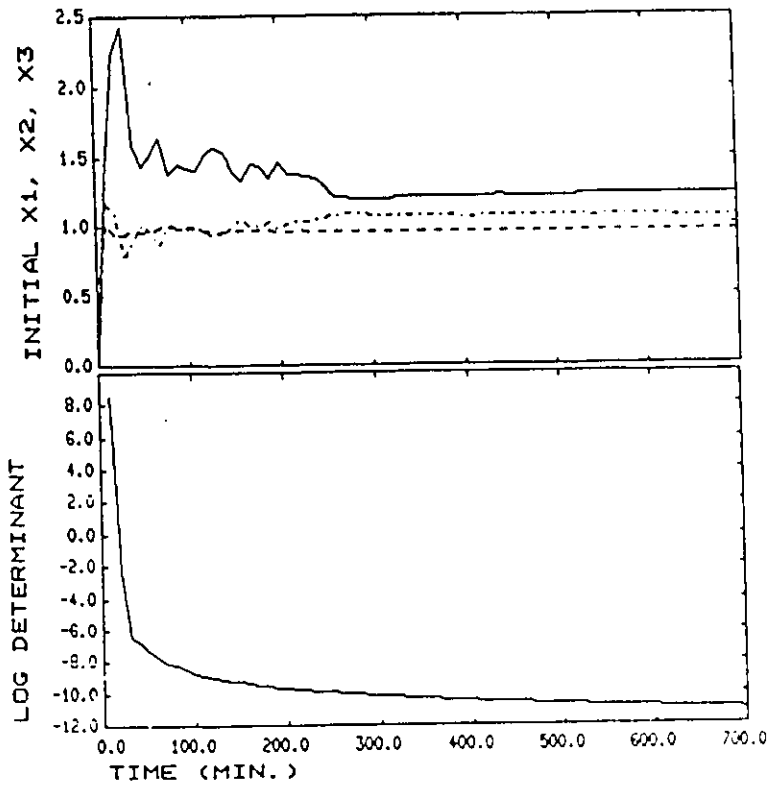

FIGURE 8.7: Nonlinear Optimization State Estimation Approach
(-) Actual Response; (--) Predicted
(a) M_t & M_b; (b) P_t & P_b; (c) Im_p; (d) N_p
(e) F_{Im_p}; (f) CTA; (g) V_pQ_0, V_pQ_1, & V_pQ_2; (h) $V_pQ_0\beta n_3$ & $V_pQ_0\beta n_4$
(i) Im_{p_0} (-), $N_{p_0}/10$ (--), $F_{Im_{p_0}}$ (..); (j) $\log|(X^TX)^{-1}|$

8.5.4. Conclusion From SBR Estimation Study With No Model Mismatch

The purpose of this section was to evaluate three different approaches to the problem of nonlinear state estimation in a semi-batch SBR emulsion reactor where some initial states were unknown. The approaches considered have been extended Kalman filtering, a reiterative extended Kalman filter, and an on-line nonlinear optimization approach. The three approaches were evaluated assuming the ideal situation of no structural and parameter model mismatch.

An extended Kalman filter with the correct nonstationary states accounted for was found to be a useful and practical approach provided that nonstationary disturbance and parameter states are correctly accounted for in the formulation, and that considerable effort is made through repeated simulation to arrive at a suitable set of tuning matrices. Relative to the sampling period of the measurements, this method provided very fast filtered state estimates. The main drawback of the approach is that convergence tends to be slow because of the recursive nature of the algorithm.

A modification was proposed whereby a second extended Kalman filter was combined with the one above to provide recursive updating of the uncertain initial state estimates x_0. By reiterating the first extended Kalman filter with every updated x_0 estimate from the second filter, improved convergence can be obtained. The second extended Kalman filter was formulated by defining the states to be the initially unknown states (x_0) of the first filter. With this formulation, the second extended Kalman filter turned out to be the counterpart of a nonlinear recursive least squares (or recursive prediction error) algorithm for these unknown initial state parameters. The modification was found to lead to a significant improvement in the convergence of the filtered state estimates. A small increase in the computational effort would be required relative to the first approach provided that the reiterative procedure is terminated once no further improvement is found.

The nonlinear optimization approach of Jang et al. (1986) was used to find maximum likelihood estimates of the unknown initial states for the purpose of state estimation. An advantage of this method over the previous two approaches described above was that far fewer tuning parameters had to be specified. The optimization problem was performed when each sampled measurement became available. The method was found to be robust to the measurement sensor noise and converged to bias free state estimates. Convergence of the nonlinear optimization approach was found to be significantly better than the first extended Kalman filter but slightly worst than the reiterative extended Kalman filter. The major problem with this approach was the significant computational effort required which was far greater than either of the methods above. The nonlinear optimization approach may only be practically usable if the computational efficiency can be

substantially improved and/or the optimization is solved less frequently. However, there is little incentive to pursue this matter since there appears to be no benefit with this method as far as convergence is concerned relative to the reiterative Kalman filter approach. Another problem with the optimization approach is the assumption that the unknown disturbance or parameter states are time invariant over the optimization horizon. This can be a very poor assumption for the system investigated in a real process environment.

Based on the results of this section, it is recommended that the most practical approach to the problem of state estimation in a semi-batch SBR emulsion reactor is the proposed reiterative extended Kalman filter that has been demonstrated to offer the best compromise between computational effort and convergence.

8.6. SIMULATION STUDIES WITH MODEL MISMATCH

It may be argued that an estimation case study with no model mismatch is of limited practical value since dynamic models of chemical processes are rarely accurate. For a nonlinear state estimation procedure to be useful in a real process environment, it must be demonstrated to be robust to both parameter and structural types of mismatch and shown to contain sufficient nonstationary disturbance and parameter states so that model predicted measurements will always be consistent with actual measurements in the region of operation. In general, these requirements cannot be met if the number of nonstationary states is less than the number of measurements. Parrish and Brosilow (1988) have stressed that if the latter requirement is not satisfied, the state estimator may contain bias, and not be capable of tracking changing conditions. This has been a common failing of almost all Kalman filtering applications described in the process control literature. The lack of consistency in the state estimator would also prevent the possibility of control with reset action if feedback control is to be applied. Unfortunately, the modifications required to make nonlinear state estimators consistent and effective are case dependent, requiring some understanding of the process mechanism and sources of model deviation. Of course nonstationary states can always be arbitrarily added to the state estimator simply to meet the consistency requirement. The consequence of such a blind approach would be a poorly performing state estimator with poor prediction of the future progress of the process.

The following sections in this chapter will take a close look at the effect of different types of model mismatch when inferring states using the extended Kalman filter for the SBR example. The aim will be to determine which type of model mismatch the previously described extended Kalman filter will be robust to,

the types of model mismatch that will introduce bias, and to introduce modifications to the state estimation algorithm by introducing a set of reasonable and hopefully meaningful parameter states in order to allow consistent state estimation in the presence of model mismatch.

8.6.1. Mismatch Affecting Average Number Of Radicals Per Particle

In this section, the effect of model mismatch where only $\bar{n}$, the average number of radicals per particle, is affected shall be investigated. In the SBR model, $\bar{n}$ appears in the reaction rate expression as

$$R_i = k_i[A_i]_p \frac{\bar{n} N_p V_w}{N_A V_p} \tag{8.26}$$

where R_i is the rate of reaction of some reactive species A_i with radicals, and k_i is the associated effective rate constant. In a real process environment, factors such as errors in the specification of Im_p, Im_w, k_{Im_p}, and f, for example, may be significant and will result in a bias in the open-loop prediction of $\bar{n}$. Unfortunately, observability limitations will not permit the estimation of all the parameter and states affecting $\bar{n}$. If one would suspect that many factors contribute significantly to deviations in $\bar{n}$ relative to the open-loop case, a simple approach to the estimation problem would be to avoid detailed modelling of all the influences on $\bar{n}$ and introduce $\bar{n}$ as a nonstationary random walk state

$$\bar{n}_{k+1} = \bar{n}_k + w_k^{\bar{n}} \tag{8.27}$$

to be estimated. This approach would also be very appealing if no mechanistic detail were available on the effect of the important states and parameters that influence $\bar{n}$. A strategy similar to this was adopted by Stephanopoulos and San (1984) where detailed modelling of the relationship between parameters and states was neglected for simplicity by replacing these dependencies with nonstationary parameter states at appropriate locations in a bioreactor model. The use of the nonstationary parameter state described by (8.27) will satisfy consistency requirements for any type of model mismatch that directly affects the prediction of $\bar{n}$.

In the previous extended Kalman filter formulations, the deviation between the model predicted and actual $\bar{n}$ was assumed to be only a result of an incorrect specification of the amount of reactive impurity Im_p in the reactor. The effect of Im_p on $\bar{n}$ was arrived at from a detailed mechanistic understanding of the relationship between these terms. Bias-free compensation for errors in the specification of the reactive impurities was made possible by including the meaningful nonstationary disturbance parameter F_{Im_p} in the filter formulation. In a real process application, the organic phase reactive impurities will be expected to be the most significant cause of $\bar{n}$ deviations from the open-loop case. If the mechanism proposed for the variation of $\bar{n}$ based on Im_p and

F_{Im_p} is correct, the state estimates based on this modelling approach would be expected to be much more precise than an approach based on (8.27) where no knowledge is assumed. The quality of future state predictions would also be improved and the state estimates would be expected to be less noisy relative to (8.27) which would likely require a significant noise component in $w_1^{\bar{n}}$ to achieve acceptable convergence in order to compensate for the unmodelled dynamics of $\bar{n}$. This detailed modelling approach to incorporate meaningful disturbances or parameter variations could have also been made if mismatch in Im_w, f, k_{Im_p}, or k_{I_2} for example, were expected to be the major source of error in the prediction of $\bar{n}$.

For the extended Kalman filter, formulated with Im_p and F_{Im_p} to be useful in a real process environment, it must be demonstrated to provide, through some fictitious adjustment, consistent compensation for any other type of unaccounted mismatch error that directly affects $\bar{n}$. In this section, it will be demonstrated that the extended Kalman filter formulated in section 8.5.1 will be robust to this particular class of model uncertainty. The types of mismatch to be demonstrated will be errors in F_{Im_p}, k_{Im_p}, and f.

Figure 8.8 shows the performance of the extended Kalman filter when the true impurity flow rate to the reactor is given by $F_{Im_p} = 5x10^{-7}$ $gmol/\min$ and $F_{Im_w} = 5x10^{-7}$ $gmol/\min$ rather than $F_{Im_p} = 1.09x10^{-6}$ $gmol/\min$ and $F_{Im_w} = 0$ as in the previous studies. It can be observed that the extended Kalman filter appears to provide biased-free estimates of all the deterministic states needed for control. The effect of the water soluble impurity in the true process was compensated by simply increasing the estimated amount of F_{Im_p} to the reactor to allow $\bar{n}$ to match the true $\bar{n}$ that results from the effect of both impurities in the reactor.

Figure 8.9 shows the effect of k_{Im_p} being set 30% too low in the model used by the extended Kalman. As before, with the exception of Im_p and F_{Im_p}, biased free estimates appear to be evident in the observable states. Mechanistically, this mismatch will only affect $\bar{n}$ and the rate of impurity depletion. The estimator compensated for this by raising the level of F_{Im_p}, and hence Im_p, as can be seen in Figures 8.9(c) and 8.9(e).

Figure 8.10 shows the effect of f being estimated 30% too low in the model used by the extended Kalman filter. The effect of the larger f will be to over estimate the radical entry rate to the particles and hence over estimate $\bar{n}$. As with the other cases, the estimator compensates for this by assuming a higher Im_p level, as is shown in Figures 8.10(c) and 8.10(e). Unlike the previous two examples, a much higher fictitious level for Im_p is needed to compensate for the modelling error. This fictitious higher level for Im_p leads to a noticeable, but still small, deviation in the V_pQ_0, V_pQ_2, and $V_pQ_0Bn_3$, and $V_pQ_0Bn_4$ predictions, shown in Figures 8.10(g) and 8.10(h). Since these states are not observable from the property measurements, a bias in these states cannot be avoided. At typical operating conditions, chain transfer to CTA dominates the molecular weight properties.

If the true impurity level is not expected to significantly affect the molecular weight moments in the region of operation, it may be more effective to remove the effect of the impurity terms on these states in the model used for state estimation. In this way excessively high or low fictitious impurity levels will not seriously affect the predictions of the nonobservable molecular weight moments states V_pQ_0 and V_pQ_1. However, if a large amount of Im_p really does exist, this most certainly would be a bad move.

It can be shown that the extended Kalman filter used in this section will also be robust to similar types of modelling errors associated with initiation, radical entry, the presence of multiple impurities, and diffusion controlled termination effects. All of the modelling errors discussed in this section are considered to be important in a real process environment, and the results have at least demonstrated that the extended Kalman filter formulated in section 8.5.1 does have some favorable robustness properties with respect to these model deviations.

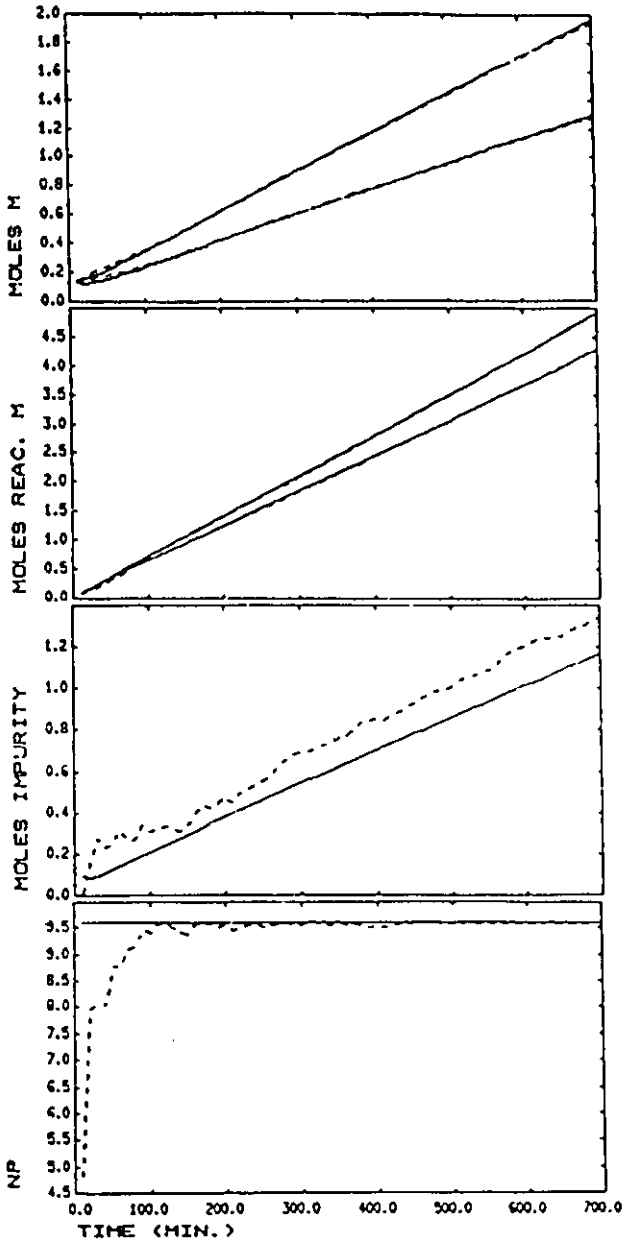
MOLES M
MOLES REAC. M
MOLES IMPURITY
NP
TIME (MIN.)
0.0
100.0
200.0
300.0
400.0
500.0
600.0
700.0

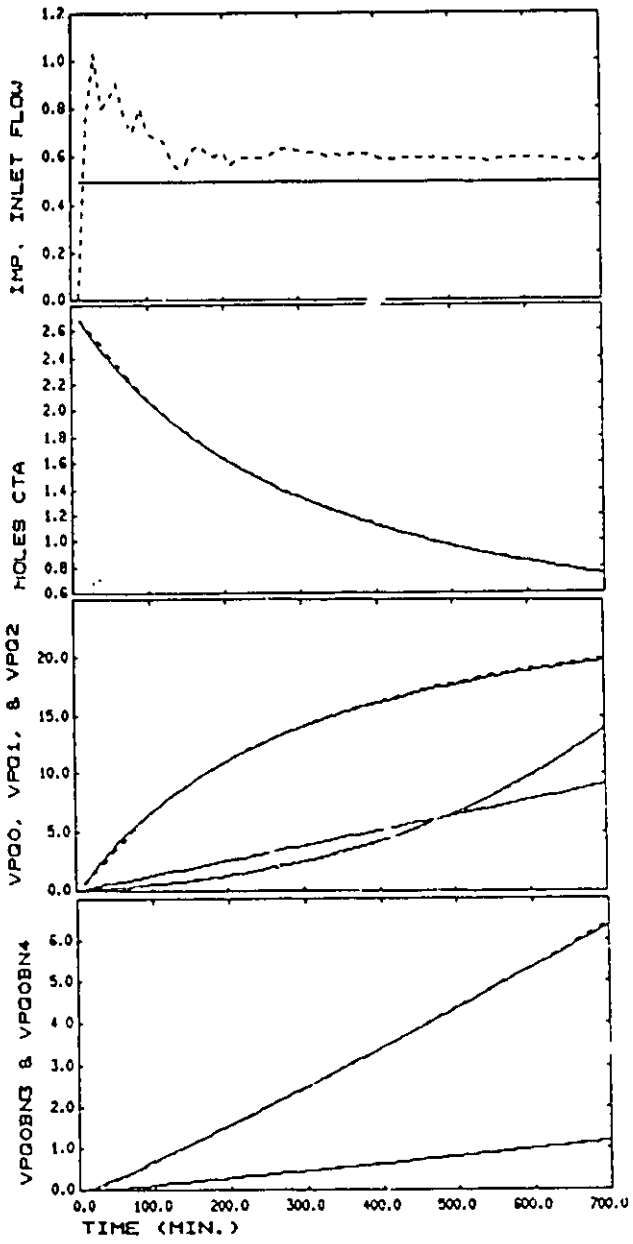

FIGURE 8.8: Extented Kalman Filter: Water Phase Impurity Model Mismatch
(-) Actual Response; (--) Predicted
(a) M_t & M_b; **(b)** P_t & P_b; **(c)** Im_p; **(d)** N_p
(e) F_{Im_p}; **(f)** CTA; **(g)** V_pQ_0, V_pQ_1, & V_pQ_2; **(h)** $V_pQ_0Bn_3$ & $V_pQ_0Bn_4$

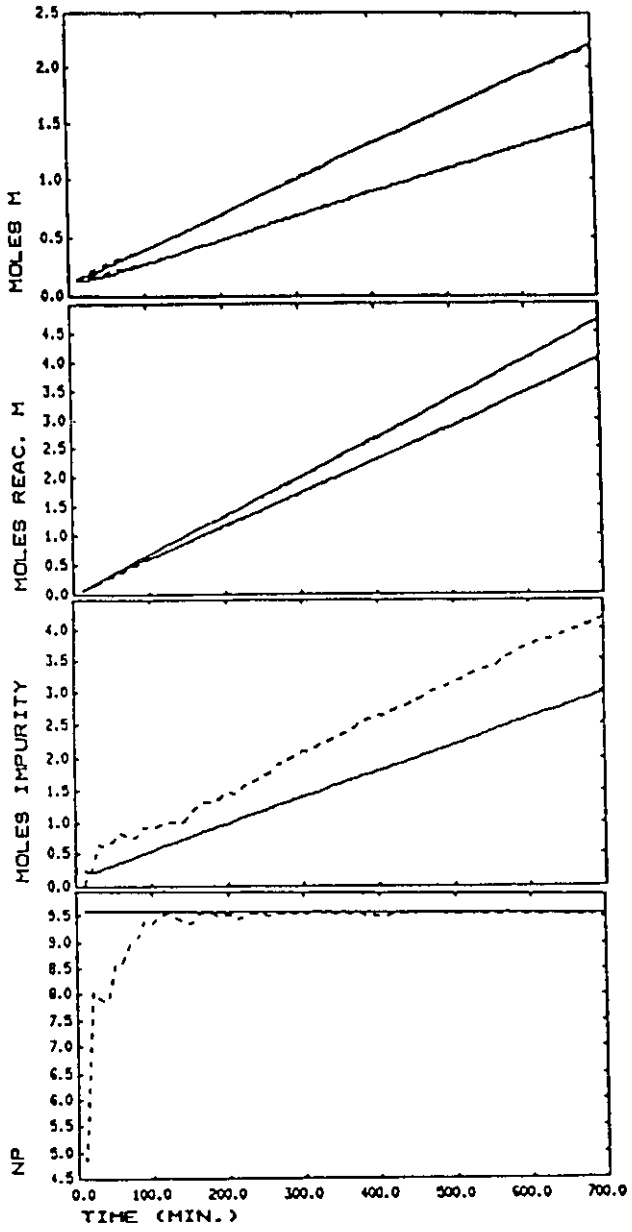
MOLES M
MOLES REAC. M
MOLES IMPURITY
NP
TIME (MIN.)
0.0
100.0
200.0
300.0
400.0
500.0
600.0
700.0

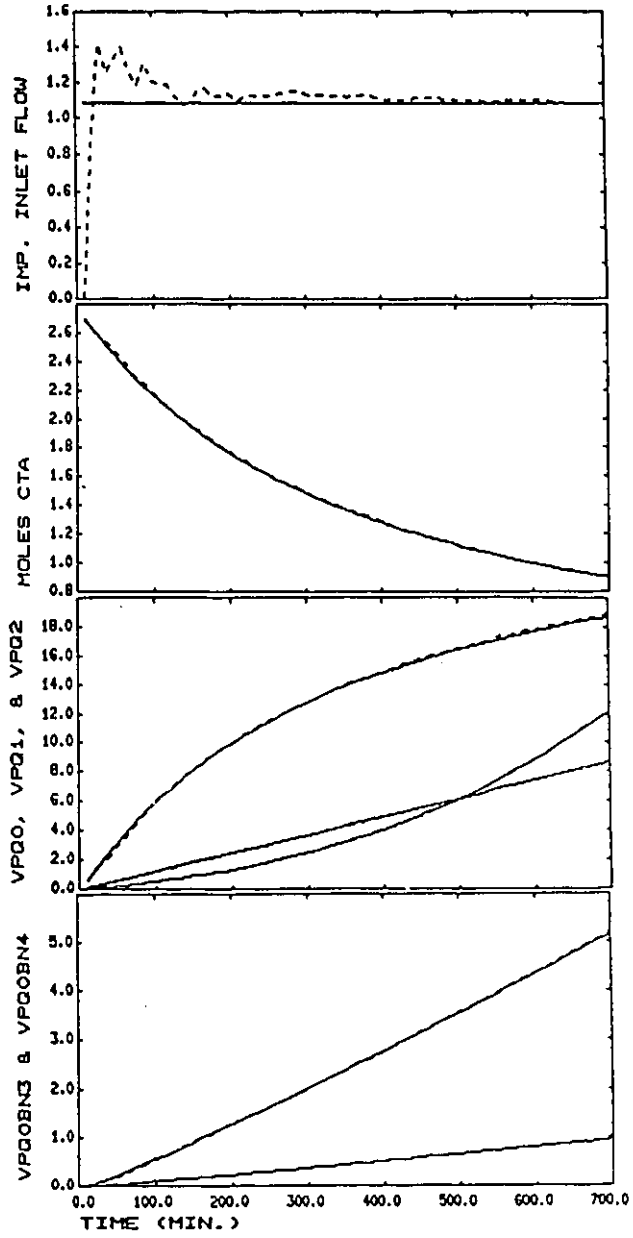

FIGURE 8.9: Extented Kalman Filter: k_{lm_p} Model Mismatch
(-) Actual Response; (--) Predicted
(a) M_s & M_b; (b) P_s & P_b; (c) Im_p; (d) N_p
(e) F_{lm_p}; (f) CTA; (g) V_pQ_0, V_pQ_1, & V_pQ_2; (h) $V_pQ_0Bn_3$ & $V_pQ_0Bn_4$

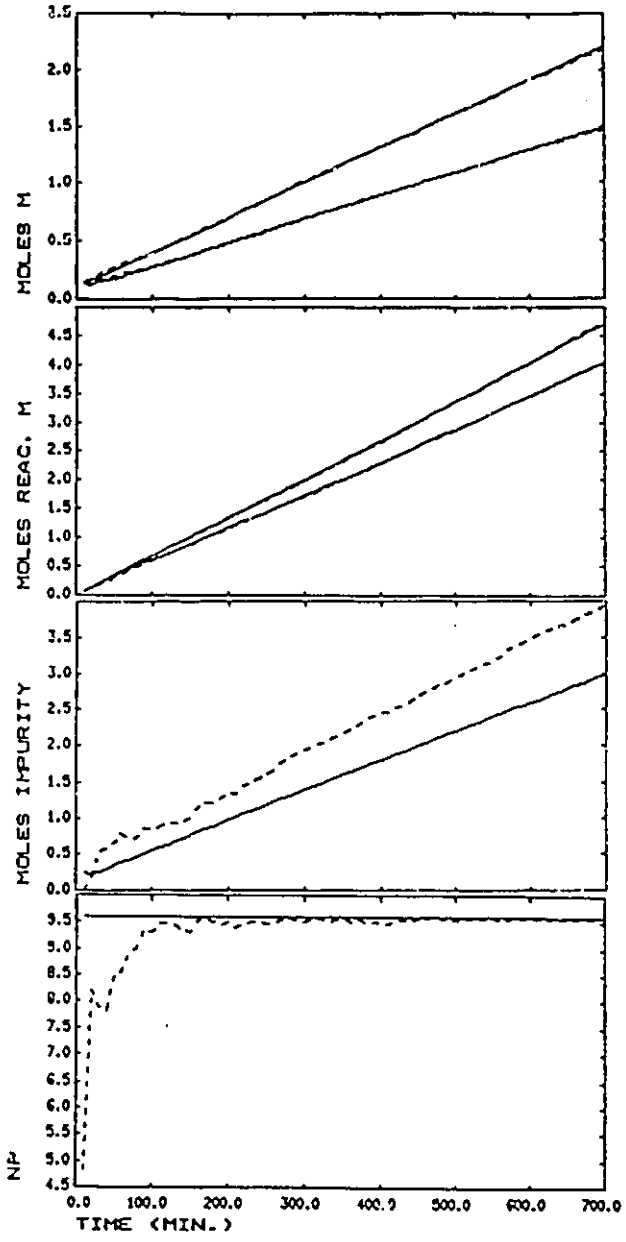
MOLES M
MOLES REAC. M
MOLES IMPURITY
NP
TIME (MIN.)
0.0
100.0
200.0
300.0
400.0
500.0
600.0
700.0

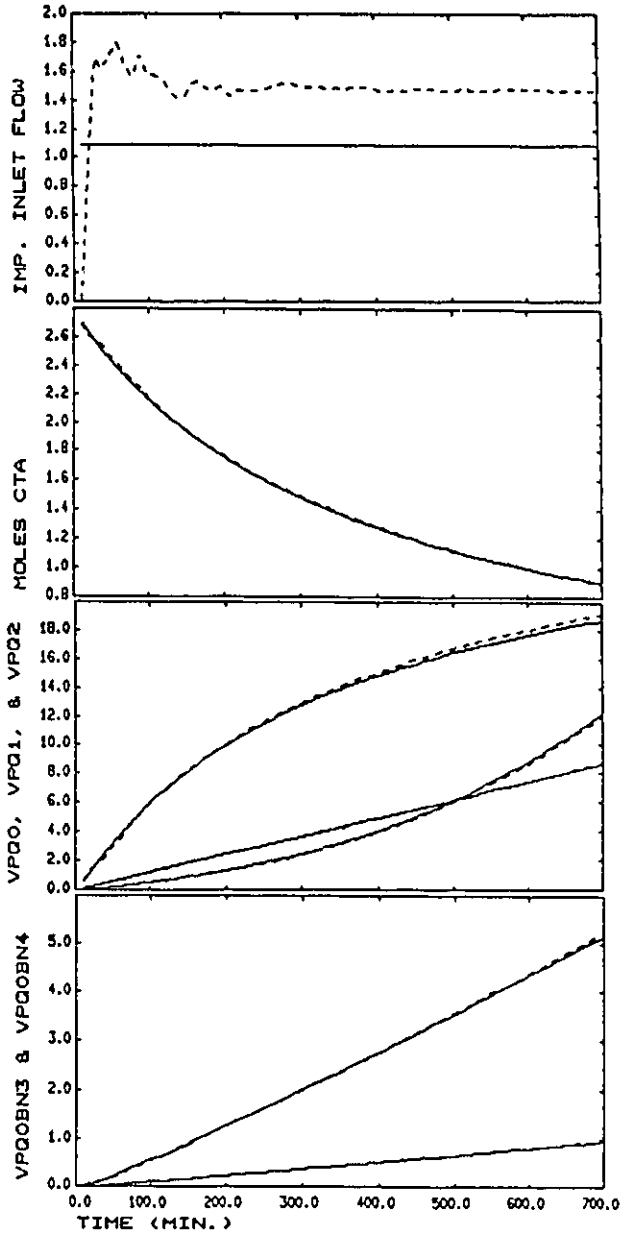

FIGURE 8.10: Extented Kalman Filter: Initiator Efficiency Model Mismatch
(-) Actual Response; (--) Predicted
(a) M_s & M_b; (b) P_s & P_b; (c) Im_p; (d) N_p
(e) F_{Im_p}; (f) CTA; (g) V_pQ_0, V_pQ_1, & V_pQ_2; (h) $V_pQ_0Bn_3$ & $V_pQ_0Bn_4$

8.6.2. Mismatch Associated With Propagation And Chain Transfer

The following section will be concerned with mismatch corresponding to errors in rate constants associated with propagation and transfer to modifier. The objective will be first to demonstrate that the extended Kalman filter formulated in 8.5.1, in general, will not be robust to this important class of model mismatch, and can lead to biased state estimates. The second objective will be to propose modifications to the extended Kalman filter of section 8.5.1 by introducing nonstationary model mismatch states that will eliminate bias in some of the state estimates and provide improved estimates in others.

The first parameter model mismatch to be examined will be an error in the propagation rate constants where both k_{pss} and k_{pbb} are increased 30% in the model used in the extended Kalman filter of section 8.5.1. The simulated results are shown in Figure 8.11. The extended Kalman filter can be observed to perform poorly under this type of model mismatch, where a significant bias problem can be observed to be present.

The poor performance of this extended Kalman filter can be easily explained. The rate of reaction of each monomer to produce polymer, and the rate of depletion of *CTA* is given by the expressions below:

$$R_{ps} = \Phi_s [M_s]_p \frac{\overline{n} N_p V_w}{N_A V_p} \tag{8.28}$$

$$R_{pb} = \Phi_b [M_b]_p \frac{\overline{n} N_p V_w}{N_A V_p} \tag{8.29}$$

$$R_{CTA} = k_{fCTA} [CTA_p]_p \frac{\overline{n} N_p V_w}{N_A V_p} \tag{8.30}$$

where R_{ps}, R_{pb}, and R_{CTA} refer to the rate of depletion of styrene, butadiene, and modifier respectively. In the equations above Φ_s, Φ_b, and k_{fCTA} refer to the effective copolymer reaction rate constants for styrene, butadiene, and *CTA* with radicals respectively. The effect of a 30% increase in both propagation rate constants, k_{pss} and k_{pbb}, leads to a 30% increase in both Φ_s and Φ_b pseudo copolymerization rate constants in (8.28) and (8.29). To compensate for this error and make the extended Kalman filter model predictions consistent with measured M_s and M_b, the estimator would have to decrease the estimated N_p and/or $\overline{n}$ through a fictitious increase in the impurity level. However, these modifications would be inconsistent with both the particle size measurement and the *CTA* differential equation (8.30). No adjustment to both N_p and $\overline{n}$ can be tolerated for consistency with the *CTA* measurement, since k_{fCTA} is unaffected by both k_{pss} and k_{pbb}, and the D_p measurement. Therefore the bias is a result of the inability of the nonstationary disturbance and parameter states to fictitiously reconstruct the observed measurements.

A similar mismatch problem as the one demonstrated above will be encountered when the error is present in the rate constants for the reaction of *CTA* with radicals. Figure 8.12 shows the simulated results when both k_{fiCTA} and k_{fbCTA} are increased by 30% in the model used in the extended Kalman filter. A serious bias problem in all the state estimates is again evident. The effect of the modelling error is to over estimate k_{fCTA} by 30% in (8.30). The only way that the estimator could compensate for this in (8.30) is by either or both a decrease in N_p and an increase in the level of impurity. However, this adjustment would create inconsistencies with model predicted and measured D_p, and M_s and M_b since in the rate expressions Φ_s and Φ_b are not effected in (8.28) and (8.29).

The results above have demonstrated that the extended Kalman filter formulated in section 8.5.1 will, in general, not be robust to independent errors in propagation and chain transfer rate constants. However, there is a special case where the filter will be robust to errors in these parameters. Figure 8.13 presents the simulated results where k_{pai}, k_{pbb}, k_{fiCTA}, and k_{fbCTA} are together estimated 30% too high in the extended Kalman filter model. The results show that in this situation the performance of the extended Kalman filter is much improved. The reason for this is that the simultaneous 30% increase in Φ_s, Φ_b, and k_{fCTA} as a result of the mismatched parameters can be compensated for in a consistent manner by reducing $\overline{n}$ through the same fictitious increase in the level of impurity. The predictions of V_pQ_0, V_pQ_2, $V_pQ_0Bn_3$, and $V_pQ_0Bn_4$ are biased due to errors in the estimated values of Im_p and $\overline{n}$ which must be known exactly for these states to be predicted correctly.

A modification to the extended Kalman filter of section 8.5.1 must be made in order that it provide consistent state estimates with the available measurements. The mismatch cases considered above showed that a fictitious increase in $\overline{n}$ to account for independent errors in the propagation rate constants will be inconsistent with the *CTA* material balance differential equation. To bring about consistency in the state estimation algorithm, a fictitious mismatch parameter state, x^{14}, is introduced as a multiplicative correction factor for $k_{fCTA}[CTA]_p$ wherever it appears in the model. With this modification, the rate expression for the depletion of *CTA* becomes

$$R_{CTA} = x^{14} k_{fCTA}[CTA]_p \frac{\overline{n} N_p V_w}{N_A V_p} \tag{8.31}$$

With no information known about the dynamic variations of x^{14}, x^{14} is modelled as a stochastic nonstationary random walk of the form

$$x^{14}_{k+1} = x^{14}_k + w^{14}_k \tag{8.32}$$

in order to eliminate the bias problem.

Figure 8.14 shows the simulated performance of the modified extended Kalman filter when both k_{pss} and k_{pbb} are assumed 30% too high. The tuning used in this filter was

$$R_w = Diag$$

$$(5x10^{-6}, 5x10^{-6}, 5x10^{-6}, 5x10^{-6}, 5x10^{-6}, 10^{-4}, 10^{-6}, 5x10^{-6}, 5x10^{-6}, 5x10^{-6}, 5x10^{-6}, 5x10^{-6}, 5x10^{-6}, 0.0001)$$

$$R_v = Diag(0.002, 0.002, 200, 0.002)$$

$$P_0 = Diag(0.0001, 0.0001, 0.0001, 0.0001, 1, 5, 1, 0.0001, 0.0001, 0.0001, 0.0001, 0.0001, 0.0001, 0.01)$$

and x^{14} was initialized to 1. Relative to the former Kalman filter design shown in Figure 8.11, the bias problem has been eliminated in the observable states, with the exception of Im_p and F_{Im_p}, and reduced in some of the nonobservable states. A similar improvement will also be observed when a modelling error is introduced to k_{fCTA}, or either k_{pss} or k_{pbb} alone.

The introduction of x^{14} parameter mismatch state has been shown to improve the consistency of the extended Kalman filter when modelling discrepancies occur between the propagation and *CTA* material balance expression. However, other types of rate constant errors can be introduced where the modified extended Kalman filter proposed will still not be adequate. Figure 8.15 shows the simulated performance of the modified extended Kalman filter when r_b has been assumed 30% too high. A significant bias problem in some of the observable states has been introduced as result of this error which cannot be accounted for though the impurity disturbance state and x^{14}. The problem is again due to inconsistency in the state estimation algorithm as a result of the model mismatch. The error in r_b effects both Φ_s and Φ_b in (8.28) and (8.29) respectively, but the effect on each term is different. Hence a consistent fictitious correction to $\overline{n}$ through the organic impurity level cannot be found to account for simultaneous unequal errors in Φ_s and Φ_b.

An additional modification to the extended Kalman filter can be made to make it consistent to the type of mismatch as the one previously described where an inconsistency exists between M_s and M_b material balances. A second fictitious model mismatch state x^{15} can be introduced as a multiplicative correction factor to $\Phi_b[M_b]_p$ everywhere in the model used for estimation. With this modification, the rate expression for the reaction of butadiene to produce polymer is given by

$$R_{pb} = x^{15}\Phi_b[M_b]_p \frac{\overline{n}N_pV_w}{N_AV_p} \tag{8.33}$$

Again, without any knowledge about the dynamics associated with x^{15}, the assumption will be made that x^{15} can be modelled as a stochastic nonstationary random walk according to

$$x_{k+1}^{15} = x_k^{15} + w_k^{15} \tag{8.34}$$

which should be effective in eliminating the bias problem in the observable states resulting from the class of model mismatch described above.

Figure 8.16 shows the simulated performance of the doubly modified extended Kalman filter when r_b is assumed 30% too high. The extended Kalman filter was tuned using

$$R_w = Diag(5x10^{-6}, 5x10^{-6}, 5x10^{-6}, 5x10^{-6}, 5x10^{-6}, 10^{-4}, 10^{-6}, 5x10^{-6}, 5x10^{-6}, 5x10^{-6}, 5x10^{-6}, 5x10^{-6}, 5x10^{-6}, 0.0001, 0.0001)$$

$$R_v = Diag(0.002, 0.002, 200, 0.002)$$

$$P_0 = Diag(0.0001, 0.0001, 0.0001, 0.0001, 1, 5, 1, 0.0001, 0.0001, 0.0001, 0.0001, 0.0001, 0.0001, 0.01, 0.01)$$

and initialized with $x^{14} = 1$ and $x^{15} = 1$. Relative to the previous filter, shown in Figure 8.15, the prediction of most of the states can be observed to be consistent with the state predictions.

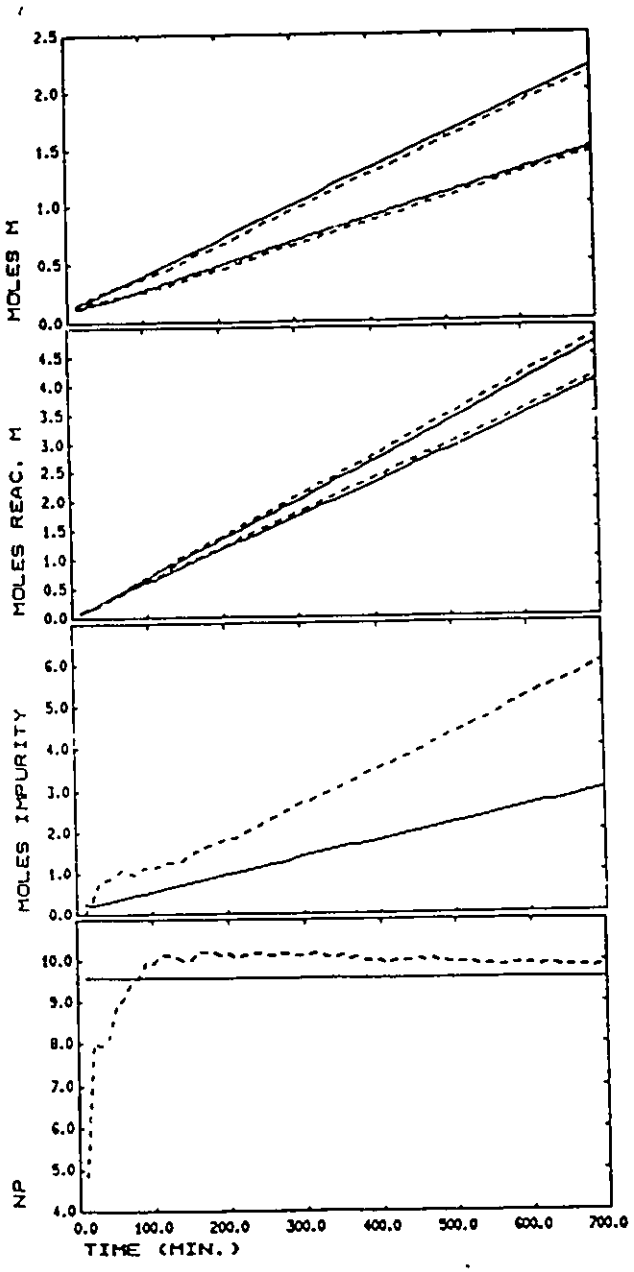
MOLES M
2.5
2.0
1.5
1.0
0.5
0.0
MOLES REAC. M
4.5
4.0
3.5
3.0
2.5
2.0
1.5
1.0
0.5
0.0
MOLES IMPURITY
6.0
5.0
4.0
3.0
2.0
1.0
0.0
NP
10.0
9.0
8.0
7.0
6.0
5.0
4.0
0.0
100.0
200.0
300.0
400.0
500.0
600.0
700.0
TIME (MIN.)

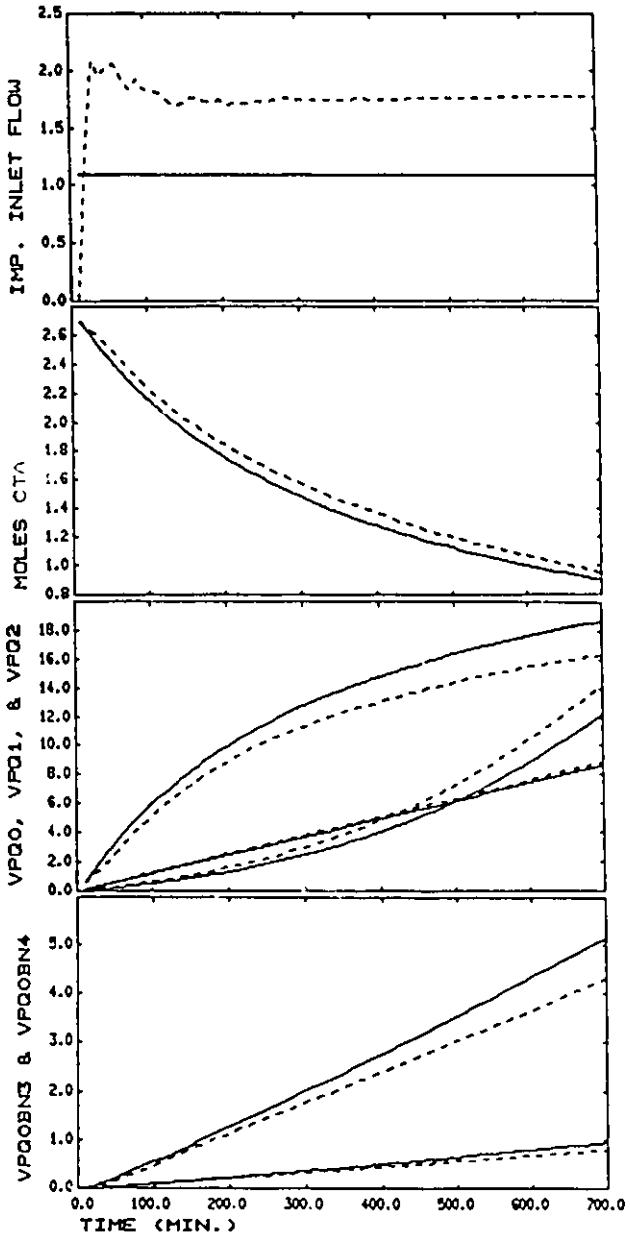

FIGURE 8.11: Extented Kalman Filter: k_{pss} & k_{pbb}Model Mismatch
(-) Actual Response; (--) Predicted
(a) M_s & M_b; (b) P_s & P_b; (c) Im_p; (d) N_p
(e) F_{Im_p}; (f) CTA; (g) V_pQ_0, V_pQ_1, & V_pQ_2; (h) $V_pQ_0Bn_3$ & $V_pQ_0Bn_4$

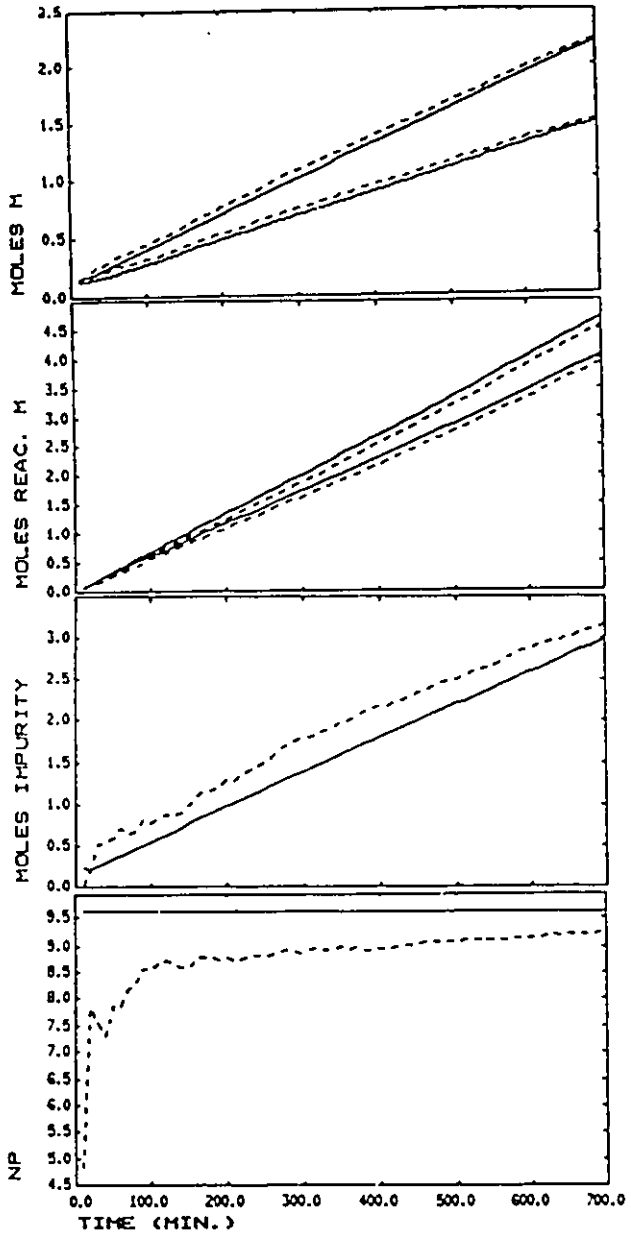
MOLES M
MOLES REAC. M
MOLES IMPURITY
NP
TIME (MIN.)
0.0
100.0
200.0
300.0
400.0
500.0
600.0
700.0

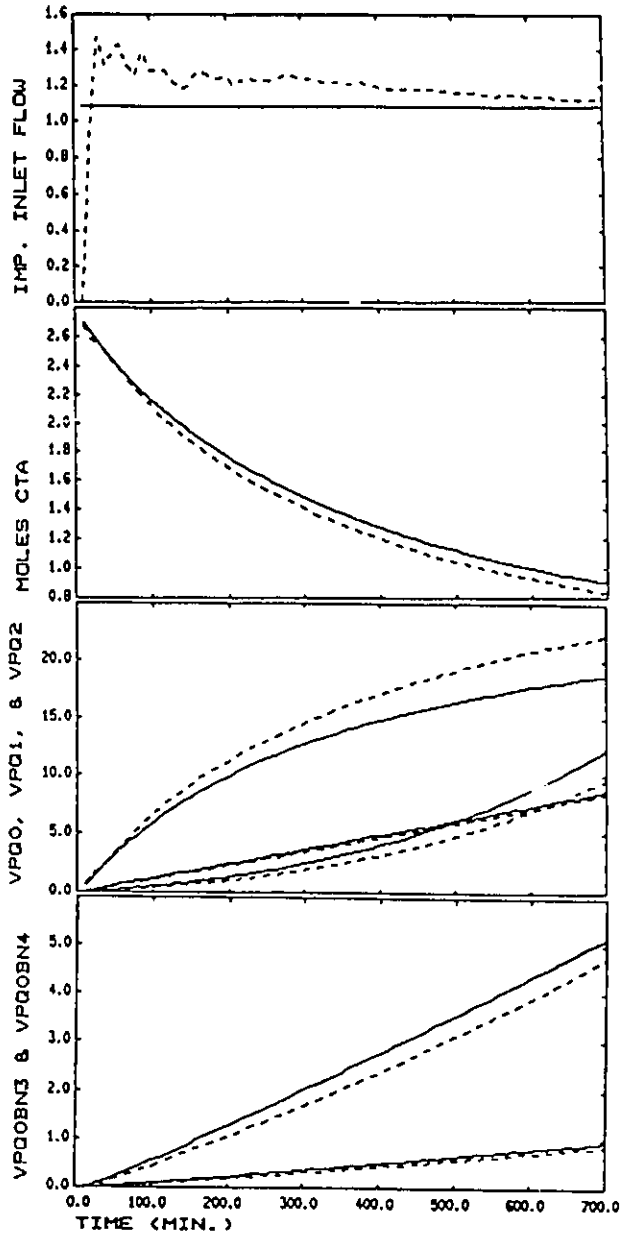

FIGURE 8.12: Extended Kalman Filter: k_{fCTA} Model Mismatch
(-) Actual Response; (--) Predicted
(a) M_s & M_b; (b) P_s & P_b; (c) Im_p; (d) N_p
(e) F_{Im_p}; (f) CTA; (g) V_pQ_0, V_pQ_1, & V_pQ_2; (h) $V_pQ_0Bn_3$ & $V_pQ_0Bn_4$

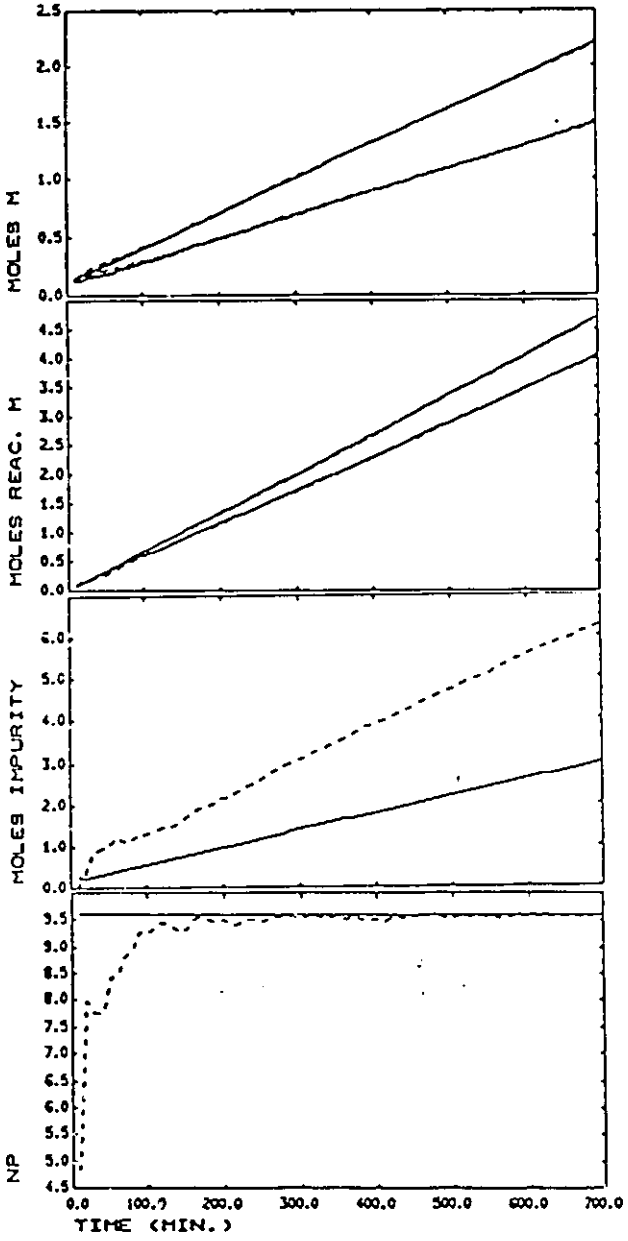
MOLES M
MOLES REAC. M
MOLES IMPURITY
NP
TIME (MIN.)
0.0
100.0
200.0
300.0
400.0
500.0
600.0
700.0

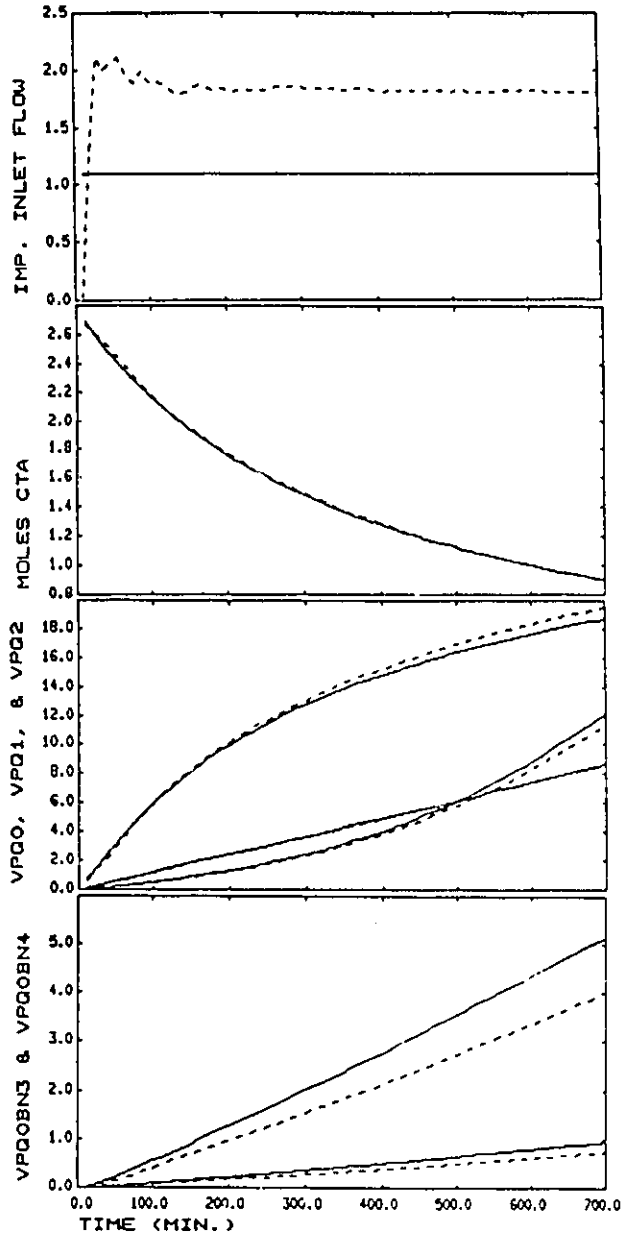

FIGURE 8.13: Extented Kalman Filter: k_{pss}, k_{pbb}, & k_{fCTA} Model Mismatch
(-) Actual Response; (--) Predicted
(a) M_s & M_b; (b) P_s & P_b; (c) Im_p; (d) N_p
(e) F_{Im_p}; (f) CTA; (g) V_pQ_0, V_pQ_1, & V_pQ_2; (h) $V_pQ_0Bn_3$ & $V_pQ_0Bn_4$

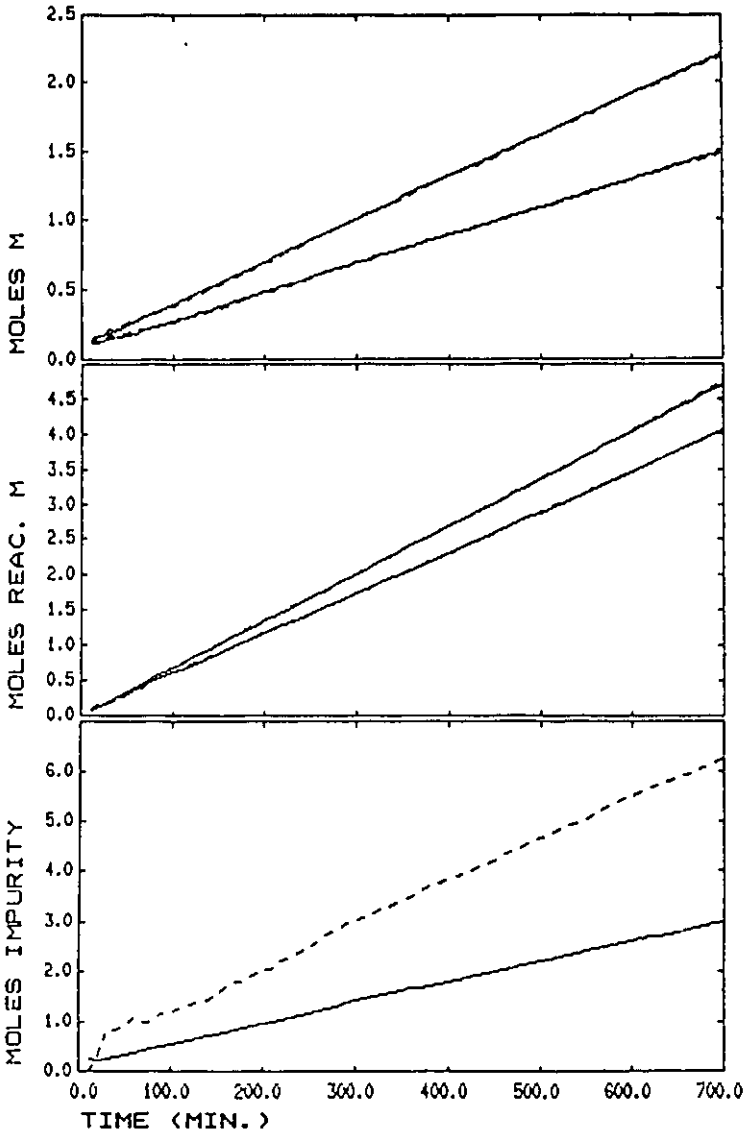
MOLES M
2.5
2.0
1.5
1.0
0.5
0.0
MOLES REAC. M
4.5
4.0
3.5
3.0
2.5
2.0
1.5
1.0
0.5
0.0
MOLES IMPURITY
6.0
5.0
4.0
3.0
2.0
1.0
0.0
0.0
100.0
200.0
300.0
400.0
500.0
600.0
700.0
TIME (MIN.)

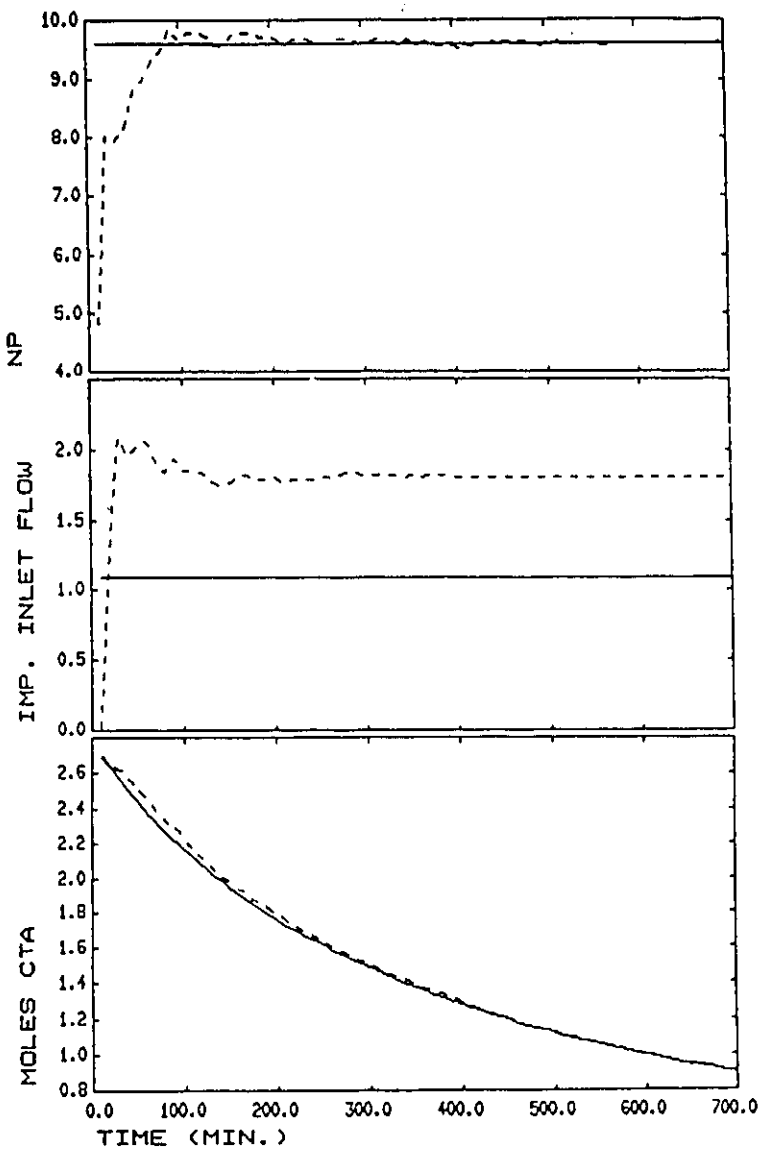
NP
10.0
9.0
8.0
7.0
6.0
5.0
4.0
IMP. INLET FLOW
2.0
1.5
1.0
0.5
0.0
MOLES CTA
2.6
2.4
2.2
2.0
1.8
1.6
1.4
1.2
1.0
0.8
0.0
100.0
200.0
300.0
400.0
500.0
600.0
700.0
TIME (MIN.)

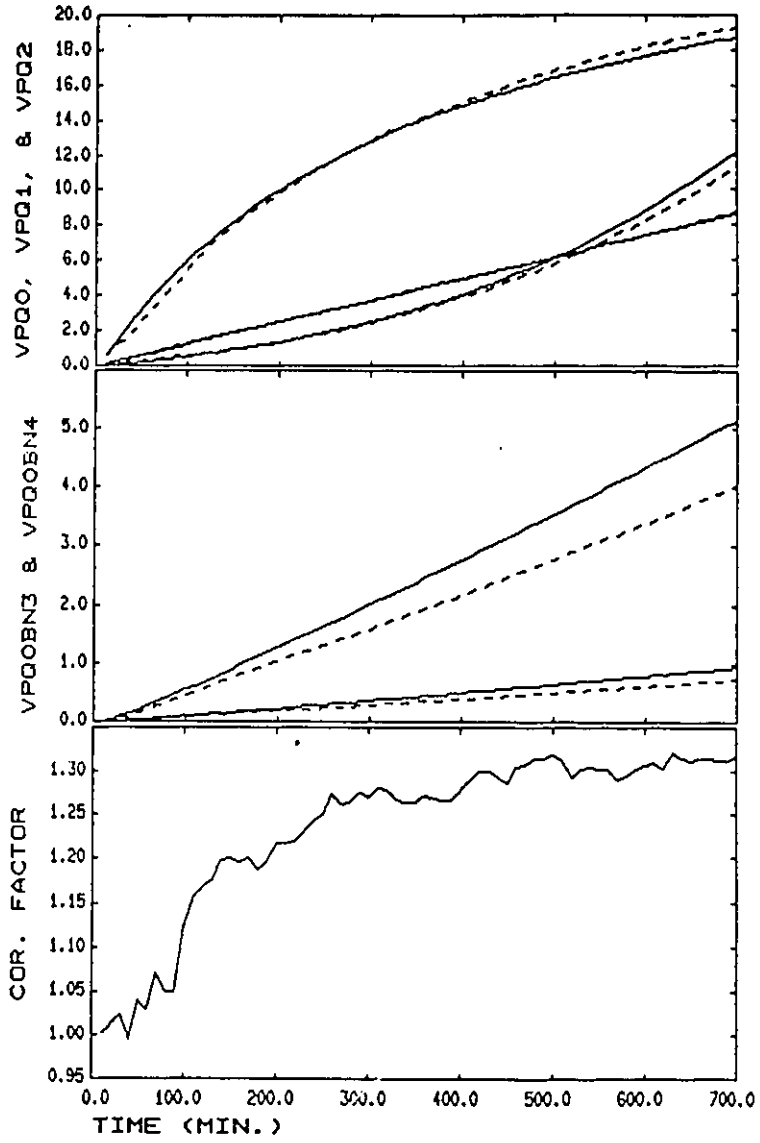

FIGURE 8.14: Extended Kalman Filter With x^{14}: k_{pss} and k_{pbb} Model Mismatch
(-) Actual Response; (--) Predicted
(a) M_s & M_b; (b) P_s & P_b; (c) Im_p; (d) N_p
(e) F_{Im_p}; (f) CTA; (g) V_pQ_0, V_pQ_1, & V_pQ_2; (h) $V_pQ_0Bn_3$ & $V_pQ_0Bn_4$; (i) x^{14}

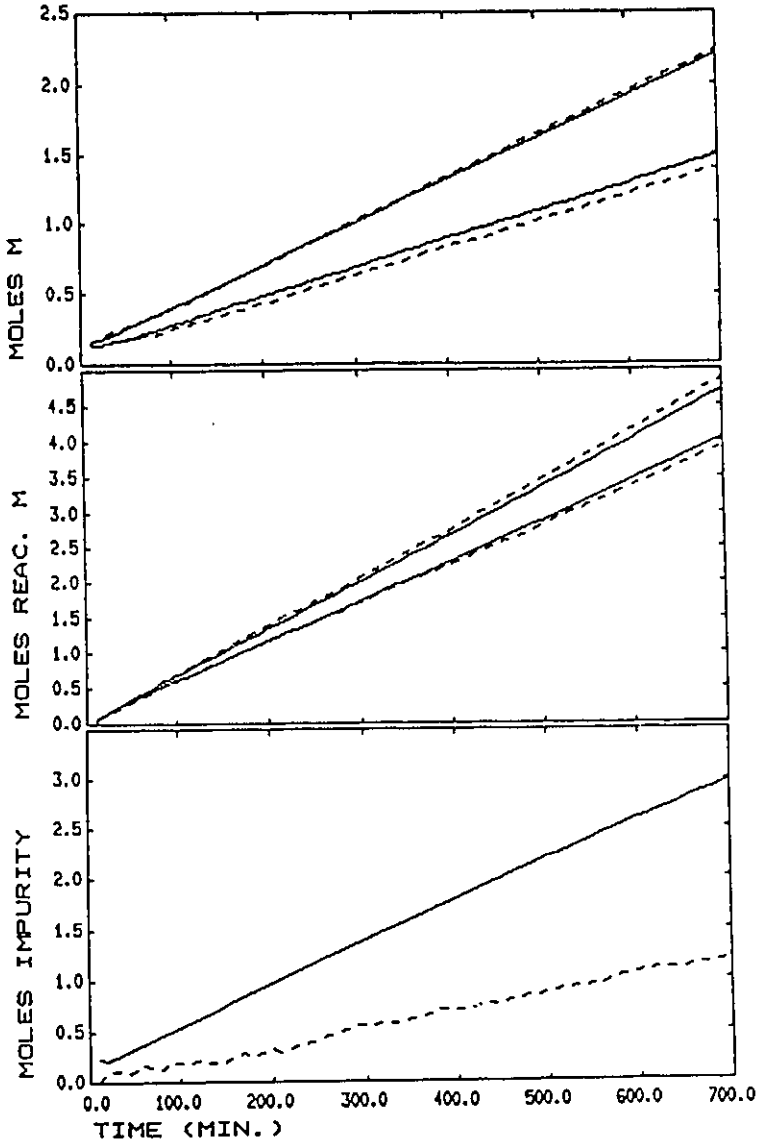
MOLES M
2.5
2.0
1.5
1.0
0.5
0.0
MOLES REAC. M
4.5
4.0
3.5
3.0
2.5
2.0
1.5
1.0
0.5
0.0
MOLES IMPURITY
3.0
2.5
2.0
1.5
1.0
0.5
0.0
0.0
100.0
200.0
300.0
400.0
500.0
600.0
700.0
TIME (MIN.)

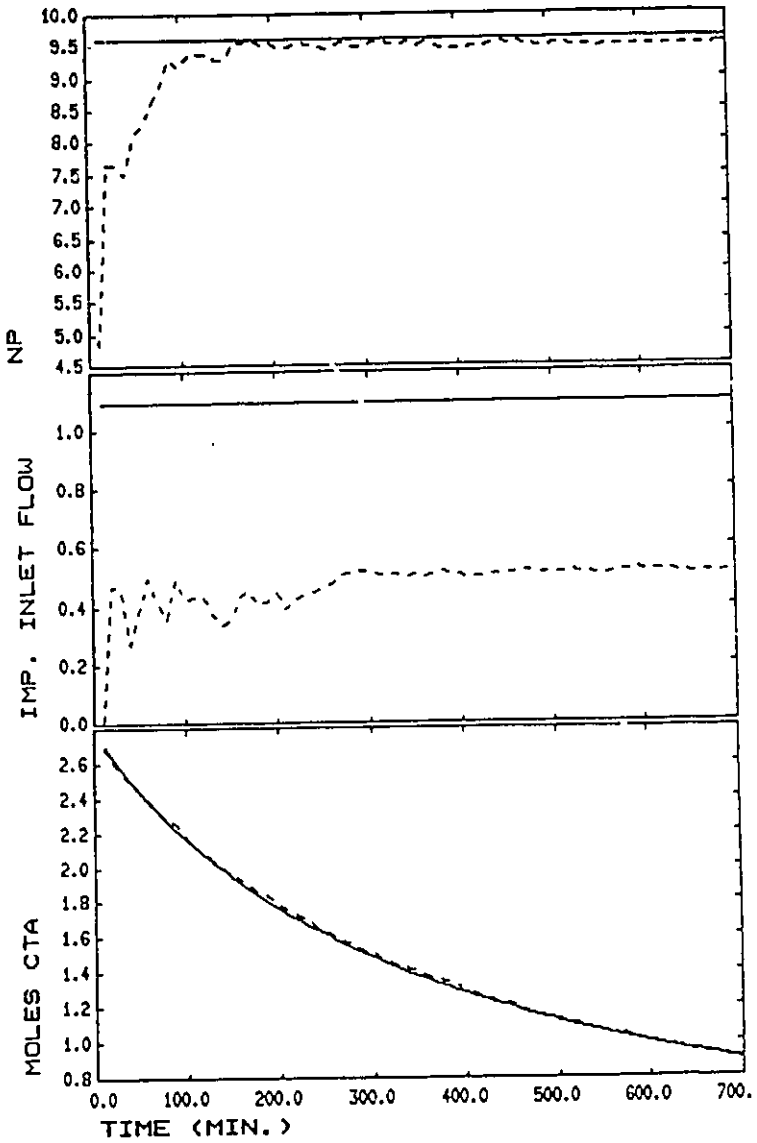
NP
10.0
9.5
9.0
8.5
8.0
7.5
7.0
6.5
6.0
5.5
5.0
4.5
IMP. INLET FLOW
1.0
0.8
0.6
0.4
0.2
0.0
MOLES CTA
2.6
2.4
2.2
2.0
1.8
1.6
1.4
1.2
1.0
0.8
0.0
100.0
200.0
300.0
400.0
500.0
600.0
700.
TIME (MIN.)

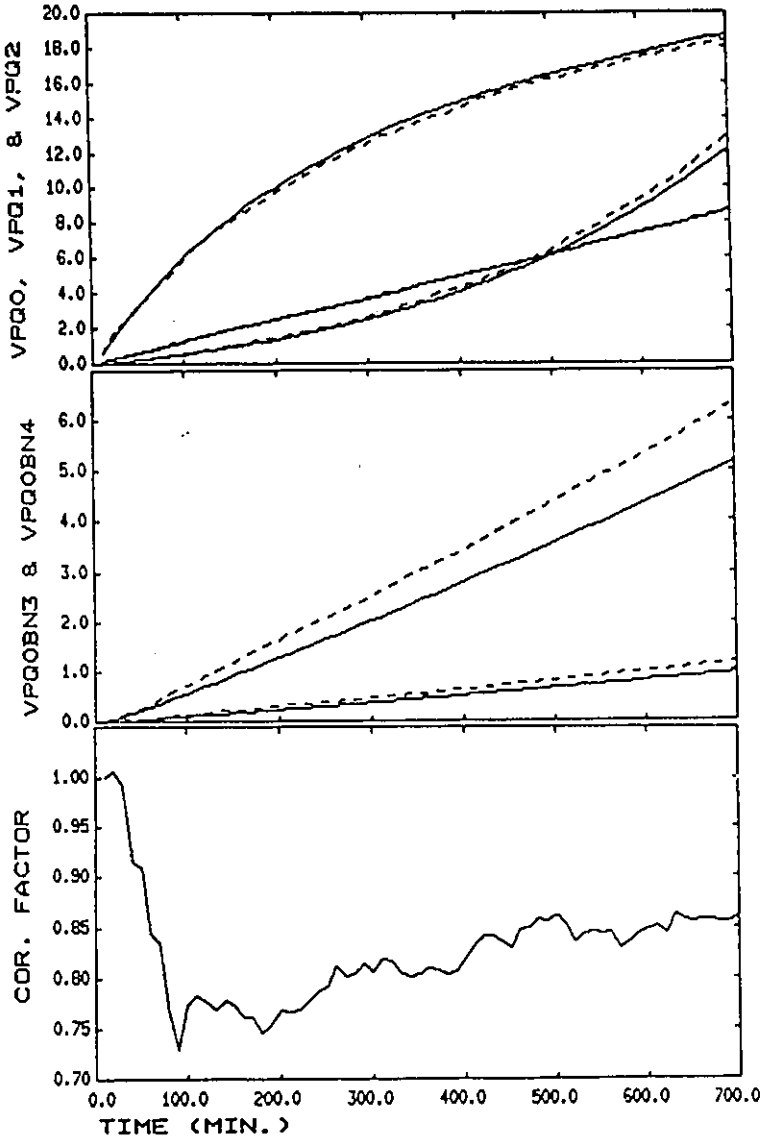

FIGURE 8.15: Extented Kalman Filter With x^{14}: r_b Model Mismatch
(-) Actual Response; (--) Predicted
(a) M_s & M_b; (b) P_s & P_b; (c) Im_p; (d) N_p
(e) F_{Im_p}; (f) CTA; (g) V_pQ_0, V_pQ_1, & V_pQ_2; (h) $V_pQ_0Bn_3$ & $V_pQ_0Bn_4$; (i) x^{14}

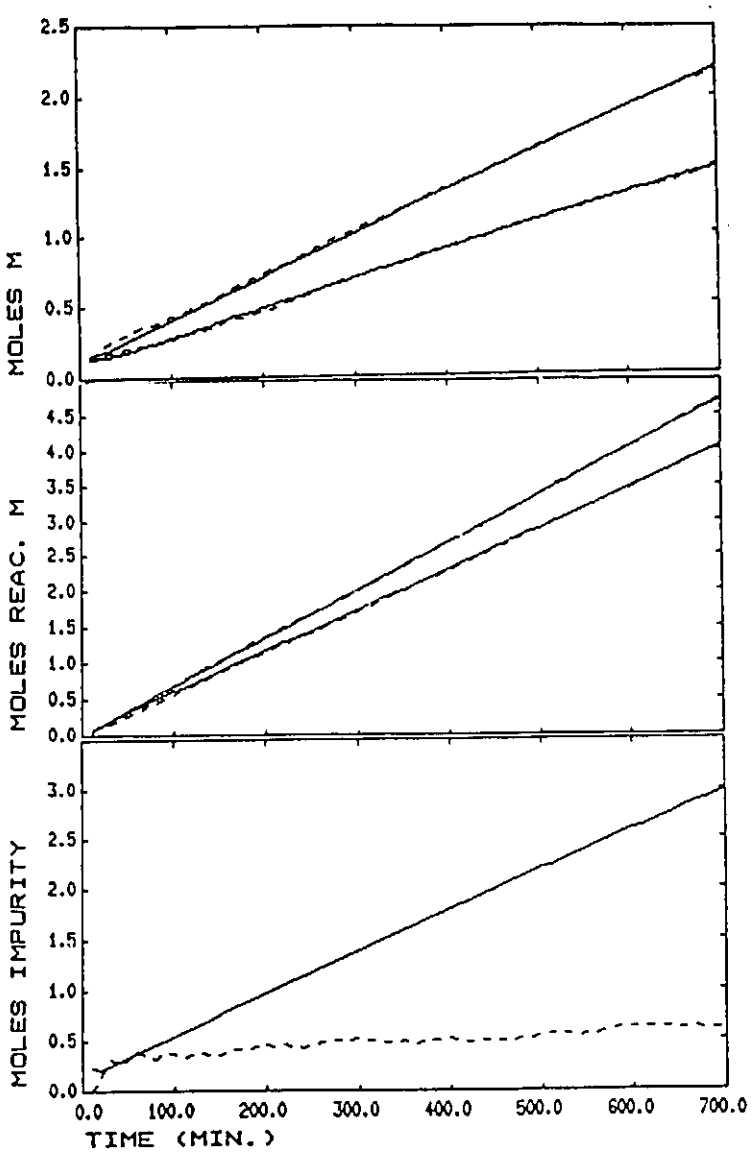
MOLES M
2.5
2.0
1.5
1.0
0.5
0.0
MOLES REAC. M
4.5
4.0
3.5
3.0
2.5
2.0
1.5
1.0
0.5
0.0
MOLES IMPURITY
3.0
2.5
2.0
1.5
1.0
0.5
0.0
0.0
100.0
200.0
300.0
400.0
500.0
600.0
700.0
TIME (MIN.)

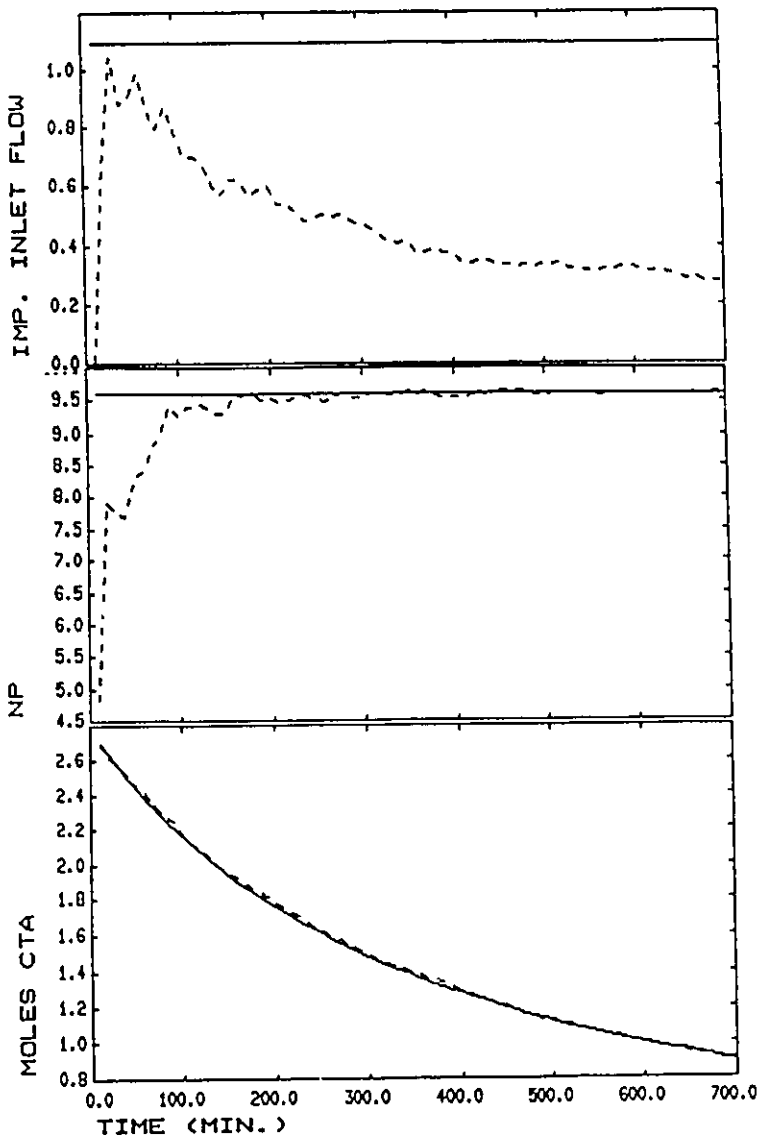
IMP. INLET FLOW
1.0
0.8
0.6
0.4
0.2
0.0
NP
9.5
9.0
8.5
8.0
7.5
7.0
6.5
6.0
5.5
5.0
4.5
MOLES CTA
2.6
2.4
2.2
2.0
1.8
1.6
1.4
1.2
1.0
0.8
0.0
100.0
200.0
300.0
400.0
500.0
600.0
700.0
TIME (MIN.)

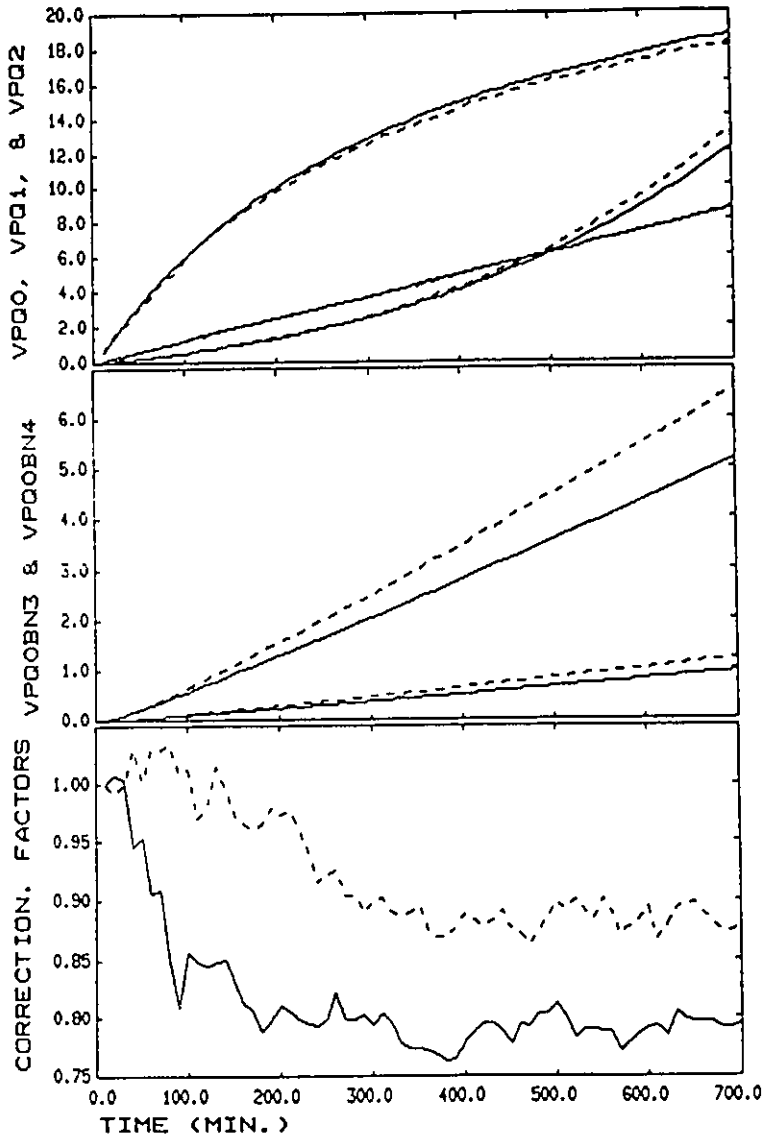

FIGURE 8.16: Extented Kalman Filter With x^{14} & x^{15}: r_b Model Mismatch
(-) Actual Response; (--) Predicted
(a) M_s & M_b; (b) P_s & P_b; (c) Im_p; (d) N_p
(e) F_{Im_p}; (f) CTA; (g) V_pQ_0, V_pQ_1, & V_pQ_2; (h) $V_pQ_0Bn_3$ & $V_pQ_0Bn_4$;
(i) x^{14} (-) & x^{15} (--)

8.6.3. Structural Mismatch Associated With Mass Transfer

In this section we examine the consequence of a structural error in modelling the distribution of monomers between the particle and monomer droplet phases. The model used in the extended Kalman filter assumes constant partitioning through fixed K_{smp} and K_{bmp}, while the true process will be modelled assuming particle swelling according to Flory-Huggins theory (see previous chapter).

Figure 8.17 shows the simulated performance of the doubly modified extended Kalman filter of section 8.6.2 when subjected to the type of uncertainty described above. The extended Kalman filter can be observed to perform well, and leads to consistent state estimates with respect to the measurements. The effect of the mass transfer prediction error can be shown to affect $\Phi_s[M_1]_p$, $\Phi_b[M_1]_p$, and $k_{fCTA}[CTA]_p$. In general, each of these terms will be affected differently. It can be shown that incorporation of the organic phase impurity together with model mismatch states x^{14} and x^{15} in the extended Kalman filter satisfies the necessary conditions for consistency.

Modelling errors with respect to the partitioning of monomers between monomer droplet and particle phases will often not be important in a semi-batch mode of SBR production. Usually, one would expect the amount of each monomer to be sufficiently low so that no significant monomer droplet phase is present and most of the unreacted monomer can be found in the particle and water phases. Nevertheless, the robustness of the extended Kalman filter to these errors if present has been clearly demonstrated.

Other species distribution errors are also expected to be significant, but can be shown to be handled consistently with the modified extended Kalman filter. Nomura (1988) has shown that modelling of the *CTA* distribution assuming equilibrium distribution through constant partition coefficients can lead to significant model prediction error. However, the error appears to be most significant when both monomer droplets and particle phases are present, and as discussed above, usually will not be present in the semi-batch mode of operation. If a serious error in prediction is present, it can be shown that the nonstationary mismatch state x^{15} will account for it.

The modified extended Kalman filter will also consistently account for errors associated with impurity and initiator distribution, since these can be easily accounted for through modification to the fictitious impurity level.

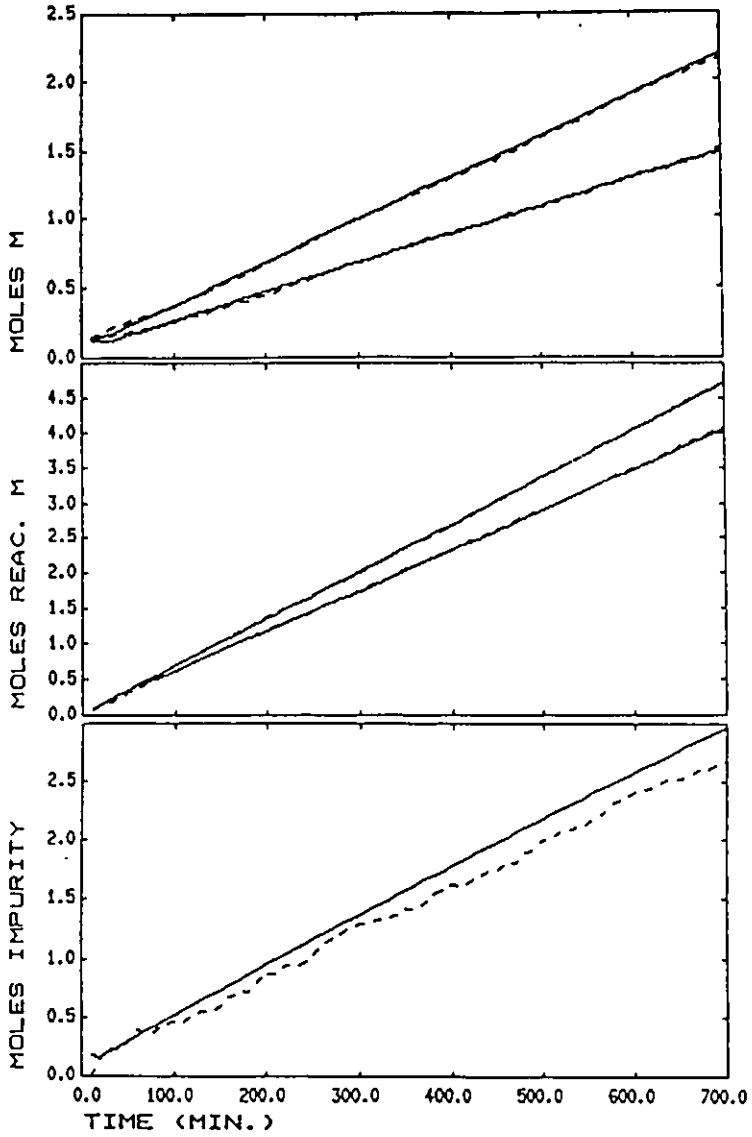
MOLES M
2.5
2.0
1.5
1.0
0.5
0.0
MOLES REAC. M
4.5
4.0
3.5
3.0
2.5
2.0
1.5
1.0
0.5
0.0
MOLES IMPURITY
2.5
2.0
1.5
1.0
0.5
0.0
0.0
100.0
200.0
300.0
400.0
500.0
600.0
700.0
TIME (MIN.)

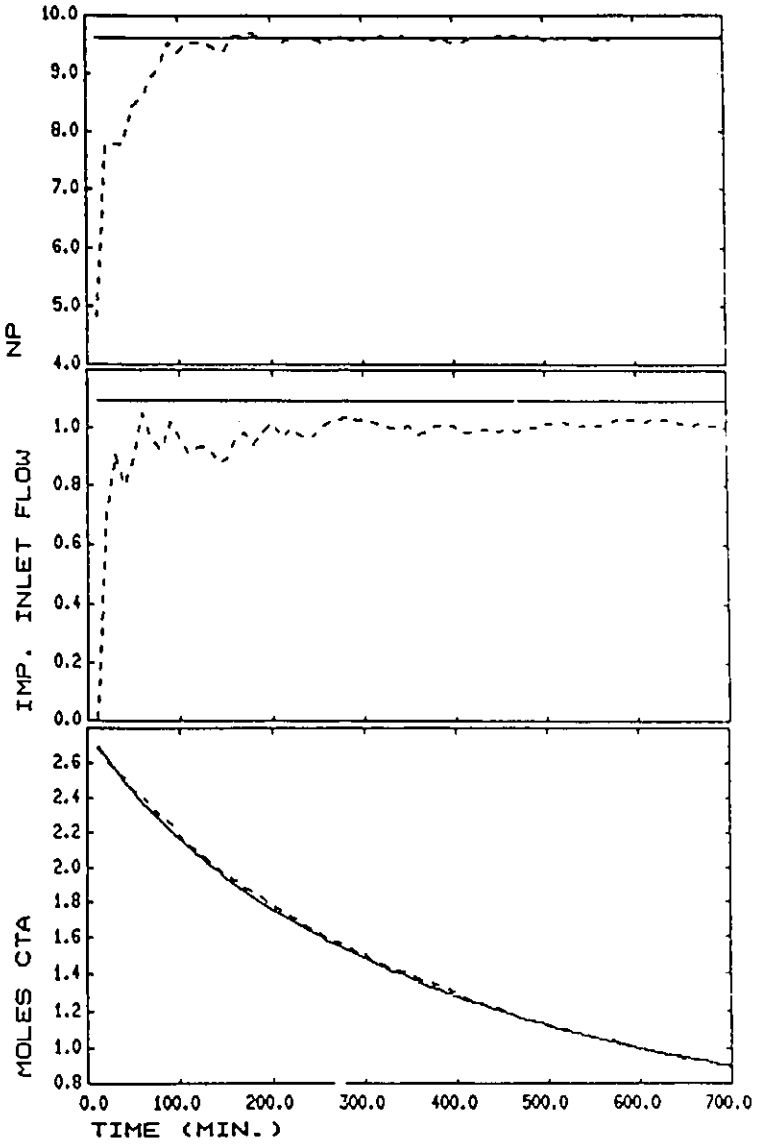
NP
IMP. INLET FLOW
MOLES CTA
TIME (MIN.)
0.0
100.0
200.0
300.0
400.0
500.0
600.0
700.0

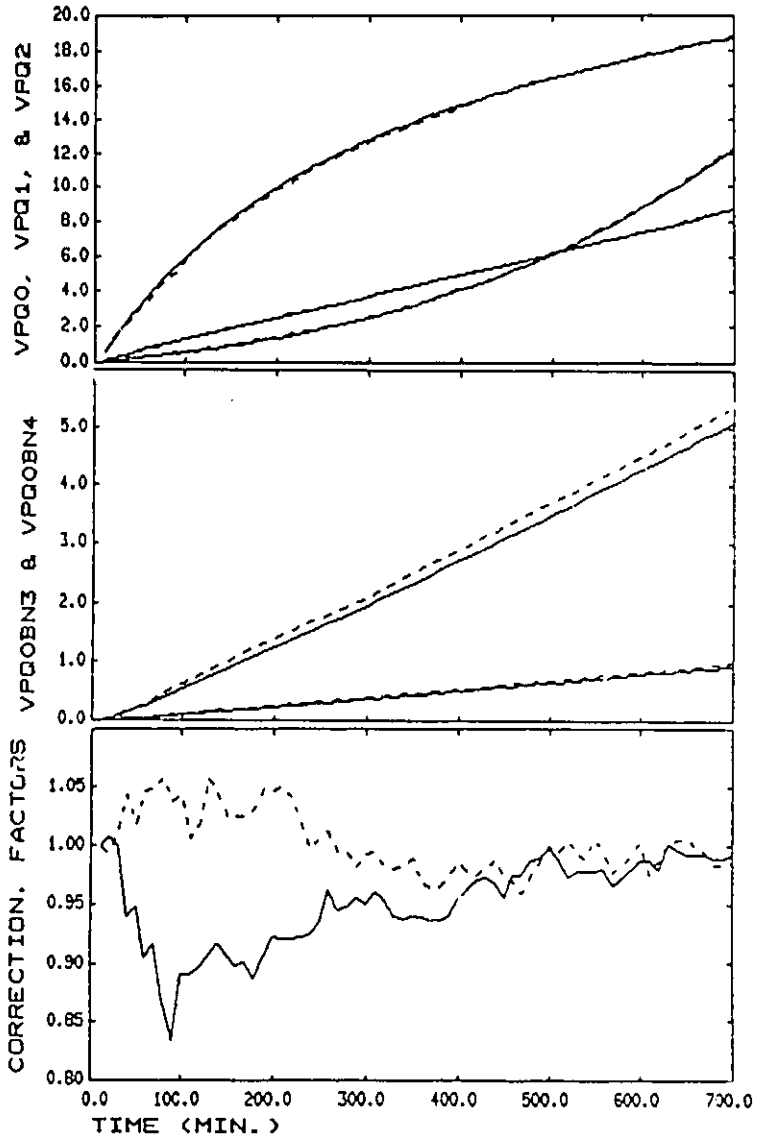

FIGURE 8.17: Extented Kalman Filter With x^{14} & x^{15}: K_{smp} & K_{bmp} Model Mismatch
(-) Actual Response; (--) Predicted
(a) M_s & M_b; (b) P_s & P_b; (c) Im_p; (d) N_p
(e) F_{Im_p}; (f) CTA; (g) V_pQ_0, V_pQ_1, & V_pQ_2; (h) $V_pQ_0Bn_3$ & $V_pQ_0Bn_4$;
(i) x^{14} (-) & x^{15} (--)

8.6.4. Particle Size Uncertainty

One important form of model mismatch is the assumption made about the particle size distribution. The model assumes that the particle size distribution is monodispersed. In a real process environment some statistical broadening will exist, and as a result, the volume average particle size may not be in agreement with the average obtained from a dynamic light scattering instrument (Korti, 1989). The development of a dynamic model with population balances and the effect of statistical broadening accounted for is far from trivial. Nevertheless, the effect on the doubly modified extended Kalman filter will be to adjust the estimated number of particles and the impurity to allow for consistency with the measurements and filtered states. The same effect would result if an error is made in estimating the density of copolymer produced. This type of mismatch might be noticeable when a significant copolymer composition drift exists due to bad control.

8.6.5. Molecular Weight And Branching Uncertainty

The prediction of the molecular weight moments and branching frequencies is seriously vulnerable to model mismatch since these states are not observable. Unfortunately, there is little hope as far as the state estimation algorithm is concerned to solve this problem. The main difficulty is the lack of any on-line instrumentation that measures properties of a polymer latex related to molecular weight and branching. All that can be done in a practical process environment is to follow the progress of the model in predicting these properties from subsequent off-line property analyses on semi-batch runs and adapt the model when appropriate.

8.6.6. Conclusion From Robustness Study

In this chapter, an exhaustive robustness study was carried out on the extended Kalman filter formulated in section 8.5.1, and a modification of it. The aim was to determine if this nonlinear estimation scheme could provide consistent state estimates when subjected to important types of mismatch, and to propose the necessary modifications for consistency if needed. The requirement of consistency (Parrish and Brosilow, 1988) must be met for unbiased tracking of the important states.

The results demonstrated that the extended Kalman filter of 8.5.1, in general, does not display consistency to all the important types of model mismatch. However, two very simple modifications were proposed to make the extended Kalman filter consistent and improve state predictions when all the important

types of model mismatch are present. The modifications were the introduction of two fictitious nonstationary model mismatch states x^{14} and x^{15} at appropriate locations in the semi-theoretical model to satisfy consistency requirements. The modifications were shown to lead to a very significant improvement in the performance of the filter relative to the original formulation.

It is recommended that the modified extended Kalman filter be combined with the extended Kalman filter of section 8.5.2 that iterates for unknown initial states Im_p, $N_p V_w$, and F_{Im_p} assuming no model mismatch. Although the iterated values of the for unknown initial states may not be correct when mismatch is present, it is expected that the mismatch will not be serious enough to significantly degrade the convergence properties of the reiterated extended Kalman filter relative to standard extended Kalman filter alone. Alternatively, x^{15} can be added to EKF 2 as an additional state to provide an improved initial starting estimates of this state in the modified EKF 1. When model mismatch becomes a serious concern, it may be much more logical to retune the model using data from on-line and off-line semi-batch runs in order to realize the potential for quality control.

8.7 NOTATION

A_k	state transition matrix of linearized state space model
A_k^d	deterministic component of A_k
A_k^s	stochastic state component of A_k
Bn_i	i'th branch frequency per copolymer chain
CTA	moles of unreacted chain transfer agent
d_i	density of i
D_p	unswollen volume average particle size
E	moles of emulsifier
f	initiator efficiency
$f^d(x,u,t)$	nonlinear state space equation indicating time rate of change of x^d
f^s	nonlinear state space equation indicating time rate change of x^s
F_{Im_p}	feed rate of Im_p
F_{Im_w}	feed rate of Im_w

F_{M_b}	feed rate of butadiene
F_{M_s}	feed rate of styrene
h	nonlinear equation relating outputs to x
H_k	output/state matrix of linearized state space model
I_n	moles of initiator
Im_p	moles unreacted organic phase reactive impurity
Im_w	moles of unreacted water phase reactive impurity
J	cost function in nonlinear optimization state estimation approach
k	sampling interval
k_{fCTA}	copolymer pseudo rate constants for *CTA*
K_k	extended Kalman filter gain at interval k
M_b	moles of butadiene
M_s	moles of styrene
M_{W_i}	molecular weight of i
$\overline{n}$	average number of radicals per particle
N_p	number of polymer particles per unit volume water
N_A	Avogadro's number
P_0	covariance matrix for initial error in x
P_k	covariance matrix of state estimation error at k
P_b	moles of butadiene reacted to form copolymer
P_s	moles of styrene reacted to form copolymer
Q_i	i'th copolymer moment concentration
R_{CTA}	rate of *CTA* reaction
R_{pb}	rate of polymerization of butadiene
R_{ps}	rate of polymerization of styrene
R_v	covariance matrix of v_k
R_w	covariance matrix of w_k

t	time
T	reactor temperature
u	manipulated input vector
v_k	additive output white noise vector at interval k
V_p	volume polymer particle phase
V_w	volume of water
w_k	additive Gaussian state white noise vector at interval k
x	vector of modelled process differential states
x_0	x at starting time
x^1	state vector corresponding to EKF 1 in reiterative extended Kalman filter
x^2	state vector corresponding to EKF 2 in reiterative extended Kalman filter
x^{14}	nonstationary stochastic state to compensate for model mismatch in R_{CTA}
x^{15}	nonstationary stochastic state to compensate for model mismatch errors in R_{pb}
x^d	deterministic component of x
x^s	nonstationary stochastic component of x
X	matrix of sensitivity coefficients
y	measurement vector
y^M	actual process measurement vector

Greek Letters

Φ_b	copolymer pseudo rate constant for butadiene
Φ_s	copolymer pseudo rate constant for styrene

OPEN-LOOP POLICIES FOR SEMI-BATCH POLYMERIZATION REACTORS

9. OPEN-LOOP OPERATING POLICIES FOR SEMI-BATCH POLYMERIZATION REACTORS

9.1 INTRODUCTION

The purpose of this chapter is to propose open-loop operating policies for the production of SBR latex in a semi-batch mode. In order for the results to be industrially relevant, the policies developed must not only be demonstrated to yield a wide range of SBR latex property specifications but must also be shown to be well suited for application in conjunction with on-line feedback control to compensate for state initialization errors, disturbances, and model mismatch. The latter issue is often neglected in the development of open-loop control policies, and is of extreme importance in SBR latex manufacture were quality control and product reproducibility is of concern (Taylor, 1988). The policies developed in this work will be specific to SBR latex production. However, it is expected that much of the ideas from this work can be extended to other semi-batch chemical process.

A wide range of examples can be found in the chemical process control literature where finite time, optimal open-loop policies were developed. A classical approach is often taken to arrive at some solution to the open-loop trajectory control problem in batch or semi-batch systems. Usually the problem is stated mathematically as

$$\underset{u(t)}{\text{Min}} \quad J(u(t)) \;=\; G(x(t_f)) \;+\; \int_0^{t_f} D(x,u,t)dt \tag{9.1}$$

given the process model

$$\dot{x} \;=\; f(x,u,t) \tag{9.2}$$

and general operating constraints in the form

$$c(x,u,t) \;\leq\; 0 \tag{9.3}$$

In the equations above, $u(t)$ is the vector of open-loop control actions to be determined, J is the objective functional, G is an end point contribution to J, D is an integrated contribution to J over period 0 to t_f, and x is the vector of internal model states that changes with time according to the nonlinear state space model defined by (9.2). A solution to (9.1) may be arrived at from the well-known maximum principle (Ray, 1981),

or instead through the transformation of the dynamic optimization problem into an equality constrained nonlinear program (NLP) using an orthogonal collocation procedure (Biegler, 1984; Cuthrell and Biegler, 1987; Cuthrell and Biegler, 1989). For discrete time control problems, (9.1) to (9.3) can be expressed in an equivalent discrete form and solved in an analogous discrete manner. In the general multivariable case, the solution to the problem posed in (9.1) to (9.3) will be quite involved, making the approach suited only for off-line use. The consequence of this can be serious when disturbances and/or model mismatch are encountered, which requires the recomputation of the optimal solution once this information becomes known. In the case of polymerization reactors, it would not generally be acceptable to simply apply a feedback control scheme that would drive the states back to their precomputed trajectories.

Depending on the nature of the open-loop control problem, arriving at a suitable form for the objective function may or may not be straightforward. For instance, in many petrochemical processes, a suitable form for J is obvious. These operations are often concerned with yield maximization subject to constraints on the feasible range of inputs. Hence, in the case of reactors, the logical choice for J would often be in the form of a batch time minimization or conversion maximization. When dealing with these processes there is often the advantage that the quality control variables are well understood and measurable in terms of the end product use, and therefore easily incorporated into (9.1). Unfortunately, polymer reactors represent a special class of control problems. The main problem with polymer reactors is arriving at a suitable form for (9.1) is by no means trivial. The difficulty arises from the fact that polymer properties in terms of their ultimate end use are very difficult to relate quantitatively to the chemical and macroscopic polymer properties that the models provide. Furthermore, depending on the end use of the polymer product, the important end properties of the polymer product can change significantly. As previously indicated, the expected end use of the latex would be either a coating (paint) or an adhesive. Some properties that are important in evaluating latex coatings (Koenecke, 1967; Martens, 1981) are oxidation resistance, ultraviolet resistance, flexibility, toughness, hydrophobic properties, chemical inertness, solubility, and so on. To evaluate latexes for adhesive applications the important end properties of concern (Autenrieth, 1977) would be tack, cohesive strength, shear adhesion, peel strength, resistance to creep, and so on. Qualitatively, it is known that molecular weight, copolymer composition, branching and crosslinking, and particle size properties contribute significantly to the end use properties regardless of the polymer end use. Hence it is by no means clear how these modelled properties should be effectively combined into an objective function in the form of (9.1) to allow a suitable diverse range of latexes to be produced.

Nevertheless, in light of the discussion above, examples can be found in the literature where a classical multiobjective optimization approach was applied to arrive at some useful open-loop policies for batch/semi-batch polymerization problems. Tirrel and Gromley (1981) derived conditions for constant copolymer composition control of styrene/acrylonitrile through reactor temperature adjustments. This composition control policy will only be applicable when certain conditions are satisfied on the activation energies of the propagation rate constants (Ray and Gall, 1969). This policy cannot be applied to SBR since in the temperature range of interest it is known that temperature has no influence on copolymer composition (Miller, 1968; Tate and Bethea; 1985). The authors also derived discrete time policies for discrete temperature manipulations via the discrete maximum principle. The objective was arbitrarily chosen to be the integrated composition drift weighted by the polymerization rate, and the weighted final conversion.

Tsoukas et al. (1982) viewed batch/semi-batch polymerization control as multiobjective in nature. For a final end point constraint on conversion and molecular weight their objective was to minimize both the weighted composition drift and molecular weight distribution in batch/semi-batch copolymerization of styrene/acrylonitrile. The manipulations to be made were temperature and/or the monomer addition rate. In their work they recognized the importance of choosing the most effective weighting in the multiobjective problem so that the best trade off in terms of the final desired polymer properties could be found. To do so they recommended a very involved procedure whereby all the noninferior or Pareto solutions be found for the multiobjective problem posed so that the best trade off is found.

Cawthon and Knaebel (1989) also viewed the problem of batch/semi-batch open-loop trajectories as multiobjective in nature. An objective function was formulated to find the best trade off between the integrated composition deviations, polydispersity, and time. These authors also suggest that all noninferior solution be computed to find the best trade off. Temperature and reactant flow rates were considered as manipulated inputs to be determined via the maximum principle. The solution free radical polymerization of acrylonitrile and styrene was considered.

Hicks et al. (1969) used the maximum principle to arrive at the best temperature and initiator policy to optimize an objective containing the molecular weight distribution, final molecular weight, and the final conversion. The free radical polymerization of styrene was considered.

Sacks et al. (1973) also used the maximum principle to arrive at temperature trajectories that minimize and maximize the spread of the molecular weight distribution for chain addition polymerization in batch reactors subject to a constraint on final conversion and molecular weight.

Ponnuswamy et al. (1987) developed open-loop and closed-loop policies for batch solution polymerization of MMA. For a specified final conversion and number average molecular weight, three optimization problems, two minimum time, the final a minimum polydispersity, were posed and solved via the maximum principle. Optimal initiator or temperature trajectories were considered. The solution provided optimal trajectories for properties to be monitored during reaction such as inferred conversion and molecular weight. The authors, recognizing the importance of process disturbances, proposed that a feedback controller be used to maintain the properties to be monitored along the computed off-line open-loop trajectory. No consideration was made to the fact that following an off-line trajectory once unaccounted disturbances or model mismatch becomes present may become suboptimal.

Farber and Laurence (1986) computed minimum time batch temperature trajectories for bulk polystyrene production subject to a final conversion and final molecular weight constraint. The maximum principle was used to obtain the optimal temperature trajectories.

Hsu and Chen (1988) determined minimum time policies subject to final conversion and molecular weight constraints for solution free radical polymerization of styrene. Unlike the previous work, piecewise initiator and temperature policies were computed via the maximum principle.

Jang and Yang (1989) developed and experimentally applied minimum, semi-batch time initiator addition policies subject to constraints concerned with heat removal and the maximum amount of initiator that may be added. The optimal policies were obtained off-line through a modification of the orthogonal collocation approach proposed by Biegler (1984). The reported CPU times to arrive at the optimal trajectories would not be practical for on-line use.

Choi and Butola (1987), recognizing the drawbacks with classical approaches, proposed a simplified suboptimal scheme for arriving at open-loop trajectories in batch/semi-batch systems. A fictitious feedback controller approach on the polymer properties that are to be controlled in an off-line simulation was used as a means to derive suboptimal open-loop input manipulations. Time varying monomer and reactor temperature profiles were computed through the fictitious feedback controller approach to control copolymer composition and molecular weight of styrene/acrylonitrile. The important issue of the design of the fictitious feedback controller was not discussed in their work.

Rather than directly optimizing an objective function like (9.1) through some numerical search algorithm, it is often possible from one's fundamental understanding of polymerization reactors to find an exactly equivalent set of necessary and sufficient conditions that must hold if (9.1) is to be optimized. Such a procedure will always be much more computationally efficient in arriving at an optimal trajectory than a

more general search based technique. This idea has been used to develop simple procedures for obtaining industrially useful optimal semi-batch policies based on the control of instantaneous rather than integral polymer properties. Although these procedures can be shown to provide an optimal solution to some form of (9.1) to (9.3), to a polymer reaction engineer, policies derived from specifications on instantaneous conditions would be much more meaningful than ones derived from cumulative (integral) properties. In general, it is desirable to produce copolymer with a consistent set of properties throughout the batch run. The production of copolymer should not be viewed as blending problem, whereby off-specification copolymer made at one point in time is compensated for by a different off specification copolymer made at some other point in time. Therefore, a sufficient condition for producing a consistent polymer with certain desired final properties is to ensure that the instantaneous polymer being produced at every instant of time throughout the batch has these desired properties.

Using this idea above, Hamielec et al. (1987) and Broadhead et al. (1985) proposed policies for copolymer composition control based on conditions for maintaining fixed instantaneous copolymer composition. Two different policies were proposed. Policy I consisted of adding all the slower reacting monomer to the reactor at the beginning and some of the faster reacting monomer. The flow rate of the faster reacting monomer is determined so that the condition for fixed instantaneous composition is maintained. Policy II consist of charging the reactor with a small amount of each monomer at the beginning in a a suitable ratio and then feeding each monomer so that the concentration of each monomer, and hence copolymer composition, is fixed with time. In addition, an operating policy was also proposed in Hamielec et al. (1987), termed calorimetric control, for on-line application of copolymer control through the measurement of the reaction heat flux. Arrival at the solution for the monomer flow rates in these policies was shown to be very straightforward.

Beste and Hall (1966) also considered the control of free radical polymerization through the control of instantaneous properties. Analytical expressions were derived for molecular weight control based on initiator, monomer, modifier, and chain stopper policies.

The method that will be advocated in the work that follows will be a generalization of the univariate ideas of Hamielec et al. (1987) and Beste and Hall (1966) to the multivariable case. Generally stated, SBR semi-batch open-loop policies will be obtained from the solution of

$$\frac{dp}{dt} = P(x,u,t) = 0 \tag{9.4}$$

where p is a vector of instantaneous copolymer properties and/or conditions to be kept uniform during the semi-batch run. The solution for the open-loop control actions $u(t)$ can be observed in (9.4) to only require the solution of a nonlinear system of equations rather than the solution of a general optimization problem, and therefore has the potential for on-line use in an open-loop/feedback control strategy. By defining different copolymer properties in p, a vast range of SBR operating policies are possible for meeting a wide range of SBR property specifications. This indirect procedure for arriving at optimal policies is chosen over a more general classical approach such as (9.1) because maintaining control over instantaneous conditions would be expected to be far more meaningful to a polymer reaction engineer even though (9.4) can always be expressed in the form of (9.1) to (9.3). Another advantage when working with condition (9.4), as will be discussed in chapter 10, is that a trivial modification can be made to (9.4) to allow for the application of feedback control actions to compensate for state initialization errors, disturbances, and model mismatch.

The sections to follow will present different SBR open-loop operating policies that can be obtained through different choices for p. Policies that have already proposed (Hamielec et al., 1987; Beste and Hall, 1966) are generalized, and some new ones are also proposed. The implication of using the different policies in an on-line recomputation strategy is also addressed. The open-loop control of copolymer properties and conditions such as composition, conversion, molecular weight, crosslinking and branching, and time optimality shall be considered. Trade-off type policies are also presented. Simulated results from some of the policies proposed shall be presented.

9.2 SEMI-BATCH REACTOR CONFIGURATION

The work that follows shall focus on developing policies for the simplified semi-batch reactor configuration shown in Figure 9.1.

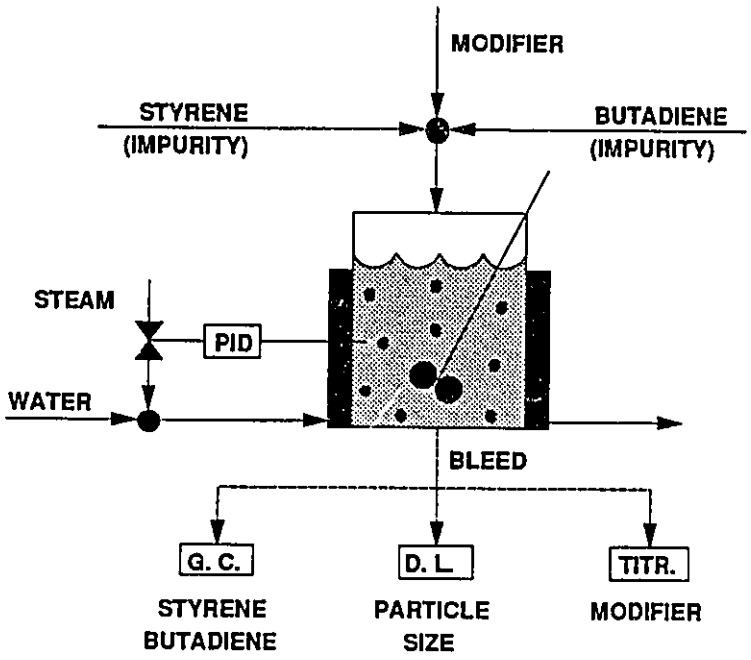

FIGURE 9.1: SEMI-BATCH SBR REACTOR CONFIGURATION FOR CONTROL

The reactor will be initially seeded with SBR copolymer. The reactor will be operated isothermally, with temperature control provided by the water coolant temperature through the reactor jacket. For the purpose of copolymer property control, the feed rates of styrene, butadiene, and modifier shall be considered. The remaining components of the copolymer recipe is initially charged to the reactor. The control over final particle size and percent solids is addressed through the specification of the number of seed particles and the volume of water to be charged respectively. Unless stated otherwise, the open-loop simulations to follow shall be carried out with the following common initial and operating conditions:

Common Initial Reactor Conditions

P_s	0.32 *gmol*
P_b	1.81 *gmol*
N_p	$2.5x10^{15}$ l^{-1}
V_pQ_0	$4.72x10^{-3}$ *gmol*
V_pQ_1	2.13 *gmol*
V_pQ_2	9595.6 *gmol*
$V_pQ_0Bn_3$	$1.766x10^{-4}$ *gmol*
$V_pQ_0Bn_4$	$9.578x10^{-4}$ *gmol*
V_w	4 *l*
E	0.122 *gmol*
I_a	0.03 *gmol*
Im_p	0
Im_w	0

Common Operating Conditions

T	55° *C*
V_r	10 *l*
F_{I_a}	0
F_{V_w}	0
F_E	0
F_{Im_p}	0
F_{Im_w}	0

Although the control strategies to follow shall pertain to the control configuration shown in Figure 9.1, the theory will easily extend to the more general case of nonisothermal operation and additional reactor feeds. Practical considerations would demand a water and emulsifier feed in a pre-emulsification stage with the monomers and CTA so that effective mixing is obtained. This detail, which is of no consequence as far as the control theory is concerned, has been left out to simplify the presentation of the important contributory results that follow.

9.3 COPOLYMER COMPOSITION

An important property of a copolymer is its composition (see section 7.3). For example, copolymer composition can have an important influence in end use properties such as strength, flexibility, and glass transition temperature. A wide range of SBR latex properties may be obtained through different SBR copolymer composition specifications. The optimal SBR copolymer composition can change significantly depending on

its end use. For instance, SBR used for making pressure sensitive adhesives might contain approximately 25% by weight styrene while SBR used in the manufacture of coatings might contain 60% (1:1 mole ratio) styrene.

In general, the objective for the open-loop policy is to maintain conditions such that a constant composition copolymer is made throughout the batch/semi-batch run. The work that follows will present three different open-loop strategies for copolymer composition control. All three strategies will achieve the desired copolymer composition through manipulation of the monomer feed rate(s). The use of a temperature trajectory for composition control (Ray and Gall, 1969) is not considered in this work since temperature does not have a significant effect on SBR copolymer composition (Miller, 1968; Tate and Bethea; 1985).

9.3.1 Copolymer Composition: Policy 0

To establish the necessary operating conditions for the production of copolymer with constant composition, the instantaneous copolymer composition with respect to styrene, given by

$$F_s = \frac{R_{ps}V_p}{R_{ps}V_p + R_{pb}V_p} \tag{9.5}$$

must remain constant with time. Hence, the first policy that we will be concerned with pertains to $p = F_s$. If one inserts the expressions for $R_{ps}V_p$ and $R_{pb}V_p$, given by

$$R_{ps}V_p = \Phi_s[M_s]_p \frac{\bar{n}N_pV_w}{N_A} \tag{9.6}$$

$$R_{pb}V_p = \Phi_b[M_b]_p \frac{\bar{n}N_pV_w}{N_A} \tag{9.7}$$

into (9.5) one obtains

$$F_s = \frac{\Phi_s[M_s]_p}{\Phi_s[M_s]_p + \Phi_b[M_b]_p} \tag{9.8}$$

where Φ_s and Φ_b are given by (7.6) and (7.7) respectively. Equation (9.8) shows that instantaneous copolymer composition is only a function of states M_s, M_b, P_s, P_b, V_w, and T for the general copolymer case. Taking the derivative of F_s with respect to time, and application of the chain rule leads to

$$\frac{dF_s}{dt} = \frac{\partial F_s}{\partial M_s}\frac{dM_s}{dt} + \frac{\partial F_s}{\partial M_b}\frac{dM_b}{dt} + \frac{\partial F_s}{\partial P_s}\frac{dP_s}{dt} + \frac{\partial F_s}{\partial P_b}\frac{dP_b}{dt} + \frac{\partial F_s}{\partial V_w}\frac{dV_w}{dt} + \frac{\partial F_s}{\partial T}\frac{dT}{dt} \tag{9.9}$$

The desired condition is given by

$$\frac{dF_s}{dt} = 0 \tag{9.10}$$

Substituting

$$\frac{dM_s}{dt} = F_{M_s} - R_{ps}V_p \tag{9.11}$$

and

$$\frac{dM_b}{dt} = F_{M_b} - R_{pb}V_p \tag{9.12}$$

into (9.9) and setting (9.9) to 0 gives the desired result

$$F_{M_b} = R_{pb}V_p - \left(\frac{\partial F_s}{\partial M_b}\right)^{-1}\left[\frac{\partial F_s}{\partial M_s}\left(F_{M_s} - R_{ps}V_p\right) + \frac{\partial F_s}{\partial P_s}R_{ps}V_p + \frac{\partial F_s}{\partial P_b}R_{pb}V_p + \frac{\partial F_s}{\partial V_w}F_{V_w} + \frac{\partial F_s}{\partial T}\frac{dT}{dt}\right] \tag{9.13}$$

Therefore, to produce copolymer with constant composition $F_s(t=0)$, F_{M_s} is specified, and F_{M_b} is computed through (9.13). This general composition control policy is referred to as Policy 0 in this work.

An alternative approach may be taken to achieve the same objective as above by imposing conditions on the ratio of monomers in the polymer particles. Hamielec et al. (1985) have shown that (9.8) can also be expressed as

$$F_s = \frac{(r_s - 1)f_{sp}^2 + f_{sp}}{(r_s + r_b - 2)f_{sp} + 2(1 - r_b) + r_b} \tag{9.14}$$

where r_s and r_b are the respective reactivity ratios for styrene and butadiene, and f_{sp}, the mole fraction of styrene in the particle monomer phase is given by

$$f_{sp} = \frac{[M_s]_p}{[M_s]_p + [M_b]_p} \tag{9.15}$$

Assuming isothermal conditions, or that r_s and r_b are temperature independent (good assumption with SBR), equations (9.14) and (9.15) show that an equivalent condition for constant copolymer composition is that f_{sp}, or equivalently, the ratio of $[M_s]_p$ to $[M_b]_p$ remain constant. Hence, an equivalent condition for the production of copolymer with constant composition can be obtained by maintaining constant $p = ([M_s]_p)/([M_b]_p)$. The condition to be satisfied is given by

$$\frac{d}{dt}\left(\frac{[M_s]_p}{[M_b]_p}\right) = 0 \tag{9.16}$$

where

$$[M_a]_p = \frac{M_a}{V_m K_{amp} + V_w K_{awp} + V_p} \tag{9.17}$$

$$[M_b]_p = \frac{M_b}{V_m K_{bmp} + V_w K_{bwp} + V_p} \tag{9.18}$$

Inserting (9.17) and (9.18) into (9.16), and application of the chain rule to obtain the required monomer feed conditions leads to

$$F_{M_b} = R_{pb}V_p + \left[\frac{M_a}{M_b^2}\zeta - \left(\frac{M_a}{M_b}\right)\frac{\partial\zeta}{\partial M_b}\right]^{-1}$$
$$\left(\left(\frac{\zeta}{M_b} + \left(\frac{M_a}{M_b}\right)\frac{\partial\zeta}{\partial M_a}\right)\left(F_{M_a} - R_{pa}V_p\right) + \left(\frac{M_a}{M_b}\right)\left(\frac{\partial\zeta}{\partial P_a}R_{pa}V_p + \frac{\partial\zeta}{\partial P_b}R_{pb}V_p + \frac{\partial\zeta}{\partial V_w}F_{V_w}\right)\right) \tag{9.19}$$

where

$$\zeta = \frac{V_m K_{bmp} + V_w K_{bwp} + V_p}{V_m K_{amp} + V_w K_{awp} + V_p} \tag{9.20}$$

Application of (9.19) to obtain F_{M_b} with F_{M_a} specified (or vice versa) will maintain $[M_a]_p/[M_b]_p$ constant at $([M_a]_p/[M_b]_p)_{t=0}$, and therefore maintain the necessary condition for constant copolymer composition.

From the point of view of an off-line policy computation, it makes no difference whether F_{M_b} or F_{M_a} is obtained from (9.13) or (9.20). However, if the composition control policy is to be applied on-line with state estimation being carried out as discussed in chapter 8, a serious difference may arise. This is due to differences in observability of the instantaneous property being controlled. Provided that $R_{pb} = x^{15}\Phi_b[M_b]_p\bar{n}N_pV_w/N_A$ is used in the state estimator (refer to section 8.6.2) and in the monomer flow rate computations, the estimator should converge to the correct F_a in the presence of initialization errors, model mismatch, and disturbances. This is due to the M_a and M_b measurements that provide sufficient information to observe $R_{pa}V_p$ and $R_{pb}V_p$. This condition does not hold for $[M_a]_p/[M_b]_p$ because both $[M_a]_p$ and $[M_b]_p$ are not observable. If errors are present in the modelled predictions $[M_a]_p$ and $[M_b]_p$, the estimator will fictitiously compensate for this by adjusting $\bar{n}$ and x^{15} in order to match the observed $R_{pa}V_p$ and $R_{pb}V_p$. The consequence of an error in the prediction of the monomer concentrations in the particle would be a bias in the monomer feed rate computation from its correct value that can only be corrected though the application of feedback control. Hence (9.13) would be the preferred condition to apply since the computed monomer feed rate when operating on-line at

nonideal conditions will at least provide a correct monomer feed rate to maintain copolymer composition at the estimated level. Procedures for correcting the open-loop monomer flow rates once error are encountered on-line shall be discussed in chapter 10.

Figure 9.2 shows the results from a policy 0 simulation. The reactor was initially charged with $M_a = 0.228 \quad gmol, M_b = 0.9 \quad gmol$, and $CTA = 8 \quad gmol$. The feed rate of styrene and CTA was fixed at 0.018 gmol/min and 0 gmol/min respectively. When the maximum amount of styrene that can be added, as determined by the reactor volume constraint, was reached F_{M_a} was set to 0. In Figure 9.2(b) the cumulative copolymer composition (seeds not included) can be observed to be constant at all time. The required flow rate for F_{M_b} to maintain constant copolymer composition is shown in Figure 9.2(d). The effect that the policy has on other properties (seeds not included) such as conversion (9.2(a)), % solids (9.2(c)), cumulative weight average molecular weight (9.2(e)), cumulative number average molecular weight (9.2(f)), cumulative polydispersity (9.2(g)), and cumulative degree of branching and crosslinking (9.2(h)) is also shown.

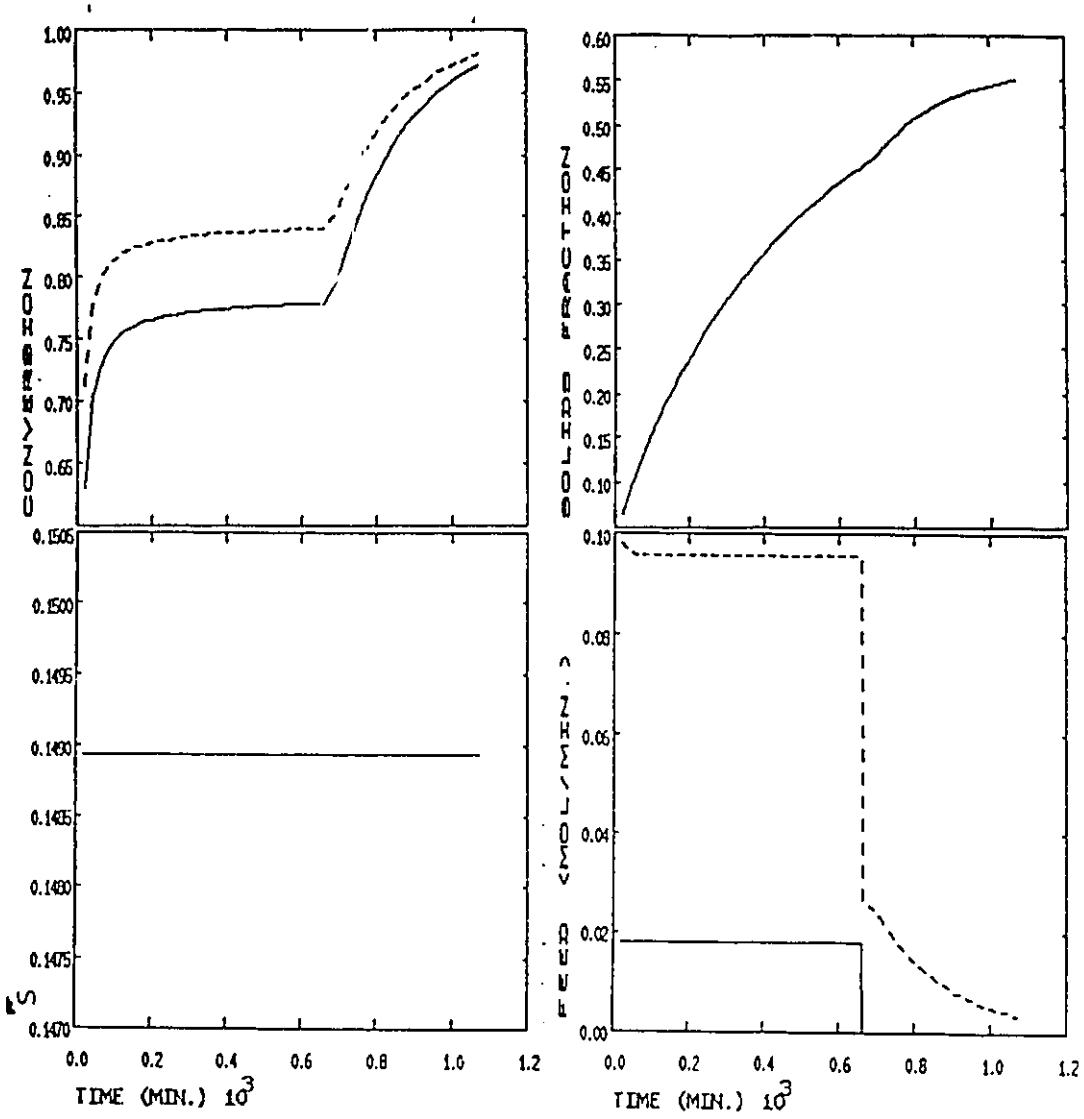
CONVERSION
1.00
0.95
0.90
0.85
0.80
0.75
0.70
0.65
0.1505
0.1500
0.1495
0.1490
0.1485
0.1480
0.1475
0.1470
ES
0.0
0.2
0.4
0.6
0.8
1.0
1.2
TIME (MIN.) 10^3
SOLID PRODUCT
0.60
0.55
0.50
0.45
0.40
0.35
0.30
0.25
0.20
0.15
0.10
0.10
0.08
0.06
0.04
0.02
0.00
SOLVENT LEVEL
0.0
0.2
0.4
0.6
0.8
1.0
1.2
TIME (MIN.) 10^3

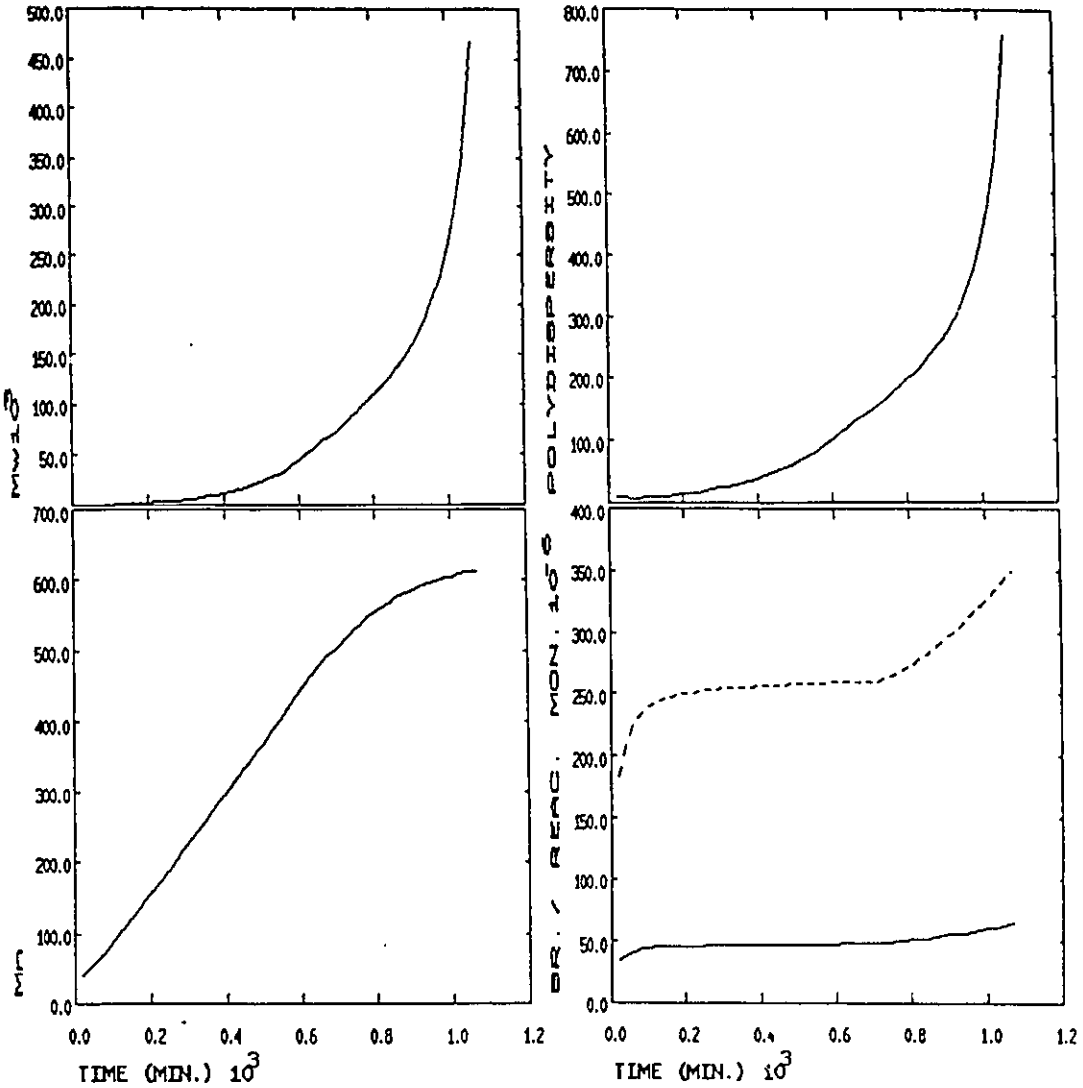

FIGURE 9.2: Simulated Policy 0
(a) M_s (-) & M_b (--) conversion; (b) $\overline{F_s}$; (c) % solids;
(d) F_{M_s} (-) & F_{M_b} (--); (e) $\overline{M_{W_W}}$; (f) $\overline{M_{W_N}}$;
(g) $\overline{\rho}$; (h) $\overline{Br}$ (-) & $\overline{X_L}$ (--)

9.3.2 Copolymer Composition Control: Policy I

Broadhead (1984) and Broadhead et al. (1985) proposed a composition control policy whereby all the slower reacting monomer (styrene) is charged to the reactor at the start along with some of the faster reacting monomer (butadiene) in the correct ratio needed to obtain the desired F_i at t=0. The feed rate of butadiene is determined so that $[M_a]_p/[M_b]_p$, and hence copolymer composition is fixed with time. This method of copolymer composition control was referred to as Policy I. Policy I is just a special case of Policy 0 with F_{M_i} set to zero, and therefore (9.13) or (9.19) may be used to obtain F_{M_b} when applying Policy I. In the work of Broadhead (1984) and Broadhead et al. (1985) a simplifying assumption was made that the amount of monomer in the water phase is negligible and no monomer droplet phase exists. These assumptions were found to introduce some error in the computation of F_{M_b} and therefore the use of (9.13) or (9.19) where these simplifying assumptions are not made is recommended.

Figure 9.3 shows a simulated application of Policy I. In the simulation, 12.5 gmol of styrene and 47.5 gmol of butadiene were added to obtain the desired initial monomer ratio. All the CTA (0.115 gmol) was charged initially. The fixed instantaneous (and cumulative) copolymer composition is shown in Figure 9.3(b) and the required butadiene flow rate is shown in Figure 9.3(d). Information on other properties and conditions are also provided. Relative to Figure 9.2, very different copolymer properties are obtained.

Although Policy I is useful as far as copolymer composition control is concerned, it posses some inherent problems as far as reactor operation is concerned. The first problem is that a large quantity of monomer is initially charged to the reactor. If error is made concerning the reactor operating conditions the potential exists for producing a significant quantity of off specification polymer before an appropriate corrective action can be taken. If the error is serious enough, the batch may have to be terminated and necessitate a costly waste of raw materials or recovery procedures. The second problem with the policy is that the initial high level of monomer concentration would require a high heat removal rate that might not be possible to maintain and lead to a reactor runaway. Finally, by charging a large quantity of monomer at the beginning, the reactor operating conditions will more closely resemble true batch conditions where conditions within the reactor can change significantly with time. The consequence of this is important when one would like to indirectly influence other copolymer properties while making constant composition copolymer. Although there are problems with applying Policy I through the semi-batch run, it is still very useful when applied as a finishing

off stage after the application of a different composition control policy once the maximum amount of the slower reacting monomer as been added because of the reactor volume constraint. This procedure was taken in the example shown in Figure 9.2 where Policy 0 was initially applied.

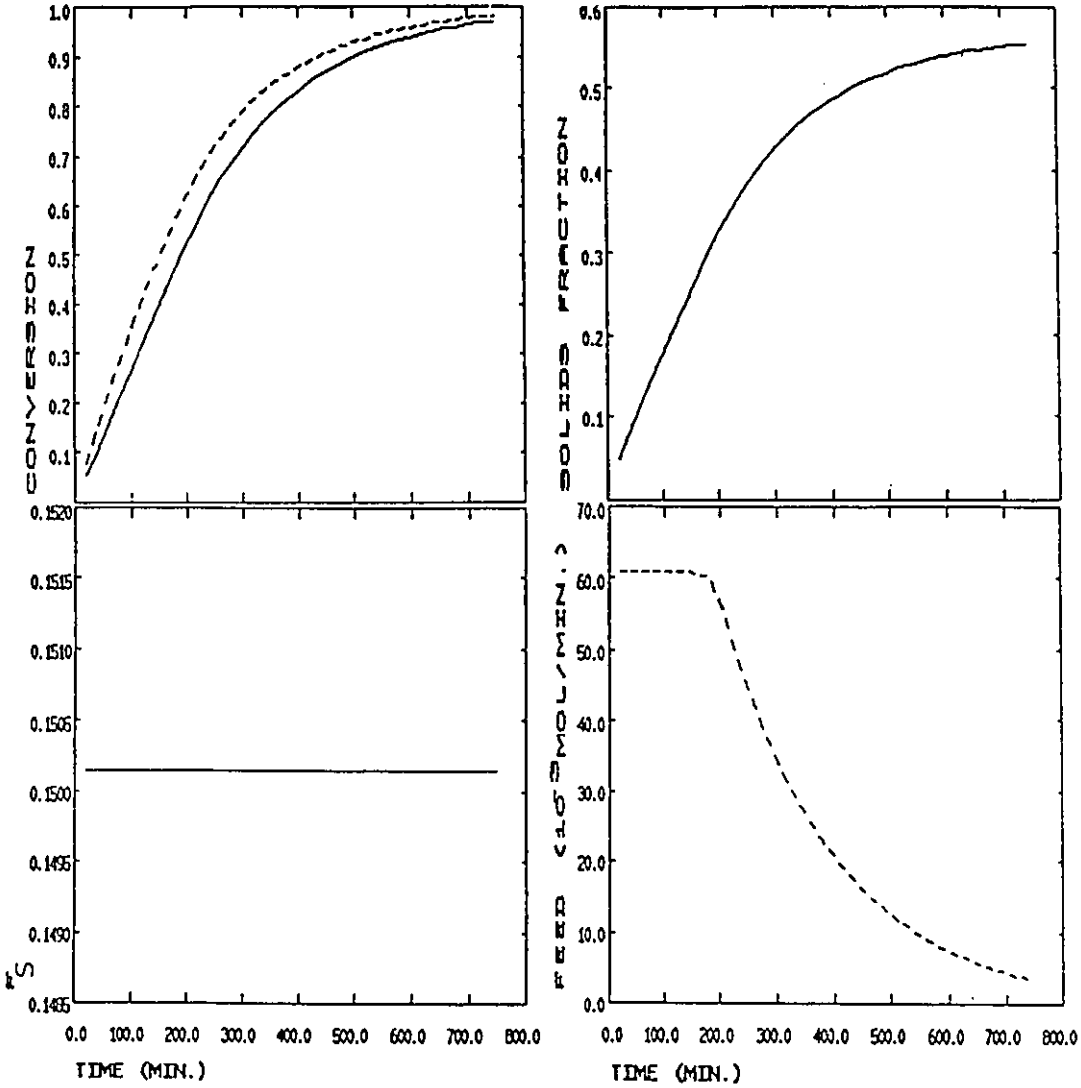
CONVERSION
SOLIDS FRACTION
FS
FEED (LBS MOL/MIN.)
TIME (MIN.)
TIME (MIN.)

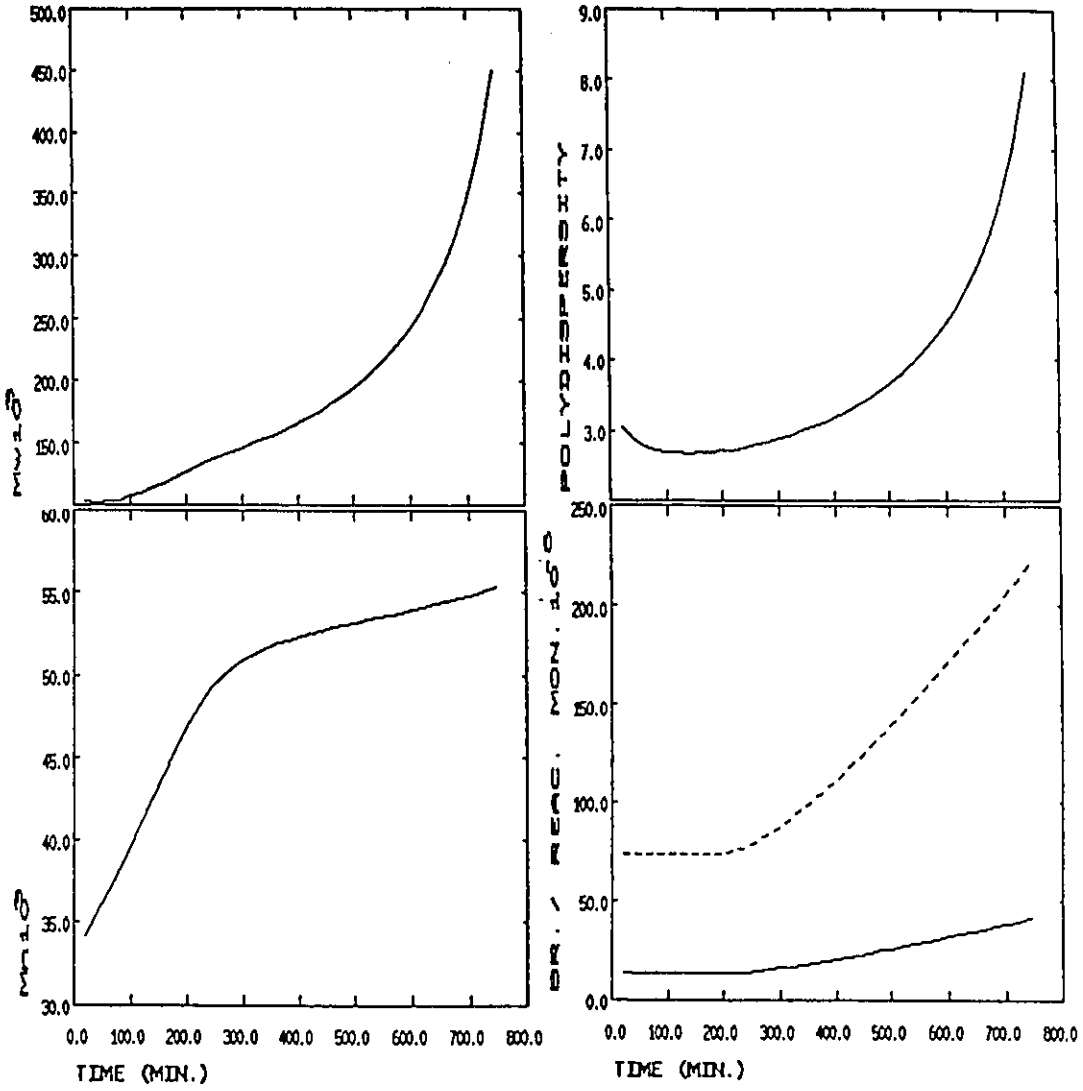

FIGURE 9.3: Simulated Policy I
(a) M_s (-) & M_b (--) conversion; (b) $\overline{F_r}$; (c) % solids;
(d) F_{M_s} (-) & F_{M_b} (--); (e) $\overline{M_{w_w}}$; (f) $\overline{M_{w_N}}$;
(g) $\overline{\rho}$; (h) $\overline{Br}$ (-) & $\overline{X_L}$ (--)

9.3.3 Copolymer Composition Control: Policy II

In section 9.3.1 it was shown that the condition for producing copolymer with constant composition can be satisfied indirectly by maintaining fixed $[M_a]_p/[M_b]_p$ with time. One way of ensuring this is to specify that both $[M_a]_p$ and $[M_b]_p$ remain constant with time. From the point of view of instantaneous property control this would correspond to the selection of $p_i^T = ([M_a]_p, [M_b]_p)$. Broadhead (1984) and Broadhead et al. (1985) proposed a solution for the necessary monomer feed rates to maintain constant $[M_a]_p$ and $[M_b]_p$. The policy that was derived was referred to as Policy II. In their work, the assumption was made that the amount of monomer in the water phase is negligible and that no monomer droplet phase exists. The results to follow will relax these assumptions.

The necessary conditions that must be maintained when applying policy II are given by

$$\frac{d[M_a]_p}{dt} = 0 \tag{9.21}$$

and

$$\frac{d[M_b]_p}{dt} = 0 \tag{9.22}$$

where expressions for $[M_a]_p$ and $[M_a]_p$ are given by (9.17) and (9.18) respectively. Substituting (9.17) and (9.18) into (9.21) and (9.22) respectively and solving for F_{M_a} and F_{M_b} leads to

$$F_{M_a} = R_{pa}V_p + \left[\alpha_a + M_a\frac{\partial\alpha_a}{\partial M_a} - \left(M_a\frac{\partial\alpha_a}{\partial M_b}\right)\left(\alpha_b + M_b\frac{\partial\alpha_b}{\partial M_b}\right)^{-1}\left(M_b\frac{\partial\alpha_b}{\partial M_a}\right)\right]^{-1} \left[\left(M_a\frac{\partial\alpha_a}{\partial M_b}\right)\left(\alpha_b + M_b\frac{\partial\alpha_b}{\partial M_b}\right)^{-1}M_b\beta_b - M_a\beta_a\right] \tag{9.23}$$

$$F_{M_b} = R_{pb}V_p - \left[M_a\frac{\partial\alpha_a}{\partial M_b}\right]^{-1}\left[\left(\alpha_a + M_a\frac{\partial\alpha_a}{\partial M_a}\right)\left(F_{M_a} - R_{pa}V_p\right) + M_a\beta_a\right] \tag{9.24}$$

with

$$\beta_a = \frac{\partial\alpha_a}{\partial P_a}R_{pa}V_p + \frac{\partial\alpha_a}{\partial P_b}R_{pb}V_p + \frac{\partial\alpha_a}{\partial V_w}F_{V_w} \tag{9.25}$$

$$\beta_b = \frac{\partial\alpha_b}{\partial P_a}R_{pa}V_p + \frac{\partial\alpha_b}{\partial P_b}R_{pb}V_p + \frac{\partial\alpha_b}{\partial V_w}F_{V_w} \tag{9.26}$$

$$\alpha_a = \frac{1}{V_m K_{amp} + V_w K_{amp} + V_p} \tag{9.27}$$

$$\alpha_b = \frac{1}{V_m K_{bmp} + V_w K_{bwp} + V_p} \tag{9.28}$$

The advantage of Policy II over Policy I and 0 is that the former maintains a steady state condition within the polymer particle with respect to monomer and polymer concentration. By maintaining this quasi steady state condition it is possible that other properties other than copolymer composition may also be kept constant, as shall be shown in section 9.5. Another advantage of policy II is that by feeding in both monomers heat transfer limitations can be met by placing an upper bound on $[M]_p$. Finally by introducing less raw material into reactor to start, we are less susceptible to producing a high percentage of off specification polymer during the initial period of operation when sufficient measurement information to apply feedback action is not available.

Although Policy II is a very useful approach to copolymer composition control, the disadvantage with it is that the instantaneous properties to be controlled, $[M_a]_p$ and $[M_b]_p$, are not observable from the measurements, as has been discussed in section 9.3.1. The consequence of this may be a bias in the observed copolymer composition from one might expect for the estimated $[M_a]_p$ and $[M_b]_p$. As stated before, accommodation with have to be made to the feedforward open-loop monomer flow rates through application of feedback control on the observable F_a estimate.

Figure 9.4 shows a simulated application of Policy II. The reactor was initially charged with $M_a = 0.114 \ \ gmol$, $M_b = 0.45 \ \ gmol$, and $CTA = 0.003 \ \ gmol$. Figure 9.4(b) shows that both the instantaneous and cumulative composition is maintained at about 15%. The feed rates of F_{M_b} and F_{M_a} are shown in Figure 9.4(d). It can be observed that both feeds are approximately constant when Policy II is applied. When the maximum amount of styrene was fed, as determined by the reactor volume constraint, Policy II was terminated, and the reactor operation was finished off with Policy I.

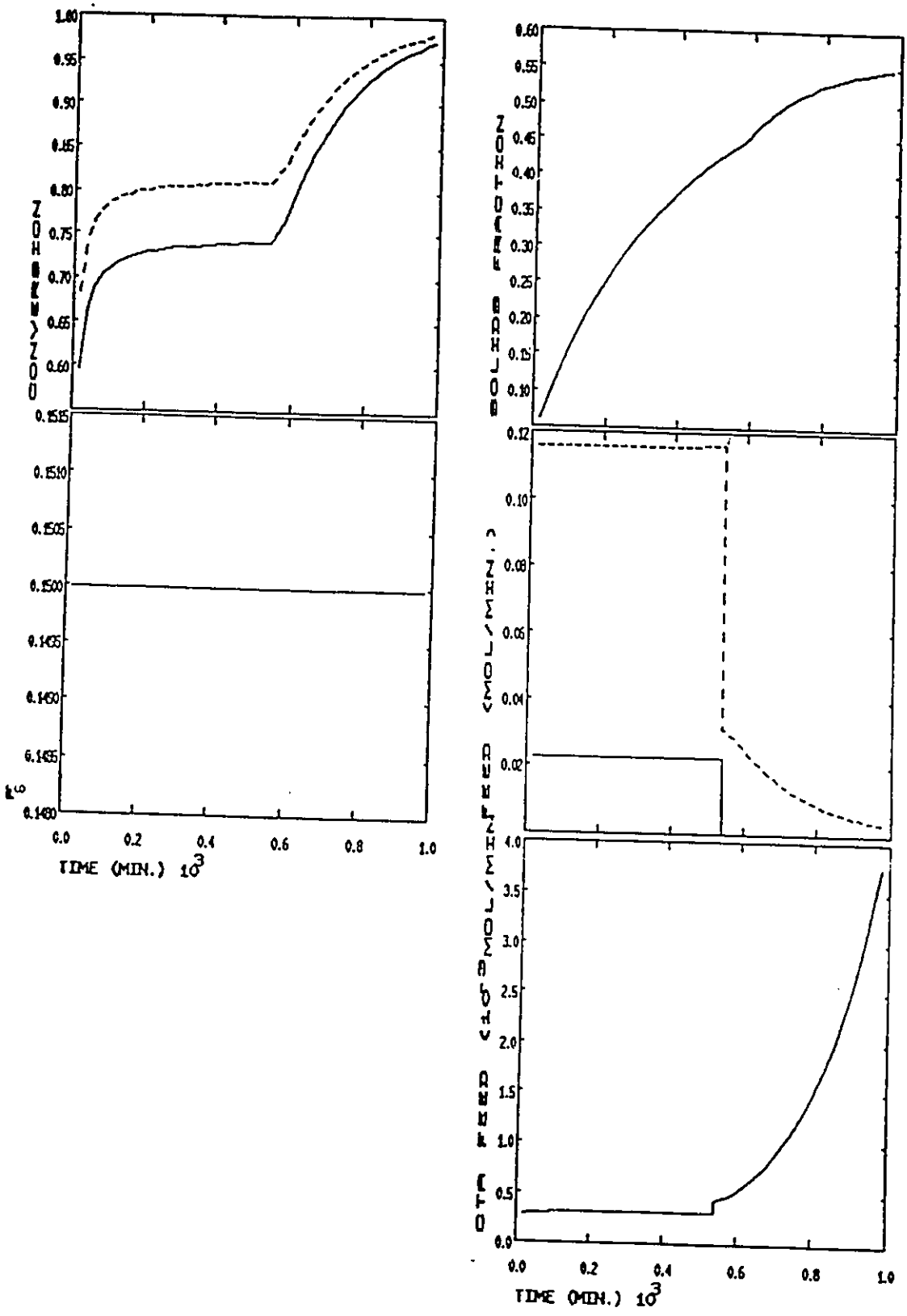
ZONE(M)/ZOO
TIME (MIN.) 10^3
SOLIDS FRACTION
TIME (MIN.) 10^3

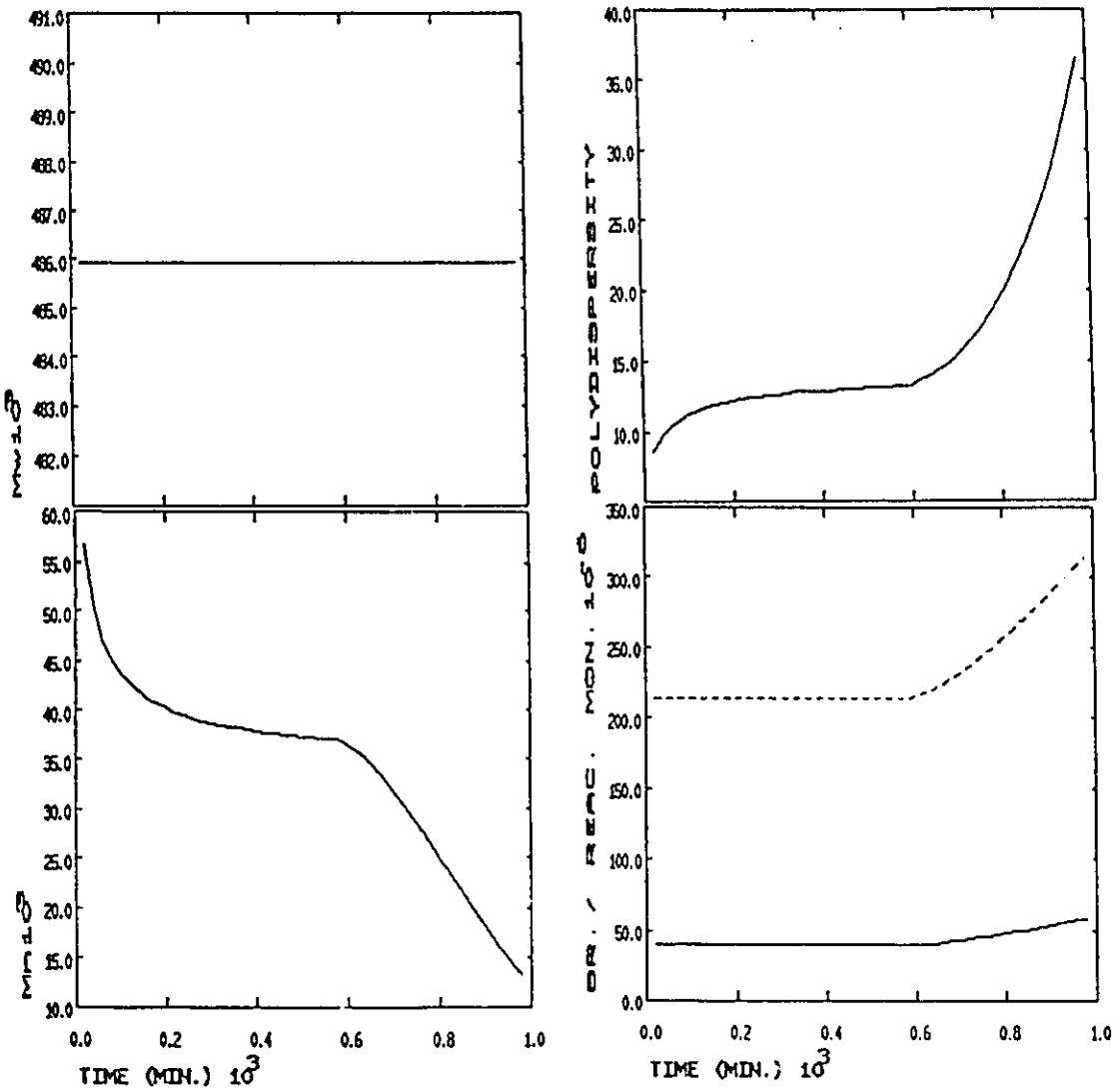

FIGURE 9.4: Simulated Policy II With r_W Control
(a) M_a (-) & M_b (--) conversion; (b) $\overline{F_s}$; (c) % solids;
(d) F_{M_a} (-) & F_{M_b} (--); (e) F_{CTA}; (f) $\overline{M_{W_W}}$;
(g) $\overline{M_{W_N}}$; (h) $\overline{\rho}$; (i) $\overline{Br}$ (-) & $\overline{X_L}$ (--)

9.4 CONVERSION CONTROL: POLICY X

In section 9.3.3 it was stated that the advantage of Policy II compared to Policy I was that some steady state operating condition was maintained at all time within the polymer particle. By maintaining some fixed condition indirect control over other copolymer properties might be achieved. An alternative to maintaining fixed monomer concentration within the particle would be to chose $p_i = X$, where X, the over conversion level in the reactor, is given by

$$X = \frac{P_a + P_b}{M_a + M_b + P_a + P_b} \tag{9.29}$$

A big advantage when using X as opposed to policies based on maintaining fixed monomer concentration conditions within the polymer particles is that X is observable when the state estimator is applied on-line (provided that $R_{pb}V_p = x^{15}[M_b]_p \Phi_b \bar{n} N_p V_b / N_A$ is used in the estimator). Therefore the progress of a policy based on X can be monitored on-line and errors due deviations from ideal conditions may be compensated for.

The required condition to be satisfied to maintain overall conversion at $X(t = 0)$ is given by

$$\frac{dX}{dt} = 0 \tag{9.30}$$

It is trivial to show that (9.30) will be satisfied when

$$F_{M_a} = \frac{R_{pa}V_p + R_{pb}V_p}{X} - F_{M_b} \tag{9.31}$$

This expression shows that X may be controlled using either one or both monomer feed rates. Alternatively, reactor temperature may be used if the monomer flow rates are used for the control of other properties or conditions. The temperature trajectory is determined so that (9.31) is satisfied at all time. The use of temperature to control conversion would be expected to be less effective than using monomer flow rate since perfect temperature control along some trajectory can only be approximated in practice. In some copolymer systems initiator feed rate might be considered for maintaining condition (9.31). However, since seeded SBR follows case II emulsion polymerization kinetics, the level of initiator in the reactor theoretically has no effect on conversion unless high impurity levels exist or a strong gel effect is encountered.

A useful policy for the production of copolymer would be obtained through $p^T = (F_a, X)$, where (9.13) and (9.31) are used to obtain F_{M_a} and F_{M_b}. In this work, the policy is referred to as Policy X. A simulated application of Policy X is shown in Figure 9.5. The reactor was initially charged with 0.114 gmol M_a, 0.45

gmol M_b, and 0.003 gmol CTA. In Figure 9.5(b) overall conversion (seeds included) can be observed to be maintained just below 80%, while Figure 9.5(c) shows the fixed cumulative and instantaneous composition at 15 mole percent styrene. The required feed rates for F_{M_a} and F_{M_b} are shown in Figure 9.5(c).

At first glance it would appear that Policy X might be equivalent to Policy II under conditions where $V_m = 0$. If we assume absence of the monomer droplet phase and apply Policy II it can be shown that

$$X = \frac{(V_w K_{awp} + V_p)[M_a]_{P_0} + (V_w K_{bwp} + V_p)[M_b]_{P_0}}{(V_w K_{awp} + V_p)[M_a]_{P_0} + (V_w K_{bwp} + V_p)[M_b]_{P_0} + [P]_{P_0} V_p} \tag{9.32}$$

where

$$[P]_{P_0} = P_a + P_b \tag{9.33}$$

In (9.32) $[M_a]_{P_0}$, $[M_b]_{P_0}$, and $[P]_{P_0}$ are constant due to the conditions required for the application of policy II.

A close examination of (9.32) will show that the application of Policy II will lead to constant X only when both K_{awp} and K_{bwp} are equal to zero (both monomers completely water insoluble). In many emulsion systems, and particularly with SBR, $V_w K_{awp}$ and $V_w K_{bwp}$ will usually be small relative to V_p. Therefore the application of Policy X should closely approximate the conditions for Policy II. Note that the approximation error will be largest at t=0 where V_p has its lowest value. The importance of this result is that, unlike Policy II, the conditions that must be maintained constant can be observed on-line with the state estimator. Therefore there are practical advantages for approximating Policy II with Policy X.

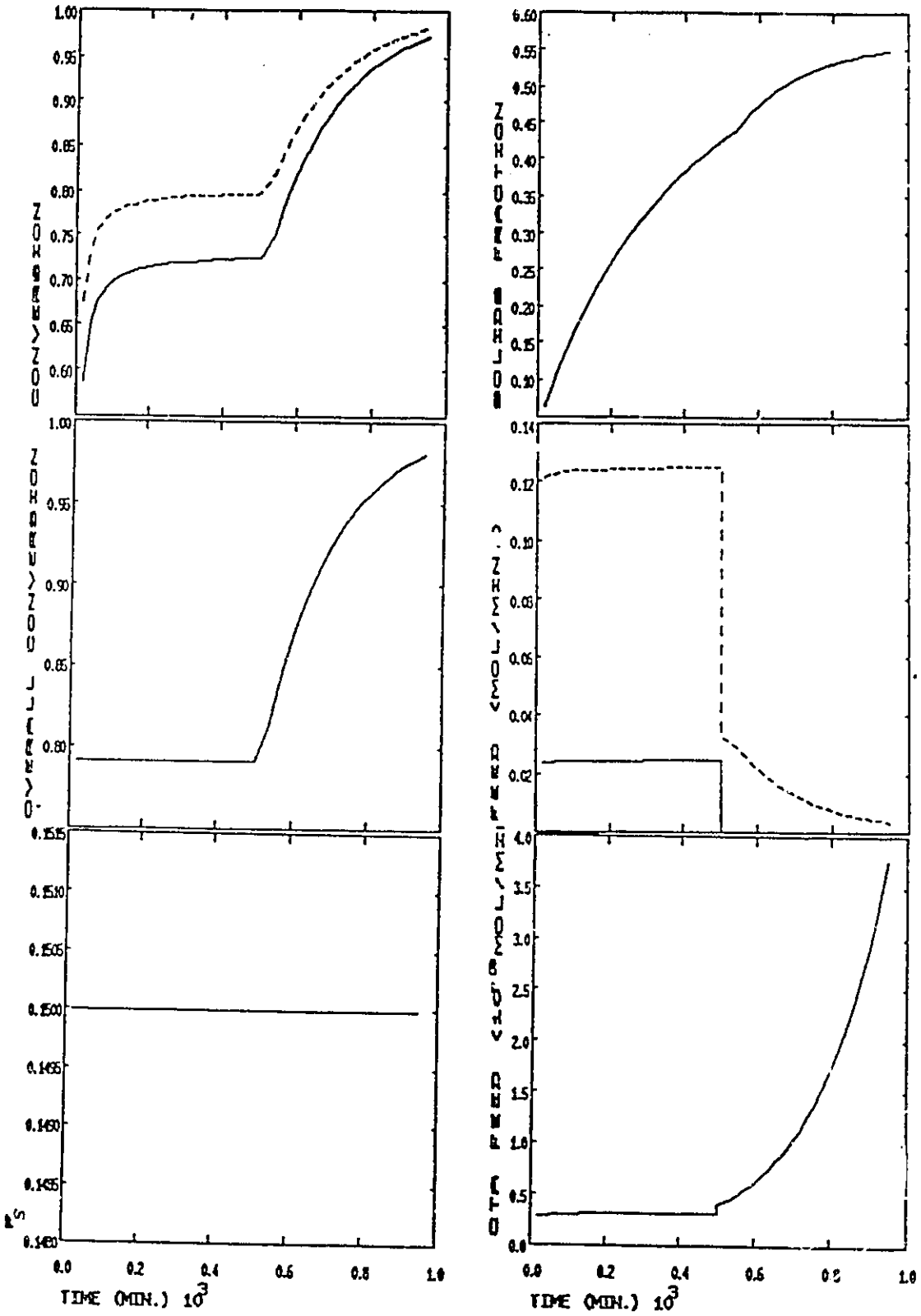
TIME (MIN.) 10^3
TIME (MIN.) 10^3

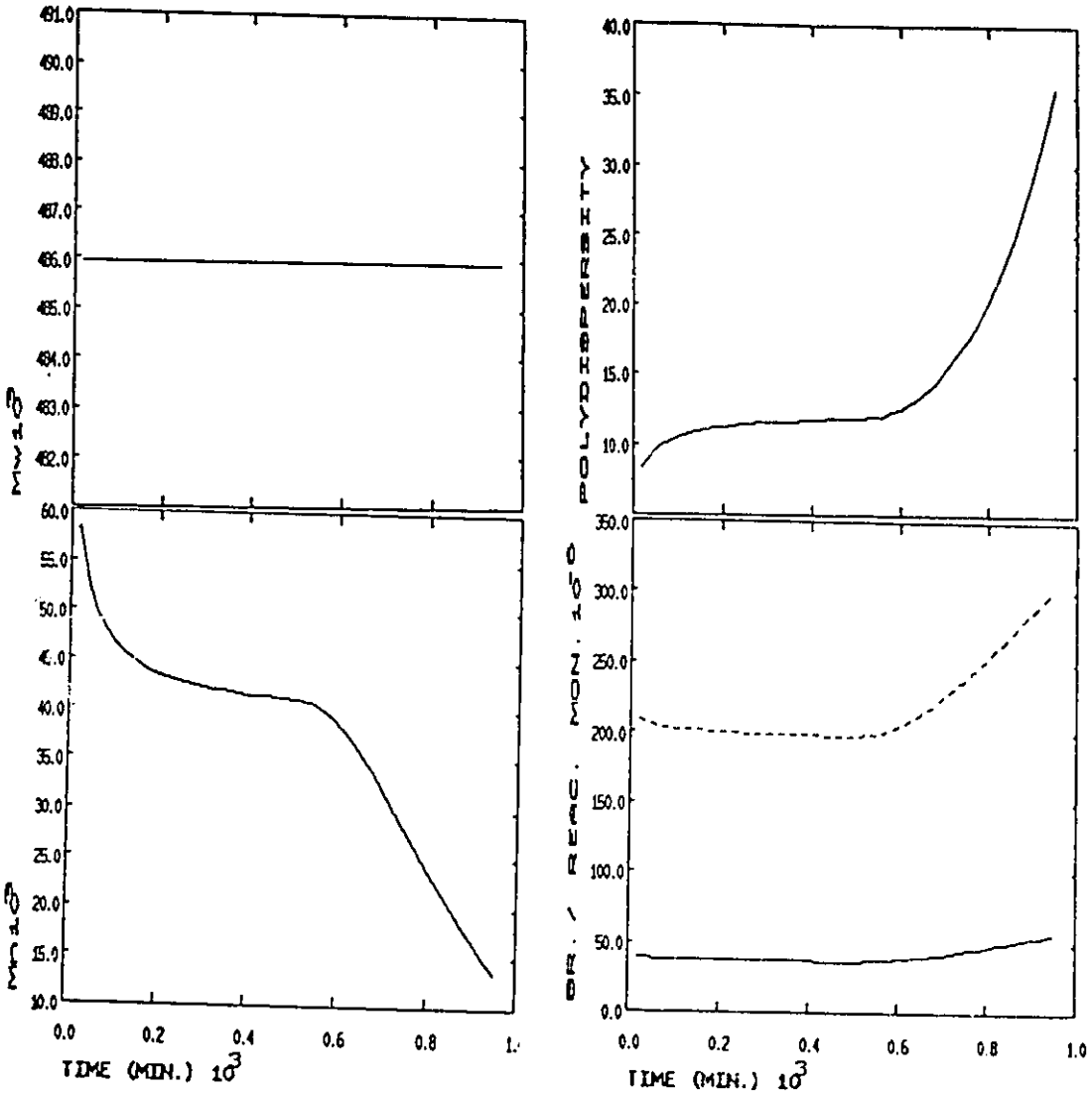

FIGURE 9.5: Simulated Policy X
(a) M_a (-) & M_b (--) conversion; (b) X (seeds included); (c) $\overline{F_s}$; (d) % solids;
(e) F_{M_a} (-) & F_{M_b} (--); (f) F_{CTA}; (f) $\overline{M_{w_w}}$;
(h) $\overline{M_{w_N}}$; (i) $\overline{\rho}$; (j) $\overline{Br}$ (-) & $\overline{X_L}$ (--)

9.5 CONTROL OF BRANCHING AND CROSSLINKING

The degree of branching and crosslinking affects important copolymer properties such as, modulus, elongation, and swell. An industrial relevant (Taylor, 1988) specification for the degree of branching and crosslinking would be given by the number of branches and crosslinks per reacted monomer units or carbons. Hence, in this work, the cumulative degree of branching is defined as

$$\overline{Br} = \frac{V_p Q_0 Bn_3}{V_p Q_1} = \frac{Total \quad Branches}{Total \quad Reacted \quad Monomer \quad Units} \tag{9.34}$$

and the cumulative degree of crosslinking as

$$\overline{X}_L = \frac{V_p Q_0 Bn_4}{V_p Q_1} = \frac{Total \quad Crosslinks}{Total \quad Reacted \quad Monomer \quad Units} \tag{9.35}$$

Similarly, instantaneous degree of branching can be defined as

$$Br = \frac{d(V_p Q_0 Bn_3)/dt}{d(V_p Q_1)/dt} \tag{9.36}$$

and the instantaneous degree of crosslinking as

$$X_L = \frac{d(V_p Q_0 Bn_4)/dt}{d(V_p Q_1)/dt} \tag{9.37}$$

The production of copolymer with a specified degree of branching or crosslinking can be obtained by maintaining conditions for fixed Br or X_L. Therefore, the objective is to establish the necessary conditions for maintaining fixed instantaneous branching (Br) and crosslinking (X_L).

If one inserts the expressions for $d(V_p Q_0 Bn_3)/dt$, $d(V_p Q_0 Bn_4)/dt$, and $d(V_p Q_1)/dt$ (refer to section 7.8) into (9.36) and (9.37) one obtains

$$Br = \frac{C_p^{\bullet} Q_1}{[M]_p} \tag{9.38}$$

$$X_L = \frac{C_p^{\bullet\bullet} Q_1}{[M]_p} \tag{9.39}$$

where the expressions for $C_p^{\bullet}$ and $C_p^{\bullet\bullet}$ are given by (7.46) and (7.48) respectively. If the assumption is made that an isothermal composition control policy will be applied and that the cumulative copolymer composition

of the seeds is at the desired instantaneous level it can be shown that both C_p^* and C_p^{**} remain fixed with time. Therefore, a policy that maintains a fixed degree of branching and crosslinking is one where $Q_1/[M]_p$ is fixed with time. Given that

$$Q_1 = \frac{(P_a + P_b)}{V_p} = [P]_p \tag{9.40}$$

the necessary condition to maintain fixed $Q_1/[M]_p$ is that $[M]_p$ remain constant. Since copolymer composition control is being applied $[M_a]_p$ and $[M_b]_p$ will also have to be constant, and therefore, according to the discussion in section 9.3.3, indicates that the control of branching and crosslinking together with copolymer composition is achieved through the application of Policy II.

A simulated application of copolymer Policy II followed by Policy I was previously shown in Figure 9.4. Figure 9.4(i) shows $\overline{Br}$ and $\overline{X}_L$ with time. As expected, during the phase where Policy II was applied, constant $\overline{Br}$ and $\overline{X}_L$ can be observed. A drift in the degree of branching and crosslinking can be observed when Policy II is terminated and replaced with Policy I as a result of the reactor volume constraint. If the subsequent drift in the degree of branching and crosslinking cannot be tolerated, the reaction must terminated when Policy II can no longer be applied. Such action may necessitate a subsequent monomer stripping procedure to eliminate residual monomer.

In section 9.4 it was suggested that Policy II be approximated by Policy X due to the advantage offered by the latter approach when applied on-line. Although Policy X, in general, does not maintain constant $[M_a]_p$ and $[M_a]_p$ with time, these conditions should be closely approximated, and therefore some control over branching and crosslinking should be exercised. The results from a simulated application of Policy X has already been shown in Figure 9.5. Figure 9.5(j) shows the cumulative degree of branching and crosslinking with time. During the period where Policy X was applied only a very a slight drift in $\overline{Br}$ and $\overline{X}_L$ can be observed, showing that the Policy X approximation does not introduce serious error.

If the previously assumed conditions are not valid, it can be shown that the general condition to be satisfied for constant crosslinking (fixed (9.39)) will be provided by

$$F_{M_a} = P_{pa}V_p - \left(\frac{\partial X_L}{\partial M_a}\right)^{-1}\left[\left(\frac{\partial X_L}{\partial M_b}\right)\left(F_{M_b} - R_{pb}V_p\right) + \left(\frac{\partial X_L}{\partial P_a}\right)P_{pa}V_p + \left(\frac{\partial X_L}{\partial P_b}\right)R_{pb}V_p + \left(\frac{\partial X_L}{\partial V_w}\right)F_{V_w} + \left(\frac{\partial X_L}{\partial T}\right)\frac{dT}{dt}\right] \tag{9.41}$$

Condition (9.41) may be satisfied through the use of monomer flow rate or alternatively, through a reactor temperature trajectory. The application of (9.41) will require that the cumulative butadiene copolymer composition in the seeds not be equal to zero (styrene seeds not permitted) since in this situation at t=0 it

impossible to form any crosslinks. It styrene seeds are to be used, condition (9.41) should only be applied once the cumulative degree crosslinking has reached its desired level. The same procedure used above can also be applied for controlling the degree of branching.

9.6 TIME OPTIMAL SEMI-BATCH POLICY

Sometimes the production of copolymer in the minimum amount of time would be the economical choice. Intuitively, a time optimal policy would be one where the monomer concentration in the polymer particles is set to its maximum and the temperature of the reactor is set to its highest acceptable level. This would provide the necessary condition for the highest rate of polymerization. In other polymer systems, the level of initiator in the reactor might also be considered to obtain time optimality. However, in a seeded SBR latex polymerization, initiator theoretically has no effect on the rate of polymerization under ideal operating conditions. Based on the discussion above, an operating policy such as Policy I or Policy 0 with particles maintained at maximum swelling, will provide the necessary conditions for time optimality since the amount of monomer in the reactor will always be at a maximum. Unfortunately, the high rate of reaction obtained when applying such a policies will demand high heat removal rates that may not be provided by the reactor cooling system. Therefore, unless the maximum possible monomer concentration within the particles can be maintained without reactor runaway, a time optimal policy will be one where the reactor is operated at its maximum cooling capacity.

By carrying out a heat balance on the reactor at some steady operating condition, the condition for time optimal copolymer production subject to the heat transfer constraint can be determined. The time optimal condition is given by

$$(F_{M_a}Cp_a + F_{M_b}Cp_b + F_{V_w}d_wCp_w)(T_{set} - T_{in}) \;=\; R_{pa}(-\Delta H_{pa})V_p \;+\; R_{pb}(-\Delta H_{pb})V_p \;-\; UA_j(T_{set} - T_{j,\min}) \;-\; Q_R \qquad (9.42)$$

where $T_{j,\min}$ is the lowest possible temperature for the coolant fed to the reactor. At isothermal conditions, time optimality may be maintained through the monomer flow rates according to (9.42) ($p_i = T$). Since two monomer flow rates are available, a copolymer property such as composition (9.13) may also be combined with the time optimal policy. Alternatively, if both F_{M_a} and F_{M_b} are needed to control other properties or conditions, reactor set point (T_{set}) may be used. The maximum reactor operating set point is determined so

that (9.42) is satisfied. In practice, the use of reactor set point will only provide an approximate solution since perfect reactor temperature is not possible, especially when working with large reactors having large volume to heat transfer surface ratios. The use of a temperature time optimal policy would be useful to apply during a Policy I finishing off stage where the polymerization rate can be very low due to the high level of conversion.

9.7 MOLECULAR WEIGHT PROPERTY CONTROL

Molecular weight and molecular weight distribution affects important end-use copolymer properties such as viscosity, elasticity, strength, tack, toughness, and solvent resistance for example. In this section we consider policies for controlling both a single and a trade-off between different molecular weight properties. The optimal molecular weight property or properties to be controlled will depend on the SBR end-use, and should be determined from experience or through laboratory studies.

9.7.1 Control Of A Single Molecular Weight Property

In some situations it may be sufficient to obtain the desired molecular weight properties through the control of one molecular weight property. Common molecular weight properties that one may be interested in controlling are listed below:

Number Average Molecular Weight

$$\overline{M_{W_N}} = \left(M_{W_a}\overline{F_a} + M_{W_b}\overline{F_b}\right)\frac{Q_1}{Q_2} \tag{9.43}$$

Weight Average Molecular Weight

$$\overline{M_{W_W}} = \left(M_{W_a}\overline{F_a} + M_{W_b}\overline{F_b}\right)\frac{Q_2}{Q_1} \tag{9.44}$$

Polydispersity

$$\overline{\rho} = \frac{\overline{M_{W_W}}}{\overline{M_{W_N}}} \tag{9.45}$$

Other possibilities such as viscosity average molecular weight, or higher moment molecular weight averages might also be considered. To provide control at all times over any one of the above cumulative molecular

weight properties, it is necessary to maintain operating conditions whereby their respective instantaneous molecular weight property is constant at all times. The instantaneous molecular weight properties corresponding to the cumulative ones above are listed below:

Instantaneous Number Average Molecular Weight

$$M_{W_N} = \left(F_a M_{W_a} + F_b M_{W_b}\right) r_N \tag{9.46}$$

Instantaneous Weight Average Molecular Weight

$$M_{W_W} = \left(F_a M_{W_a} + F_b M_{W_b}\right) r_W \tag{9.47}$$

Instantaneous Polydispersity

$$\rho = \frac{r_W}{r_N} \tag{9.48}$$

where

$$r_N = \left(\frac{C_t[CTA]_p}{[M]_p} + C_m + \frac{C_{Im_p}[Im_p]_p}{[M]_p} - \frac{C_p^{**}Q_1}{[M]_p}\right)^{-1} \tag{9.49}$$

$$r_W = \frac{2\left(1+\frac{C_p^{**}Q_2}{[M]_p}\right)\left(1+\frac{C_t[CTA]_p}{[M]_p}+C_m+\frac{C_p^{*}Q_2}{[M]_p}+\frac{C_p^{**}Q_2}{[M]_p}\right)}{\left(\frac{C_t[CTA]_p}{[M]_p}+C_m+\frac{C_p^{*}Q_1}{[M]_p}+\frac{C_{Im_p}[Im_p]_p}{[M]_p}\right)} \tag{9.50}$$

In (9.49) and (9.50), r_N and r_W refer to the number and weight average copolymer chain lengths respectively.

Suppose one were interested in maintaining control over weight average molecular weight. Such a policy would be useful if one were interested in producing a copolymer with a low gel content. The assumption shall be made that a copolymer composition control policy will be applied. The necessary conditions for constant M_{W_W} will be provided by choosing $p_i = r_W$, and requires at all time that

$$\frac{dr_W}{dt} = 0 \tag{9.51}$$

The molecular weight properties of SBR are strongly influenced by radical chain transfer to modifier. Hence a suitable manipulated input for controlling molecular weight properties would be the feed rate of *CTA* given by F_{CTA}. The optimal F_{CTA} trajectory for r_W control can be obtained by inserting (9.50) into (9.51), differentiating, and applying the chain rule. The optimum F_{CTA} is given by

$$F_{CTA} = R_{CTA}V_p - \left(\frac{\partial r_W}{\partial CTA}\right)^{-1}\Gamma_W \tag{9.52}$$

where

$$\Gamma_W = \frac{\partial r_W}{\partial M_a}\left(F_{M_a} - R_{pa}V_p\right) + \frac{\partial r_W}{\partial M_b}\left(F_{M_b} - R_{pb}V_p\right) + \frac{\partial r_W}{\partial P_a}R_{pa}V_p + \frac{\partial r_W}{\partial P_b}R_{pb}V_p +$$

$$\frac{\partial r_W}{\partial Im_p}\frac{dIm_p}{dt} + \frac{\partial r_W}{\partial V_W}F_{V_W} + \frac{\partial r_W}{\partial V_pQ_1}\frac{dV_pQ_1}{dt} + \frac{\partial r_W}{\partial V_pQ_2}\frac{dV_pQ_2}{dt} + \frac{\partial r_W}{\partial T}\frac{dT}{dt} \qquad (9.53)$$

$$R_{CTA}V_p = k_{fCTA}[CTA]_p\frac{\overline{n}N_pV_w}{N_A} \qquad (9.54)$$

Alternatively, one may attempt to follow a temperature trajectory such that r_W remains constant. A big advantage of F_{CTA} over temperature or monomer flow rate to control r_W is that the control of molecular weight properties with flow rate of modifier is completely decoupled from the other properties or conditions that have been considered. This feature can lead to simplification when feedback control is to be applied.

Figure 9.4 showed a simulated application of Policy II followed by Policy I. In the run shown r_W was also controlled using F_{CTA}. In Figure 9.4(f) constant cumulative weight average molecular weight can be observed. The computed *CTA* feed rate is shown in Figure 9.4(e). The effect of this policy on $\overline{\rho}$ and $\overline{M_{W_N}}$ can be seen in Figures 9.4(h) and 9.4(g) respectively. As the computed F_{M_a} and F_{M_b} shown in Figure 9.4(d), the flow for F_{CTA} is almost constant with time during the application of Policy II. This implies that of one does not plan to apply feedback control the monomer feeds and modifier may be premixed in the appropriate flow rate ratios. An r_W control policy was also used in the simulation previously shown in Figure 9.5 with Policy X ($p^T = (X, F_s, r_W)$, $u^T = (F_{M_a}, F_{M_b}, F_{CTA})$) followed by Policy I ($p^T = (F_s, r_W)$, $u^T = (F_{M_b}, F_{CTA})$). Since the same initial conditions exist in both Figures 9.4 and 9.5, almost identical molecular weight properties can be observed.

Instead of controlling weight average molecular one may choose to control the number average molecular weight. This choice would be appropriate if one were producing a highly gelled SBR copolymer such as used for coating applications, where theoretically, r_W is infinite. Again, assuming a constant composition control policy will be applied and F_{CTA} will be used for control, it can be shown that the necessary condition to maintain

$$\frac{dr_N}{dt} = 0 \qquad (9.55)$$

is given by

$$F_{CTA} = R_{CTA}V_p - \left(\frac{\partial r_W}{\partial CTA}\right)^{-1}\Gamma_N \qquad (9.56)$$

with

$$\Gamma_N = \frac{\partial r_N}{\partial M_a}\left(F_{M_a} - R_{pa}V_p\right) + \frac{\partial r_N}{\partial M_b}\left(F_{M_b} - R_{pb}V_p\right) + \frac{\partial r_N}{\partial P_a}R_{pa}V_p + \frac{\partial r_N}{\partial P_b}R_{pb}V_p + \frac{\partial r_N}{\partial Im_p}\frac{dIm_p}{dt} + \frac{\partial r_N}{\partial V_W}F_{V_W} + \frac{\partial r_N}{\partial V_p Q_1}\frac{dV_p Q_1}{dt} + \frac{\partial r_N}{\partial T}\frac{dT}{dt} \qquad (9.57)$$

As was the case with r_W, following a temperature trajectory may also be possible for controlling r_N.

Figure 9.6 shows the application of Policy II followed by policy I with r_N control. The initial condition for this simulation is the same as for the simulation shown in Figure 9.4 where r_W control was applied instead of r_N. Comparing Figures 9.4 and 9.6, it can be observed that very different molecular weight properties are obtained. The constant cumulative number average molecular weight can be observed in Figure 9.6(g), and the required F_{CTA} is shown in Figure 6(e). Figure 9.6(f) shows that this Policy leads to infinite weight average molecular weight, and therefore indicates the production of a gelled copolymer. As with the Policy II/r_W case, this policy requires almost constant monomer and modifier feed rate. If no feedback control is expected, the feeds may be premixed in the correct ratios.

Polydispersity is influenced by the molecular weight distribution of the polymer chains and may have important implications on the end-use properties of SBR. It is known that the ease of processing of SBR is affected by its polydispersity. The polydispersity of SBR is very important when used to make pressure sensitive adhesives. In this case it is important to find the correct balance between the high molecular weight chains which provide long term strength and the short molecular chains that are needed for quick stick. Therefore, if one would like to control the molecular weight distribution and also produce a low gel copolymer (ρ is infinite at gel point) a constant instantaneous polydispersity policy may be of use. Taking the same assumptions as above, the necessary condition for controlling instantaneous polydispersity can be obtained from (9.51) to (9.54) with ρ replacing r_W everywhere it appears.

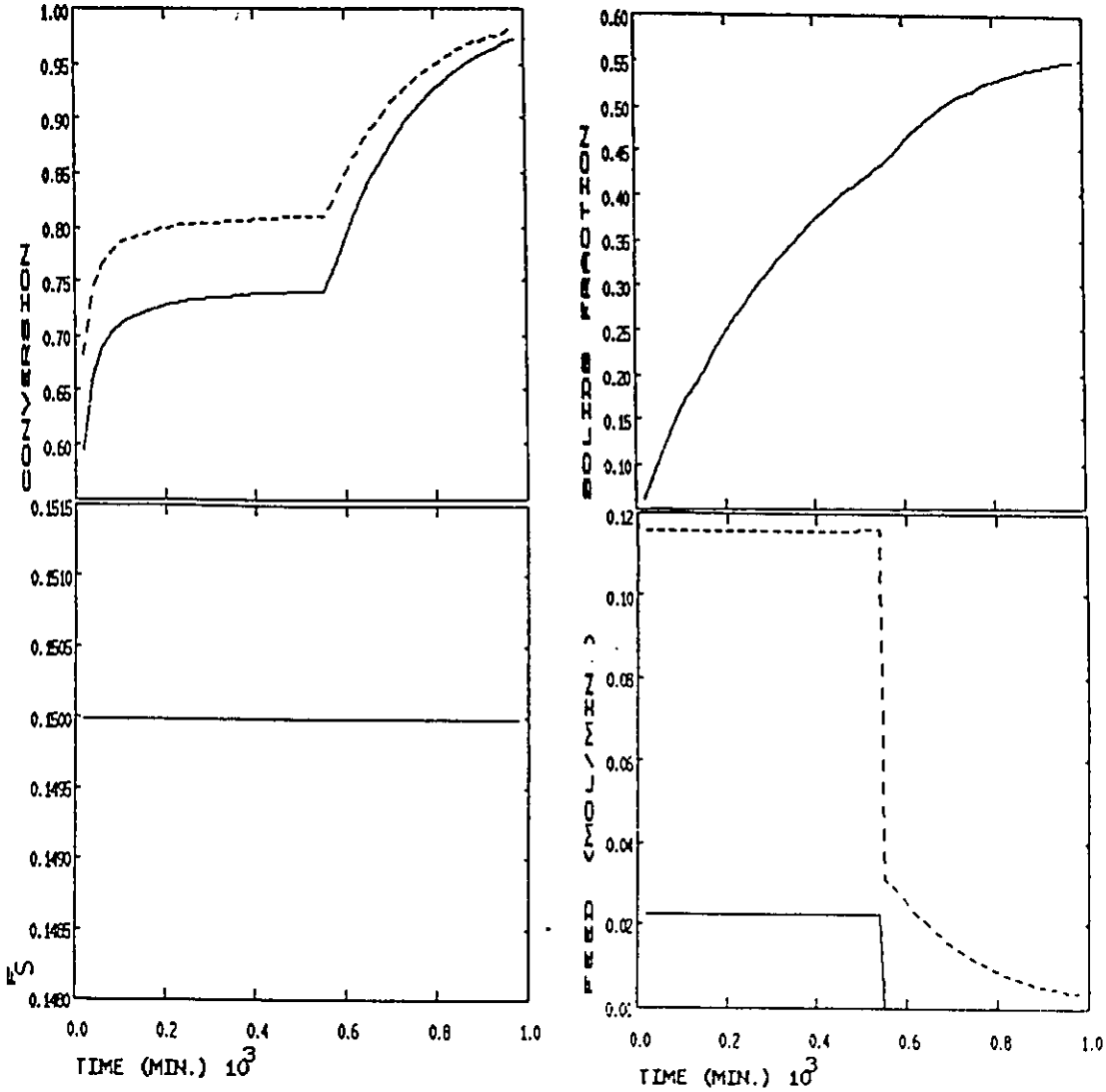
CONVERSION
1.00
0.95
0.90
0.85
0.80
0.75
0.70
0.65
0.60
FS
0.1515
0.1510
0.1505
0.1500
0.1495
0.1490
0.1485
0.1480
0.0
0.2
0.4
0.6
0.8
1.0
TIME (MIN.) 10^3
SOLKDB FRACTION
0.60
0.55
0.50
0.45
0.40
0.35
0.30
0.25
0.20
0.15
0.10
FEED (MOL/MIN.)
0.12
0.10
0.08
0.06
0.04
0.02
0.0
0.0
0.2
0.4
0.6
0.8
1.0
TIME (MIN.) 10^3

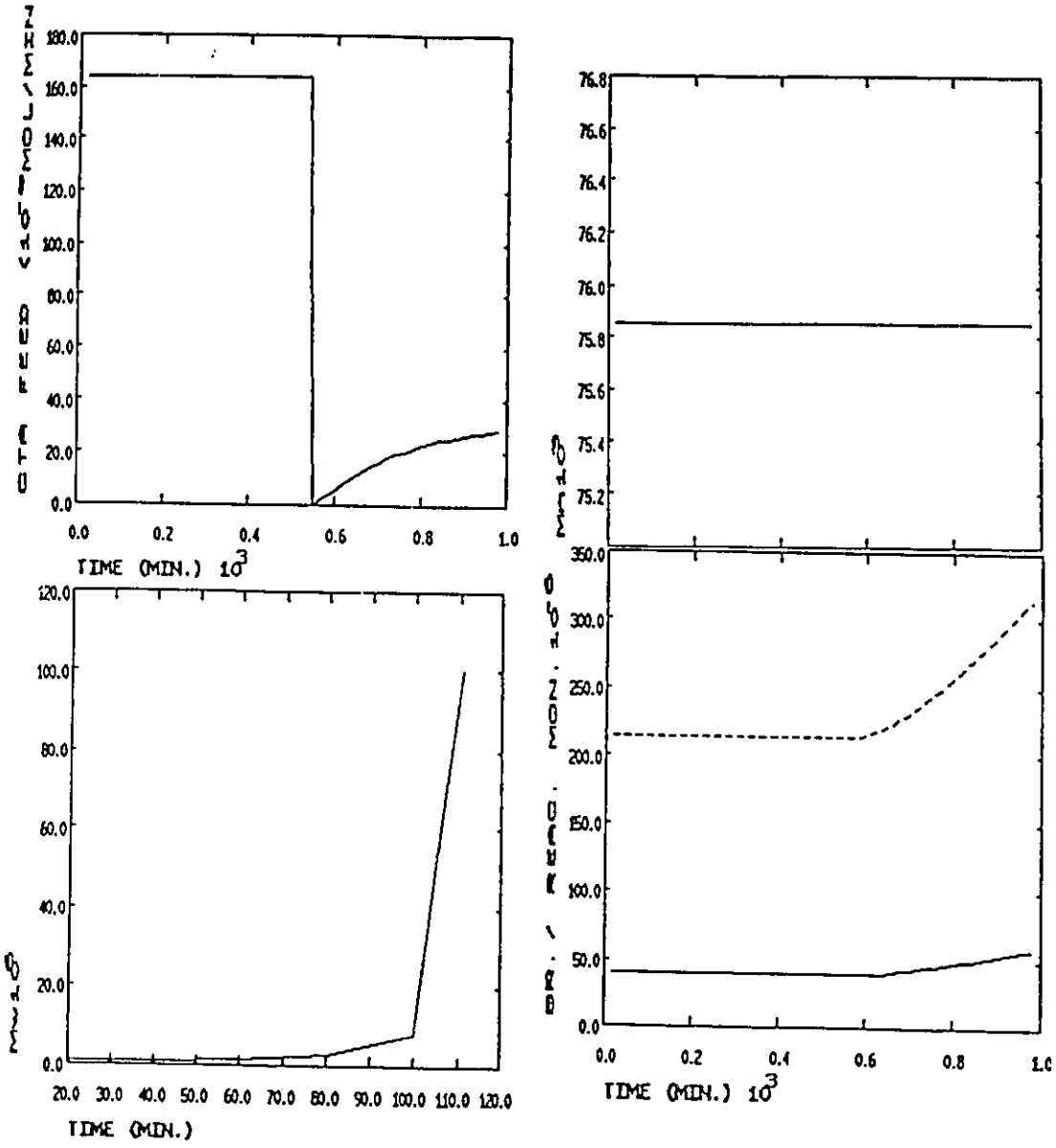

FIGURE 9.6: Simulated Policy II With r_N Control
(a) M_s (-) & M_b (--) conversion; (b) $\overline{F_s}$; (c) % solids;
(d) F_{M_s} (-) & F_{M_b} (--); (e) F_{CTA}; (f) $\overline{M_{W_W}}$;
(g) $\overline{M_{W_N}}$; (h) $\overline{Br}$ (-) & $\overline{X_L}$ (--)

9.7.2 Trade-Off Molecular Weight Policies

In some situations it would not be adequate to control only one molecular weight property as was shown in section 9.7.1. Sometimes one would prefer a trade-off between different molecular weight properties that one would ideally like to obtain. A trade-off is usual necessary since molecular weight properties, in general, are not independent. For example, suppose that one would like to manufacture SBR with a specific M_{W_w} and ρ. Knowing that it may not be possible to meet both specifications, one may wish to find an optimal trade-off between properties. Suppose that an optimal trade-off is to be determined through

$$J_{MW} = W_1(r_{W,set} - r_W)^2 + W_2(\rho_{set} - \rho)^2 \tag{9.58}$$

where W_1 and W_2 are weighting parameters, and $r_{W,set}$ and ρ_{set} are the desired r_W and ρ respectively. The assumption will be made that a constant composition control policy will be applied. As discussed in the previous section, a useful input trajectory for minimizing (9.58) would be F_{CTA}. If one inserts expressions for r_W (9.50) and ρ (9.48) into (9.58), it can be shown that J_{MW} is a function of $[CTA]_p$. Therefore, the minimization of (9.58) at all time during operation will require that the concentration of modifier in the polymer particles at all time satisfy

$$\frac{\partial J_{MW}}{\partial [CTA]_p} = 0 \tag{9.59}$$

where

$$\frac{\partial J_{MW}}{\partial [CTA]_p} = -2W_1(r_{W,set} - r_W)\frac{\partial r_W}{\partial [CTA]_p} - 2W_2(\rho_{set} - \rho)\frac{\partial \rho}{\partial [CTA]_p} \tag{9.60}$$

$$\frac{\partial \rho}{\partial [CTA]_p} = \frac{1}{r_N}\frac{\partial r_W}{\partial [CTA]_p} - \frac{r_W}{r_N^2}\frac{\partial r_N}{\partial [CTA]_p} \tag{9.61}$$

$$\frac{\partial r_N}{\partial [CTA]_p} = -\frac{C_t}{[M]_p r_N^2} \tag{9.62}$$

$$\frac{\partial r_W}{\partial [CTA]_p} = \frac{\frac{C_t}{[M]_p} r_W}{\left(1 + \frac{C_t[CTA]_p}{[M]_p} + C_m + \frac{C_p^* Q_2}{[M]_p} + \frac{C_p^{**} Q_2}{[M]_p}\right)} - \frac{\frac{C_t}{[M]_p} r_W}{\left(\frac{C_t[CTA]_p}{[M]_p} + C_m + \frac{C_p^* Q_1}{[M]_p} + \frac{C_{tm_p}[m_p]_p}{[M]_p}\right)} \tag{9.63}$$

Condition (9.59) is used to compute the optimal $[CTA]_p$ at t=0. Once $[CTA]_p$ at t=0 is determined, the required initial *CTA* charge can be computed. For t>0 the condition for optimality (9.59) must be maintained and will require that

$$\frac{d}{dt}\left(\frac{\partial J_{MW}}{\partial [CTA]_p}\right) = 0 \tag{9.64}$$

Hence, the fixed instantaneous pseudo property to be held constant in this example would be $p_i = \partial J_{MW}/\partial [CTA]_p$, the gradient of the objective with respect to the concentration of chain transfer agent in the particle. By inserting the expression for $p_i = \partial J_{MW}/\partial [CTA]_p$ into (9.64), one obtains required trajectory for F_{CTA} to maintain constant $\partial J_{MW}/\partial [CTA]_p$. The result is in the form of (9.51) to (9.54) but with $\partial J_{MW}/\partial [CTA]_p$ replacing r_W wherever it appears.

Other policies like the one above can be developed for trading-off molecular weight properties such as r_N and ρ, or r_N and r_W. As an alternative to CTA, one may also choose to use temperature.

A a trade-off policy like (9.58) might be very useful during a finishing off stage where Policy I may be applied. The combined r_W, Policy II approach in Figure 9.4 did not lead to very large change in polydispersity with time. However, when Policy II was stopped and replaced by Policy I, a very large drift in ρ can be seen. In this situation it may be worthwhile to switch from a r_W policy to a trade-off one to prevent excessive changes in the different molecular properties.

9.8 TRADE-OFF POLICIES IN GENERAL

The ideal of trading-off different instantaneous copolymer properties or conditions, as was demonstrated in section (9.7.2) for molecular weight properties, may be extended to the general case. Let p_i represent a vector of instantaneous properties or operating conditions that are to be traded-off in some objective function $J(p_i)$. The instantaneous property vector p_i may be effected by a different set of instantaneous operating conditions c_i. The first derivative of c_i with respect to time can be controlled through manipulated inputs u_i. The optimal trade-off condition is given by

$$p_{pseudo} = \frac{\partial J(p_i(c_i))}{\partial c_i} = 0 \quad | \quad t = 0 \tag{9.65}$$

$$\frac{dp_{pseudo}}{dt} = 0 \quad | \quad t > 0 \tag{9.66}$$

where p_{pseudo} is gradient of the objective with respect to controllable operating conditions c_i. One can view p_{pseudo} as a pseudo instantaneous property vector that must be equal to zero all times. At t=0 (9.65) is solved for $c_i(t=0)$ to establish starting optimal conditions. At t>0 u_i is determined so that condition (9.66) is satisfied at all time.

9.9 IMPLICATION OF CONSTRAINTS

The policies that have been outlined in the previous section make no accommodation for operating constraints on the manipulated inputs. When arriving at a suitable instantaneous policy it is expected that a preliminary simulation will be carried out beforehand to detect if operating constraints will be violated. If constraint violations are detected, several courses of action can be taken. First, one can simply recognize that the operating conditions and copolymer specification are not attainable and determine through a simulation study a reasonable set of alternatives that will not violate the operating constraints. However, such a procedure may not be adequate, especially if the off specification copolymer cannot be sold. If the desirable copolymer properties must be obtained in order to meet end-use specifications it may be preferable, if possible, to make changes to the design of the reactor system. For example, if monomer flow rates are determined to be too high it may be much more economical to replace pumps and/or valves, change reactors, adjust the seed specification, or reduce the batch size.

Another procedure that may prove effective for addressing operating constraints would be the transformation of the constraint problem to an equivalent instantaneous condition that must be satisfied during operating. This procedure has already been demonstrated in section (9.6) where a time optimal policy subject to heat removal constraints was proposed. This same idea can be extended to other types of operating constraints.

Finally, if all of the above suggestions prove to be inadequate, a formal optimization problem such as (9.1) to (9.3) may have to be solved to provide a useful trajectory for $u(t)$. The drawback with such an approach is that the computational effort required may restrict it to only off-line use. When applying such a procedure off-line one should always be on the look out for properties or conditions that are nearly constant using the optimum input trajectory. This would allow the optimal solution to be approximated by some equivalent constant property policy which may be computed in some on-line control strategy. Note that it would be

impossible to propose that a constrained optimization be solved at all time based on some cost function of the instantaneous properties or conditions. The reason for this is that at time t the manipulated inputs only affect, at best, the first derivative of the instantaneous properties or conditions.

9.10 RANGE OF COPOLYMER PROPERTY SPECIFICATIONS

Since many different operating policies have already been described at this point, it would useful to provide some indication of the range of SBR property specifications that one might obtain by combining some molecular weight control policy with some composition control policy. Consider combining a constant r_s control policy with Policy X followed by Policy I, as was shown in Figure 9.5. The three tables shown below provide information on the effect of changing the initial level of conversion (X_0), *CTA* charge, and isothermal operating temperature on the cumulative branching, crosslinking, and molecular weight properties. The time required to reach the termination point of 98% conversion with about 55% solids has also been provided. Additional information concerning the reactor operator conditions can be found in section (9.2). In all of the results below, copolymer composition was specified at 15 mole percent styrene.

Table 9.1 shows the effect of changing the level of conversion during the application of Policy X. The reactor was initially charged with 0.003 gmol of *CTA* and operated isothermally at 55° *C*. It can be observed that conversion affects all of the properties shown. With the exception of number average molecular weight, increased conversion levels led to increased property values. Increased conversion level also leads to a very significant increase in reaction time.

Table 9.1: POLICY X/r_W.

Effect Of Conversion On Copolymer Properties

X_0	$\overline{Bn_3}$	$\overline{Bn_4}$	$\overline{M_{W_W}}$	$\overline{M_{W_N}}$	$\bar{\rho}$	Time (min.)
60%	$4.19x10^{-5}$	$2.27x10^{-4}$	$4.84x10^{5}$	$1.57x10^{4}$	30.8	759
70%	$4.63x10^{-5}$	$2.51x10^{-4}$	$4.67x10^{5}$	$1.54x10^{4}$	30.2	812
80%	$5.77x10^{-5}$	$3.13x10^{-4}$	$4.92x10^{5}$	$1.32x10^{4}$	37	960
90%	$9.77x10^{-5}$	$5.30x10^{-4}$	$6.53x10^{5}$	$6.40x10^{3}$	101	1496

Table 9.2 shows the same information but with changes made to the initial charge of chain transfer agent. All runs in Table 9.2 were carried out an 80% initial conversion. The results clearly indicate that the *CTA* level affects molecular weight properties but not branching, crosslinking, or the reactor operation time.

Table 9.2: Policy X/r_W

Effect Of CTA On Copolymer Properties

$CTA_{t=0}$ *(gmol)*	$\overline{Bn_3}$	$\overline{Bn_4}$	$\overline{M_{W_W}}$	$\overline{M_{W_N}}$	$\bar{\rho}$	Time (min.)
0.007	$5.77x10^{-5}$	$3.13x10^{-4}$	$2.16x10^{5}$	$1.92x10^{4}$	11.3	960
0.005	$5.77x10^{-5}$	$3.13x10^{-4}$	$3.00x10^{5}$	$1.72x10^{4}$	17.4	960
0.003	$5.77x10^{-5}$	$3.13x10^{-4}$	$4.92x10^{5}$	$1.32x10^{4}$	37	960

Table 9.3 demonstrates the effect of reactor temperature operation on copolymer properties. In all of the runs shown, initial conversion was set to 80% and 0.003 gmol of chain transfer agent was present in the

initial charge. Temperature can be observed to influence all of the variables shown. Increasing temperature decreases branching, number average molecular weight, and reactor operation time, and increases crosslinking, weight average molecular weight, and polydispersity.

Table 9.3: Policy X/r_W

Effect Of Temperature On Copolymer Properties

T (C)	$\overline{Bn_3}$	$\overline{Bn_4}$	$\overline{M_{W_W}}$	$\overline{M_{W_N}}$	$\bar{\rho}$	Time (min.)
50	$7.19x10^{-5}$	$2.79x10^{-4}$	$4.18x10^{5}$	$1.68x10^{4}$	24.9	1205
55	$5.77x10^{-5}$	$3.13x10^{-4}$	$4.92x10^{5}$	$1.32x10^{4}$	37.0	960
60	$4.66x10^{-5}$	$3.50x10^{-4}$	$5.81x10^{5}$	$1.01x10^{4}$	57.8	778

To investigate the influence of the instantaneous molecular weight control policy on the copolymer properties, a simulation was carried out with number average molecular weight control instead of weight average. Table 9.4 shows the same information as was shown in Table 9.2 for this Policy X / r_N run. As before, different initial chain transfer charges will only influence molecular weight properties. Comparing Tables 9.2 and 9.4, it can observed that the number average molecular weight policy can lead to significantly different molecular weight properties relative to the weight average control policy.

Table 9.4: Policy X/r_N

Effect Of CTA On Copolymer Properties

$CTA_{,=0}$ $(gmol)$	$\overline{Bn_3}$	$\overline{Bn_4}$	$\overline{M_{W_W}}$	$\overline{M_{W_N}}$	$\bar{\rho}$	Time (min.)
0.007	$5.77x10^{-5}$	$3.13x10^{-4}$	$1.57x10^{5}$	$2.63x10^{4}$	5.96	960
0.005	$5.77x10^{-5}$	$3.13x10^{-4}$	$8.07x10^{5}$	$3.88x10^{4}$	20.0	960
0.003	$5.77x10^{-5}$	$3.13x10^{-4}$	∞	$7.23x10^{4}$	∞	960

9.11 SUMMARY

This chapter essential provides a catalog of different semi-batch operating policies for the manufacture of SBR latex. All of the policies discussed can generalized in the form

$$\frac{dp}{dt} = P(x,u,t) = 0 \tag{9.67}$$

where p is a vector of fixed instantaneous copolymer properties or reaction conditions to be held constant, x is the vector of internal model states, u is the manipulated input trajectory to be determined. The solution for u can be observed in (9.67) to only require the solution of a nonlinear set of equations, and therefore may be applied in some on-line computation scheme. These policies would be very meaningful to a polymer reaction engineer whose main concern would often be to operate the reactor so that consistent copolymer properties are obtained at all time. A big advantage when applying these policies is the quasi-state established on some conditions within the reactor. Intuitively, this should provide some simplification to the design of a feedback controller if required. The open-loop polices based on (9.67) can always be shown to be optimal with respect to some classical optimal control problem in the form of (9.1) to (9.3). The procedure used in this work to obtain the optimal trajectory for $u(t)$ would be recognized by optimization expects to be the most numerically efficient approach.

In this work several useful policies related to open-loop control of copolymer properties and operating conditions have been discussed. Instantaneous control policies that were previously proposed (Hamielec et al., 1987; Beste and Hall, 1966) have been extended, and new ones have been added. Open-loop policies related to the control of copolymer properties and operating conditions such as copolymer composition, conversion, particle monomer concentration, branching and crosslinking, molecular weight, polydispersity, and time optimality are proposed. In addition, a simple procedure for trading-off different instantaneous specifications was also shown. The policies proposed would be expected be very useful for many different industrial applications, and would allow a wide range SBR latex specifications to obtained for its different end uses.

9.12 NOTATION

A_j	heat transfer area for reactor cooling jacket
Bn_i	i'th branch frequency per copolymer chain
Br	instantaneous degree of branching

$\overline{Br}$	cumulative degree of branching
c	nonlinear matrix expression defining operating constraints in trajectory optimization problem
C_{Im_p}	ratio of organic impurity rate constant to pseudo copolymer propagation rate constant
C_m	ratio of pseudo copolymer rate constant for transfer to monomer to pseudo copolymer propagation rate constant
C_p^*	ratio of pseudo copolymer rate constant for branch formation to pseudo copolymer propagation rate constant
C_p^{**}	ratio of pseudo copolymer rate constant for crosslink formation over pseudo copolymer propagation rate
Cp_i	heat capacity of i
C_t	ratio of pseudo copolymer chain transfer rate constant to pseudo copolymer propagation rate constant
CTA	moles of unreacted chain transfer agent
d_i	density of i
D	integrated contribution to objective functional
E	moles of emulsifier
f	nonlinear matrix describing time rate of change of x
f_{sp}	mole fraction of styrene in monomer contained in polymer particle phase
F_b	instantaneous butadiene copolymer composition
$\overline{F_b}$	cumulative butadiene copolymer composition
F_E	feed rate of emulsifier
F_{Im_p}	feed rate of organic phase reactive impurity
F_{Im_w}	feed rate of water phase reactive impurity
F_{I_a}	feed rate of initiator
F_{M_b}	feed rate of butadiene
F_{M_s}	feed rate of styrene
F_s	instantaneous styrene copolymer composition
$\overline{F_s}$	cumulative styrene copolymer composition

F_{V_w}	feed rate of water
G	end-point contribution in objective functional
Im_p	moles unreacted organic phase reactive impurity
Im_w	moles of unreacted water phase reactive impurity
I_n	moles of unreacted initiator
ΔH_{pb}	heat of polymerization for butadiene
ΔH_{ps}	heat of polymerization of styrene
J	objective functional in classical optimal control approach
J_{MW}	trade-off cost function for instantaneous molecular weight property control
k_{fCTA}	pseudo copolymer rate constant for chain transfer agent
K_{ijk}	ratio of concentration of i in phase j to phase k
M_b	moles of unreacted butadiene
M_s	moles of unreacted styrene
M_{W_i}	molecular weight of i
M_{W_N}	instantaneous number average molecular weight
M_{W_W}	instantaneous weight average molecular weight
$\overline{M_{W_N}}$	cumulative number average molecular weight
$\overline{M_{W_W}}$	cumulative weight average molecular weight
N_A	Avogadro's number
N_p	number of polymer particles per unit volume of water
p	instantaneous copolymer property vector to be controlled
P	total amount of P_s and P_b
$P(x,u,t)$	nonlinear matrix expression describing the time rate of change of p
P_b	moles of butadiene
P_s	moles of styrene
Q_i	concentration of i'th moment

r_b	butadiene copolymer reactivity ratio
r_s	styrene copolymer reactivity ratio
r_N	number average copolymer chain length
r_W	weight average copolymer chain length
R_{CTA}	rate of reaction of chain transfer agent
R_{pb}	rate of butadiene polymerization
R_{ps}	rate of styrene polymerization
t	time
t_f	stop time
T	temperature
T_{in}	temperature of reactor feed
$T_{j,min}$	lowest temperature for coolant feed to reactor jacket
T_{set}	reactor temperature set point
u	manipulated input vector
U	overall heat transfer coefficient for reactor cooling jacket
V_i	volume of phase i
W_i	weighting parameters in optimization cost function
x	modelled differential state vector
X	overall monomer conversion
X_L	instantaneous degree of crosslinking
$\overline{X_L}$	cumulative degree of crosslinking

Subscripts

b	butadiene
m	monomer phase
p	polymer phase
s	styrene
w	water phase

Greek Letters

α_b	expression given by (9.28)
α_s	expression given by (9.27)
β_b	expression given by (9.26)
β_s	expression given by (9.25)
Γ_N	expression given by (9.57)
Γ_W	expression given by (9.53)
ζ	expression given by (9.20)
ρ	instantaneous polydispersity
$\bar{\rho}$	cumulative polydispersity
Φ_b	pseudo copolymer copolymerization rate constant for butadiene
Φ_s	pseudo copolymer copolymerization rate constant for styrene

FEEDBACK CONTROLLER DESIGN FOR SEMI-BATCH COPOLYMER REACTORS

10. FEEDBACK CONTROLLER DESIGN FOR SEMI-BATCH COPOLYMER REACTORS

10.1 INTRODUCTION

Open-loop operating policies, such as described in chapter 9, provide useful operating trajectories for optimally producing copolymer in some sense. Unfortunately, the optimal trajectories that these procedures provide are only valid when the assumed initial operating conditions are correct, no disturbances enter the process, and the dynamic model provides perfect prediction of the dynamic response of the actual process. The implication of these assumptions is serious when producing copolymer latex. The existing models of these processes have limited accuracy, and therefore one can expect that an optimal trajectory arrived at from these models will contain some significant error. Furthermore, it is known (Huo et al, 1988; Ahlberg and Cheyne, 1976) that the dynamic response of these systems is highly sensitive to trace levels of reactive impurities that would be encountered in an industrial operation. Hence the operation of copolymer reactors based solely on these off-line computed trajectories may not be very economical since one will determine only after the batch/semi-batch operation if the desired copolymer property specifications have been met. This could lead to a costly waste of raw materials in spoiled batches that may not be possible to sell or have to be sold at reduced profit. One would also expect the operating procedure described above to yield poor product reproducibility if variations in the process operating conditions exist.

Examples of the application of feedback control to improve batch process operating conditions can be found in the literature. Relative to continuously operating processes, the application of feedback control in this circumstance has been studied to a far lesser extent. General review papers on the application of feedback control to polymer reactors are provided by Amrehn (1977), Juba and Hamer (1986), and Elicabe and Meira (1988). Many examples of the application of feedback control for controlling batch reactor temperature can be found (Kiparissides and Shah, 1983; Jutan and Uppal, 1984; Garcia, 1984; Juba and Hamer, 1986). The application of linear quadratic state space control for controlling conversion and molecular weight in MMA polymerization using temperature as a manipulated input was demonstrated by Ponnuswamy et al. (1987). Kiparissides et al. (1987) used the same control problem to compare the performance of linear quadratic state

space control with DMC and an extended STR control strategy. In all of the literature cited above, the feedback control strategies described are used to control some variable(s) along some precomputed on-line trajectory. The feedback control is used to correct the off-line input action for disturbances and/or model mismatch. Although the feedback controller will allow the process to closely follow the precomputed off-line optimal trajectory in these approaches, there is no guarantee that such a strategy will maintain optimality since disturbances and model mismatch, in general, affect the optimal off-line trajectory to be followed. To maintain optimal operating conditions, the optimal trajectory must be recomputed on-line making use of the available measurements provided during operation. The computational effort required to do so may not be practical in practice. Kravaris et al. (1989), rather than apply control along some precomputed cumulative property trajectory, considered the design of a feedback controller for the control of an instantaneous copolymer property. In their work the control of copolymer composition using temperature and monomer feed rate was considered. A global input/output linearizing transformation was used in their application so that standard linear feedback controller designs may be applied. The approach was demonstrated to meet copolymer property specifications in the presence of initialization errors, model mismatch, and disturbances, but required an unrealistic a direct property measurement for these features to be realized.

The purpose of this chapter is to propose a feedback control strategy to correct for errors made in the assumed operating conditions for the instantaneous open-loop control policies discussed in chapter 9. The block diagram of the proposed structure is shown in Figure 10.1.

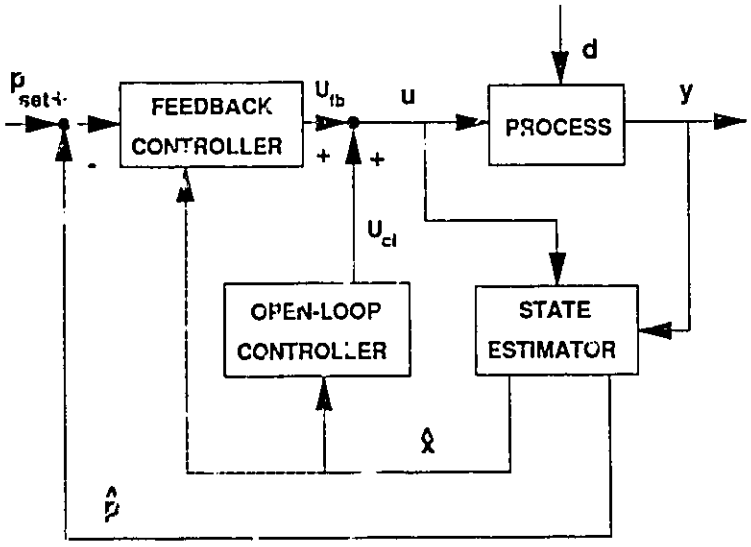

Figure 10.1: Semi-Batch Feedforward/Feedback Control Block Diagram

It consists of a nonlinear state estimator to infer instantaneous copolymer properties ($\hat{p}$) to be controlled from the available measurements ($y^T = (M_n, M_b, D_p, CTA)$). The state estimator in Figure 10.1 will be the reiterative extended Kalman filter proposed in chapter 8. The open-loop controller represents some open-loop instantaneous control policy discussed in chapter 9. This open-loop controller provides a feedforward control action u_{ol} to maintain fixed $\hat{p}$, as determined through $\hat{x}$, and thus establishes near quasi-steady state conditions on the instantaneous copolymer properties to be controlled. If the current value of $\hat{p}$ is not at the desired set point, a feedback correction must be added to the open-loop/feedforward input to eliminate the deviation from set point. This is the purpose of the feedback block in the control scheme of Figure 10.1. Several different possibilities for the design of the feedback controller block shall be discussed, such as conventional PID control, a decoupling global input/output linearizing transformation approach (Freund, 1973, 1975, 1982), and model-based optimal feedback control. Simulation results will be presented for PID control and the approach based on the decoupling global input/output linearization. The robustness of the latter approach to state initialization errors, model mismatch, and unaccounted for disturbances is also examined.

This chapter is essentially the climax of all the chapters related to the semi-batch polymerization control problem. For the first time, procedures related to dynamic polymer modelling, nonlinear state estimation, open-loop operating policies, and feedback control are effectively tied together to arrive at an optimal, or suboptimal, nonlinear inferential feedback controller that would be well-suited for application to batch/semi-batch industrial polymerization processes. The proposed scheme will offer a very simple alternative to computationally intensive on-line optimization approaches that, in general, would not be practical to apply. The economic advantage and improvement in reactor operation when applying the proposed strategy would definitely be appreciated by polymer manufactures, where quality control and product reproducibility is a main concern (Taylor, 1988). The results also demonstrate, from the point of view of quality control, the advantage of using operating policies based on instantaneous properties rather than cumulative ones where time varying trajectory tracking provided by some off-line solution is often required. As will be demonstrated, the former policies when combined with state estimation and feedback control, can be easily driven to optimal operating conditions during on-line application when nonideal operating conditions are encountered.

10.2 FEEDBACK CONTROL CASE STUDY

The simulations to follow shall be concerned with the process operation configuration shown below:

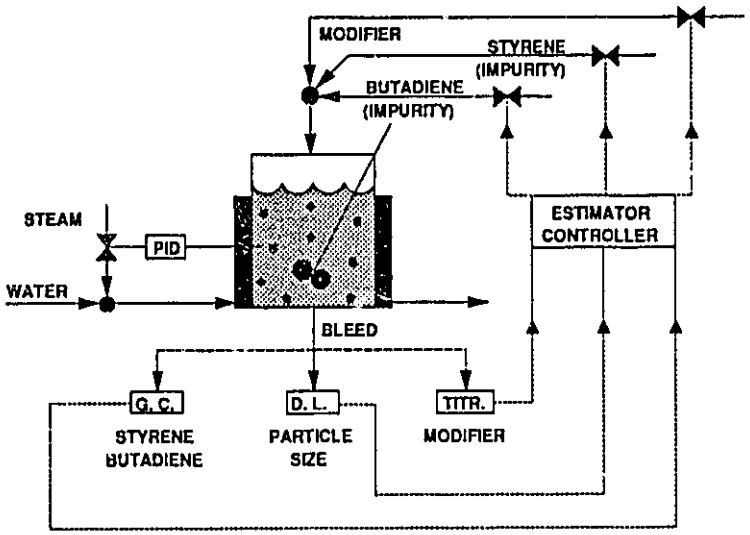

Figure 10.2: Closed-Loop SBR Process Configuration

As was the case in chapter 9, the reactor will be operated isothermally and only styrene, butadiene, and modifier shall be fed to the reactor. Unless stated otherwise, the following actual process operating conditions are to be assumed:

Initial Conditions For Feedback Controller Simulations

M_a	0.07 *gmol*
M_b	0.27 *gmol*
P_a	0.32 *gmol*
P_b	1.81 *gmol*
I_n	0.03 *gmol*
E	0.122 *gmol*
CTA	0.0051 *gmol*
Im_p	$1.25x10^{-5}$ *gmol*
Im_w	0.0 *gmol*
N_p	$1.75x10^{18}$ l^{-1}
V_w	4.0 *l*
V_pQ_0	$4.72x10^{-3}$ *gmol*
V_pQ_1	2.13 *gmol*
V_pQ_2	$9.6x10^{3}$ *gmol*
$V_pQ_0Bn_3$	$1.77x10^{-4}$ *gmol*
$V_pQ_0Bn_4$	$9.58x10^{-4}$ *gmol*

Common Operating Conditions

T	55° *C*
V_r	10 *l*
F_{I_n}	0.0
$F_{V_{cr}}$	0.0
F_E	0.0
F_{Im_w}	0.0
F_{Im_p}	$5x10^{-6}F_{M_a} + 4.5x10^{-5}F_{M_b}$

In the operating conditions shown above, the organic impurity is assumed to be present in the monomer feeds. Since butadiene would be expected to contain more impurities than styrene, the amount of impurity in the butadiene monomer feed was set to a higher level.

The operating policy that will be used as a case study for the application of feedback control will be concerned with the control of instantaneous copolymer composition, conversion, and instantaneous weight average molecular weight ($p^T = (F_s, X, r_W)$). This mode of operation was referred to as policy X/r_W in chapter 9. This policy will be applied until the maximum amount of styrene, as determined by the reactor volume constraint, is reached. Thereafter, the flow rate of styrene is set to zero, and the operating policy will be reduced to the control of instantaneous composition and weight average molecular weight (Policy I/r_W, $p^T = (F_s, r_W)$). The open-loop control actions provided by these policies (u_{ol}) are computed during the feedback control run using estimates of the internal model states ($\hat{x}$) provided by the nonlinear estimator block. Model mismatch states, x^{14} and x^{15} (refer to section 8.6.2) are also incorporated into the open-loop calculations.

To evaluate controller design performance, the model used in the estimator and in the control action computations is initialized with the assumption that no impurity is present (Im_p, $F_{Im_p} = 0$), and with the number of polymer particles seeds over estimated by 30% ($N_p = 2.5x10^{18}$). An over estimation in the particle count can occur in practice when polymer particle coagulation occurs. Figure 10.3 shows the consequence of applying the instantaneous open-loop policy without the model states corrected by the estimator and without feedback control when the initialization error is made. These figures provide information on the actual instantaneous response (-), desired instantaneous set point (--), and the estimated instantaneous response provided by the state estimator (..). Under ideal operating conditions, instantaneous composition (10.3(a)), conversion (10.3(b)), and instantaneous molecular weight (10.3(c)) should be constant at the indicated set points during the application of Policy X/r_W. The initialization error clearly leads to a significant deviation from the expected copolymer properties under ideal operating conditions. The purpose of the feedback control will be to correct the monomer and modifier feed rates so that these deviations, once detected, can be eliminated as quickly as possible. The use of a conservative control strategy, such as is often found to be acceptable in continuously operating petrochemical processes, would not be suitable since one would not want a high percentage of off specification polymer that cannot be removed to be present in the final product.

As mentioned earlier, the nonlinear estimator to be used in this study will be the reiterative extended Kalman filter proposed in chapter 8. The first extended Kalman filter is formulated using internal model states

$$x^T = \left(M_s, M_b, P_s, P_b, Im_p, N_p V_w, F_{Im_p}, CTA, V_p Q_0, V_p Q_1, V_p Q_2, V_p Q_0 Bn_3, V_p Q_0 Bn_4, x^{14}, x^{15}\right)$$

and measurement vector

$$y^T = (M_s, M_b, D_p, CTA)$$

The measurements will corrupted with Gaussian white noise having a covariance matrix Diag(0.002,0.002,200,0.002). For the operating conditions discussed above, the following tuning parameters for the scaled model states (refer to section 8.5 for scaling) was found to lead to acceptable performance:

$$R_w = Diag\{10^{-4}, 10^{-4}, 10^{-4}, 10^{-4}, 10^{-4}, 1, 10^{-4}, 10^{-4}, 10^{-4}, 10^{-4}, 10^{-4}, 10^{-4}, 10^{-4}, 10^{-3}, 10^{-3}\}$$

$$R_v = Diag\{0.002, 0.002, 200.0, 0.002\}$$

$$P_0 = Diag\{10^{-3}, 10^{-3}, 10^{-3}, 10^{-3}, 1, 500, 1, 10^{-3}, 10^{-3}, 10^{-3}, 10^{-3}, 10^{-3}, 10^{-3}, 10^{-2}, 10^{-2}\}$$

The second extended Kalman filter which is used to estimate unknown initial states was formulated using

$$x^T = \left(Im_{p_0}, N_{p_0}, F_{Im_{p_0}}, x_0^{15}\right)$$

as the states and with the measurement vector

$$y^T = (M_t, M_b, D_p)$$

The tuning parameters that led to acceptable results for the operating conditions described are given below:

$$R_w = Diag\{0, 0, 0.01, 0\}$$

$$R_v = Diag\{0.002, 0.002, 200\}$$

$$P_0 = Diag\{1, 500, 1, 0.01\}$$

The first extended Kalman filter was reiterated only for the first 10 sampling intervals with improved unknown initial state estimates provided by the second extended Kalman Filter. After the first 10 sampling periods, only the first extended Kalman filter was used to provide state estimates in the conventional recursive manner.

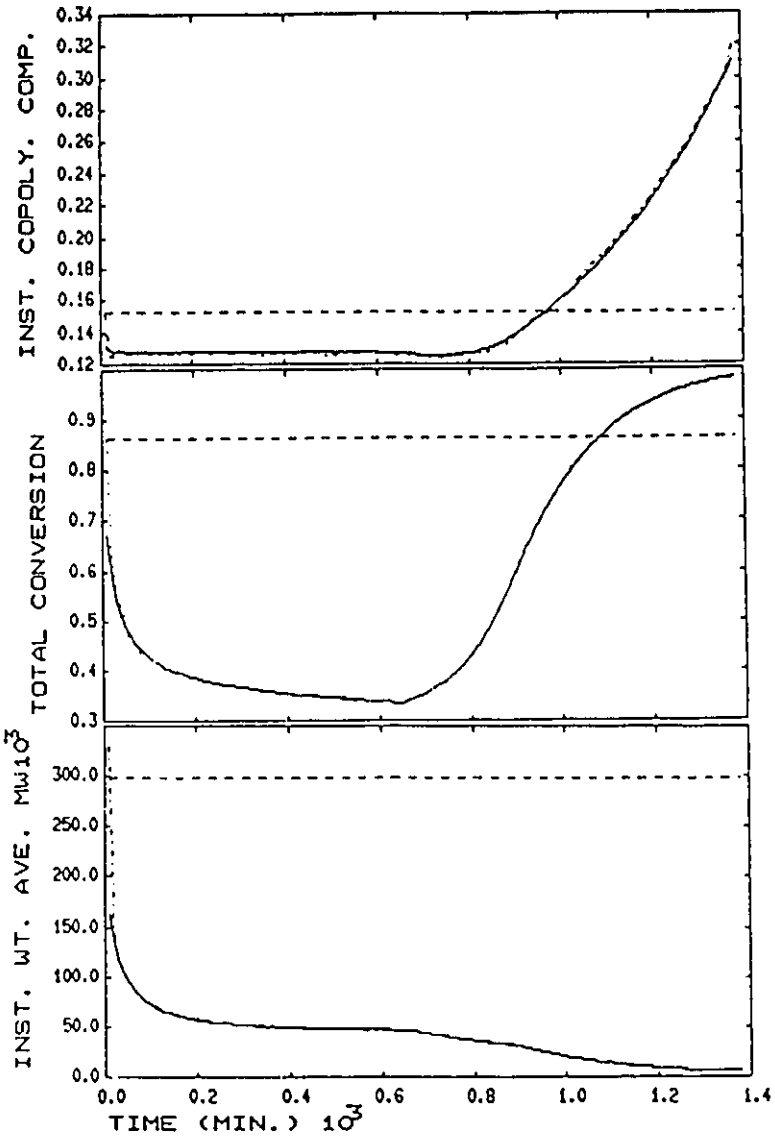
INST. COPOLY. COMP.
0.34
0.32
0.30
0.28
0.26
0.24
0.22
0.20
0.18
0.16
0.14
0.12
TOTAL CONVERSION
0.9
0.8
0.7
0.6
0.5
0.4
0.3
INST. WT. AVE. MW10^{-3}
300.0
250.0
200.0
150.0
100.0
50.0
0.0
0.0
0.2
0.4
0.6
0.8
1.0
1.2
1.4
TIME (MIN.) 10^{-3}

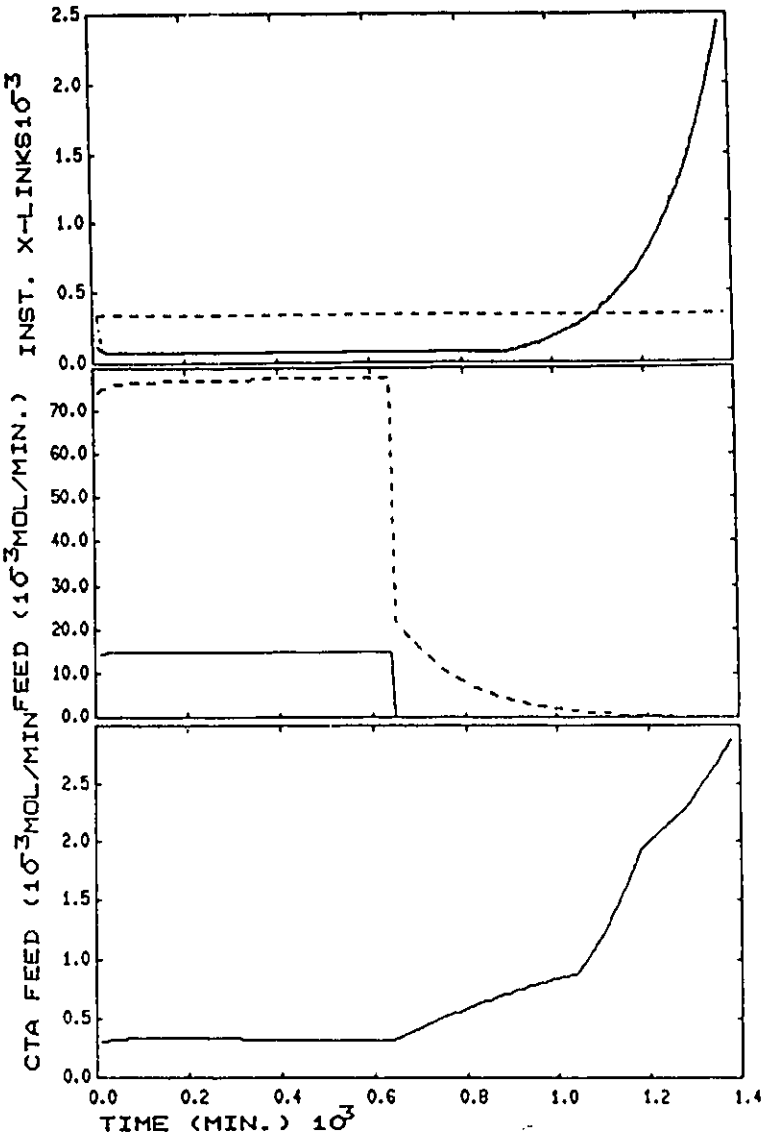

FIGURE 10.3: Open-loop Instantaneous Policy With Initialization Error And No Feedback
a: Copolymer Composition; b: Overall Conversion
c: Instantaneous Weight Average Molecular Weight; d: Instantaneous Cross-Linking
(-) Actual Response, (--) Set Point, (..) Estimated Response
e: Monomer Feed Rates, (-) styrene, (--) butadiene
f: CTA Feed Rate

10.3 PAIRED PID CONTROL

If one is concerned with a single input/single output control policy or can find suitably decoupled input/output pairings in a multivariable control policy, a classical, non-model based PID feedback control strategy may prove to be adequate. Taking this approach in the strategy proposed in Figure 10.1, the j'th manipulated input u_j used to control i'th instantaneous property p_i can be determined by

$$u_j = u_{ol,j} + u_{fb,j} \tag{10.1}$$

$$u_{fb,j} = K_{c_j}\left\{e_i + \frac{1}{\tau_{I_j}}\int e_i dt + \tau_{d_j}\dot{e}_i\right\} \tag{10.2}$$

$$e_i = (p_{i,set} - \hat{p}_i) \tag{10.3}$$

In (10.1), $u_{ol,j}$ represents the feedforward/open-loop action that attempts to maintain constant $\hat{p}_i$. The feedback control action $u_{fb,j}$ in (10.1) provides a correction to this feedforward term to allow the specified instantaneous conditions $\hat{p}_i$ to be reached when an error is estimated.

The effectiveness of the PID approach will depend on the amount of multivariable interaction between the different pairings and on the process nonlinearities. If the dynamics of the process change considerably with time, a considerable effort in prior simulation studies will have to be carried out to specify the large number of PID tuning parameters. When these situations are encountered, the use of paired PID control will far less convenient than the methods to be discussed in the sections to follow.

Figure 10.4 shows the simulated performance of a paired PI feedback design when applied to the operating conditions described in section 10.2. In the run shown, the PI inputs were used to correct the open-loop control actions according to

$$F_{M_s} + F_{M_b} = u_{PID,1}\left(F_{M_s} + F_{M_b}\right)_{open\ \ loop} \tag{10.4}$$

$$\frac{F_{M_s}}{F_{M_b}} = u_{PID,2}\left(\frac{F_{M_s}}{F_{M_b}}\right)_{open\ \ loop} \tag{10.5}$$

$$F_{CTA} = u_{PID,3}(F_{CTA})_{open\ \ loop} \tag{10.6}$$

during the phase where Policy X/r_W was applied. The feedback inputs, $u_{PID,1}$, $u_{PID,2}$, and $u_{PID,3}$ were paired with controlling conversion, instantaneous composition, and r_W respectively. These pairings were found to lead to minimal interaction. After an exhaustive simulation study, the following PI tuning parameters were found to be acceptable:

PI Tuning Parameters During Policy X/r_W

$$K_{c_1} = -7 \qquad \tau_{I_1} = 30 \quad \text{min.}$$

$$K_{c_2} = -2 \qquad \tau_{I_2} = 1000 \quad \text{min.}$$

$$K_{c_3} = -1 \qquad \tau_{I_3} = 400 \quad \text{min.}$$

During the finishing off phase where Policy I/r_W was applied, the feedback corrections were changed to

$$F_b = u_{PID,1}\left(F_{M_b}\right)_{open\ \ loop} \tag{10.7}$$

$$F_{CTA} = u_{PID,2}(F_{CTA})_{open\ \ loop} \tag{10.8}$$

where $u_{PID,1}$ and $u_{PID,2}$ were paired with the control of instantaneous composition and r_W respectively. The PI tuning parameters that were used are listed below:

PI Tuning Parameters During Policy I/R_W

$$K_{c_1} = -7 \qquad \tau_{I_1} = 30 \quad \text{min.}$$

$$K_{c_2} = -1 \qquad \tau_{I_2} = 400 \quad \text{min.}$$

Figures 10.4(a) to 10.4(c) provides information on the actual (-), desired (--), and estimated (..) instantaneous copolymer composition, conversion, and instantaneous molecular weight respectively. In all cases reasonably tight control can be observed. Figure 10(d) also provides information on the instantaneous degree of crosslinking. In section 9.5, the use of Policy X was suggested for indirectly controlling crosslinking since a constant conversion condition closely approximates the required condition for constant instantaneous crosslinking. In Figure 10(d) the control of instantaneous degree of crosslinking can be observed to be very good even though significant initialization errors were present. Figure 10(e) shows the actual feed rate of styrene (-) and butadiene (--) during the controlled run. The flow rate of modifier is shown in Figure 10(f). The inputs can be observed to be well behaved during the entire control run, and respond quickly to establish the desired instantaneous operating conditions once the effect of the initialization error was detected. Relative to Figure 10.3, where only open-loop flow rates were applied, the application of this feedback control strategy leads to a tremendous improvement in copolymer property control. The only drawback with the this PI feedback control approach, from the point of view of controller design, was the substantial effort required in simulation runs to arrive at suitable choice for the six PI tuning parameters.

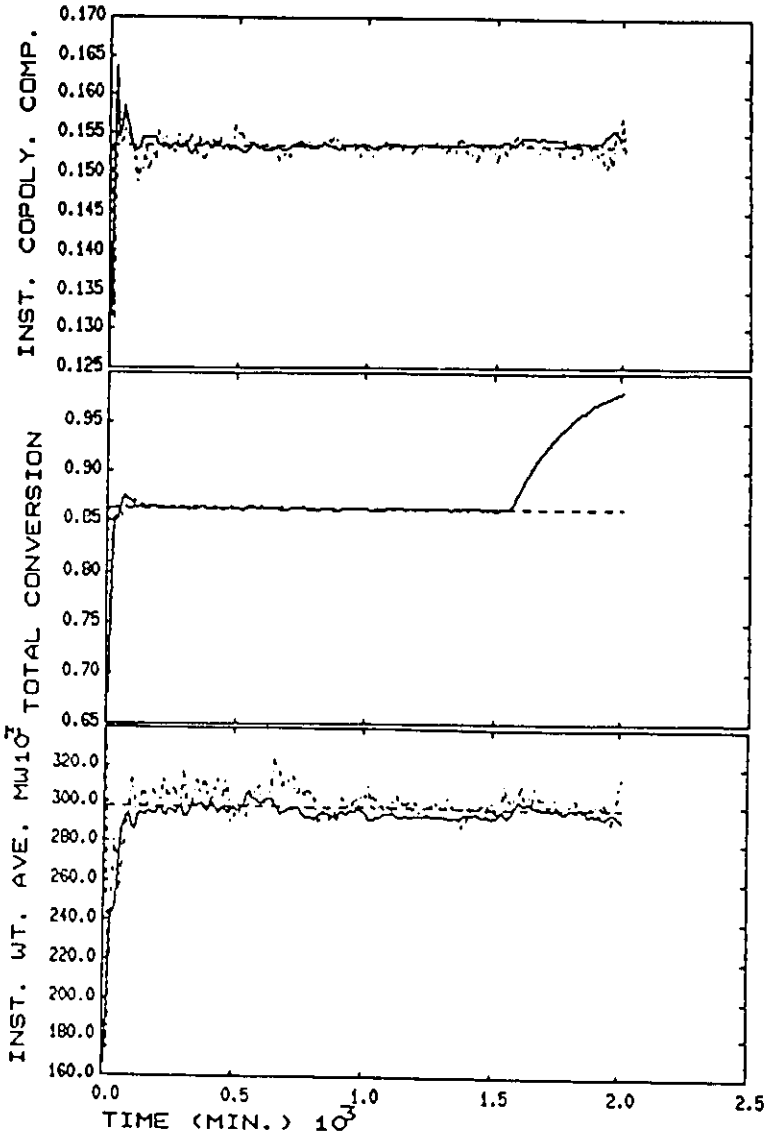
INST. COPOLY. COMP.
0.170
0.165
0.160
0.155
0.150
0.145
0.140
0.135
0.130
0.125
TOTAL CONVERSION
0.95
0.90
0.85
0.80
0.75
0.70
0.65
INST. WT. AVE. MW10^-3
320.0
300.0
280.0
260.0
240.0
220.0
200.0
180.0
160.0
0.0
0.5
1.0
1.5
2.0
2.5
TIME (MIN.) 10^3

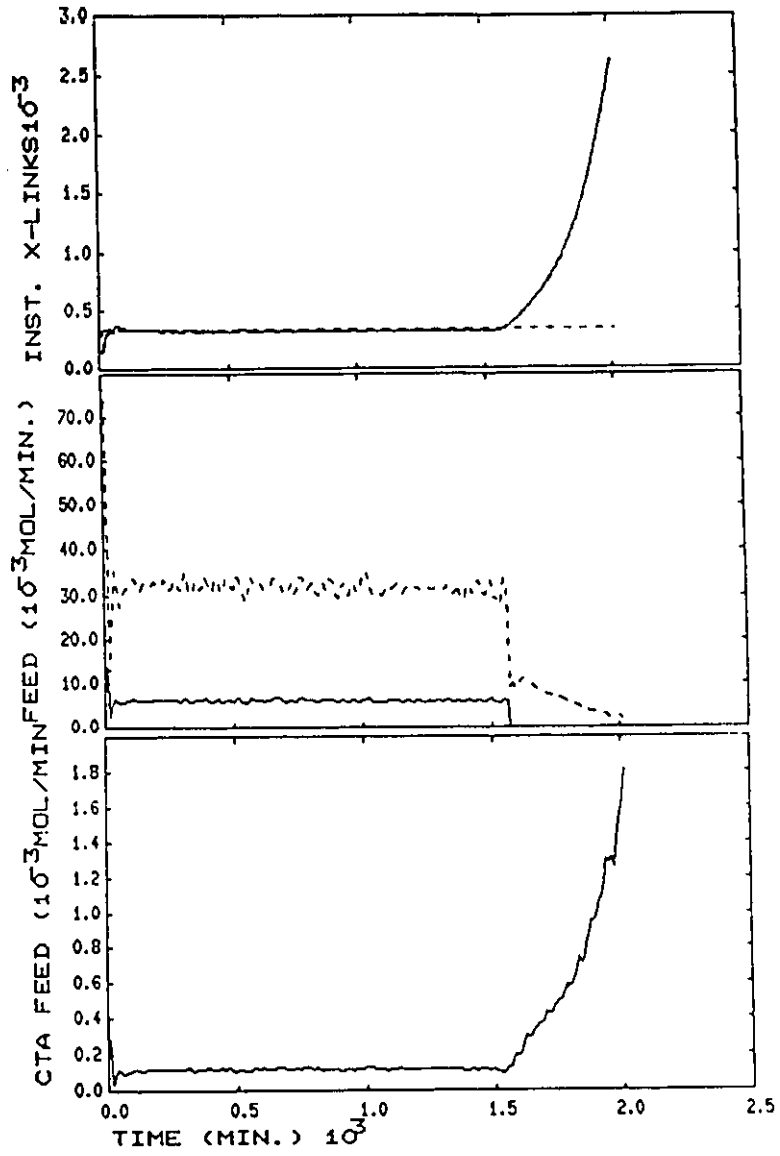

FIGURE 10.4: Instantaneous Property Control With Paired PI Design
curve identification as in Figure 10.3

10.4 GLOBAL INPUT/OUTPUT LINEARIZATION

The use of input/output linearization transformations for simplifying nonlinear control problems is well-known. This approach will only be useful if a straightforward input/output transformation can be found to obtain a linear space with respect to transformed variables. If a transformation can be found in a nonlinear control problem all well-known control theory developed for linear systems can be conveniently applied to the transformed linear space.

Freund (1973,1975,1982) provides a general input/output transformation for linearizing and decoupling nonlinear multivariable control problems of the form

$$\dot{x} = A(x,t) + B(x,t)u(t) \tag{10.9}$$

$$p(t) = P(x,t) + D(x,t)u(t) \tag{10.10}$$

Dynamic polymerization models in general will exist in the form of (10.9) and (10.10). In this approach, the input variable $u(t)$ is transformed to fictitious input variable $v(t)$ through the relationship

$$u(t) = F(x,t) + G(x,t)v(t) \tag{10.11}$$

Expressions for $F(x,t)$ and $G(x,t)$ can be found in Freund (1973,1975,1982). Use of (10.11) leads to the linear decoupled output/transformed input space

$$p_i^{(d_i)}(t) + \delta_{d_i-1,i}p_i^{(d_i-1)}(t) + \ldots + \delta_{0,i}p_i(t) = \theta_i v_i(t) \tag{10.12}$$

where index i refers to i'th decoupled fictitious input/output pairing, and d_i is the derivative order of output i with respect to the input. The parameters $\delta_{j,i}$ and θ_i can be arbitrarily specified to establish the poles and gain respectively in the linear decoupled input/output space. To make use of this transformation in a feedback control strategy one would design fixed linear multiloop controllers to control p_i with v_i based on model (10.12). Once the feedback action for $v_i(t)$ is obtained, the actual input to the process is determined through (10.11).

The transformation procedure described above is well-known in robotics controller design applications (Asada and Slotine, 1986; Spong and Vidyasagar, 1989). Kravaris and Chung (1987), apparently unaware of the earlier work by Freund (1973, 1975, 1982), have rederived the results shown above for the special case of SISO nonlinear control problems. In their work they referred to this procedure as global input/output linearization synthesis. Kravaris et al. (1989) reported of a successful application of this theory in a copolymer composition control problem. Lee and Sullivan (1988a,b) advocate a special case of the general procedure

outlined by Freund (1973,1975,1982) and Kravaris and Chung (1987) for controller design which they have coined Generic Model Control (GMC). Boye and Brogan (1986) have also proposed a similar transformation approach to nonlinear control design. Unlike the work above, their paper was more concerned with a less meaningful first derivative trajectory tracking problem.

The order of p_i (d_i in (10.12)) is determined by the differential order of the nonlinear system with respect to the inputs. In previous chapters it was shown that the manipulated flow rate inputs to the SBR semi-batch polymerization process affects the first derivative of the instantaneous properties to be controlled. This implies that $d_i = 1$. In most batch/semi-batch reactor control problems the manipulated inputs will affect first derivative of the outputs being controlled and therefore the case were $d_i = 1$ would be most common. This is especially true for batch/semi-batch copolymerization process. However, a differential order of 1 would not be expected for different polymer reactor configurations, such as reactor trains. In this case the differential order of input manipulations made to the first reactor with respect to outputs in the final reactor in the reactor train would be at least equal the number of reactors in the train.

Given that $d_i = 1$, a convenient selection for $\delta_{0,i}$ and θ_i must be made. The most simple choice which leads to the least computational effort to arrive at feedback control actions is given by

$$\delta_{0,i} = 0 \tag{10.13}$$

$$\theta_i = 1 \tag{10.14}$$

This choice simplifies the multivariable control problem to designing SISO controllers for a decoupled set of integrating linear processes with time domain dynamics

$$\dot{p}_i = P_i(x,u,t) = v_i(t) \tag{10.15}$$

and Laplace transfer function

$$\frac{p_i(s)}{v_i(s)} = \frac{1}{s} \tag{10.16}$$

Virtually any continuous time nonlinear controller design procedure can be applied to (10.16) in a straightforward manner. In this work it was considered convenient to select a SISO design procedure that is simple to tune with meaningful tuning parameters in terms of a desired closed-loop output response. Hence a Dahlin (1968) or Internal Model Control (Garcia and Morari, 1982) pole-placement design specification given by

$$\frac{p_i}{p_{set,i}} = \frac{1}{1 + \tau_{c_i} s} \tag{10.17}$$

was taken. This specification will lead to a first order step response to step set changes or set disturbances at the process output. The only design parameters that have to be specified are the closed-loop first order time constants of each output (τ_{c_i}). It can be shown that the Dahlin closed-loop specification will lead to the feedback controller

$$v_i(t) = \frac{1}{\tau_{c_i}} e_i(t) \tag{10.18}$$

where $e_i(t)$ is given by (10.3). Inserting (10.18) into (10.15) will lead to

$$\dot{p}_i(t) = P(x,u,t) = \frac{1}{\tau_c} e(t) \tag{10.19}$$

This is the final form of open-loop feedforward/feedback control action to be applied on-line. If we recall back to the open-loop control strategies proposed in chapter 9 that were in the form

$$\dot{p}(t) = P(x,u,t) = 0 \tag{10.20}$$

we can observe that the only difference between (10.19) and (10.20) lies on the right hand side where 0 is replace by $\tau_c^{-1} e(t)$ when feedback correction is applied. Hence the nonlinear pole-placement procedure based on the input/output linearization transformation ultimately leads to only a trivial modification to the open-loop input control action.

The form of the control law given above can be modified to correspond with control block diagram proposed in Figure 10.1. It can be shown that process model (10.9) and (10.10) can be rearranged into the form

$$\dot{p}(t) = P_1(x,t) + P_2(x,t)u(t) \tag{10.21}$$

Inserting (10.19) into (10.21) and solving for $u(t)$ leads to

$$u(t) = P_2^{-1}(x,t)\frac{1}{\tau_c} e(t) - P_2^{-1}(x,t)P_1(x,t) \tag{10.22}$$

The first term of the right side of (10.22) is the feedback control block contribution to $u(t)$ ($u_{fb}(t)$). This term can be observed to be a product of a time varying nonlinear term and the linear control action. The second term on the right hand side represents the feedforward open-loop control block contribution to $u(t)$ (u_{ol}) provided from some instantaneous operating policy.

The literature reporting the use of global input/output linearization synthesis have taken a different approach to the design of the feedback controller in the linear space. Kravaris and Chung (1987), Kravaris et al. (1989), Lee and Sullivan (1988a,b) proposed the use of a PI controller in form

$$v(t) = K_{c_i}\left\{e(t) + \frac{1}{\tau_{I_i}}\int e_i(t)dt\right\} \tag{10.23}$$

that leads to the closed-loop transfer function response

$$\frac{p_i(s)}{p_{sst,i}(s)} = \frac{2\tau_{c_i}\zeta_i s + 1}{\tau_{c_i}^2 s^2 + 2\tau_{c_i}\zeta_i s + 1} \tag{10.24}$$

where

$$\tau_{c_i} = \frac{1}{\sqrt{\frac{K_{c_i}}{\tau_{I_i}}}} \tag{10.25}$$

$$\zeta_i = \frac{K_{c_i}}{2}\tau_{c_i} \tag{10.26}$$

This type of feedback design is also used in robotic control applications (Spong and Vidyasagar, 1989; Asada and Slotine, 1986). Relative to controller design procedure previously described, their design approach would be considered by many process control engineers to be far less appealing. By adding the integral term in (10.23) relative to (10.18) they have doubled the number of tuning parameters that need to specified. The resulting closed-loop response, given by (10.24) is much less meaningful and more difficult to specify than (10.17). It is difficult imagine why anyone would desire to work with such an unusual closed-loop response design. Their justification in adding the integral term to (10.23) relative to (10.18) has to do with model mismatch. Without much reflection on the matter, their argument does seem plausible. When model mismatch is present, the open-loop feedforward term in (10.22) and the linearizing transformation between $u(t)$ and $v(t)$ may become biased. If model mismatch causes this bias to persist or increase with time, the proportional feedback term in (10.22) will not be capable of eliminating this error in an asymptotically constant sense. Hence the use of the integral term in (10.23) was suggested as a simple ad hoc approach for eliminating a persistent bias due to model mismatch. Of course their procedure will only be valid for the simple case where one can directly measure the outputs to be controlled.

Based on arguments above, one would expect the computation of feedback control through (10.18) to be inadequate for practical process implementation since no accommodation is provided in the feedback design for model mismatch. However, this will not be true when using (10.18) in the control scheme of Figure 9.1.

The model mismatch problem in the overall control strategy proposed by the authors above was not an inherent difficulty in the control design procedure. The problem was rather due to the fact that they failed to design a consistent output estimator (refer to chapter 8.6 for a discussion on state estimator consistency). In their work no nonstationary disturbance or model mismatch states were introduced in the model to account for observed differences between the ideal model predicted responses and observed ones. Hence they had no choice but to resort to the ad hoc feedback design specification (10.23) since no use is made of the information on the deviation between model predicted outputs and the observed ones to adapt the model, and eliminate bias in the feedforward and feedback control actions. As stated above, this ad hoc approach for compensating for model mismatch in the feedback control design will only work when a direct output measurement is available. One might consider their a approach useful alternative in this case since the design of a state estimator may be avoided. On the other hand, if one invests a considerable effort in a arriving at a mechanistic or semi-theoretical nonlinear dynamic process model for high performance control, it would make little sense to fall short of identifying meaningful sources of disturbances and/or model mismatch. Intuitively, by incorporating more knowledge about distances and sources of model uncertainty into the overall controller design scheme, one would expect improved convergence of the control actions to desired values, and hence overall improved control. The consequence of not meeting the consistency requirement will be very serious when outputs must be inferred using a state estimator, as is the case with this SBR semi-batch problem. Not meeting the consistency requirement in the estimator will led to biased output predictions that will be impossible to correct with feedback control since in this case one has no actual property measurement. As was discussed in chapter 8, the state estimator used in this work meets the consistency requirement on the important observable state that are needed for property predictions. Therefore, the use of the use of the much more convenient control law (10.18) is adopted in this work.

Figure 10.5 shows the simulated application of the proposed nonlinear pole-placement feedback design. The controller shown was tuned with all τ_{c_i} set to 20 minutes. The operating conditions are the same as the PI simulation run shown in Figure 10.4. The same instantaneous property and flow rate information as was shown in Figure 10.4 is also provided. Relative to the open-loop policy shown in Figure 10.3, a tremendous improvement in copolymer property control can be observed in Figure 10.5. The quality of control relative to the PI design in Figure 10.4 is approximately the same. A slight improvement can be observed in the instantaneous copolymer composition response to the intialization error with the nonlinear pole-placement design. The flow rate manipulations, shown in Figure 10(e), respond quickly to the initialization error once detected and are well-behaved during the entire run. In Figure 10.5(c), a small bias can be observed between

the actual instantaneous molecular weight (-) and its estimated level (..). This problem is not the fault of feedback control but rather due to the estimator, since the estimated instantaneous molecular weight can be observed to be controlled quite well at its set point. The bias is due to molecular weight properties not being observable from the available measurements used in the state estimator. Even through some error was encountered, the deviation was not very significant, and much improved over the open-loop run response in Figure 10.3.

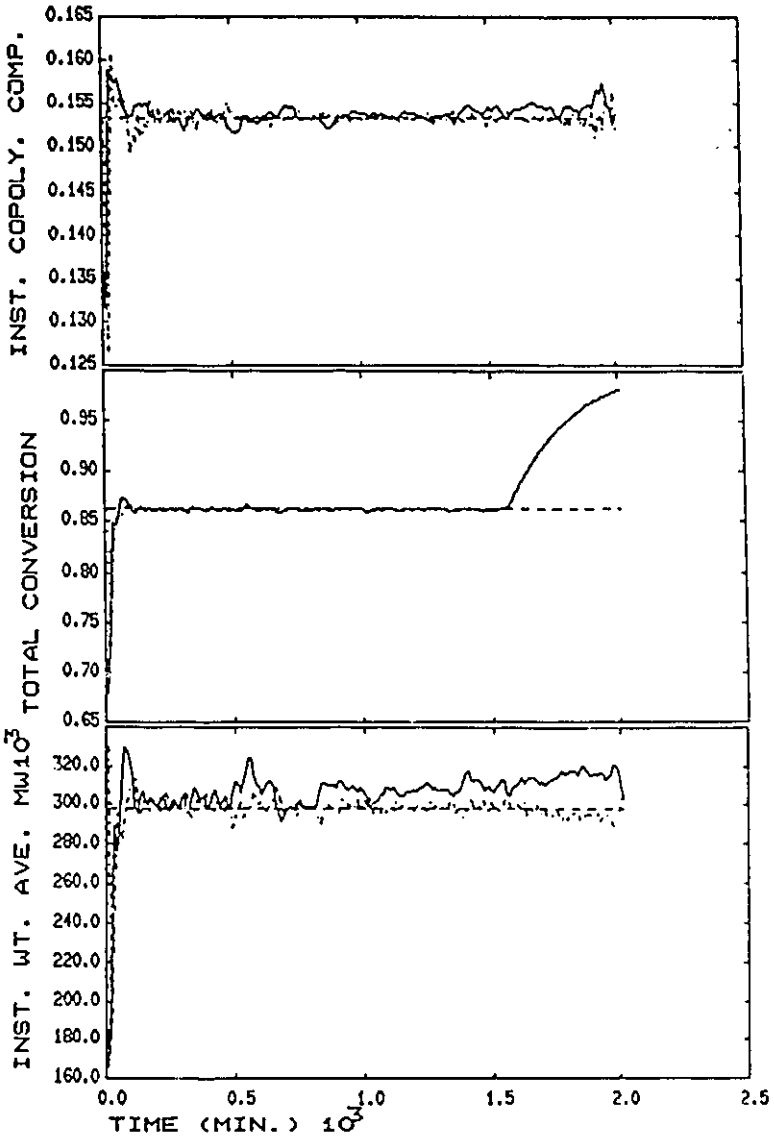
INST. COPOLY. COMP.
0.165
0.160
0.155
0.150
0.145
0.140
0.135
0.130
0.125
TOTAL CONVERSION
0.95
0.90
0.85
0.80
0.75
0.70
0.65
INST. WT. AVE. MW10^{-3}
320.0
300.0
280.0
260.0
240.0
220.0
200.0
180.0
160.0
0.0
0.5
1.0
1.5
2.0
2.5
TIME (MIN.) 10^{-3}

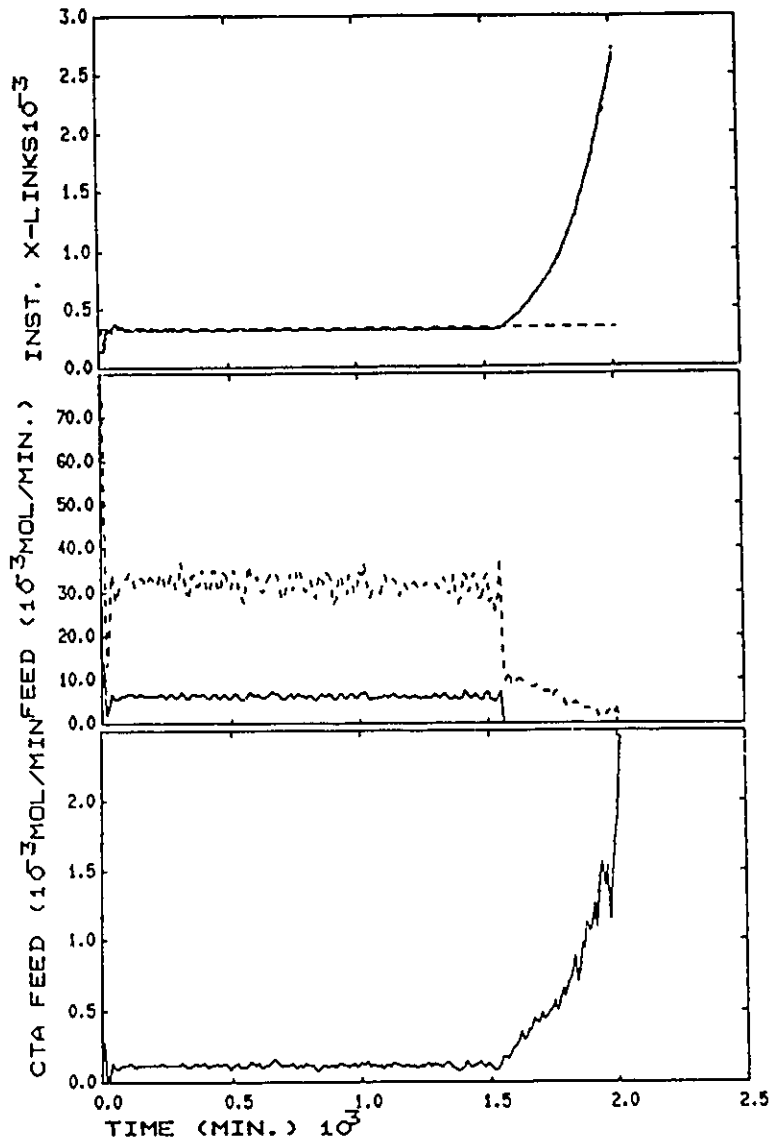

FIGURE 10.5: Instantaneous Property Control With Linearized Decoupled Design curve identification as in Figure 10.3

As discussed earlier, the state estimator used in this work meets consistency requirements. By incorporating the nonstationary stochastic states $x^{s^T} = \left(N_p, F_{Im_p}, x^{14}, x^{15}\right)$ (refer to chapter 8 for details) in the state estimator, it was shown that the important observable states needed for property calculations can estimated without bias even in the presence of model mismatch. During the control run, these nonstationary state estimates together with the estimated deterministic ones are used in both the feedback and feedforward control runs. Therefore, convergence to the desired closed-loop response, even in the presence of model mismatch, should be achieved for the observable properties.

Figure 10.6 shows the performance of the proposed nonlinear pole placement design when unaccounted for model mismatch is introduced. In the program used to simulate the true dynamic response of the process, the previously used inlet organic impurity feed F_{Im_p}, given by $5x10^{-6}F_{M_a} + 4.5x10^{-5}F_{M_b}$, was replaced with $3x10^{-6}F_{M_a} + 2.7x10^{-5}F_{M_b}$, and an inlet water phase impurity feed F_{Im_w} equal to $1x10^{-5}(F_{M_a} + F_{M_b})$ was introduced. In section 8.6.1, it was pointed out that this type of model mismatch can be shown to introduce error in the prediction of $\overline{n}$, the average number of radicals per particle. The control of the observable properties copolymer composition and conversion, shown in Figures 10.6(a) and 10.6(b) is still quite good and without offset in the presence of this specific type of model mismatch. The observed closed-loop response of the controller when the result of the initialization error was detected in these properties is still very good compared to the nominal response shown in Figure 10.5. The input manipulations, shown in Figures 10.6(e) and 10.d(f) do not go unstable and are well-behaved during the run. The control of copolymer composition can be observed to be a little more noisy about the set point relative to the nominal case. A small drift in copolymer conversion can be observed to occur at the time when the styrene feed was stopped. By comparing actual copolymer composition (-) with its estimated value (..), it can be observed that the problem is not due to the controller but rather a convergence problem in the estimator that requires some time for convergence to a new suitable fictitious level for F_{Im_p} once operating conditions are significantly changed. Unlike the control of copolymer composition and conversion, a small off-set in the control of molecular weight can be observed in Figure 10.6(c). This can expected since molecular weight is not observable. Nevertheless, the observed bias is not very large, and much closer to set point that one would obtain through the application just an open-loop operating policy. The control of crosslinking, shown in Figure 10.6(d), can be observed to be very good in the presence of model mismatch since constant monomer concentration in the polymer particles was approximately maintained. The required conversion level of controlling instantaneous degree of crosslinking was shown in section 9.5 to be independent from the level of impurity. The observed favorable robustness properties of the proposed design will extended to other types of model mismatch where the prediction of the

average number of radical per particle is affected, such as important model mismatch associated with initiation, multiple impurities, radical entry, and diffusion controlled termination effects for example. For a more detailed discussion refer to section 8.6.1.

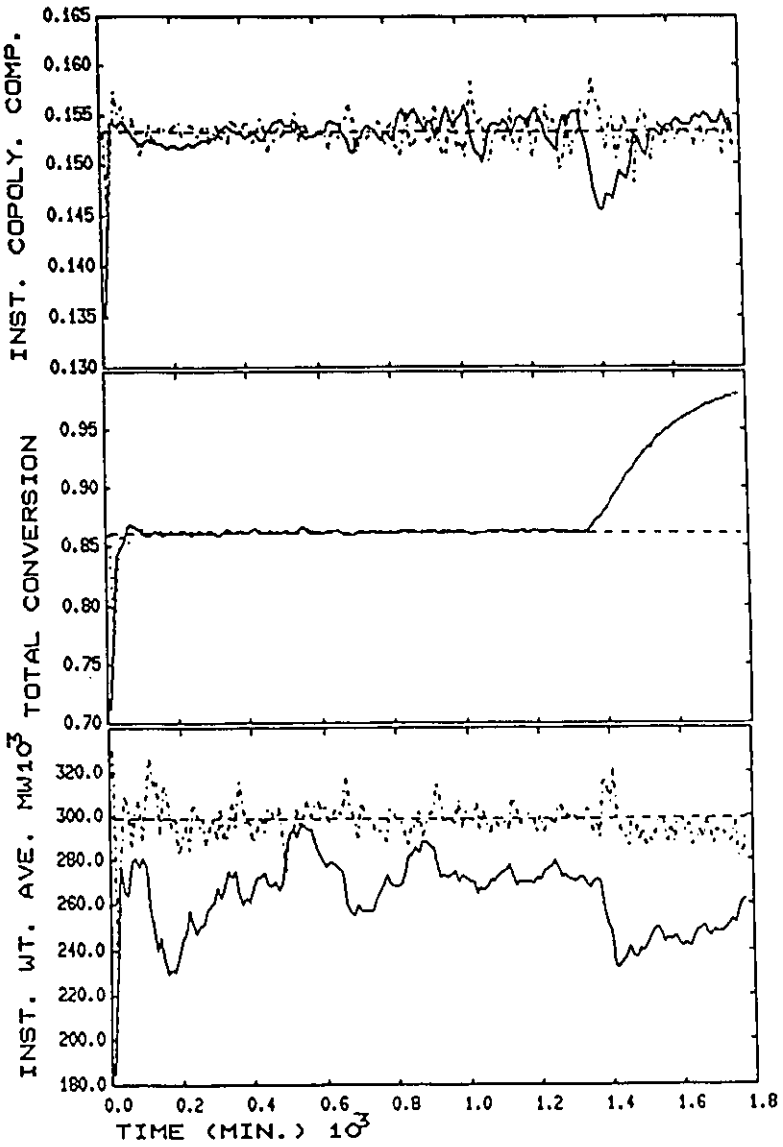
INST. COPOLY. COMP.
0.165
0.160
0.155
0.150
0.145
0.140
0.135
0.130
TOTAL CONVERSION
0.95
0.90
0.85
0.80
0.75
0.70
INST. WT. AVE. MW10^3
320.0
300.0
280.0
260.0
240.0
220.0
200.0
180.0
0.0
0.2
0.4
0.6
0.8
1.0
1.2
1.4
1.6
1.8
TIME (MIN.) 10^3

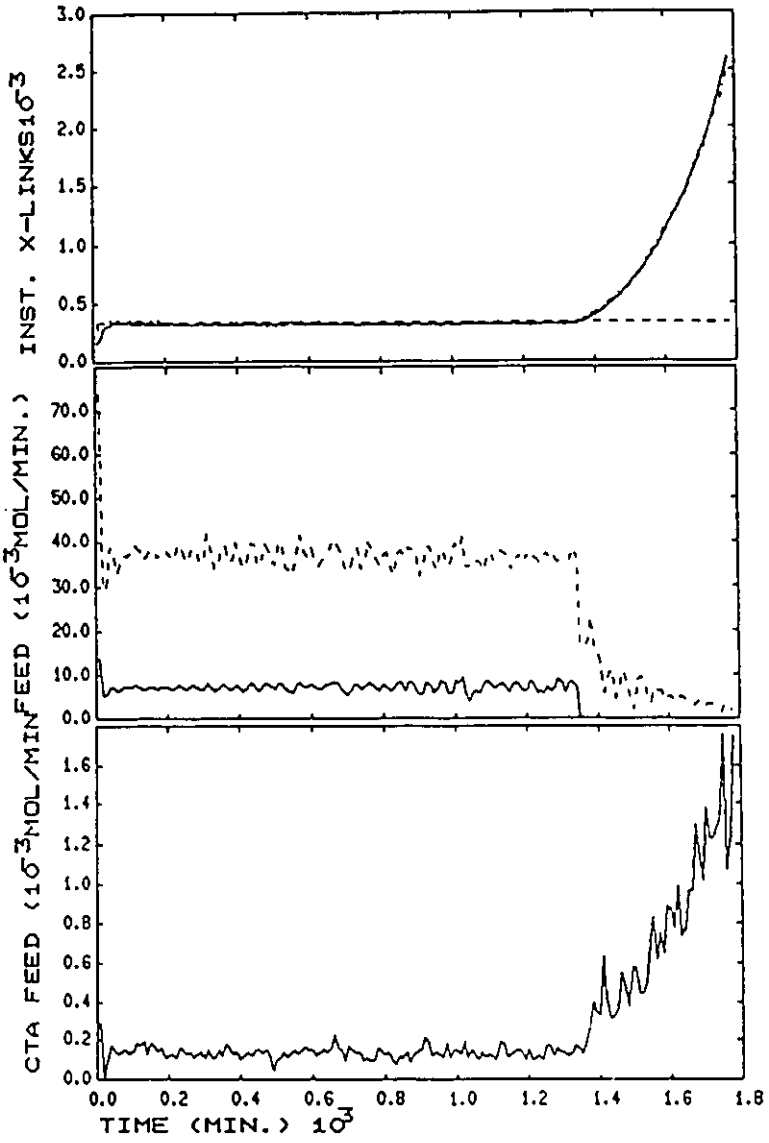

FIGURE 10.6: Control With Linearized Decoupled Design: Water Phase Impurity Model Mismatch
curve identification as in Figure 10.3

Figure 10.7 shows the performance of the nonlinear pole-placement design to a completely different type of model mismatch. In this run, the propagation rate constant for butadiene (k_{pb}) and its copolymer reactivity ratio with styrene (r_b) were increased by 30% in the model used to simulate the actual process. Relative to the nominal model response in Figure 10.5, the control of the copolymer composition and conversion is still good and free from offset when subjected to this significant type of model mismatch. The controlled molecular weight response to the initialization error, shown in 10.7(c), has degraded relative to the nominal case, but does eventually converge to the desired set point in a reasonable period of time. The result is still very impressive given that this output is not observable, and that the mismatch introduced does influence the molecular weight. In Figure 10.7(d) an offset from the desired degree of crosslinking can be observed, even though the estimator provided biased-free predictions. It can be shown that the mismatch introduced does influence the required monomer concentration in the polymer particles for a specified degree of crosslinking. Hence, the problem can only be corrected by changing the conversion level. If one is really more concerned with controlling crosslinking the use of a direct crosslinking control policy, such as described in section 9.5, would prove to be more effective in this case. The closed-loop performance of the manipulated inputs in Figures 10.7(e) and 10.7(f) are stable and well behaved. Based on the discussion in chapters 8.6.2 and 8.6.3, the results from this mismatch case study can used to infer that the robustness properties of the proposed design will also perform well for the important class of model mismatch associated propagation, chain transfer, and mass transfer. This mismatch case study, along with the previous one provides sufficient evidence that the control strategy procedure posses favorable robustness properties with respect to important model mismatch that one would encounter during implementation.

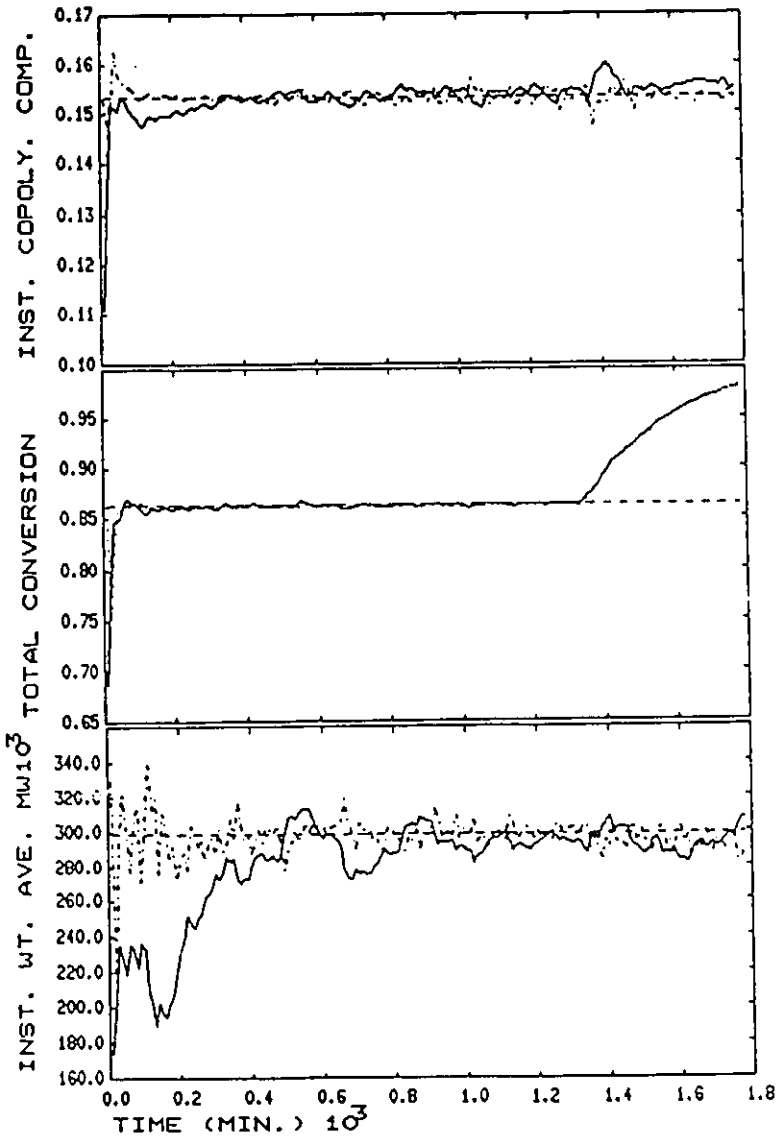
INST. COPOLY. COMP.
0.17
0.16
0.15
0.14
0.13
0.12
0.11
0.10
TOTAL CONVERSION
0.95
0.90
0.85
0.80
0.75
0.70
0.65
INST. WT. AVE. MW10^3
340.0
320.0
300.0
280.0
260.0
240.0
220.0
200.0
180.0
160.0
0.0
0.2
0.4
0.6
0.8
1.0
1.2
1.4
1.6
1.8
TIME (MIN.) 10^3

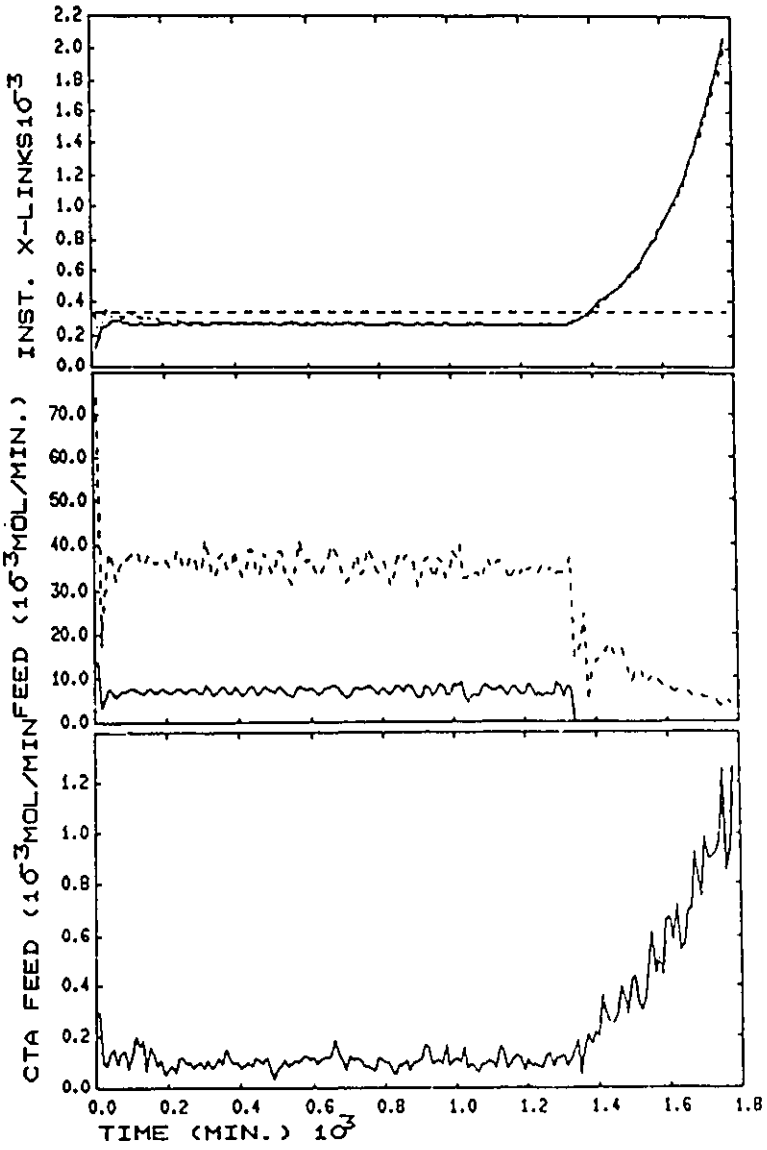

FIGURE 10.7: Control With Linearized Decoupled Design: Rate Constant And Reactivity Ratio Model Mismatch
curve identification as in Figure 10.3

The previous two mismatch case studies were concerned with prediction errors present in the dynamic process model. A different type prediction mismatch which is also important has to do with unaccounted for state initialization error. Recall that the state estimator used in this work focused on initializations errors in Im_p, N_p, and F_{Im_p}. In an actual industrial implementation of the control strategy proposed an error can also be introduced in the remaining model states as a result of a late detection in the start of reaction. Figure 10.8 shows performance of the controller design for the extreme case where the estimator and controller is started one full sampling interval too late (10 minutes). During the undetected period, the monomer level in the reactor dropped from 0.07 and 0.27 to 0.031 and 0.083 gmoles of styrene and butadiene respectively. Relative to the nominal run in Figure 10.5, control of copolymer composition, conversion, and degree of branching are not seriously degraded by the intialization error. However, Figure 10.8(c) shows that the initialization error leads to a significant loss in performance for molecular weight control. Performance is still much improved over the open-loop case shown in Figure 10.3(c). The only possible improvement that one might try to reduce the problem would to take a measurement from the process at t=0, and use the measurement to improve some of the starting model state estimates. Not much more can be done because of the lack of a suitable measurement that would allow one to observe molecular weight.

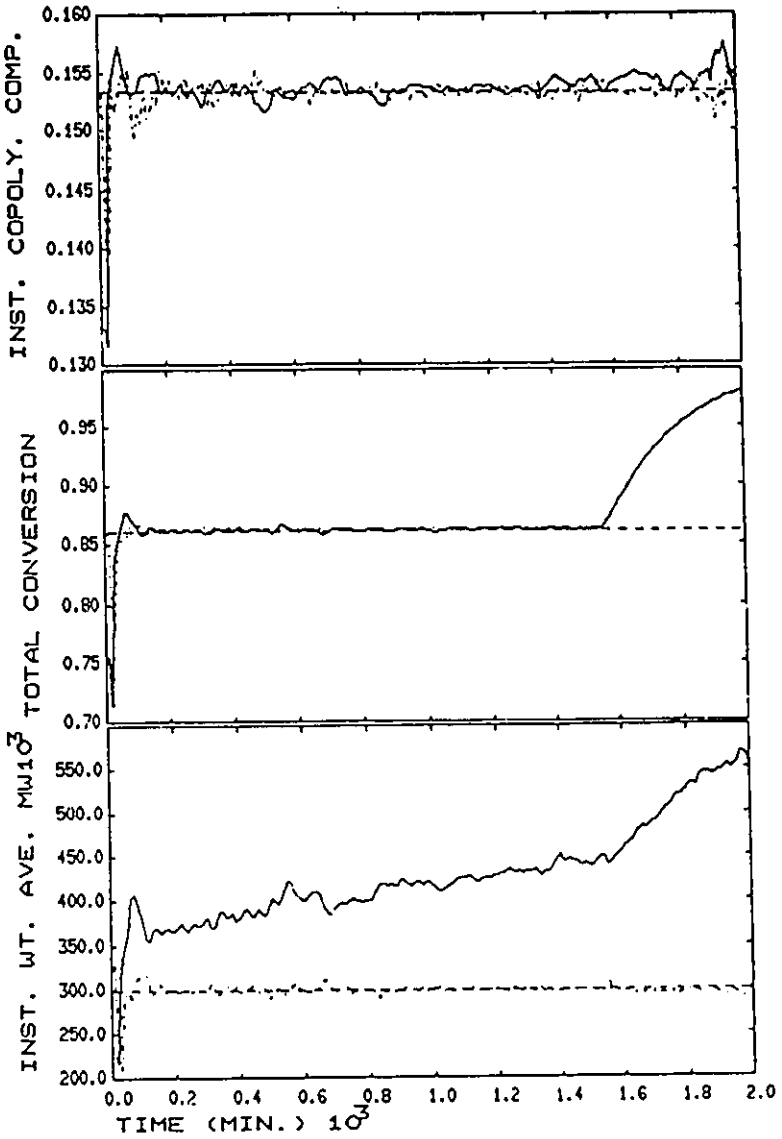
INST. COPOLY. COMP.
0.160
0.155
0.150
0.145
0.140
0.135
0.130
TOTAL CONVERSION
0.95
0.90
0.85
0.80
0.75
0.70
INST. WT. AVE. MW10^3
550.0
500.0
450.0
400.0
350.0
300.0
250.0
200.0
0.0
0.2
0.4
0.6
0.8
1.0
1.2
1.4
1.6
1.8
2.0
TIME (MIN.) 10^3

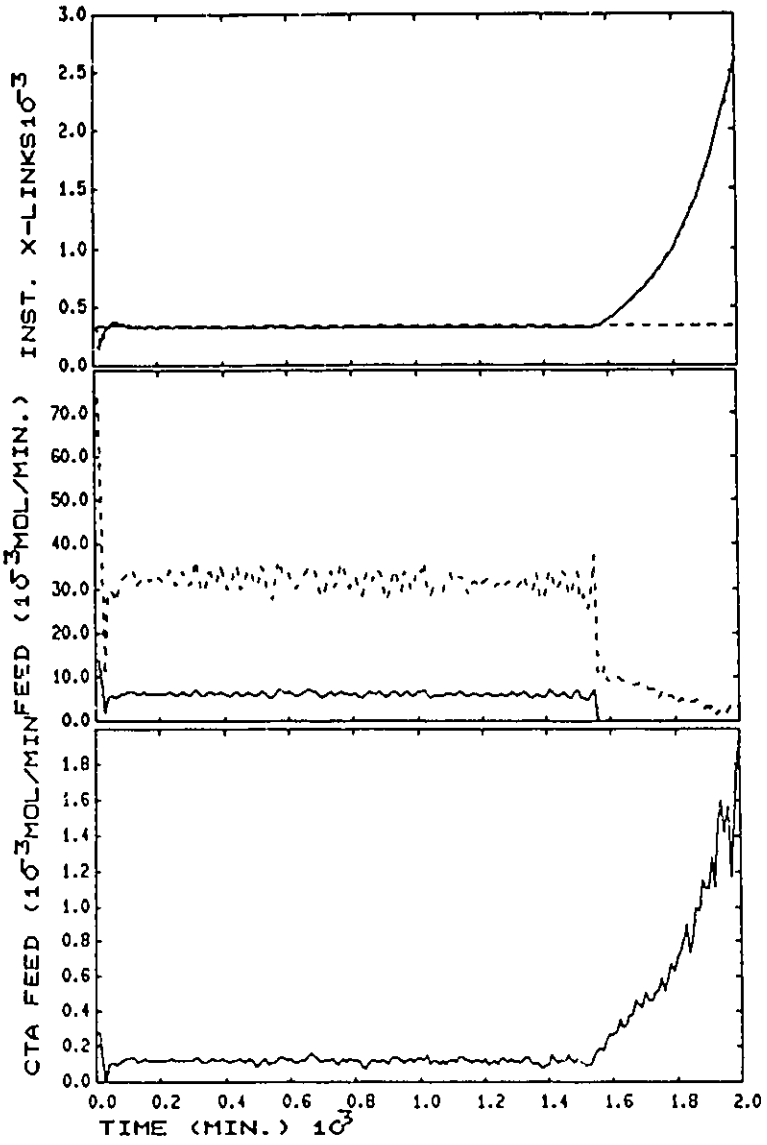

FIGURE 10.8: Control With Linearized Decoupled Design: Initialization Error Model Mismatch
curve identification as in Figure 10.3

The results of this section have demonstrated that global nonlinear input/output linearization approach of Freund (1973,1975,1982) is very well-suited for applying nonlinear multivariable feedback in the nonlinear inferential control scheme shown in Figure 10.1. The application of feedback control when taking this procedure requires only a trivial modification to the open-loop policies described in chapter 8. The modification required, in terms of prior programming effort, is even more trivial than the in the PID design approach of section 10.3. A feedback controller in the linearized space based on a Dahlin (1968) closed-loop specification was found to be very effective in controlling instantaneous properties at both nominal and important model mismatch conditions. The use of the Dahlin (1968) closed-loop specification only requires the specification of one meaningful tuning parameter for each controlled output. This is an improvement over the suboptimal PID design procedure where much more, less meaningful tuning parameters need to specified. The Dahlin design specification in the overall approach taken in Figure 10.1 is also far more meaningful and more generally applicable than other reported approaches using input/output linearizations (Kravaris and Chung, 1987; Kravaris et al., 1989, Lee and Sullivan, 1988a,b) where no account for disturbances or model mismatch was taken in the estimation procedure. The only restrictions with the input/output linearization approach are that it is not well-suited for general nonsquare control problems, systems with deadtime, and control problems with constraints. The case of more outputs that inputs may be indirectly handled through the trade-off policies discussed in section 9.7.2. Even though these limitations exist, the approach will still be expected to be useful for a wide range of industrially relevant problems, and therefore the simplicity offered by this method should not be overlooked.

10.5 MODEL-BASED OPTIMAL FEEDBACK CONTROL

If the simple control strategies in sections 10.3 and 10.4 are not well-suited for high performance feedback control, one might consider instead the use of some model-based optimal feedback design. In the control literature, there exists a plethora of different optimal model-based design procedures. No attempt shall be made to cover all the different approaches that one might try. Only a brief outline on the method for using the more popular optimal and optimal designs at quasi-linearized conditions shall be discussed. The main issue is the method for incorporating model based design procedures in the strategy proposed in Figure 10.1. This main idea should be conveyed in the designs to be discussed below.

A commonly used objective function for determining optimal feedback control moves ∇u is given by

$$\underset{\nabla u_1, \nabla u_2, \ldots, \nabla u_m}{\text{Min}} \quad J_{fb} = \sum_{i=1}^{h} \sum_{j=1}^{n} (p_{j,sst} - \hat{p}_{j,t+i})^2 Q_{i,j} + \sum_{i=1}^{m} \sum_{j=1}^{r} \nabla u_{j,t+i-1}^2 W_{i,j} \tag{10.27}$$

In (10.27), h refers to the future output horizon, n is the number of outputs to be controlled, m is the number of future control moves to be made, r is the number of inputs, and $Q_{i,j}$ and $W_{i,j}$ are weighting parameters. All of these parameters are specified to design the controller. The inputs in (10.27) are taken to be piecewise continuous for simplicity. The number of piecewise control actions to be taken between the measurement interval must also be specified. Logically, the future output horizon h would extend to the time of the next measurement interval, or multiples of it, and the optimization problem posed in (10.27) would be resolved at every measurement interval. General operating constraints may also added to problem posed above that must be satisfied at the control intervals.

The level of difficulty in arriving at optimal feedback control actions in (10.27) depends heavily on the type of process model to be used in (10.27), and of course the nature of operating constraints if present. Consider the case where one makes use of a process model in the form

$$\dot{\bar{x}} = \bar{f}(\bar{x}, \bar{u}, t) \tag{10.28}$$

$$\bar{p} = \bar{P}(\bar{x}, t) \tag{10.29}$$

to arrive at nonlinear optimal control actions. The nonlinear model above is presented in deviation form about some feedforward/open-loop trajectory provided by some instantaneous control policy. If this nonlinear model is used, an on-line nonlinear optimization search approach will have to be carried out to arrive at the optimal input actions. Several researchers have advocated the use of this type of on-line optimization procedure for computing nonlinear control actions in closely related class of nonlinear controller design approaches. Included in this class are Nonlinear Internal Model Control (NIMC) (Economou and Morari, 1986; Li and Biegler, 1988), Nonlinear Model Predictive Control (NMPC) (Patwardhan et al., 1988), Nonlinear Inferential Control (Parrish and Brosilow, 1988), Universal Dynamic Matrix Control (UDMC) (Morshedi, 1986), and an on-line optimization using a two phase approach (Chen and Joseph, 1987; Jang et al., 1987). The use of these approaches will involve a tremendous prior programing effort for implementation relative to the strategies described in sections 10.3 and 10.4. During implementation, a significant computational effort will have to be made relative to the previous approaches, even when adopting computationally efficient solution procedures that some of the authors above have suggested. Depending on the size of the control problem posed, the on-line computational effort required may not be practical. Much of the success that the authors above have reported were based on much more simple nonlinear problems than the SBR semi-batch problem considered

in this work. Another important potential problem that one must face when adopting this approach is that there is no guarantee of convergence to a solution during application since a general nonlinear problem is involved. When applying a controller to an industrial profit making process, integrity is a very important concern.

Often the level of detail provided by the dynamic model would not justify the application of the brute force approach described above. This would certainly be true for the SBR model used in this work. Also, in many circumstances, the optimal solution for (10.27) can be approximated reasonably well through a quasi-linearization of the process at each control interval. If the deviation nonlinear process model about the open-loop/feedforward trajectory is linearized and discretized at control interval k, one obtains

$$\tilde{x}_{k+1} = \tilde{A}_k \tilde{x}_k + \tilde{B}_k \tilde{u}_k \tag{10.30}$$

$$\tilde{p}_{k+1} = \tilde{P}_k \tilde{x}_k \tag{10.31}$$

Given (10.30) and (10.31), a future horizon, linear quadratic (LQ) model-based design, such as Dynamic Matrix Control (Cutler and Ramaker, 1979), can be easily applied. The approach has the advantage of being capable of handling linear operating constraints. Background material on DMC can be found in chapter 5. During on-line implementation, the step response coefficients needed to obtain the dynamic matrix can be obtained recursively through (10.30) and (10.31) by setting $\tilde{u}_{k_j} = 1$. The future projected error vector without control, e_{k+1} (refer to chapter 5), in the DMC algorithm can be obtained by recursively solving (10.30) and (10.31) forward in time with $\tilde{u}_k$ set to 0. Alternatively, a hybrid procedure could be applied whereby e_{k+1} is computed by integrating the nonlinear model forward in time. This hybrid approach was used by Garcia (1984) when applying DMC to control temperature in a batch polymerization reaction. Relative to a formal nonlinear optimization feedback controller design, the use of DMC would be expected to substantially reduce the on-line computation effort. A big advantage of DMC is that convergence to a unique solution can be guaranteed, provided that singular control problem has not be posed.

If process operating constraints are of no concern, one may want to make use of an analytical design procedure for computing LQ optimal feedback actions. Linear quadratic state space feedback control is well-known and is often found to be useful when working with state space process models. Given a linearized and discretized model in the form (10.30) and (10.31) at some control interval k, a control law in the form

$$\tilde{u}_k = L_k \tilde{x}_k \tag{10.32}$$

can be found that will minimize

$$J_{p_k} = \vec{p}^T Q \vec{p} + \sum_{i=1}^{h-1} (\vec{p}_i^T Q \vec{p}_i + \vec{u}_i^T W \vec{u}_i) \tag{10.33}$$

The solution for L_k is well-known, and can found elsewhere (Astrom and Wittenmark, 1984; Kwakernaak and Sivan, 1972). The use of this feedback control strategy has been successfully applied to batch polymerization applications (Ponnuswamy et al., 1987; Kiparissides et al., 1987). Unfortunately, for the feedback control strategy being considered in this work, the control law given by (10.32) will not be useful. The form of (10.32) is only suitable for controlling the process model states along some predetermined open-loop trajectory. In this work we wish to modify the state trajectory so that the desired p is obtained. An estimated deviation in an instantaneous property $\vec{p}$ cannot be uniquely related to $\vec{x}$ since $\vec{P}$ is nonsquare. Therefore, the use of an input/output control law is required.

Using (10.30) and (10.31), the pulse transfer function relationship between $\vec{u}$ and $\vec{p}$ at control interval k is given by

$$\vec{p}(z) = G_k(z)\vec{u}(z) \tag{34}$$

with

$$G_k(z) = z^{-1}\vec{P}_k(I - \vec{A}_k z^{-1})^{-1}\vec{B}_k \tag{10.35}$$

This process transfer function model can used to obtain a LQ optimal control law in the form

$$\vec{u}_k = C_k(z)(p - \vec{p})_k \tag{10.36}$$

for the special case of (10.33) with $h = \infty$. The LQ optimal solution for $C_k(z)$ can be found in Harris and MacGregor (1987). Alternatively, (10.35) can instead by used in IMC design procedure presented in chapter 4. The solution for $C_k(z)$ can be recomputed on-line at every control interval. When taking this approach, one should consider the use of some fixed average $C(z)$ over the operating conditions to be expected. This simplification, if found acceptable, would lead to a significant reduction in on-line computation.

The methods described above can be useful for correcting the open-loop/feedforward inputs for errors due to nonideal operating conditions. The drawback with these approaches is that they will all require a considerable prior programming effort and a substantial computational effort during on-line application relative to both the PID design strategy in section 10.3 and the input/output linearization approach of section 10.4. Hence, there is no incentive to apply these procedures in such a clumsy fashion to the control strategy in Figure 10.1, especially when both the PI design and the input/output linearization approach performed so well. The only situations where one would benefit by taking these approaches is when a serious constraint problem is

encountered or when process deadtime is significant. Since both of these problems are not considered to be important in the semi-batch SBR problem, the use of these optimal model-based control strategies were not considered in this work.

10.6 SUMMARY AND CONCLUSIONS

In this chapter, the design of the feedback controller block in the nonlinear inferential control scheme of Figure 10.1 was addressed. Three different basic design approaches were considered, and two were evaluated. Controller designs were evaluated in a simulated application of a semi-batch operating policy where copolymer composition, conversion, and weight average molecular weight were controlled using monomer flow rate and modifier flow rate as manipulated inputs. Performance of the controller designs to initialization errors in the level of organic reactive impurity and particle number with noise corrupted measurements was investigated.

The first approach to controller design considered was classical PID input/output pairing control. This method is simple to apply in strategy of Figure 10.1, and for the case study considered, led to good control once suitable decoupled input/output pairing and PI tuning parameters were found. Copolymer property control was greatly improved compared to the case where a fixed off-line computed policy was applied. The drawback with the approach is that large number of optimal PID parameters for the range of operating conditions that need to be determined by exhaustive prior simulation.

The second approach considered made use of a global decoupling input/output linearization transformation proposed by Freund (1973, 1975, 1982). The procedure was shown to lead to a very trivial modification of open-loop control policy computation suggested in chapter 9 for obtaining input trajectories. The linear feedback controller design proposed for decoupled output/linearized input space was based on the Dahlin (1968) response specification. This closed-loop design specification was considered far more convenient and meaningful relative to previously proposed design strategies (Kravaris and Chung, 1987, Kravaris et al, 1989, Lee and Sullivan, 1988a,b). It was pointed out that the Dahlin closed-loop specification was only possible because of the presence of the nonlinear estimator in Figure 10.1 which meets consistency requirements. This approach provided good copolymer property control in the simulation case study investigated. The performance of this design was also demonstrated to be robust to model mismatch,

disturbances, and initialization errors. Performance of this multivariable design relative to the PID approach was about the same. This approach was preferred over the PID design since less prior program effort is required and tuning is far more straightforward.

Finally, model-based optimizing feedback control strategies were considered. Relative to the designs discussed above, these approaches require a far greater programming effort and on-line computation. For the semi-batch SBR problem in this work, optimal feedback control design offers little or no advantage over the methods proposed above, and therefore its use was not investigated in this work.

The results of this chapter also provided the completion of the work on the development of a nonlinear inferential control strategy for a semi-batch copolymerization process. In this chapter, concepts related to dynamic polymer modelling (chapter 7), nonlinear state estimation (chapter 8), open-loop optimal operating policies (chapter 9), and feedback control design (chapter 10) are tied together, for the first time, to arrive at a simple and yet very effective, inferential nonlinear feedback control strategy for application to industrial semi-batch polymerization control problems. The proposed strategy is a much more simple alternative to computationally intensive on-line optimization procedures which would not be practical to apply in many circumstances and which would often not be considered acceptable by plant operating personnel. The performance of the overall design strategy was demonstrated in this chapter to be robust to process model mismatch, state initialization errors, and disturbances. In all cases investigated, copolymer property control was greatly improved over a fixed operating policy determined off-line. The results clearly demonstrate that use of the operating policies and control strategies advocated in this work have the potential for greatly improving product reproducibility and quality control in polymer manufacturing industries.

10.7 NOTATION

$A(x,t)$ nonlinear state transition matrix in nonlinear state space model (10.9)

$\tilde{A}_k$ linearized state transition matrix at control interval k along open-loop trajectory

$B(x,t)$ nonlinear input matrix in nonlinear state space model (10.9)

$\tilde{B}_k$ linearized state space input matrix at interval k along open-loop trajectory

Bn_i i'th branch frequency per copolymer chain

CTA moles of chain transfer agent

d disturbance vector

D_p unswollen volume average particle size

e error vector of instantaneous properties p from set point

E moles of emulsifier

$\vec{f}$ expression for derivative of $\vec{x}$

F_{CTA} molar feed rate of chain transfer agent

F_E molar feed rate of emulsifier

F_{Im_p} molar feed rate of organic phase impurity

F_{Im_w} molar feed rate of water soluble impurity

F_{I_n} molar flow rate of initiator

F_{M_b} molar feed rate of butadiene

F_{M_s} molar feed rate of styrene

F_s instantaneous styrene copolymer composition

F_{V_w} volumetric feed rate of water

G_k linearized input/output transfer function matrix at control interval k

h future output horizon for discrete feedback control

Im_p moles of unreacted organic phase impurity

Im_w moles of unreacted water phase impurity

I_n moles of unreacted initiator

J_{fb} cost function for model based feedback control

K_{C_j} proportional term in PID controller for j'th input

L_k proportional gain matrix at interval k in state space optimal feedback design

m future input horizon in model predictive feedback controller design

M_s moles of styrene

M_b moles of butadiene

n number of outputs

N_p number of polymer particles

$\hat{p}$	estimated instantaneous property vector
p_{set}	instantaneous property vector set point
$\tilde{p}$	instantaneous property vector in deviation form about open-loop trajectory
P	matrix expression representing the derivative of p with respect to time
$\tilde{P}$	nonlinear matrix relating $\tilde{p}$ to $\tilde{x}$
$\tilde{P}_k$	linearized output/state matrix at interval k along open-loop trajectory
P_b	moles of reacted butadiene in copolymer
P_0	initial covariance matrix of x in extended Kalman filter
P_s	moles of reacted styrene in copolymer
$Q_{i,j}$	output weighting for model prediction controller design
r	number of inputs
r_W	weight average copolymer chain length
R_v	covariance matrix of y in extended Kalman filter
R_w	covariance matrix of x in extended Kalman filter
s	Laplace transform
T	reactor temperature
Q_i	i'th molecular weight moment concentration
u	manipulated input vector
$\tilde{u}_k$	deviation input vector along open-loop trajectory at interval k
u_{fb}	feedback contribution to u
u_{ol}	open-loop/feedforward contribution to u
v	fictitious input vector obtained after decoupled global input/output linearization
V_p	volume of polymer particle phase
V_r	reactor volume
V_w	volume of water
$W_{i,j}$	input move weighting in model predictive controller design
x	model state vector

$\hat{x}$	estimated model state vector
$\tilde{x}$	model state vector in deviation form about open-loop trajectory
x^{14}	nonstationary stochastic mismatch state to compensate for model errors in rate of *CTA* reaction
x^{15}	nonstationary stochastic mismatch state to compensate for model errors in rate of M_b reaction
X	overall monomer conversion
y	measurement vector
z^{-1}	backward shift operator

Greek Letters

$\delta_{j,i}$	j'th degree coefficient of pole polynomial for i'th output in linearized decoupled space
ζ_i	2'nd order damping factor for closed-loop output response of i
θ_i	i'th output gain in linearized decoupled space
τ_{c_i}	closed-loop time constant specification for output i
τ_{d_j}	derivative term in PID controller for j'th input
τ_{I_j}	reset term in PID controller for j'th input

THESIS SUMMARY AND CONCLUSIONS

11. THESIS SUMMARY AND CONCLUSIONS

This section provides a summary of major results and conclusions made in this thesis. The summary is presented according to the three areas of in MIMO controller design research considered in this work, as described in the thesis introduction.

11.1. LINEAR MULTIVARIABLE CONTROLLER DESIGN: ROBUSTNESS AND APPROXIMATE INVERSES

Chapters 2 and 3 provided a review on currently popular frequency domain approaches for analyzing the robustness properties of linear multiple input/multiple output (MIMO) transfer function controller designs. The purpose of this work was to both evaluate and apply these popular approaches for predicting relative robustness properties of linear MIMO Internal Model controller designs in some general sense. Using these theories, three approaches to relative robustness assessment were considered. The first approach was based on a singular value and condition number analysis of the approximate model inverse used in the linear controller design. The second method made use of a singular value analysis where a single norm bounded, multiplicative output perturbation block in the frequency domain is used to characterize model mismatch (Doyle and Stein, 1981). The final approach investigated was a new method of relative robustness assessment proposed in this work. This approach was based on an equal percentage disk uncertainty radii in all elements of the nominal model transfer function at each frequency. The amount by which the equal percentage disk uncertainty radii at each frequency can be increased before the closed-loop system goes unstable was used as a measure of relative robustness. This new measure of relative robustness (κ) was introduced to reduce conservatism in the uncertainty characterization relative to the second approach. The computation of κ was shown to require the use of structured singular value theory (Doyle, 1982). In two model mismatch simulation case studies with different controller designs it was found that the prediction of relative robustness trends provided first and third approaches were always in agreement with the observed trends. The second approach was shown to always be at odds with the other robustness assessment methods and the observed simulation trends. The results showed that assessment of relative robustness is very dependent upon the model uncertainty

characterization used. Different characterizations can lead to totally contradictory results. It appears that a much more thorough understanding of the nature of the uncertainties is necessary if one is to put much faith in the conclusion of any robustness analysis.

The design of stable and causal approximate inverses model inverses for Internal Model Controllers (IMCs) was addressed in chapter 4. A linear quadratic optimal, matrix spectral factorization approach was proposed as a straightforward and computationally efficient method for obtaining inverses which yield excellent controller performance and robustness properties. Unlike any other approach proposed, this procedure automatically handles multivariable process transfer function matrices of arbitrary order, with unbalanced deadtime, with noninvertible zeros, and nonsquare systems. In two simulation case studies, it was shown that these inverses lead to improved nominal performance and robustness properties compared to the more traditional IMC designs where tunable diagonal filters are used with fixed, but usually suboptimal, inverses.

11.2. DISTURBANCE PREDICTION IN DYNAMIC MATRIX CONTROLLERS

In chapter 5, a new, and straightforward modification to the standard Dynamic Matrix Control (DMC) algorithm was proposed to improve to disturbance regulation. The optimality of DMC for disturbance regulation was generalized for all types of MIMO disturbances. The formal approach will lead to improved disturbance regulation when the standard DMC assumption that disturbances enter as decoupled deterministic steps at the process outputs is suboptimal. The proposed procedure makes use of autoregressive, integrated moving average disturbance models to predict the future response of disturbances, and is more computationally efficient and straightforward to apply relative to other approaches that have been reported. Three simulation case studies showing the benefits of the modification to the DMC algorithm were presented.

11.3. NONLINEAR INFERENTIAL FEEDBACK CONTROL FOR POLYMERIZATION REACTORS

Chapters 6 through 10 dealt with the different stages of the development of an inferential nonlinear feedback control strategy for a semi-batch copolymerization reactor. The strategy proposed featured a nonlinear state estimator to infer copolymer properties from limited indirect noisy measurements, a nonlinear open-loop feedforward compensator to maintain fixed instantaneous copolymer properties, and a linear

feedback controller to correct for errors in the feedforward control actions. In this work, the control of styrene/butadiene rubber (SBR) latex copolymer properties was considered. The strategy was evaluated in simulation study using a semi-theoretical SBR copolymerization model described in chapter 7.

The first problem examined was the design of a useful nonlinear state estimator. The nonlinear state estimator is required to infer copolymer properties to be controlled from limited, indirect noisy process measurements taken from the process during operation. Three approaches, extended Kalman filtering, extending Kalman filtering with global reiteration, and state estimation using an on-line nonlinear optimization approach were examined. The second approach was found to be most effective for semi-batch SBR state estimation, and was therefore adopted. The new results showing the relative performance of each strategy disputes the work of Jang et al. (1986), where performance of a nonlinear optimization approach was claimed to be far superior to extended Kalman filtering. The results of this work also demonstrate the importance of introducing sufficient meaningful nonstationary states in order to have consistent, biased free state estimates when nonideal process operating conditions are encountered. This important issue had been neglected in previously reported work where state estimators were developed for batch/semi-batch polymerization reactors, operating under ideal conditions.

Using the knowledge of the modelled chemical reaction mechanisms, open-loop/feedforward operating policies were proposed based on establishing conditions for maintaining fixed instantaneous copolymer properties. Well-known univariate approaches for instantaneous copolymer property control were extended to the multivariable case, and new policies were proposed. These optimal operating policies are very meaningful to polymer reaction engineers. The instantaneous control policies offer the advantage of computational simplicity in arriving at feedforward manipulated input trajectories, and because of this, can be recomputed on-line with improved state estimates provided by the nonlinear state estimator. The open-loop/feedforward actions provided by these policies serve to establish quasi-steady state conditions on the instantaneous copolymer properties to be controlled. This feature is shown to greatly simplify the subsequent feedback controller design. It is shown in this work that the use of instantaneous copolymer property or reactor condition control policies can allow one to produce copolymer with a wide range of property specifications.

The final subproblem of the semi-batch control strategy addressed was the design of a useful feedback controller. Three approaches, conventional paired PI, a multivariable decoupling and linearizing transformation approach, and model based optimal feedback control were considered. The second approach was found to be most convenient for use in the semi-batch control scheme. This approach was demonstrated

to provide excellent control over copolymer properties. The performance of the design was demonstrated to be robust to state intialization errors, disturbances, and model mismatch. In all cases examined, control over copolymer properties was far superior to the case where an off-line computed open-loop policy was applied. The results of this work demonstrate that the simple, but yet effective, semi-batch control strategy proposed in this work is a very useful alternative to computationally intensive on-line optimization approaches, which in many circumstances, would not be practical. This work also clearly demonstrates that the use of the operating policies and control strategies advocated in this work have the potential for greatly improving product reproducibility and quality control in polymer manufacturing industries.

LITERATURE CITED

12 LITERATURE CITED

Ahlberg, D.T. and I. Cheyne, "Adaptive Control Of A Polymerization Reactor", *AIChE Symposium Series*, No. 159, Vol. 72, 221 (1976)

Allison, B.J. and P.A. Taylor, "On The Experimental Application Of Computer Control To A Time-Varying pH Neutralization Process, Part III: The Use Of An Extended Kalman Filter As A Nonlinear State Estimator", Technical Report 1010, McMaster University, Hamilton, Canada (1986)

Amrehn, H., "Computer Control In The Polymerization Industry", *Automatica*, Vol. 13, 533 (1977)

Asada, H. and J.E. Slotine, "*Robot Analysis And Control*", Wiley, (1986)

Astrom, K.J. and B. Wittenmark, "*Computer Controlled Systems*", Prentice-Hall, N.J. (1984)

Autenreith, J.S., "Resins For Rubber-Based Adhesives", *Handbook Of Adhesives*, 2nd Edition, Van Nostrand Reinhold, New York (1977)

Beck, J.V. and K.J. Arnold, "*Parameter Estimation In Engineering And Science*", Wiley, New York (1977)

Bekey, G.A. and G.N. Saridis, "Identification And System Parameter Estimation. 1982", Proceedings of the Sixth IFAC Symposium, Washington, DC (1982)

Bergh, L.G., Ph.D. Thesis, McMaster University, Hamilton, Ontario, Canada (1987)

Beste, L.F. and H.K. Hall, "Equations For Continuous Control Of Molecular Weight Distribution In Homogeneous Free-Radical Polymerizations", *Journal Of Macromolecular Chemistry*, Vol. 1, No. 1, 121 (1966)

Biegler, L.T., "Solution Of Dynamic Optimization Problems By Successive Quadratic Programming And Orthogonal Collocation", *Computers And Chemical Engineering*, Vol. 8, No. 3/4, 243 (1984)

Billmeyer, F.W., "*Textbook Of Polymer Science*", Wiley, New York (1984)

Boye, A.J. and W.L. Brogan, "A Non-Linear System Controller", *Int. J. Control*, Vol. 44, No. 5, 1209 (1986)

Box, G.E.P and G.M. Jenkins, "*Time Series Analysis Forecasting And Control*", Holden-Day, Oakland (1976)

Brash, J. and A.E. Hamielec, "Introduction To Polymerization Kinetics", An Intensive Short Course On Polymer Production Technology, McMaster University (1986)

Broadhead, T.O, "Dynamic Modelling Of The Emulsion Copolymerization Of Styrene/Butadiene", M.Eng. Thesis, McMaster University, Hamilton, Canada (1984)

Broadhead, T.O. et al., "Dynamic Modelling Of The Batch, Semi-Batch And Continous Production Of Styrene/Butadiene Copolymers By Emulsion Polymerization", *Makromol. Chem., Suppl.*, 10/11, 105 (1985)

Brosilow, C.B., "The Structure And Design Of Smith Predictors From The View-Point Of Inferential Control", Proc. Joint Aut. Control Conf., Denver, Co. (1979)

Bueche, F., "*Physical Properties Of Polymers*", John Wiley & Sons, New York (1962)

Campbell, J.D., "Emulsion Polymerization Of Syrene", M.Eng. Thesis, McMaster University, Hamilton, Canada (1985)

Cawthon, G.D. and K.S. Knaebel, "Optimization Of Semibatch Polymerization Reactions", *Computers And Chemical Engineering*, Vol. 13, No. 1/2, 63 (1989)

Chen, C.Y. and B. Joseph, "On-line Optimization Using a Two-Phase Approach: An Application Study", *Ind. Eng. Chem. Res.*, 26, 1924 (1987)

Choi, K.Y. and D. Butala, "Control Of Batch Free Radical Polymerization Reactors", Proceedings Of The 1987 American Control Conference, Minneapolis, MN (1987)

Clarke, D.W. et al., "Generalized Predictive Control - Part I. The Basic Algorithm", *Automatica*, Vol. 23, No. 2, 137 (1987)

Clarke, D.W. et al., "Generalized Predictive Control - Part II. Extensions And Interpretations", *Automatica*, Vol. 23, No. 2, 149 (1987)

Cuthrell, J.E. and L.T. Biegler, "On The Optimization Of Differential-Algebraic Process Systems", *AIChE Journal*, Vol. 33, No. 8, 1257 (1987)

Cuthrell, J.E. and L.T. Biegler, "Simulataneous Optimization And Solution Methods For Batch Reactor Control Profiles", *Computers And Chemical Engineering*, Vol. 13, No. 1/2, 49 (1989)

Cutler, C.R., and B.L. Ramaker, "Dynamic Matrix Control - A computer Control Algorithm", 86th AIChE Meeting (1979)

Dahlin, E.B., "Designing and Choosing Digitial Controllers", *Instrum. Control Syst.*, 4, 77 (1968)

Davis, J.H. and R.G. Dickinson, "Spectral Factorization By Optimal Gain Iteration", *SIAM J. Appl. Math*, Vol. 43, No. 2 (1983)

Desoer, C.A. and M.J. Chen, "Design of Multivariable Feedback Systems With Stable Plant", *IEEE Trans. Auto. Control*, Vol. AC-26, No. 2 (1981)

Dimitratos, J. et al., "Dynamic Modelling And State Estimation For An Emulsion Copolymerization Reactor", *Computers And Chemical Engineering*, Vol. 13, No. 1/2, 21 (1989)

Doyle, J.C., "Analysis Of Feedback Systems With Structured Uncertainties", *IEE Proc.*, Vol. 129, Pt. D, No. 6, 242 (1982)

Doyle, J.C., Lecture Notes from Robust Control Workshop, The 1987 American Control Conference, Minneapolis, MN (1987)

Doyle, J.C. and G. Stein, "Performance And Robustness Analysis For A Classical/Modern Synthesis", *IEEE Trans. Auto. Control*, Vol. AC-26, No. 1, 4 (1981)

Doyle, J.C., Wall, J.E. and G. Stein, "Performance And Robustness Analysis For Sturctured Uncertainty", Proceedings Of the 21st IEEE Conference On Decision And Control, Orlando, Florida (1982)

Economou, C.G. and M. Morari, "Internal Model Control. 5. Extension To Nonlinear Systems", *Ind. Eng. Chem. Process Des. Dev.*, 25, 403, (1986)

Ekyhoff, P., "*System Identification*", Wiley, London (1974)

Elicabe, G.E. and G.R. Meira, "Estimation And Control In Polymerization Reactors. A Review", *Polymer Engineering And Science*, Vol. 28, No. 3, 121 (1988)

Farber, J.N. and R.L. Laurence, "The Minimum Time Problem In Batch Radical Polymerization: A Comparison Of Two Policies", *Chem. Eng. Commun.*, Vol. 46, 347 (1986)

Foo, Y.K. and I. Postlethwaite, "Extension Of The Small-μ Test For Robust Stability", *IEEE Tranactions On Automatic Control*, Vol. 33, No. 2, 172 (1988)

Freund, E., "Decoupling And Pole Assignment In Nonlinear Systems", *Electronic Letters*, Vol. 9, No. 16, 373 (1973)

Freund, E., "The Structure Of Decoupled Nonlinear Systems", *International Journal Of Control*, Vol. 21, No. 3, 443 (1975)

Freund, E., "Fast Nonlinear Control With Arbitrary Pole-Placement For Industrial Robots And Manipulators", *The International Journal Of Robotics Research*, 1, 65 (1982)

Froisy, J.B. and J. Richalet, "Industrial Applications Of IDCOM", Proceedings of the Third International Conference On Chemical Process Control, Asilomar, California, (1986)

Garcia, C.E., "Quadratic/Dynamic Matrix Control Of Nonlinear Processes: An Application To A Batch Reaction Process", AIChE Annual Meeting (1984)

Garcia, C.E. and M. Morari, "Internal Model Control. 1. A Unifying Review And Some New Results", *Ind. Eng. Chem. Process Des. Dev.*, 21, 308 (1982)

Garcia, C.E. and M. Morari, "Internal Model Control. 2. Design Procedure For Multivariable Systems", *Ind. Eng. Chem. Process Des. Dev.*, 24, 472 (1985)

Garcia, C.E. and M. Morari, "Internal Model Control. 3. Multivariable Control Law Computation And Tuning Guidelines", *Ind. Eng. Chem. Process Des. Dev.*, 24, 484 (1985)

Garcia, C.E. and D.M. Prett, "Advances In Industrial Model-Predictive Control", Proceedings of the Third International Conference On Chemical Process Control, Asilomar, California (1986)

Georgiou, T.T., "On a Schur-Algorithm Based Approach To Spectral Factorization: State-Space Formulae", *Systems & Control Letters*, 10, 123 (1988)

Gilles, E.D., "Some New Approaches For Controlling Complex Processes In Chemical Engineering", Proceedings of the Third International Conference On Chemical Process Control, Asilomar, California (1986)

Gilles, E.D., "Model-Based Techniques For Controlling Processing In Chemical Engineering", 10th World Congress On Automatic Control, Munich, Germany (1987)

Goodwin, G.C. and R.L. Payne, "*Dynamical System Identification: Experiment Design And Data Analysis*", Academic Press, New York (1977)

Goodwin, G.C. and K.S. Sin, "*Adaptive Filtering Prediction And Control*", Prentice-Hall (1984)

Hamielec, A.E. and T. Hoffman, "Emulsion Polymerization Polymer Reaction Engineering", An Intensive Short Course On Polymer Production Technology, McMaster University, Hamilton, Canada (1986)

Hamielec, A.E., et al., "Multicomponent Free-Radical Polymerization In Batch, Semi-Batch And Continuous Reactors", *Makromol. Chem. Macromol. Symp.*, 10/11, 521 (1987)

Hamilton, J.C. et al., "An Experimental Evaluation Of Kalman Filtering", *AIChE Journal*, Vol. 19, No. 5, 901 (1973)

Hansen, F.K. and J. Ugelstad, "Particle Nucleation In Emulsion Polymerization. III. Nucleation in Systems with Anionic Emulsifier Investigated by Seeded And Unseeded Polymerization", *Journal Of Polymer Science: Polymer Chemistry Edition*, Vol. 17, 3047 (1979)

Harris, B., Hamielec, A.E., and F.L. Marten, *Emulsion Polymers And Emulsion Polymerization*, Basset, D.R., Hamielec, A.E. (ed.), ACS Symposium Series, 165, Washington, D.C., 315 (1981)

Harris, T.J. and J. Davis, "Fast Algorithms for Discrete Matrix Spectral Factorization", submitted for publication (1989)

Harris, T.J. and J.F. MacGregor, "Design Of Discrete Multivariable Linear Quadratic Controllers Using Transfer Functions", *AIChE Journal*, Vol. 33, No. 9, 1481 (1987)

Hicks, J. et al., "The Optimal Control Of Polymerization Reactors", *The Canadian Journal Of Chemical Engineering*, Vol. 47, 590 (1969)

Hoffman, E.J., "Kinetic Modelling Of Emulsion Copolymerization Of Styrene And Acrylonitrile", M.Eng. Thesis, McMaster University, Hamilton, Canada (1984)

Holt, B.R. and M. Morari, "Design Of Resilient Processing Plants - VI. The Effect Of Right-Half-Plane Zeros On Dynamic Resilience", *Chemical Engineering Science*, Vol. 40, No. 1, 59 (1985)

Holt, B.R. and M. Morari, "Design Of Resilient Processing Plants - V. The Effect Of Deadtime On Dynamic Resilience", *Chemical Engineering Science*, Vol. 40, No. 7, 1229 (1985)

Hsia, T.C., "*System Identification*", Lexington Books, Toronto (1977)

Hsu, K.Y. and S.A. Chen, "Minimum End-Time Policies For Batchwise Radical Chain Polymerization: The Piecewise Initiator Addition Policy", *Chemical Engineering Science*, Vol. 43, No. 6, 1311 (1988)

Hubbard, M. and T. DaSilva, "Estimation Of Feedstream Concentrations In Cement Raw Material Blending", *Automatica*, Vol. 18, No. 5, 595 (1982)

Hugo, A., Ph.D. Thesis (In Progress) (1989)

Huo, B.P, et al., "The Effect Of Impurities On Emulsion Polymerization: Case II Kinetics", *Journal Of Applied Polymer Science*, Vol. 35, 2009 (1988)

Hyun, J.C. and S.G. Bankoff, "Continuous Polymerization Of Vinyl Acetate-II", *Chemical Engineering Science*, Vol. 31, 953 (1976)

Jang et al., "Comparison Of Two Approaches To On-Line Parameter And State Estimation Of Nonlinear Systems", *Ind. Eng. Chem. Process Des. Dev.*, 25, 809 (1986)

Jang, S.S, et al., "On-Line Optimization Of Constrained Multivariable Chemical Processes", *AIChE Journal*, Vol. 33, No. 1, 26 (1987)

Jang, S.S and W.L. Yang, "Dynamic Optimization Of Batch Emulsion Polymerization Of Vinyl Acetate-An Orthogonal Polynomial Initiator Policy", *Chemical Engineering Science*, Vol. 44, No. 3, 515, (1989)

Jazwinski, A.H., "*Stochastic Processes And Filtering Theory*", Academic, New York (1970)

Jecek, J. and V. Kucera, "Efficient Algorithm For Spectral Factorization", *Automatica*, Vol. 21, No. 6, 663 (1985)

Jo, J.H. and S.G. Bankoff, "Digital Monitoring And Estimation Of Polymerization Reactors", *AIChE Journal*, Vol. 22, No. 2, 361 (1976)

Johnson, M.A. and M.J. Grimble, "Recent Trends In Linear Optimal Quadratic Multivariable Control System Design", *IEE Proceedings*, Vol. 134, Pt. D. No. 1, 53 (1987)

Juba, M.R. and J.W. Hamer, "Progress And Challenges In Batch Process Control", Proceedings of the Third International Conference On Chemical Process Control, Asilomar, California (1986)

Jutan, A. and A. Uppal, "Combined Feedforward-Feedback Servo Control Scheme For An Exothermic Batch Reactor", *Ind. Eng. Chem. Process Des. Dev.*, 23, 597 (1984)

Kalman, R.E., "A new approach to Linear Filtering and Prediction Problems", *ASME Trans. J. Basic Eng.*, 82D, 35 (1960)

Kashyap, R.L. and A.R. Rao, "*Dynamic-Stochastic Models From Empirical Data*", Academic Press, New York (1976)

Kiparissides, C. and S.L. Shah, "Self-Tuning And Stable Adaptive Control Of A Batch Polymerization Reactor", *Automatica*, Vol. 19, No. 3, 225 (1983)

Kiparissides, C. et al., "A Comparative Study Of LQC, DMC And Extended STR Control Strategies", 10th World Congress On Automatic Control, Munich, Germany (1987)

Korti, T., Ph.D. Thesis, In Progess, McMaster University, Hamilton, Canada, (1989)

Kouvaritakis, B. and H. Latchman, "Necessary And Sufficient Stability Criterion For Systems With Structured Uncertainties: The Major Principle Direction Alignment Principle", *Int. J. Control*, Vol. 42, No. 3, 575 (1985)

Kozub, D.J., "Advanced Model-Based Multivariate Control Design And Application to Packed Bed Reactor Control", M.Eng. Thesis, Dept. Chem. Eng., McMaster University, Hamilton, Canada (1986)

Kozub, D.J., MacGregor, J.F. and J.D. Wright, "Application Of LQ and IMC Controllers To A Packed-Bed Reactor", *AIChE Journal*, Vol. 33, No. 9, 1496 (1987)

Kravaris, C. and C.B. Chung, "Nonlinear State Feedback Synthesis By Global Input/Output Linearization", *AIChE Journal*, Vol. 33, No. 4, 592 (1987)

Kravaris, C. et al., "Nonlinear Controllers For Trajectory Tracking In Batch Processes", *Computers Chem. Engng.*, Vol. 13, No. 1/2, 73 (1989)

Kucera, V., "*Discrete Linear Control: The Polynomial Approach*", Wiley, N.Y. (1979)

Kwakernaak, H., "Uncertainty Models And The Design Of Robust Control Systems", Lecture Notes in Control And Information Sciences, Proceedings of an International Seminar Organized By Deutsche Forschungs and Versuchsanstalt For Luft-und Ramumfahrt (DFVLR), Bonn, Germany (1985)

Kwakernaak, H. and R. Sivan, "*Linear Optimal Control Systems*", Wiley, N.Y. (1972)

Lee, P.L. and G.R. Sullivan, "Generic Model Control - Theory And Applications", IFAC Workshop On Model Based Process Control, Atlanta, Georgia, USA (1988)

Lee, P.L. and G.R. Sullivan, "Generic Model Control (GMC)", *Comput. Chem. Engng.*, Vol. 12, No. 6, 573 (1988)

Li, W.C. and L.T. Biegler, "Process Control Strategies For Constrained Nonlinear Systems", *Ind. Eng. Chem. Res.*, 27, 1421 (1988)

Li, S. et al., "A State Space Formulation For Model Predictive Control", *AIChE Journal*, Vol. 35, No. 2, 241 (1989)

Ljung, L. and T. Soderstrom, "*Theory And Practice Of Recursive Identification*", The MIT Press, Cambridge (1987)

MacGregor, J.F., Lecture Notes from An Intensive Short Course On Digital Computer Techniques For Process Identification and Control, McMaster University, Hamilton, Canada (1984)

MacGregor, J.F., "On-line Statistical Process Control", *Chemical Engineering Progress*, 84, 21 (1988)

MacGregor, J.F., et al., "State Estimation For Polymerization Reactors", IFAC Symp. On Dynamics And Control Of Chemical Reactors And Distillation Columns, Bournemouth, U.K. (1986)

Marroquin, G. and W.L. Luyben, "Experimental Evaluation Of Nonlinear Cascade Controllers For Batch Reactors", *Ind. Eng. Chem. Fundam.*, Vol. 11, No. 4, 552 (1972)

Martens, C.R., "*WaterBorne Coatings*", Van Nostrand Reinhold Co., New York (1981)

McDonald, K.A., "Characterization Of Distillation Nonlinearlity For Control System Design And Analysis", *The Shell Process Control Workshop*, Butterworths (1987)

McDonald, K.A., and A.N. Palazoglu, "Robustness Analysis Of High Purity Distillation Control Using Highly Structured Correlated Model Uncertainty Descriptions", AIChE Annual Meeting, New York (1987)

McDonald, K.A. et al., "Impact Of Model Uncertainty Descriptions For High-Purity Distillation Control", *AIChE Journal*, Vol. 34, No. 12, 1996 (1988)

Miller, F.A., "Styrene-Butadiene Latexes In Protective And Decorative Coatings", *Film-Forming Compositions*, Part II, Marcel Dekker, New York (1968)

Morari, M. and J.C. Doyle, "A Unifying Framework For Control System Design Under Uncertainty And Its Implications For Chemical Process Control", Proceedings of the Third International Conference On Chemical Process Control, Asilomar, California, 5 (1986)

Morari, M., Zafiriou, E., and B.R. Holt, "Design Of Resilient Processing Plants. New Characterization Of The Effect Of RHP Zeros" *Chemical Engineering Science*, Vol. 42, No. 10, 2425 (1987)

Morshedi, A.M., "Universal Dynamic Matrix Control", Proceedings of the Third International Conference On Chemical Process Control, Asilomar, California (1986)

Navratil, J.P et al., "Disturbance Feedback In Model Predictive Control Systems", IFAC Workshop On Model Based Process Control, Atlanta, Georgia, USA (1988)

Nomura, M.H., Personal Communication (1988)

Onderwater, D.N., "Control System Configuration And Multivariable Identification of a Packed Bed Tubular Reactor", M.Eng. Thesis, McMaster University, Canada (1985)

O'Toole, J.T., "Kinetics Of Emulsion Polymerization", *J. App. Polym. Sci.*, 9, 1291 (1965)

Palazoglu, A., "Robust Stability in IMC Framework Using the Numerical Range Approach", Proceedings Of The 1987 American Control Conference, Minneapolis, MN (1987)

Ponnuswamy, S.R. et al., "Computer Optimal Control Of Batch Polymerization Reactors", *Ind. Eng. Chem. Res.*, 26, 2229 (1987)

Parish, J.R. and C.B. Brosilow, "Nonlinear Inferential Control", *AIChE Journal*, Vol. 34, No. 4, 633 (1988)

Patwardhan, A.A. et al., "Model Predictive Control Of Nonlinear Processes In The Presence Of Constraints", AIChE Annual Meeting, Washington (1988)

Postlethwaite, I. et al., "Principle Gains And Principle Phases In The Analysis Of Linear Multivariable Feedback Systems", *IEEE Transactions On Automatic Control*, Vol. AC-26, No. 1, 32 (1981)

Ramirez, W.F., "Optimal State And Parameter Identification. An Application To Batch Fermentation", *Chemical Engineering Science*, Vol. 42, No. 11, 2749 (1987)

Rawlings, J.B. and W.H. Ray, "The Modelling Of Batch And Continuous Emulsion Polymerization Reactors - I. Model Formulation And Sensitivity To Parameters", *Polymer Eng. & Sci.*, Vol. 28, No. 5 (1986)

Ray, W.H., "*Advanced Process Control*", McGraw-Hill (1981)

Ray, W.H. and C.E. Gall, "The Control Of Copolymer Composition Distributions In Batch And Tubular Reactors", *Macromolecules*, Vol. 2, No. 4 (1969)

Richalet J., et al. "Model Predictive Heuristic Control: Application to Industrial Processes", *Automatica*, Vol. 14, 413 (1978)

Rosenbrock, H.H., "*Computer-Aided Control System Design*", Academic Press, London (1974)

Rouhani, R. and R.K. Mehra, "Model Algorithmic Control (MAC); Basic Theoretical Properties", Automatica, Vol. 18, No. 4, 401 (1982)

Sacks, M.E., et al., "Effect Of Temperature Variations On Molecular Weight Distributions: Batch, Chain Addition Polymerizations", *Chemical Engineering Science*, Vol. 28, 241 (1973)

Schuler, H. and Z. Suzhen, "Real-Time Estimation Of The Chain Length Distribution In A Polymerization Reactor", *Chemical Engineering Science*, Vol. 40, No. 10, 1891 (1985)

Schuler, H. and S. Papadopoulou, "Real-Time Estimation Of The Chain Length Distribution In A Polymerization Reactor II. Comparison Of Estimated And Measured Distributions", *Chem. Eng. Sci.*, 41, 2681 (1986)

Seinfeld, J.H., "Nonlinear Estimation Theory", *Industrial And Engineering Chemistry*, Vol. 62, No. 1, 32 (1970)

Seinfeld, J.H. "Optimal Stochastic Control Of Nonlinear System", *AIChE Journal*, Vol 16, No. 6, 1016 (1970)

Skogestad S. and M. Morari, "Design Of Resilient Processing Plant-IX. Effect Of Model Uncertainty On Dynamic Resilience", *Chemical Engineering Science*, Vol. 42, No. 7, 1765 (1987)

Spong, M.W. and M. Vidyasagar, "*Robot Dynamics And Control*", Wiley (1989)

Stephanopoulos G. and K.Y. San, "Studies On On-line Bioreactor Identification. I. Theory", *Biotechnology and Bioengineering*, Vol. XXVI, 1176 (1984)

Stripada, N.R. and D.G. Fisher, "Multivariable Optimal Constrained Control Algorithm (MOCCA) : Part 1. Formulation And Application", Proceedings Of The International Conference On Industrial Process Modelling And Control, Vol. 1, Hangzhou, China (1985)

Takamatsu, T., et al., "Design Of Adaptive/Inferential Control System And Its Application To Polymerization Reactors", *Ind. Eng. Chem. Process Des. Dev.*, 25, 821 (1986)

Tate, D.P. and T.W. Bethea, "Buadiene Polymers", *Encyclopedia Of Polymer Science And Engineering*, Vol. 2, Wiley, New York (1985)

Taylor, M., personal communication, Polysar Limited , Sarnia, Canada (1988)

Temeng, K.O. and F.J. Schork, "Adaptive Control Of Emulsion Polymerization In A Seeded Stirred Tank Reactor", Proceedings Of The 1987 American Control Conference, Minneapolis, MN (1987)

Tiao, G.C. and G.E.P. Box, "Modelling Multiple Time Series With Applications", *Journal Of The American Statistical Association*, Vol. 76, No. 376, 802 (1981)

Tirrel, M. and K. Gromley, "Composition Control Of Batch Copolymerization Reactors", *Chemical Engineering Science*, Vol. 36, 367 (1981)

Tsoukas, A. and M. Tirrel, "Multiobjective Dynamic Optimization Of Semi-Batch Copolymerization Reactors", *Chemical Engineering Science*, Vol. 37, No. 12, 1785 (1982)

Tuel, W.G., "Computer Algorithm For Spectral Factorization Of Rational Matrices", *IBM Journal*, March, 163 (1968)

Ugelstad, J. and F.K. Hansen, "Kinetics And Mechanism Of Emulsion Polymerization", *Rubber Chem. & Technol.*, 49, 536 (1976)

Ugelstad, J. et al., "Thermodynamics Of Swellling. Preparation And Application Of Some Composite, Monosized Polymer Particles", *Makromol. Chem., Suppl.*, 10/11, 215 (1985)

Wells, C.H., "Application Of Modern Estimation And Identification Techniques To Chemical Processes", *AIChE Journal*, Vol. 17, No. 4, 966 (1971)

Wilson, G.T., "Modelling Linear Systems For Multivariate Control", Ph.D. Thesis, University Of Lancaster, England (1970)

Wilson, G.T., "The Factorization Of Matrical Spectral Densities", *SIAM J. Appl. Math.*, 23, 420 (1972)

Youla, D.C. et al. "Modern Wiener-Hopf Design Of Optimal Controllers - Part II: The Multivariable Case", *IEEE Transactions On Automatic Control*, Vol. AC-21, No. 3, 319 (1976)

Young, P., "Parameter Estimation For Continuous-Time Models - A Survey", *Automatica*, Vol. 17, No. 1, 23 (1981)

Zafiriou, E. and M. Morari, "Digital Controller Design For Multivariable Systems With Structural Closed-Loop Performance Specifications", *Int. J. Control*, Vol. 46, No. 6, 2087 (1987)

Zames, G. "Feedback And Optimal Sensitivity: Model Reference Transformations, Weighted Seminorms, And Approximate Inverses", Proc. 17th Allerton Conf., 744 (1979)

Zames, G., "Feedback And Optimal Sensitivity: Model Reference Transformations, Multiplicative Seminorms and Approximate Inverses" *IEEE Trans. Auto. Control*, Vol. AC-26, No. 2, 301 (1981)